A NOVEL REACTOR WITH TWO INDEPENDENTLY-DRIVEN IMPELLERS FOR GAS-LIQUID PROCESSING

by

ARWYN JOHN

A thesis submitted to the Faculty of Enginnering
of the
University of Birmingham
for the degree of
DOCTOR OF PHILOSOPHY

School of Chemical Engineering
University of Birmingham
Birmingham
B15 2TT
United Kingdom

UNIVERSITY OF
BIRMINGHAM

University of Birmingham Research Archive

e-theses repository

This unpublished thesis/dissertation is copyright of the author and/or third parties. The intellectual property rights of the author or third parties in respect of this work are as defined by The Copyright Designs and Patents Act 1988 or as modified by any successor legislation.

Any use made of information contained in this thesis/dissertation must be in accordance with that legislation and must be properly acknowledged. Further distribution or reproduction in any format is prohibited without the permission of the copyright holder.

19912625

K0913841

ABSTRACT

Filamentous micro-organisms, grown in submerged culture, are used in a large number of fermentation processes, such as the production of penicillin and citric acid. Generally, production takes place in baffled sparged vessels agitated by either single or multiple impellers, traditionally Rushton turbines mounted on a common shaft. This configuration is satisfactory for low viscosity systems, *e.g.* yeast and some bacterial fermentations. However, in cultures of filamentous fungi, as the fermentation time progresses, the broth may become increasingly viscous, and possibly shear thinning, with the consequent onset of dead zones or stagnant regions. The resulting concentration gradients may cause a reduction in the productivity.

It may be possible to overcome these problems by using a fermenter which has two independently driven impellers and a cylindrical draft tube (IDDIDT *i.e.* an acronym for "**I**ndependently **D**riven **D**ual **I**mpeller with **D**raft **T**ube"). Studies have been undertaken in a 0.75 m Perspex proto-fermenter employing a Rushton turbine (6RT) and a Scaba 3SHP1 axial flow impeller, with test fluids such as water and CMC, under unaerated and aerated conditions. In order to fully characterise the system, important mixing aspects such as mass transfer (hold-up, k_La) and bulk blending (mixing times, circulation time distributions) were investigated and related to the power input from each impeller. At low gas rates, moderately-increased hold-up and k_La values were observed with the IDDIDT compared to single or dual Rushton turbine systems. At higher gassing rates the performance was similar for all configurations. For the IDDIDT, regardless of the proportion of the total energy dissipation rate contributed by each impeller, the k_La was the same. In addition, very rapid mixing times,

approximately 3 times faster than predicted by correlations for single impeller, single shaft systems and experimentally determined values for the dual Rushton system, were observed. Mixing times could be directly controlled by the 3SHP1 axial flow impeller, and confirmation of the increased exchange flow rate throughout the vessel was achieved via circulation time distribution (CTD) experiments.

Since very little data has been published regarding the use of fermentation broths in these systems, hygienic *Aspergillus niger* fermentations were carried out in the fermenter to clarify any improvements when using the novel reactor and also to highlight any discrepancies in the use of test fluids, such as CMC, as model broths. Although unaerated and aerated power characteristics were similar for both the test fluids and fermentation broths the hold-up values varied considerably, probably due to differing coalescence characteristics. Productivity (g/l/kWh) of batch phase *Aspergillus niger* fermentations was unaffected by system geometry, at least up to concentrations of circa 15 g/l.

To my mother and father

ACKNOWLEDGEMENTS

I would like to express my sincerest gratitude to Professor Alvin Nienow and Dr. Waldemar Bujalski for their enthusiastic support and guidance throughout the duration of the project.

The organisational skills of Bob Badham coupled with the technical expertise of Bob Sharpe and Tom Eddleston were unsurpassed and has been greatly appreciated. I would also like to thank, for their indispensable advice and assistance: Rainer Schmitz for developing the CTD work, Phil Cox for the morphology measurements, and Grainne Riley for the fermentation work. In addition, I am grateful for many helpful discussions with friends and colleagues including: the biocentre staff (Hazel Jennings, Dave Bowden, Dave French and Elaine Mitchell), the fermentation group (Colin Thomas, Ashraf Amanullah and Gopal Paul), the mixing group (Dixie Patel, Noboru Otomo and Thomas Martin), and, not forgetting, "The Brook" group (too numerous to mention).

Finally, I would like to thank Ruth Blair for proof reading this work and my parents for their endless moral and financial support throughout my student years.

CONTENTS

CHAPTER 7

CHAPTER 8

CHAPTER 9

APPENDIX I

NOMENCLATURE

APPENDIX II

CALIBRATION OF RHEOMETER

APPENDIX III

STATISTICAL ANALYSIS

APPENDIX IV

MASS TRANSFER CALCULATIONS

APPENDIX V

LABVIEW PROGRAMS

APPENDIX VI

ASPERGILLIS NIGER FERMENTATIONS

APPENDIX VII

PUBLISHED WORK

CHAPTER 1

INTRODUCTION

Large scale, fed-batch or batch fermentation processes are often governed by growth limiting factors which could be eliminated by improving the efficiency of the mixing process. In particular the primary task in a fermentation is to provide as near a homogeneous and defined environment as is possible[1]. This is in order to meet the physiological requirements of the cells. In addition , the process of mass transfer between gas and liquid is of great importance when considering the effectiveness of gas-liquid reactors and fermenters. A critical factor in the design of a fermentation system is the provision of a desired concentration of dissolved oxygen required by the cells, which in turn is limited by the transfer of the oxygen from the sparged air into the liquid phase.

Agitated, sparged vessels and bubble columns are the two main methods of aeration. Bubble columns are utilised because of their lack of moving parts, low cost and ease with which the phase residence time can be varied[2]. Mechanically agitated vessels are particularly suited to vessels with relatively low superficial gas velocities[2], providing good mass transfer, heat transfer and excellent mixing. The fermentation industries have traditionally adopted the baffled, sparged vessel of aspect ratio greater than one agitated by multiple Rushton turbines, on a common shaft, for the production of biosynthetic products. However, problems can still occur on the large scale due to heat and mass transfer limitations, resulting in reduced yields, lower productivity and poor process control. This is especially the case when highly viscous non-Newtonian fermentation broths are encountered, e.g. filamentous forms of *Penicilium chrysogenum* and *Aspergillus niger* employed for the production of Penicillin and Citric acid

respectively, or the extremely viscous xanthan gum, produced by *Xanthemonas campestris*. This problem can be overcome by the method proposed by Anderson *et al.*[1]. They suggested that a fermenter consisting of two independently driven impellers, the bottom impeller for gas dispersion and the top for bulk recirculation, could yield an improved homogeneous environment, possibly at the lowest possible power input to the system. The system can also incorporate a draft tube producing an increased heat transfer area[1] whilst providing a more defined bulk flow pattern. Such an attractive system was patented by Solomons and Le Grys[3] in 1981.

The aim of the work undertaken was to analyse such a configuration using a proto-fermenter of 0.75 m diameter (T) with a liquid height giving an aspect ratio of 2:1 with two, independently-driven impellers with and without a draft tube. The objectives were therefore to investigate the effects on the proto-fermenter performance due to:

- Operating variables; lower and upper impeller speeds, gas flow rate and power input,
- Vessel geometry; with/without draft tube,
- Fluid rheology; using simple and complex fluids,
- Morphology; using real (*Aspergillus niger*) fermentation broths.

To achieve this schedule, the project was divided into four interrelated sections:

(i) Power draw and hold-up. The power drawn by single and dual agitators, under gassed and ungassed conditions, using simple and complex fluids (water, sodium carboxy-methyl-cellulose (CMC), *Aspergillus niger* broths), with and without draft tube was investigated. The subsequent changes in gas-liquid hold-up were also measured.

(ii) Mixing/circulation times covering the same set of conditions, again with and without a draft tube.

(iii) Mass transfer coefficient, k_La. As (i) and to analyse reliability of the comparison drawn between k_La and hold-up.

(iv) Real Fermentations. To conduct mycelial fermentations within the proto-fermenter and observe the effects on and of morphology and rheology on the operating characteristics and performance of the proto-fermenter.

1.1 REFERENCES

1 . Anderson, C., LeGrys G. A. and Solomons G. L.,1982, "Concepts in the design of large-scale fermenters for viscous culture broths", *The Chemical Engineer*, 377: 43-49

2 . Paca J., Ettler, P. and Grégr V.,1976, "Hydrodynamic behaviour and oxygen transfer rate in a pilot plant fermenter", *J.Appl.Chem.Biotech.*, 26: 309-317

3 . Solomons, G. L. and LeGrys, G. A., *British Patent*, 1 584 103

CHAPTER 2

BACKGROUND INFORMATION

Agitators have been incorporated into fermentation vessels to achieve two major functions. Firstly, the provision of good bulk mixing is necessary to ensure that micro-organisms are subjected to a homogenised and well defined environment which is a prerequisite for high productivity processes. The second major requirement of an agitator is the break-up and distribution of gas bubbles leaving the sparger for oxygen mass transfer. Provided these requirements are satisfied, concentration gradients within the reactor will be minimised and sufficient mass transfer between gas bubbles and the cells and good heat transfer between the fermentation broth and the heating/cooling system will be achieved. However, as fermentations progress the rheological properties may become increasingly complex, either due to the production of a biopolymer, *e.g.* polysaccharide fermentations, or due to the interaction of hyphae in a filamentous fermentation broth, *e.g. Penicillium chrysegenum*. In such circumstances, heat and mass transfer becomes more problematic throughout the fermentation with the possible onset of dead zones (stagnant areas) where no bulk mixing occurs, resulting in regions depleted in oxygen/nutrients. In addition, on scale-up, temperature control becomes more difficult since the heat produced by the metabolic activity of the cells and the energy dissipation of the agitators increases volumetrically but the provision for heat transfer scales with area and the heat transfer coefficient goes down with increasing viscosity.

Reactor performance is generally assessed through the mass transfer and/or bulk blending characteristics as a function of specific power input and gas flow rate.

Mass transfer efficiency is usually characterised by the overall mass transfer coefficient k_La (Chapter 6), or by relation to the gassed hold-up (Chapter 5). The bulk flow, or macromixing, can be assessed by mixing time measurements (Chapter 7) or by flow follower techniques (Chapter 8).

Before investigating different bioreactor configurations it is necessary to consider some basic mixing definitions and principles which underpin the theory and data presentation throughout the thesis. Section 2.1 describes the rheological characteristics of some industrial bioprocess fluids and the test solutions used to mimic them in this study. Section 2.2 gives an introduction to mixing including some of the most important definitions and the characteristic methods of analysing and presenting the data.

2.1 Rheology

As previously mentioned, industrial fermentation processes involve the growth of filamentous organisms for the production of biosynthetic products. The behaviour of the fermentation broths is extremely important for the assessment of bioreactor performance and design, as the rheological properties can have a significant effect on the efficiency of bulk mixing, mass and heat transfer. This affects the transfer of essential nutrients and oxygen to the micro-organisms and the removal of metabolic heat by the coiling coils or water jacket. The rheological characteristics of the fermentation broth may vary as the fermentation progresses due to the increased biomass concentration and changes in morphology of the micro-organism. In order to fully investigate the flow behaviour and transport phenomena without the necessity of costly fermentations, researchers often use transparent polymer solutions to simulate the properties of fermentation broths[1].

Sufficient texts are available which discuss the rheological properties of fluids in detail [2,3,4]. In this section the basic principles of rheology will be addressed. The fluids investigated can be divided into two distinct groups, Newtonian and non-Newtonian.

2.1.1 Newtonian

From Newton's viscous law, the viscosity of a fluid is defined as:

$$\mu = \frac{\tau}{\dot{\gamma}} \tag{2.1}$$

where τ is the shear stress and $\dot{\gamma}$ is the shear rate. For Newtonian fluids viscosity is constant and independent of shear rate and hence agitation rate. Most bacterial or yeast fermentation broths exhibit Newtonian behaviour.

2.1.2 Non-Newtonian

Non-Newtonian fluids do not obey Newtons law of viscous flow. They have a non-uniform viscosity which is dependent upon shear rate and hence impeller speed. In this case, an apparent viscosity is defined as:

$$\mu_a = \frac{\tau}{\dot{\gamma}} \tag{2.2}$$

and is a function of the rate of shear.

2.1.2.1 Shear thinning/pseudoplastic fluids

Shear thinning fluids of industrial importance include mycelial fermentation broths and biopolymer solutions. The decrease in apparent viscosity with increasing shear rate occurs as the filamentous structures or long chain polymer molecules align with each other, reducing resistance to flow. Such fluids are generally described in terms of the Power law model:

$$\tau = K\dot{\gamma}^n \tag{2.3}$$

where K is the consistency index representing the apparent viscosity at any given rate of shear and n is the flow behaviour index. The flow behaviour index describes the deviation of flow from Newtonian, *i.e.* as n decreases below 1, the flow becomes increasingly shear thinning. Power law data is commonly described in the form

$$\log \tau = \log K + n \log \dot{\gamma} \qquad (2.4)$$

enabling n and K to be calculated from the gradient and intercept (log-log plot) respectively.

Combining equations 2.2 and 2.3 gives,

$$\mu_a = K\dot{\gamma}^{n-1} \qquad (2.5)$$

In stirred vessels, high shear rates near the intensely mixed impeller region produce a low apparent viscosity. Moving away from the impeller region, the shear rate falls and so the apparent viscosity increases.

2.1.2.2 Bingham Plastics

Bingham plastics behave in a similar manner to Newtonian fluids, except that the fluid will not flow until a shear stress exceeding a limiting shear stress, known as the yield stress, has been imposed. As with Newtonian liquids, a linear relationship exists between shear stress and shear rate and the flow is governed by the equation

$$\tau = \tau_o + \eta\dot{\gamma} \qquad (2.6)$$

where τ_o is the yield stress and η is the coefficient of rigidity.

2.1.2.3 Casson body model

Casson [5] describes a type of fluid that could be considered as a cross between a plastic and a pseudoplastic fluid, *i.e.* the flow follows the Power law model but only after the yield stress has been surpassed. The flow can be described by

$$\sqrt{\tau} = \sqrt{\tau_o} + K_c\sqrt{\dot{\gamma}} \qquad (2.7)$$

where K_c is the Casson viscosity.

Rheological properties of mycelial fermentation broths are often described by the Power law model due to its simplicity and widespread use. The rheological properties of a variety of test fluids and fermentation broths have been examined by many researchers and are summarised in.Table 2.1.2-1.

Table 2.1.2-1 Rheological characteristics of a variety of fermentation broths and fluids

Author	Fluid/broth	Measurement technique	Power law constants	
			K	n
Allen and Robinson[1]	*Apergillus niger* *Penicillium chrysogenum*	Turbine rheometer Rotating cylinder Pipeline	0.02-2*	1-0.4*
Reuss *et al.*[6]	*Apergillus niger*	Turbine rheometer	0.2 -10	1 - 0.2
Fatile[7]	*Apergillus niger*	Pipe flow	0.067-0.103	1-0.87
Kim *et al.*[8]	*Absidia corymbifera*	Helical ribbon rheometer	0.1-10	0.6-0.4
Warren *et al.*[9]	*Saccharopolysporery thraea* *Actinomadura roseorufa* *Sterptomyces rimosus*	Brookfield rheometer	0.2-14	1-0.258
Fanahashi *et al.*[10]	xanthan gum solution	Brookfield rheometer	8.8-80.1	0.12
Pandit and Joshi[11]	CMC	not stated	0.049-3.48	1-0.58
Pandit *et al.*[12]	CMC	not stated	0.069-6	0.81-0.55
Nienow and Elson[13]	CMC	not stated	1.24	0.51

* Turbine rheometer gave higher shear rates than other methods.

The majority of researchers found that the consistency index, K, increased with increasing biomass concentration. The flow behaviour index, n, was unequivocally reported to decrease

with increasing biomass concentration upto approximately 5-10 g/l, after which it remained relatively constant. In this study, CMC solutions were used to simulate the rheological properties of fermentation broths as a wide range of K and n values (resulting in the Reynolds number in the range of $100<Re<4000$ (see below for definition of Re)) could be attained.

2.2 Mixing definitions and dimensionless groups

2.2.1 Reynolds Number

Reynolds number represents the ratio of inertial to viscous forces and relates to whether the flow is laminar, transitional or turbulent.

$$\mathrm{Re} = \frac{\rho N D^2}{\mu} \tag{2.8}$$

When calculating the Reynolds number in non-Newtonian fluids, the apparent viscosity is found from the Metzner and Otto approach[14]. They proposed that the average shear rate, γ_{AV}, was related to impeller speed by

$$\dot{\gamma}_{AV} = k_s N \tag{2.9}$$

where k_s was dependent on impeller type and termed the Metzner-Otto constant[15] (Table 2.2.1-1). Therefore, for power law fluids:

$$\mu_a = K\left(k_s N\right)^{n-1} \tag{2.10}$$

and

$$\mathrm{Re} = \frac{\rho N^{2-n} D^2}{K k_s^{n-1}} \tag{2.11}$$

Table 2.2.1-1 Metzner-Otto constants for various impeller types

Impeller	k_s
Rushton turbine	11.5 ± 10%
Pitched blade turbine	13.5 ± 15%
Propeller	10.0 ± 10%

2.2.2 Power number

Very early studies showed the power drawn by an impeller, in low viscosity fluids, was proportional to its speed and diameter[16], *i.e.*,

$$P \propto N^3 D^5 \tag{2.12}$$

Po is a dimensionless group representing the ratio of pressure differences and is equivalent to a drag coefficient for particles,

$$Po = \frac{P}{\rho N^3 D^5} \tag{2.13}$$

Po is based on the power input to the vessel and is therefore an important parameter when considering the design of a mixing process (Chapter 4).

At low Reynolds, in the laminar regime, numbers Po is proportional to 1/Re; at higher Reynolds numbers, in the turbulent regime ($Re>10^4$), Po is constant (Chapter 4).

2.2.3 Gas flow number

The gas flow number, Fl_G, represents the ratio of gas flow rate, Q_G, to impeller pumping rate and is given by:

$$Fl_G = \frac{Q_G}{ND^3} \tag{2.14}$$

2.2.4 Froude number

The Froude number, *Fr*, gives the ratio of inertial forces to gravitational forces:

$$Fr = \frac{N^2 D}{g} \tag{2.15}$$

The Froude number was used to generate flow regime maps (Section 4.3.2.2), but was not considered as a scale-up criteria since comparison between impellers was done on a power per unit volume basis.

2.2.5 Gas power

The energy dissipation rate due to the bubbles was calculated from basic thermodynamic principles, *i.e*

$$P_{gas} = \frac{1000\, R\, T\, u_s}{22.4H} \ln\left(1+\frac{\rho\, g\, H}{p_u}\right) \tag{2.16}$$

2.3 Data presentation

Throughout this study differerent reactor configurations (all at H=2T) have been compared on the basis of increasing power consumption, due to changing impeller speeds, at constant gas flow rates. Alternatively, data has been presented as a function of gas flow rate whilst keeping total power input or impeller speed constant. Under gassed conditions data was correlated using P_T/V which represents the total power input/unit volume, *i.e.* the sum of the power input by both the impellers and the power input due to the gas. Difficulties arose in the representation of the data gained from the independently driven impeller system (IDDIDT) since both impellers were of differing diameters, operating at different speeds. Consequently, overall values of *Fr*, *Fl* and *Re* were difficult to calculate and therefore single impeller values were used as a basis for comparison. For the single shaft situation an average value of the single impeller values was used.

2.3.1 Regime analysis

In a regime analysis, a comparison of "characteristic times" or "time constants" enables the rate limiting mechanism for a bioprocess to be determined[17,18,19,20,21,22,23]. The comparison can be made from experimentally or theoretically-established rate processes. The time constants are described as the time required to reach a fraction of the final steady state value following a step change in the input. A small time constant suggests a fast mechanism, whereas a large value suggests a slow mechanism. Comparison of the time constants associated with the reactions within the micro-organism with those of the surrounding (process controlled) environment can provide information on how possible concentration fluctuations, such as oxygen or nutrients, might affect microbial productivity [19,23] (Table 2.3-1). If the reactions associated with the micro-organism exhibit characteristic times of the same order of magnitude as (or lower than) those of the processes in the surrounding environment, interactions will occur between them. Consequently, the metabolic pathways of the micro-organism will be altered.

Table 2.3-1 Important mechanisms for regime analysis of microbial fermentations [19,23]

Microbial/conversion	Environmental/transport phenomena
Oxygen consumption	Oxygen transfer, ($1/k_La$)
Substrate consumption	Gas residence time
Growth	Liquid circulation (mixing/circulation time)
Heat production	Transfer of O_2 from bubble
	Heat transfer

2.4 References

1. Allen, D.G. and Robinson, C.W., 1990, "Measurement of rheological properties of filamentous fermentation broths", *Chem.Eng.Sci.*, 45, No.1: 37-48
2. Blanch, H.W. and Bhavaraju, S.M., 1976, "Bioengineering report: Non-Newtonian fermentation broths: Rheology and mass transfer", *Biotech.Bioeng.*, 18: 745-790
3. Wilkinson, W.L., 1960, "Fluid mechanics mixing and heat transfer", Non-Newtonian fluids, 1, Pergamon Press
4. Barnes,H.A., Hutton, J.F. and Walters, K., 1989, "An introduction to rheology", Elsevier
5. Casson, N, 1959, "Flow equation for pigment-oil suspensions of the printing ink type", *Rheology of disperse Systems* (Ed C.C. Mill), Pergammon Press, Oxford: 84-104
6. Reuss, M., Dedus, D. and Zoll, G., 1982, "Rheological properties of fermentation fluids", *Chem.Eng.*, 6: 233-236
7. Fatile, I.A., 1985, "Rheological characteristics of suspensions of *Aspergillus niger*: correlation of rheological parameters with microbial concentration and shape of the mycelial aggregate", *Appl.Microbiol.Biotech.*, 21: 60-64
8. Kim, H.J., Lebeault, J.M. and Reuss, M., 1983, "Comparitive studies on rheological properties of mycelial broth in filamentous and pelleted form", *Euro.J.Appl.Micro.Biotechnol.*, 18: 11-16
9. Warren, S.J., Keshavarz-Moore, E., Ayazi Shamlou, P. and Lilly, M.D., 1995, "Rheologies and morphologies of three *Actinomycetes* in submerged cultures", *Biotech.Bioeng.*, 45:80-85
10. Fuhanashi, H., Harada, H., Taguchi, H. and Yoshida, T., 1987, "Circulation time distribution and volume of mixing regions in highly viscous xanthan gum solution in a stirred vessel", *J.Chem.Eng.Japan.*, 20, No.3:277-282
11. Pandit, A.B. and Joshi, J.B., 1983, "Mixing in mechanically agitated gas-liquid contactors, bubble columns and modified bubble columns", *Chem.Eng.Sci.*, 36, No.8: 1189-1215
12. Pandit, A.B., Rielly, C.D., Niranjan, K. and Davidson, J.F., 1989, "The convex bladed mixed flow impeller: a multipurpose agitator", *Chem.Eng.Sci.*, 44, No.11: 2463-2474

13 . Nienow, A.W. and Elson, T.P., 1988, "Aspects of mixing in rheologically complex flluids", *Chem.Eng.Res.Des.*, 66, January: 5-15

14 . Metzner, A.B. and Otto, R.E., 1957, "Agitation of non-Newtonian fluids", *A.I.Chem.E.J*, 3, No.1: 3-10

15 . Metzner, A.B., Feehs, R.H., Ramos, H.L., Otto, R.E. and Tuthill, J.D., 1961, "Agitation of Newtonian and non-Newtonian fluids", *A.I.Chem.E.J*, 7, No.1: 3-9

16 . Unwin, W.C., 1880, "On the friction of water against solid surfaces of different degrees of roughness", *Proc.Royal.Soc.*, 31: 54

17 . Ooesterhuis, N.M.G., 1984, "Scale-up of bioreactors, a scale down approach", *Ph.D. Thesis*, Delft University of Tech.

18 . Kossen, N.W.F. and Oosterhuis, 1985, "Modelling and scaling-up of bioreactors", in *Biotechnology*, (Rehm, H.J., Reed, G. and Brauer, H. (Eds.)), VCH: Weinheim, Germany: 571-605

19 . Luyben, K.Ch.A.M., 1993, "Regime analysis for the scale-down of biotechnology processes", *Proc.Bioreactor.Performance.*, March, Helsingor, Denmark: 159-169

20 . Fransden, S., Nielsen, J. and Villadsen, 1993, "Application of regime analysis of yeast fermentation for down scaling", *Proc.Bioreactor.Performance.*, March, Helsingor, Denmark: 171-179

21 . Dunn, J.I., Heinzle, E., 1993, "Types of understanding in scaling down and up, illustrated with an oxygen sensitive culture", *Proc.Bioreactor.Performance.*, March, Helsingor, Denmark: 189-203

22 . Schmitz, R., 1996, "Circulation time studies in Newtonain and non-Newtonian fluids in stirred tanks", *Ph.D. Thesis*, University of Birmingham, UK

23 . Marten, M.R., Wenger, K.S. and Khan, S.A., 1997, "Rheology, mixing time, and regime analysis for a production-scale *Aspergillus oryzae* fermentation", *Proc.4th.Int.Conf.Bioreactor.Bioprocess.Fluid.Dynamics.*, (Ed. A.W. Nienow), BHRG, Cranfield, Edinburgh, July 1-3: 295-313

CHAPTER 3

MATERIALS AND METHODOLOGY

This chapter deals with the equipment and methods that are applicable to the proceeding chapters. The methods which are specific to a chapter have been described in that particular chapter's introduction.

3.1 Proto-fermenter

3.1.1 Vessel

The schematic layout of the proto-fermenter is shown in Figure 3.1-1. The Perspex vessel had an internal diameter of 0.75 m and a total height of 2.2 m giving a maximum liquid volume of up to about 0.95 m^3 . A working volume of 0.64 m^3 was utilised in the experimental work undertaken, *i.e.* H = 2T = 1.5 m. To eliminate optical distortion and aid visualisation a square Perspex jacket, filled with water, surrounded the vessel. The fermenter had four, evenly spaced, 0.14T width stainless steel baffles. A draft tube when fitted, was fixed to these baffles, giving a diameter of 0.54 m (0.72T), so that the cross-sectional area of the annulus and the draft tube are approximately equal thereby minimising the resistance to liquid circulation [1] (Figure 3.1-1).

The fermenter was agitated by two independently-driven impellers, shown in Figure 3.1-2 and Figure 3.1-3. The lower impeller, a standard Rushton turbine (D=T/3), was used for gas distribution and the upper impeller, a SCABA Axial 3SHP1 (D=2T/3), was incorporated for bulk recirculation. The Rushton turbine and Scaba axial impellers were driven by geared 8 kW and 4 kW motors respectively. To simulate a common shaft situation both impellers were

rotated at the same speed. By removing the draft tube and replacing the 3SHP1 by a Rushton turbine (D=T/3), a comparison with the standard dual Rushton configurations could be made.

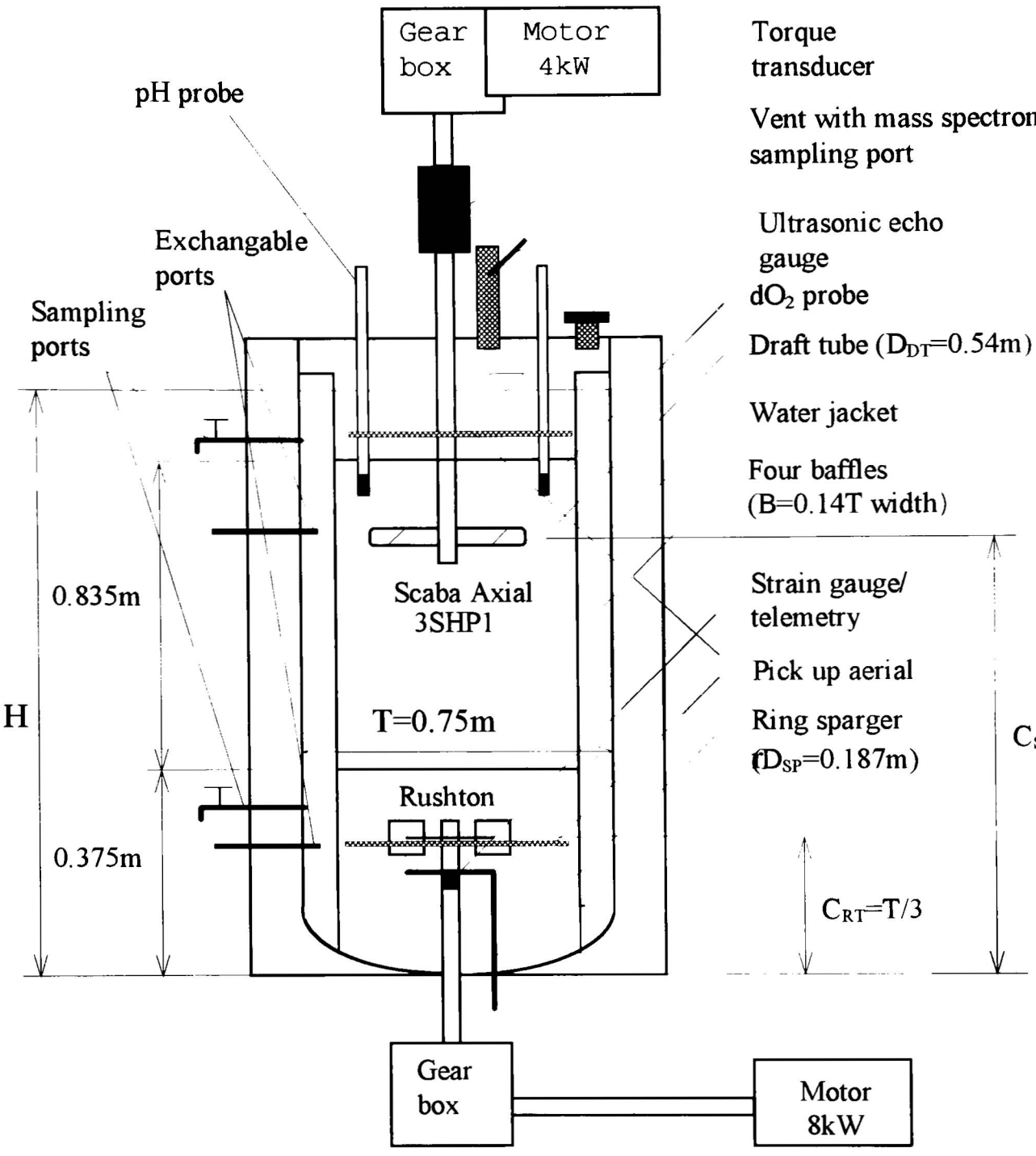

Figure 3.1-1 Schematic layout of equipment

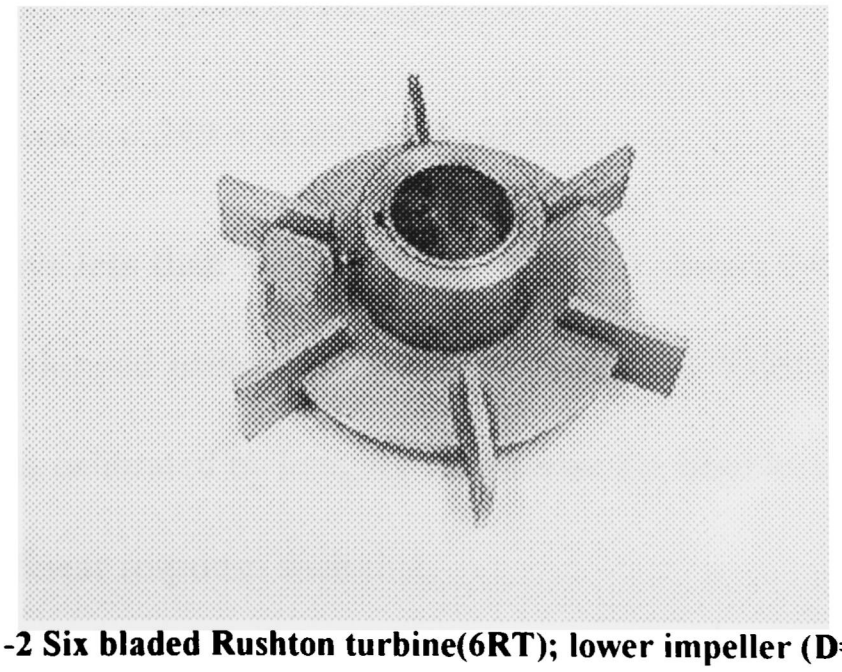

Figure 3.1-2 Six bladed Rushton turbine(6RT); lower impeller (D=T/3)

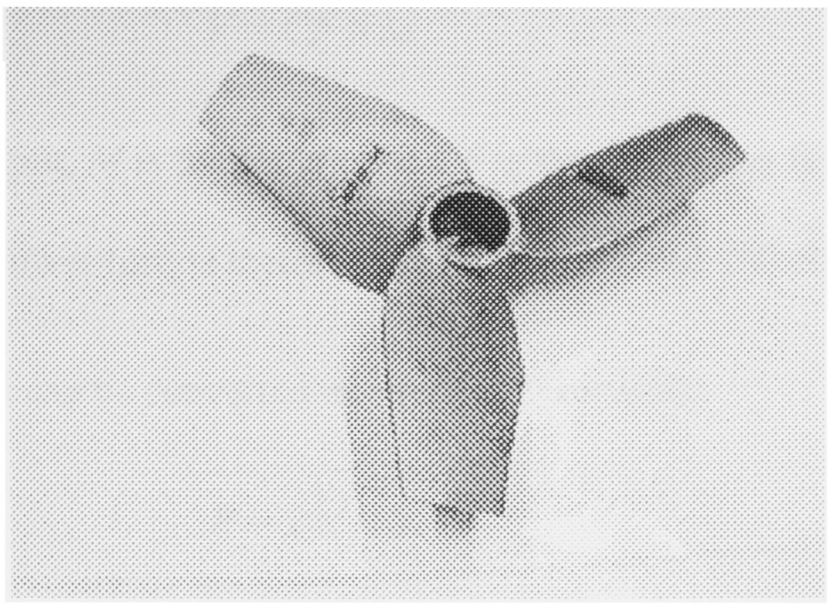

Figure 3.1-3 SCABA Axial 3SHP1; upper impeller (D=2T/3)

3.1.2 Power measurement

The torque on the bottom impeller was measured using strain gauge/telemetry technique, which is based on the principle that the electrical resistance of the metal in the strain gauge varies with the strain placed on it[2]. The change in resistance is determined by a Wheatstone bridge circuit connected to the telemetry equipment. Strain gauges mounted on the shaft allow the power consumption of the impellers to be calculated with an error of ± 3% [2,3].

Torque on the upper impeller was measured using a commercially available torque transducer (EEL Ltd.). Since this transducer was positioned outside the vessel, an allowance had to be made for torque losses encountered in the bearings. These losses were found to be a function of agitator speed and were considered when calculating the power draw. The losses were shown to be related to the agitator speed by the equation:

$$Torque\ Losses = 0.299 + 0.002N - 2\times10^{-6}N^2 \qquad (3.1)$$

(N in rpm) and were always less than 10% of the total power drawn and generally less than 3%. Torque signals were logged using a BBC Goerz metrawatt S120 chart recorder. The output from the gauges was calibrated by hanging weights on the impellers at a known distance from the axis producing a linear response such that,

$$V = CF \times M \tag{3.2}$$

where V is the voltage output, M is the torque and CF is the calibration factor. The calibration factors for the upper and lower torque meters were 46.3 Nm/V and 100 Nm/V respectively.

The torque value obtained can be converted into power draw using:

$$P = 2\,\pi N M \tag{3.3}$$

Prior to any experiment, the chart recorder and voltmeter were first zeroed. After zeroing, an ungassed power number was measured at a given speed and compared to a previously calculated value, therefore providing a check on the measurement. At the end of any experiment, the chart recorder zero was checked and any drift accounted for in the calculation of torque. A linear variation with time which had been found previously was always assumed here.

3.1.3 Impeller Speed

The impeller speeds were measured electronically using an optical relay switch that intermittently detected light passing through a 60 hole disc attached to the shaft. The values were displayed on a digital screen, giving a readout accurate to ± 1 rps (Maximum error 1.1% over experimental range).

3.1.4 Gas Sparger

Gas was sparged through ring sparger (D_{SP} = 0.187 m) positioned below the lower impeller. Gas flow rates between 60 and 395 l/min (0.09 to 0.62 vvm or 2.26 to 14.9 mm/s) were achievable. The compressed air was supplied at 10 p.s.i.g. and controlled via a calibrated rotameter. During experimentation visual checks were undertaken to ensure that no drifts in flow rate were encountered.

3.1.5 Hold-Up

The hold-up was measured using a continuous level measuring ultrasonic echo gauge (Nivosonic FMU 2780, Endress and Hauser Ltd., Manchester, UK) positioned at the top of the vessel. The unit emitted ultrasonic pulses which were reflected by the liquid surface and received by the sensor. The time delay between emitting and receiving the signal was proportional to the liquid height. The instrument was calibrated between 0 and 20 cm for which 0 % of the measuring span corresponded to the liquid level when no aeration or agitation was taking place. 100 % of the measuring span corresponded to a rise of 20 cm in the liquid level and an equivalent output of 5V. The rise in the liquid level was continuously recorded by chart recorder and converted into height by:

$$\Delta H = CF_h \times mV \tag{3.4}$$

where CF_h = 0.04 mm/mV.

The integration time was set to 35 seconds, *i.e.* if a rapid change in level from 0 to 100% occurred it would take 35 seconds before the output signal catches up with 63% of the new value. During agitation and aeration the liquid level tended to be unstable producing an unsteady reading on the chart recorder. The reading was averaged graphically to obtain a reading with a maximum error of ± 4 %. The sound waves were able to penatrate foam of upto 2 cm thickness producing an accurate measurement for the majority of test fluids used.

The hold-up was calculated from :

$$\varepsilon_G = \left(\frac{H_g - H}{H_g} \right) \times 100\% \tag{3.5}$$

where ε_G is the percentage hold-up, H_g is gassed height and H is the ungassed height.

3.1.6 Temperature control

Temperature was controlled by passing heating or cooling water through a simple stainless steel U-tube fitted between the baffles. Prior to an experiment, the vessel temperature was raised to 25°C and then controlled to ± 0.1°C for the duration of a run. Typically, cooling was required due to:

- the heat produced from the impellers,
- the exothermic decomposition of hydrogen peroxide (during k_La measurements),
- the metabolic heat of the micro-organisms (during fermentations).

Temperature was measured by two thermocouples positioned between the baffles in the upper and lower regions of the vessel.

3.1.7 Mass transfer measurement

Mass transfer coefficients were measured using the catalytic reduction of hydrogen peroxide and "live culture" methods. A full description is given in Chapter 6.

3.1.8 Mixing time measurement

Conductivity and decolorisation techniques were employed for the evaluation of the mixing time. The conductivity technique followed the concentration transient after the injection of a salt tracer. In addition to providing a global mixing time, the decolorisation technique allowed the visualisation of flow patterns occurring. The methods are fully described in Chapter 7.

3.2 Model fluids and preparation

As described in the previous chapter, researchers often use model fluids to mimic the behaviour of process fluids/fermentation broths. This allows an investigation into changing flow patterns, impeller power consumption and mass transfer properties due to a change in rheology.

Water, sodium carboxy-methyl-cellulose (CMC) and *Aspergillus niger* fermentation broths were employed as test fluids in this study.

3.2.1 Preparation

Carboxy-methyl-cellulose solutions were prepared by dissolving CMC (high molecular weight food grade 7H4CF, Aqualon, Alizay, France) in de-ionised water over a range of concentrations (0.28-1.0 % CMC). A moisture content of approximately 8 %, determined by a HOUSS moisture balance, was considered when calculating the amount of polymer powder required. Slow addition of the powder to the vessel was necessary in order to avoid the formation of large clumps. The solution was mixed overnight to allow the complete dissolution of the powder and the disengagement of small bubbles.

3.2.2 Rheology measurement

3.2.2.1 Background

Conventionally, the rheological properties of fluids have been measured using absolute measurement techniques such as concentric cylinders, cone and plate and parallel plate rheometers. However, problems exist when determining the rheological properties of viscous broths containing suspended particles, *e.g.* pellets or mycelial flocs (ca. 1mm) due to[4]:

(i) the formation of less dense layers next to the surfaces of the cylinders,

(ii) destruction of mycelial clumps or pellets since they are of similar magnitude to the annulus,

(iii) production of a non-homogeneous sample caused by settling or particle interactions.

These difficulties can be avoided by using relative measurement systems incorporating a rotating impeller (Rushton turbine/helical screw) instead of a bob[4]. The removal of the annulus eliminates aggregate damage, with solids settling minimised by the action of the agitator. The turbine rheometer has been developed for the measurement of rheological properties

encountered with filamentous broths[5,6]. However, relative systems have very complex fluid dynamics. The constitutive equations from which the fundamental rheological variables are obtained may contain some inherent system properties, and therefore cannot be solved easily. The system must be "calibrated" with systems of known rheology [5, 7, 8] In addition, turbine rheometers are only accurate at very low shear rates, *i.e.* in the laminar flow regime, and uncertain extrapolation is therefore required to predict properties in bioreactor systems which operate at higher shear rates.

3.2.2.2 Measurement technique

The rheological characteristics for all fluids were determined using a constant shear rate rheometer (Contraves Rheomat 30, Zurich, Switzerland) fitted with either concentric cylinders or a Rushton turbine and beaker arrangement (Figure 3.2-1 and Figure 3.2-2). The impeller/bob shaft was connected to the drive motor/torque-indicator system of the viscometer, and its speed was controlled via a closed loop servo system. The speed was increased stepwise (up-curve) from 7 to 350 rpm over a range of 15 increments and then decreased similarly (down-curve). Each speed was held for 20 seconds and the torque required to keep a constant rotational value was displayed on a multimeter (0 to 4.9 x 10^{-3} Nm). The up-curve and down-curve for the polymer solutions gave identical results allowing either curve to be used for the calculations of shear rates and shear stresses from concentric cylinder charts provided (Manual Rheomat 30, Contraves, Zurich, Switzerland). However, for fermentation broths, using the Rushton turbine, the high shear rate up-curve was used to fully mix the solution and the readings used for the calculation of rheological properties were recorded on the down curve[6]. Due to the complex fluid dynamics, shear rates and shear stresses could not be calculated directly and an empirical approach was necessary. The system therefore required calibration[1,8] (Appendix II). Rheological calculations were only carried out with shear rates and stresses

obtained below Reynolds numbers of 10, *i.e.* readings in the laminar flow regime. All experiments were undertaken at a temperature of 23±0.5°C.

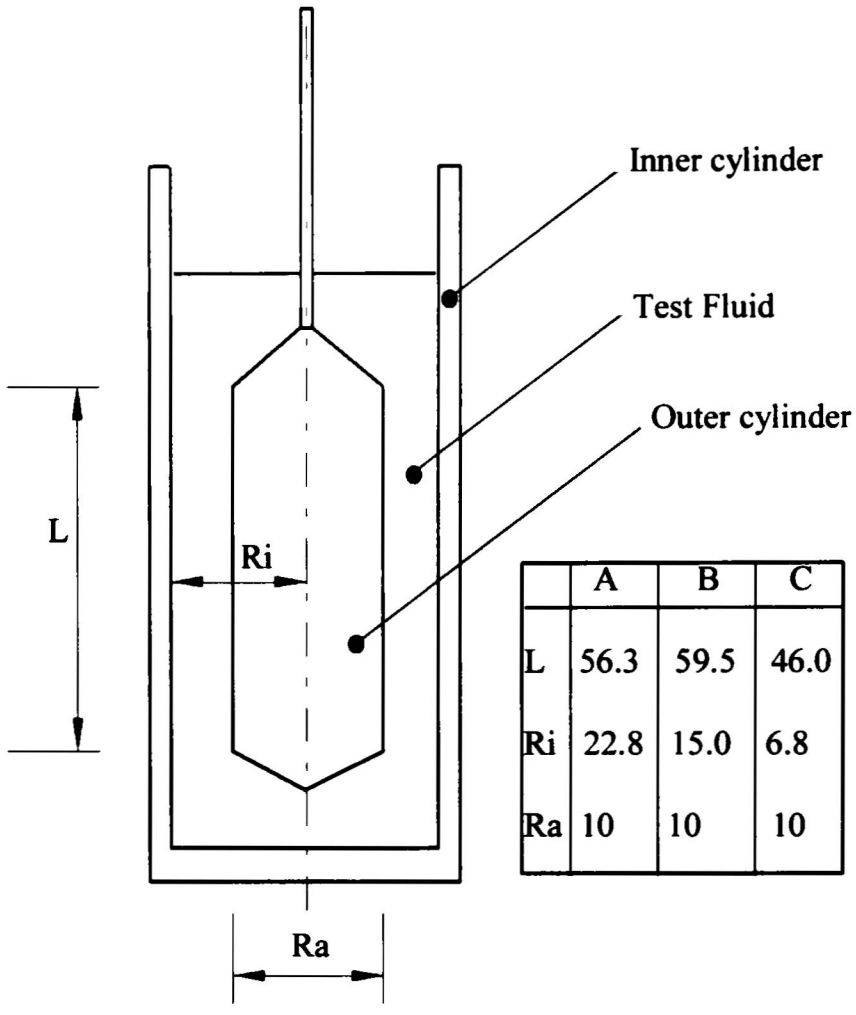

	A	B	C
L	56.3	59.5	46.0
Ri	22.8	15.0	6.8
Ra	10	10	10

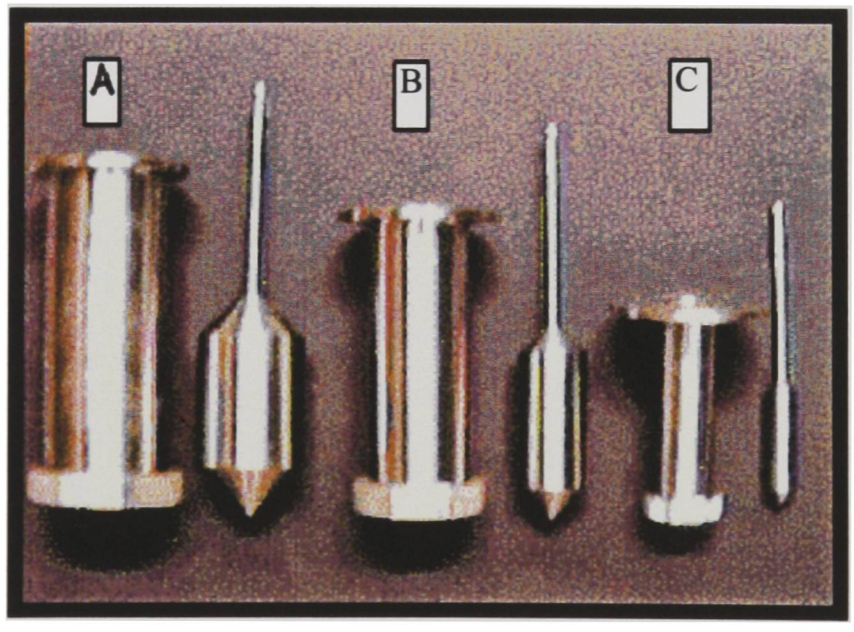

Figure 3.2-1 Concentric cylinders for Contraves shear rate rheometer

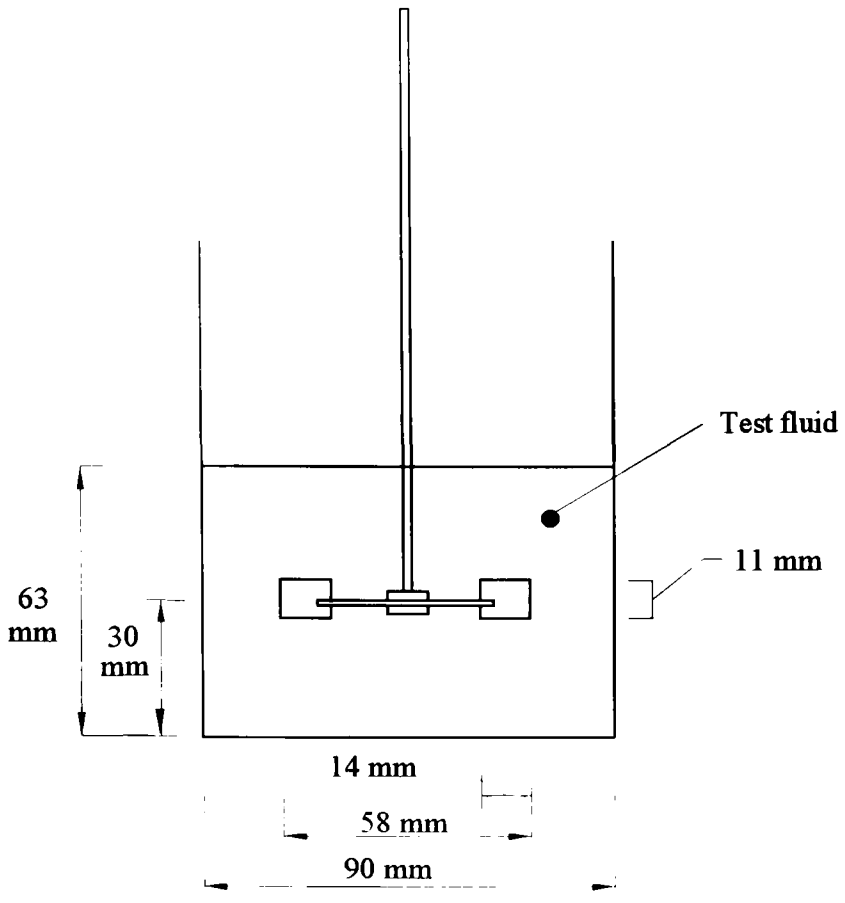

Figure 3.2-2 Rushton turbine and beaker arrangement for the Contraves rheometer

3.3 Fermentation studies

In order to examine the reactor performance in fermentation broths, a technique has been produced which permits large scale, non-aseptic, fermentations to be undertaken in Perspex tanks. The small scale pilot plant work needed to develop the method and the fermentation procedures for the large scale work (640l) are described in Appendix VI.

3.4 References

1. Jones, A.G., 1985, "Liquid circulation in a draft tube bubble column", *Chem.Eng.Sci.*, 40, No.3: 449-462
2. Kuboi, R., Nienow, A.W. and Allsford, K, 1983, "A multi-purpose stirred tank facility for flow visualisation and dual impeller power measurement", *Chem.Eng.Comm.*, 22: 43-49
3. McFarlane, C.M., "Gas-liquid mixing studies on hydrofoil impellers", 1991, *Ph.D. Thesis,* Univesity of Birmingham, U.K.
4. Bongenaar, J.J.T.M., Kossen, N.W.F., Metz, B., and Meijboom, F.W., 1973, "A method for characterising the rheological properties of viscous fermentation broths", *Biotech.Bioeng.*, 15: 201-206
5. Reuss, M., Debus, D. and Zoll, G., 1982, "Rheological properties of fermentation fluids", *Chem.Eng.*, 6: 233-236
6. Tucker, K.G. and Thomas, C.R., "Effect of biomass concentration and morphology on the rheological parameters of *Penicillium chrysogenum* fermentation broth", *Trans.I.Chem.E.*, 17, C: 111-117
7. Allen, D.G. and Robinson, C.W., 1990, "Measurement of rheological properties of filamentous fermentation broths", *Chem.Eng.Sci.*, 45, No.1: 37-48
8. Roels, J.A., van der Berg, J. and Voncken, R.M., 1974, "The rheology of mycelial broths", *Biotech.Bioeng.*, 16: 181-208

CHAPTER 4

POWER DRAW

4.1 Introduction

An important factor to be considered when assessing the performance of a bioreactor is the total power drawn by any agitators. Power costs have a direct impact on the operating costs of a fermentation process and therefore on its economic viability. Important operating characteristics such as mass transfer and mixing time can be related to the power input. In addition to providing a basis for the comparison of different agitator types and configurations, the specific power input (P/V) is a common scale up criteria for mixer, motor, drive and shaft specification for industrial size vessels.

The power characteristics of differing impellers are often coupled to local or bulk hydrodynamics and flow regimes achieved under gassed and ungassed conditions. Power characteristics and hydrodynamic behaviour of various radial and axial flow impellers have been previously reviewed[1, 2] and are addressed in the following sections.

4.1.1 Rushton Turbine (RT)

4.1.1.1 Unaerated hydrodynamic and power characteristics

The six bladed Rushton disc turbine (6RT) produces a radial flow pattern as shown in Figure 4.1-1. At the impeller tip the radial and tangential velocities are approximately equal[3], but with increasing distance from the impeller, the tangential velocities decrease more rapidly than the radial velocities[4]. Circulation loops are created by secondary axial flows produced from the interaction between the discharge fluid and the vessel walls, base and baffles.

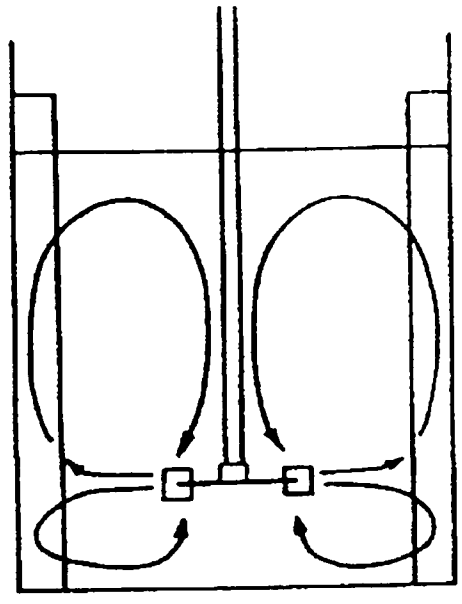

Figure 4.1-1 Radial flow pattern produced by the Rushton turbine[17]

Rushton *et al*[5]. and Bates *et al.*[6] showed, that for geometrically similar systems,

$$Po = f(\mathrm{Re}) \tag{4.1}$$

In the laminar regime (Re<10) *Po* was related by

$$Po = a\,\mathrm{Re}^{-1} \tag{4.2}$$

where a is constant and dependent on system geometry. In the turbulent regime ($\mathrm{Re} \geq 2\times10^4$)

$$Po = B \tag{4.3}$$

where B is constant, independent of *Re* but dependent on impeller type. In the transitional regime ($10 < \mathrm{Re} < 10^4$) *Po* varies non-linearly with *Re* making mathematical correlations difficult. However, using more accurate power measurements, it was shown that, in the turbulent regime, *Po* increased to a maximum and then dropped[7]. At higher impeller speeds, the decline in *Po* was rapid due to surface aeration. It was also noted that *Po* is dependent on scale and impeller dimensions, and can be accurately predicted from[8]

$$Po = 2.5\left(\frac{x_1}{D}\right)^{-0.2}\left(\frac{T}{T_o}\right)^{0.065} \tag{4.4}$$

where x_1 is the disc thickness and T_O is a reference diameter equal to 1 m.

4.1.1.2 Aerated hydrodynamics and power characteristics

The factors affecting the aerated power drawn by a Rushton turbine are extremely complex and can be explained in terms of bulk flow phenomena and the structure of the gas-filled cavities formed behind the impeller blade.

The course of bubble breakage has been studied in great detail for Rushton turbines using a de-rotational prism technique [9,10]. Under aerated conditions, gas is drawn into the low pressure vortices at the back of the impeller blades, forming gas-filled cavities. The type and size of the cavities is dependent on impeller speed and gas flow rate (Figure 4.1-2). At a constant impeller speed with an increasing gas flow rate the initial rapid drop in power draw is due to the formation of large clinging cavities behind the blades[11] (Figure 4.1-2). A further increase in gas flow rate leads to the production of "3-3" cavities and consequently a fall in power. At gas flow rates too high for the agitation conditions, ragged cavities form, the gas dominates the bulk flow, and the impeller becomes flooded (Figure 4.1-2). The flooding point coincides with a characteristic step-change in the power drawn by the impeller (Figure 4.1-4).

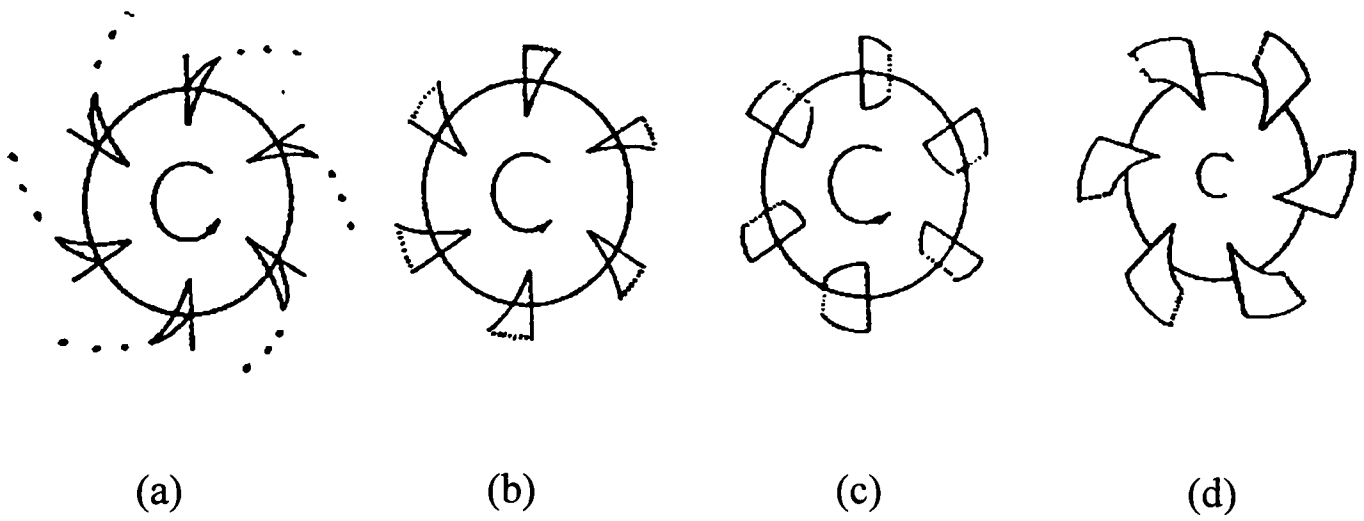

Figure 4.1-2 RT Gas filled cavities with increasing gas flow rate and constant impeller speed: (a) Vortex cavities (b) Clinging cavities (c) "3-3" structure (d) Ragged cavities[12]

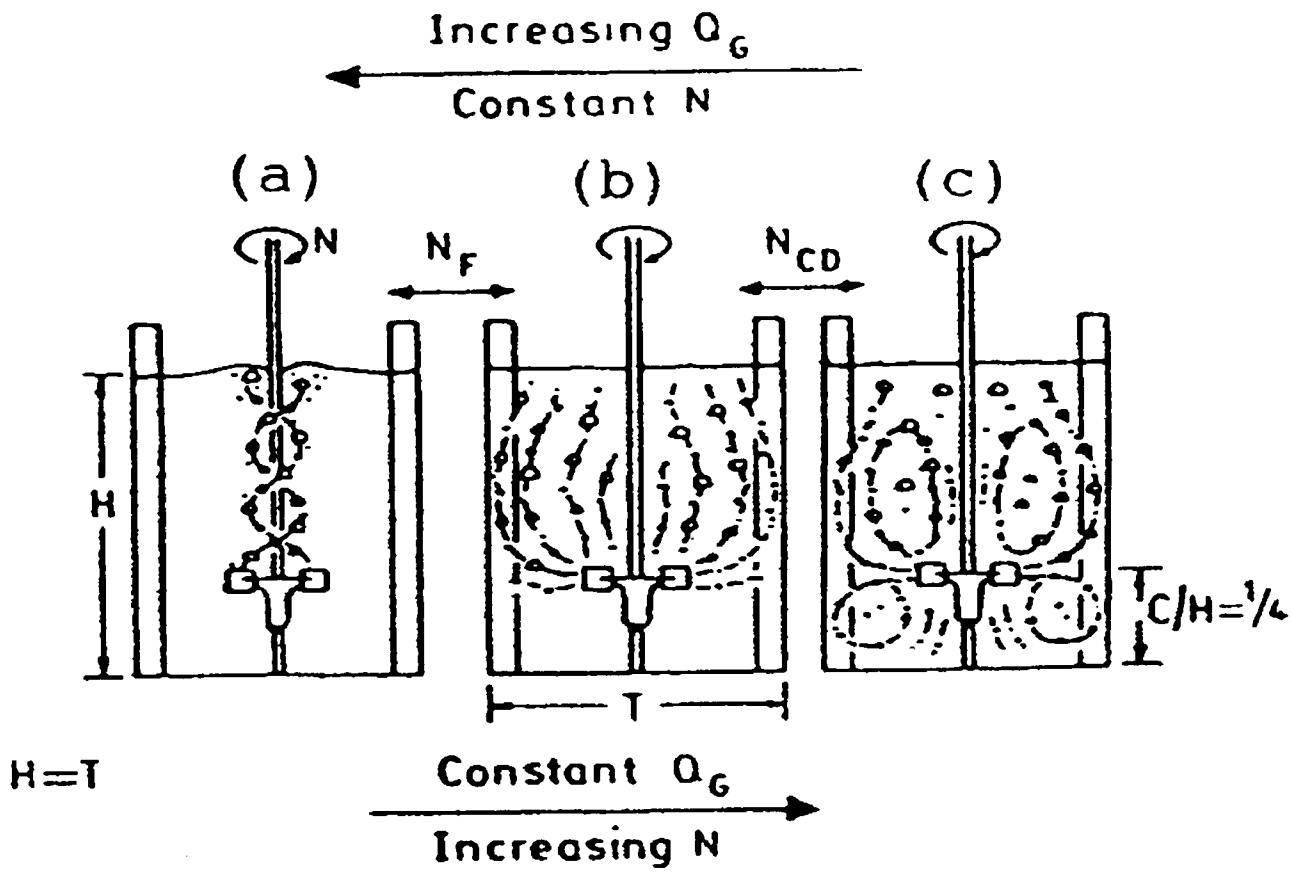

Figure 4.1-3 Aerated bulk flow pattern with constant gas flow rate and increasing RT speed[12]

Alternatively the situation can be described in terms of constant gas flow rate and increasing impeller speed. At low impeller speeds, the impeller is flooded and the gas is poorly dispersed (Figure 4.1-3). Increasing the impeller speed results in a change in cavity structure and the impeller becomes loaded, with the upper part of the vessel acting like a bubble column (Figure 4.1-3). A further increase in speed, produces a complete dispersion of gas in the lower part of the vessel. At higher speeds the gas is recirculated back into the impeller region due to the action of the secondary loops.

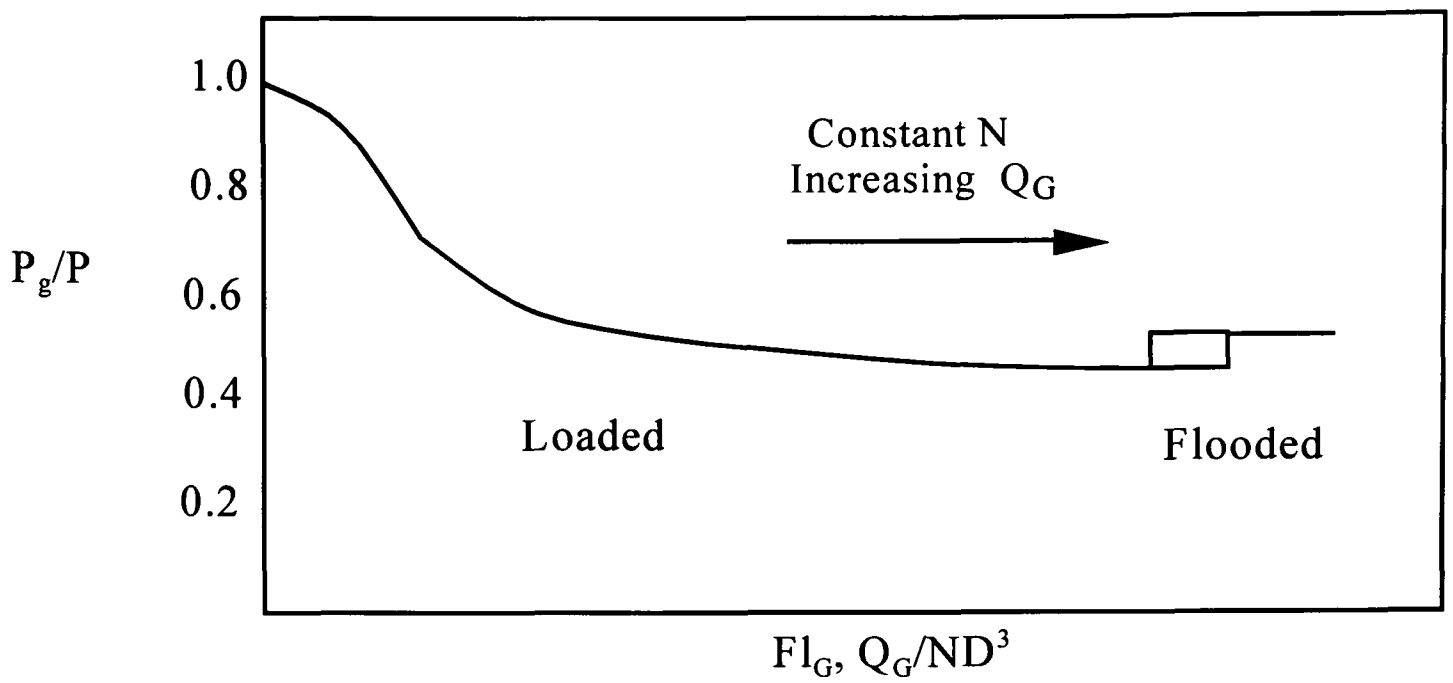

Figure 4.1-4 Example of a gassed power curve as a function of gas flow number (constant N, increasing Q_G)

For low viscosity broths, it was reported that the minimum speed required to prevent flooding (N_F) could be calculated from [2,13]

$$\left(Fl_G\right)_F = 30\left(\frac{D}{T}\right)^{3.5}\left(Fr\right)_F \qquad (4.5)$$

and for D/T = 0.33,

$$\left(Fl_G\right)_F = 0.48\left(Fr\right)_F \qquad (4.6)$$

However, the minimum speed required for complete dispersion (N_{CD}) is considered a better criteria for design purposes as it describes the speed at which the whole volume of the tank contains gas and is therefore performing optimally. Incidentally, this corresponded to a minimum point on the power curve versus *Re* or *Fr* plot[7]. In addition to the complete dispersion minima, Abradi *et al.*[14] and Sharma *et al.*[15] report a second minimum at the flooding point.

Nienow[2] proposed calculating N_{CD} from:

$$\left(Fl_G\right)_{CD} = 0.2\left(\frac{D}{T}\right)^{0.5}\left(Fr\right)_{CD}^{0.5} \qquad (4.7)$$

Bakker *et al.*[13] suggested that a minimum Froude number of 0.045 should be exceeded to ensure cavity retention and effective gas distribution. Combining this with equations (4.5) and (4.7) allowed a flow map to be created [13,14]. Flow regime maps are useful tools for design and scale-up of mixing equipment.

4.1.2 Axial Flow Impellers

4.1.2.1 Unaerated hydrodynamics and power characteristics

Although Rushton turbine impellers provide good gas dispersion in gas-liquid processes they are not noted for their blending efficiency in multiple impeller systems. Consequently, axial flow impellers have been traditionally employed for single phase bulk blending. Axial flow impellers, such as the propellor, pitched blade turbine and hydrofoil produce a predominantly axial flow which promotes good top-to-bottom mixing (Figure 4.1-5). (The pitched blade turbine is sometimes termed a mixed flow impeller as it exhibits a degree of radial flow in addition to the axial flow). Swirling due to tangential flow is stopped by the action of the baffles.

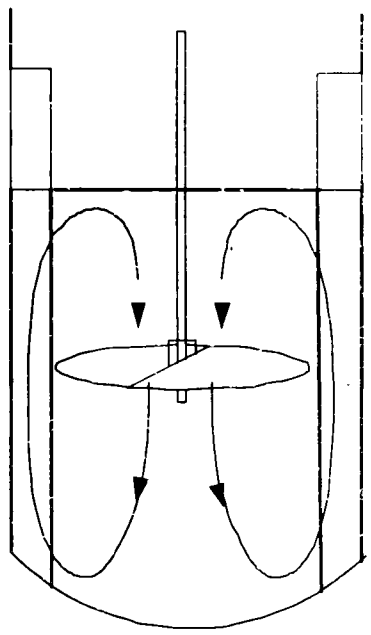

Figure 4.1-5 Unaerated flow pattern of an axial flow impeller

Although propellors provide efficient single phase blending their gas handling capability is very low and they tend to flood easily. For this reason, hydrofoil impellers were developed to provide efficient blending and gas dispersion. Hydrofoils work on the basis of aircraft wing

technology. An upward hydrodynamic thrust on the blades produces a downward flow of liquid. To provide good gas handling ability, the fraction of the swept area occupied by the blades (solidity ratio) should be high. The design also minimises drag on rotation and hence power requirements and power numbers are very much lower. Power numbers in the range of 0.4 to 1.4 have been reported (*c.f.* 5 to 6 for the RT).

The hydrofoil impellers most frequently studied include the Prochem Maxflo T and the Lightin' A315. Similarities between their flow behaviour and that of the PBT have been reported. Very little data has been published on the performance of the SCABA 3SHP1 impeller. The unaerated power numbers for the Maxflow T[16,17], A315[17] and PBT[6,18] were found to be constant in the turbulent and transitional regimes until low *Re* numbers were encountered and a slight increase in *Po* was observed. On the large scale (14 m^3), Nienow *et al.*[19] reported constant *Po* values for Maxflow T's and A315's for *Re* values down to 2000. Similarly, *Po* for the 3SHP1 was reported to be constant in both the regimes[20]. All researchers reported a drop in *Po*, with increasing *Re*, following the onset of surface aeration. As with the Rushton turbine the *Po* for the hydrofoils was found to be dependent on scale[17].

4.1.2.2 Aerated hydrodynamic and power characteristics

On aeration, as with the RT, the complex interaction between bulk flow phenomena and structure of the gas filled cavities determines the gas dispersion characteristics. Once again similarities occur between the gas-liquid flow regimes of hydrofoils and PBTs, although the terminology is often different. For hydrofoils, McFarlane[17] distinguished four cavity shapes and related their type and size to the bulk flow and power characteristics (Figure 4.1-6 and Figure 4.1-7).

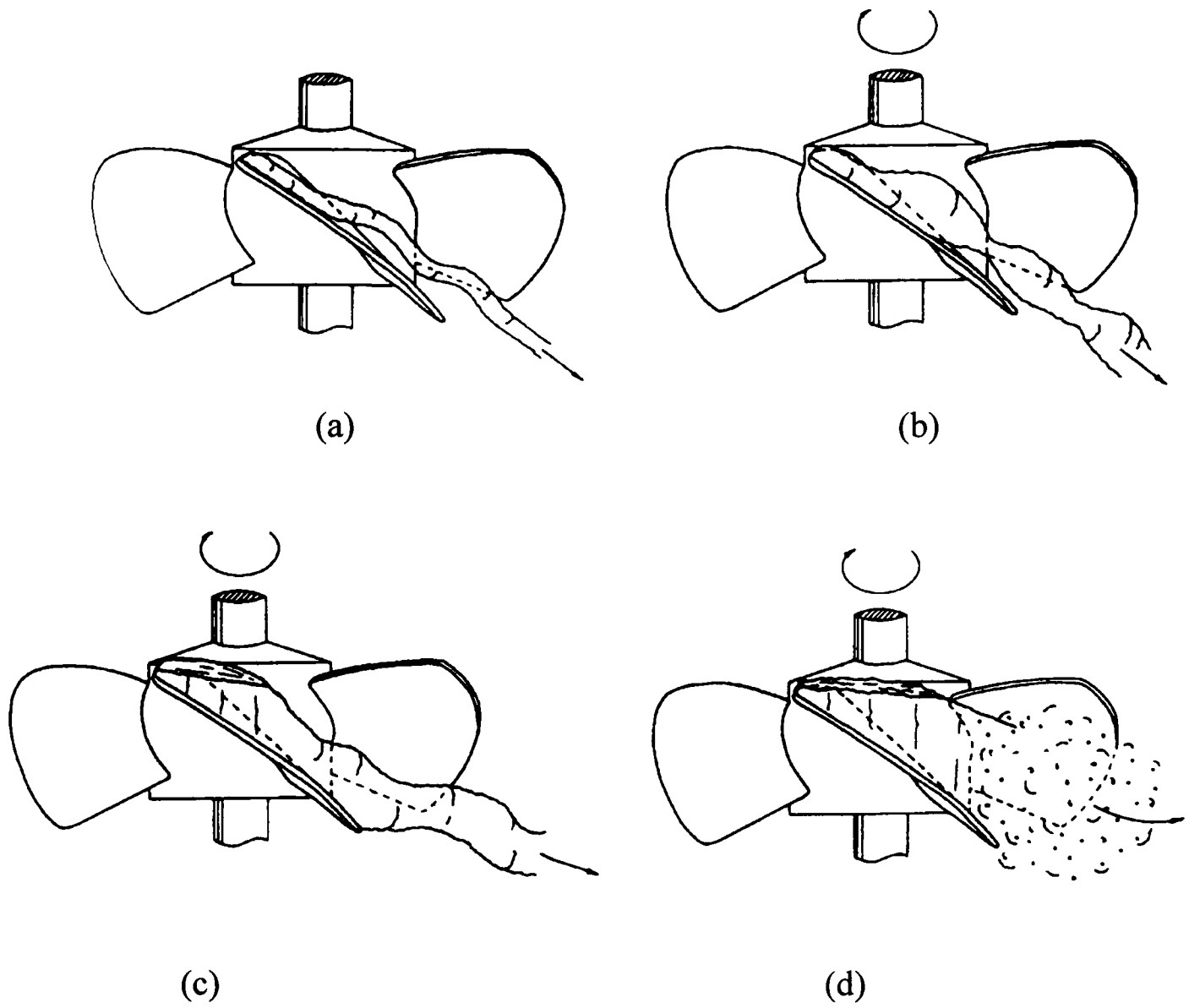

Figure 4.1-6 Gas filled cavities formed behind the blades of an axial flow impeller (Prochem); (a) vortex cavity (b) clinging cavity (c) incipient large cavity (d) large, fully developed cavity[17]

With increasing gas flow rate (or decreasing impeller speed) cavities behind the blades change in shape and size. Generally, the flow behaviour falls into two distinct regions:

1. Low gas rate / high impeller speeds: Axial flow regime[17]

The axial flow regime has also been termed the completely dispersed[1] or indirectly loaded[16,21] regime. Here, the downward force of the liquid is greater than the buoyancy force of the bubbles and the gas is displaced before reaching the impeller. The gas then enters the impeller from above after being circulated throughout the vessel. A small drop in power, dependent on the impeller speed and gas flow rate, is observed. Small clinging or vortex cavities are present.

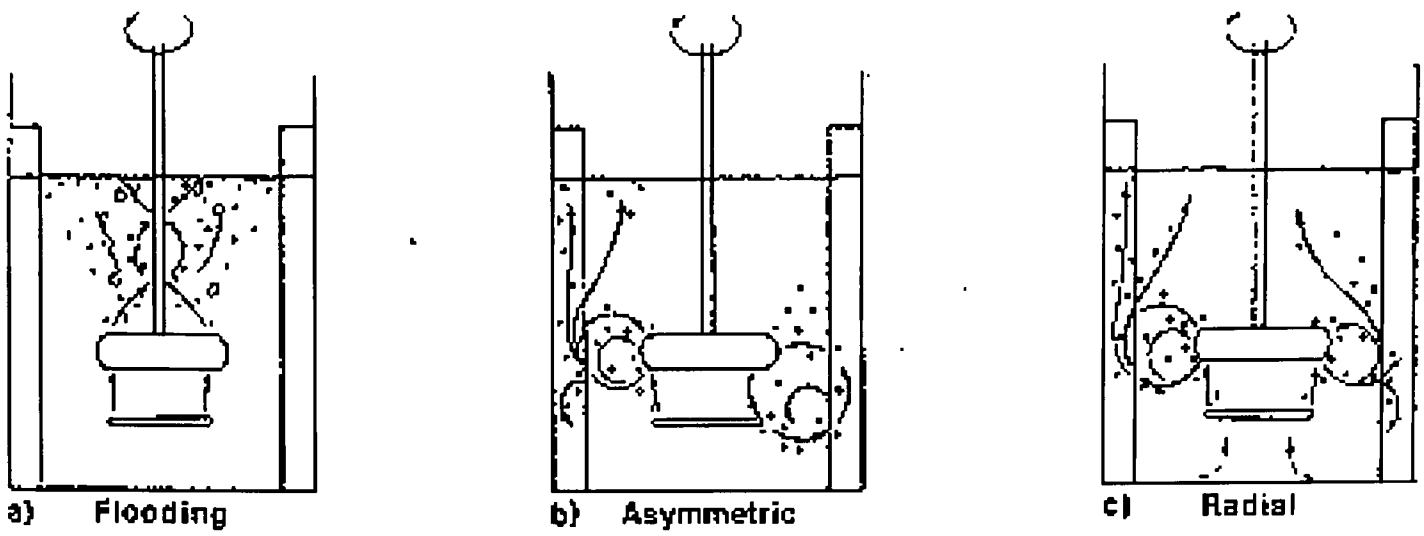

Figure 4.1-7 Aerated flow pattern for the Prochem Maxflow T[17]

2. High gas flow rate / low impeller speeds: Radial flow regime[17]

In the radial flow regime, also termed incomplete dispersion[1] or directly loaded regime[16,21], the buoyancy forces of the rising bubbles is greater than the downward flow of the liquid. Consequently, the gas enters the impeller region creating large, fully developed cavities behind the blades resulting in a dramatic drop in the power drawn. In addition, the pumping capacity of the impeller is lost and it enters a radial flow regime.

The transition from the axial to the radial regime has been termed the competitive region since the rising gas competes with the downward liquid flow[17]. This causes significant bulk flow instabilities and large power fluctuations [1,16,17,18,19,22,23] resulting in greater mechanical loads and possibly vessel vibration. Careful design of the fermenter, pipework and supporting structures should ensure that these vibrations do not cause an operating problem[19,22]. McFarlane has suggested, for the Prochem Maxflo T, calculating the minimum speed required for complete dispersion and safe operating conditions from the empirical equation

$$\left(Fl_G\right)_{CD} = 0.087\left(Fr\right)_{CD}^{1.26} \tag{4.8}$$

The author stresses that the equation is only valid for the operating conditions and geometry tested. A similar equation, based on a momentum balance over the impeller, was proposed by Chapman *et al.*[1] for PBTs:

$$N_C = 11.7\frac{Q_G^{0.5}}{D^{1.63}} \tag{4.9}$$

where N_c is the impeller speed at which the flow instabilities occur.

On aeration, the drop in power is much lower for hydrofoils compared to Rushton turbines. This suggests a greater amount of power is available for mass transfer and consequently the possibility for improved bioreactor performance is evident [19].

4.1.3 Gas dispersion and power draw in viscous fluids

In a number of industrial processes, such as xanthan gum production and mycelial fermentations, it is necessary to disperse the gas in very viscous and rheologically complex liquids.

On aerating high viscosity fluids a large, stable cavity will form behind each impeller blade[2]. The size and shape of the cavity is independent of gas flow rate. Increasing the gas flow rate will however increase the size and rate of bubble release from the cavities. The bubble distribution tends to be bimodal with a large quantity of very small bubbles and a few large bubbles. The small bubbles follow the motion of the liquid, whereas the large bubbles travel rapidly through the fluid to the surface[2,24].

Nienow *et al.* [24] studied gas dispersion using Rushton turbines in water, Newtonian and non-Newtonian solutions for Reynolds numbers ranging from 1 to 5×10^5. Three Reynolds regions were reported. At $Re > 900$ the gassed behaviour was very similar to that of water, except a higher impeller speed was required to disperse the gas. At $10 < Re < 900$, the drop in power was greater than with water and was insensitive to gas flow rate. In the laminar regime, the gassed power was equal to the ungassed power. The 6RT was unable to disperse the gas at $Re < 50$. Similarly, with a non-Newtonian fermentation broth of *Amycolatopsis mediterranei*, Velasco *et al.*[25] reported an independence of gassing rate on the power drawn by dual RTs and by a RT-PBT configuration for $Re < 1000$. In addition, as the fermentation progressed, the ratio of gassed to ungassed power became lower due to the increased viscosity and the

presence of a yield stress[25]. Such a phenomena was experienced with a RT and curved blade impellers (Chemineer CD-6) in increasingly viscous aerated Newtonian liquids[26]. In xanthan solutions, at Re values ~ 2000, the aerated power characteristics for multiple hydrofoils were very similar to those encountered in water[19]

Bujalski *et al.*[27] reported that the power characteristics for independently driven dual-impellers, with no draft tube (IDDINT), in water were almost identical to those in 1% CMC, although it was noted that the gassed power for the RT and the 3SHP1 was virtually independent of gassing rate. However, the *Re* range was not stated. Suprisingly, it was discovered that, in general, the drop in power on aeration was lower for viscous non-Newtonian *Aspergillus niger* broths than for water and decreased with increasing biomass concentration (and viscosity) when using both dual RTs and dual axial impellers[27].

4.1.4 Multiple impeller systems

More efficient design of gas-liquid contactors / fermenters has lead to the use of high aspect ratio reactors (H/T > 1) stirred by multiple impellers. However, literature on the design criteria is scarce due to the complexity arising from mixed flow impeller systems, *i.e.* radial-axial impeller combinations.

4.1.4.1 Unaerated conditions

For low viscosity broths an impeller spacing of one vessel diameter is recommended[2,28]. However, in shear thinning viscous broths, where cavern formation is likely, the impeller separation should be such that the caverns will meet at the impeller speed at which they also reach the wall[2]. Here, the power drawn by multiple impellers is the sum of the power drawn by the single impellers, and for *n* similar impellers on a single shaft[2,22,28]

$$(Po)_n = n(Po) \qquad (4.10)$$

Generally, for an independently-driven, dual-impeller system (impeller spacing T), there is no influence of either impeller on the ungassed power numbers. However, at high RT speeds (lower impeller) and low 3SHP1 speeds (upper impeller) the *Po* of the 3SHP1 was increased due to the interaction of the upper loop of the RT and the predominantly axial flow of the 3SHP1[29]. Interaction between impellers in dual RT configurations was shown to slightly decrease the power numbers compared to single impeller systems[25].

4.1.4.2 Aerated conditions

In multiple impeller systems it is reported that the lower impeller will act as a single impeller on its own and, even if the lower impeller is flooded, any upper impellers operate as if in fully dispersed conditions [2,13,22,28]. However, Abradi *et al.*[14] defined two regimes, termed ineffective and effective dispersion, for the upper impeller in RT-RT and RT-axial configurations. It was also reported that the action of the upper impeller tended to lower the speed required to completely disperse the gas[14]. In addition, provided $N > N_F$ the gassed power number was found to be a function of gas flow rate only.

At critical conditions, gross instabilities were discovered for an independently driven, dual-impeller system[27,29] (Appendix VII). Instabilities reported for single hydrofoils[17] were not always substantiated in large scale multi-impeller systems, probably due to the complex interactions between the impellers[22]. However, vibrations experienced in high viscosity systems were very much greater than in water[19].

4.2 Experimental techniques

The power drawn by an impeller is an important factor when considering the performance of a bioreactor. In order to be able to compare the experimental data obtained with that already known, characteristic plots of Power number (Po), gassed power number (Po_g) and the ratio of

gassed to ungassed power number (Po_g/Po) against variables such as gas flow rate (Q_G), impeller speed (N), flow number (Q_G/ND^3) and Reynolds number ($\rho ND^2/\mu$) must be obtained. The methods used to measure air flow rate, impeller speed and power draw have been described earlier (Chapter 3). Test fluids included water, 0.28 % CMC, 1.0 % CMC and *Aspergillus niger* fermentation broths.

4.2.1 Single impeller system

The following experiments were undertaken for each impeller acting singularly at H=2T:

Constant gas flow rate increasing impeller speeds: for an ungassed system, impeller speed was varied stepwise throughout the whole range possible. For each impeller speed, torque and hold up were measured and notes made on any flow characteristics observed. Points of particular interest included:

(i) Bulk flow patterns, *i.e.* the direction of flow through the annulus or draft tube, the amount of recirculation and any dead zones or stagnant regions,

(ii)For ungassed systems, the point of surface aeration and its subsequent effect on the power drawn by the impeller,

(iii)For gassed systems, the impeller speeds at which flooding, loading and complete dispersion occurred were of particular importance.

These observations and measurements were then repeated for 0.25vvm , 0.5 vvm and 0.62 vvm (maximum gas flow possible).

Constant impeller speed and varied gas flow rate: the 6RTDT was tested at speeds of 120, 150, 180, 200, 240 and 320 rpm and the SCABA axial impeller at speeds of 60, 90, 120, 180 and 240 rpm. It was unreasonable to increase the speed of the SCABA axial impeller above

240 rpm because increased vibrations within the vessel may have caused the draft tube to weaken and fracture.

For each impeller speed gas flow rates of 60, 80, 105, 125, 145 165, 185, 210, 230, 250, 270, 310, 330, 350, 375 and 395 l/min were used.

Once again torque, hold-up and bulk flow characteristics were noted for each setting.

4.2.2 Dual impeller system

Constant impeller speed varied gas flow rate: after checking the characteristics of the impellers when operated singularly the next stage was to operate them simultaneously. The variables, upper impeller speed and lower impeller speed where manipulated as described in Table 4.1.4.2-1. at gas flow rates from 65 l/min to 395 l/min.

Table 4.1.4.2-1 Power and hold-up experimental conditions for IDDI

6 RT rpm	3SHP1 rpm	3SHP1 rpm	3SHP1 rpm	3SHP1 rpm
120	90	120	180	240
150	90	120	180	240
180	90	120	180	240
240	90	120	180	240

Constant gas flow rate, varied impeller speed: for gas flow rates of 0, 0.25, 0.5 and 0.62 vvm three configurations were investigated. Firstly, common configurations such as single impeller and dual impeller single shaft systems were considered. It was possible to simulate a dual impeller common shaft configuration by rotating the independent impellers at the same speed. Secondly, the impellers were operated independently (IDDI), keeping the

6RT speed constant at either 200, 300 or 400 rpm and incrementally increasing the 3SHP1 speed from 60 to 240 rpm. This enabled a comparison of hold-up values achieved for the independently driven, single shaft systems and single impeller configurations to be made at equal specific energy inputs.

The power drawn by the impellers was directly calculated using:

$$P = 2\,\rho\,N\,M \qquad (4.11)$$

The power number was found from equation (2.13). Characteristic curves of Power numbers versus other variables could now be constructed.

4.3 Results and Discussion

4.3.1 Ungassed power draw

4.3.1.1 Single 6RTDT

Figure 4.3-1 displays the unaerated power number (Po) plotted against Reynolds number (Re), giving a typical power curve for a standard 6RT impeller, with an average unaerated power number of 5.4. This was slightly higher than the experimental and calculated values of Po (4.85 and 4.95 respectively) obtained for the configuration without the draft tube (same size baffles)[30]. Since the power number from a Rushton turbine is independent of clearance for $C_R \geq T/5$ in standard vessels[6], the most probable explanation for the slight increase in power number was the close proximity of the draft tube resulting in a small restriction to the discharge flow. The point of surface aeration occurred at slightly lower impeller speeds than when no draft tube was present [20,27]. But, the drop in power occurred at an impeller speed three times greater than that required for surface aeration as without the draft tube present [20,27].

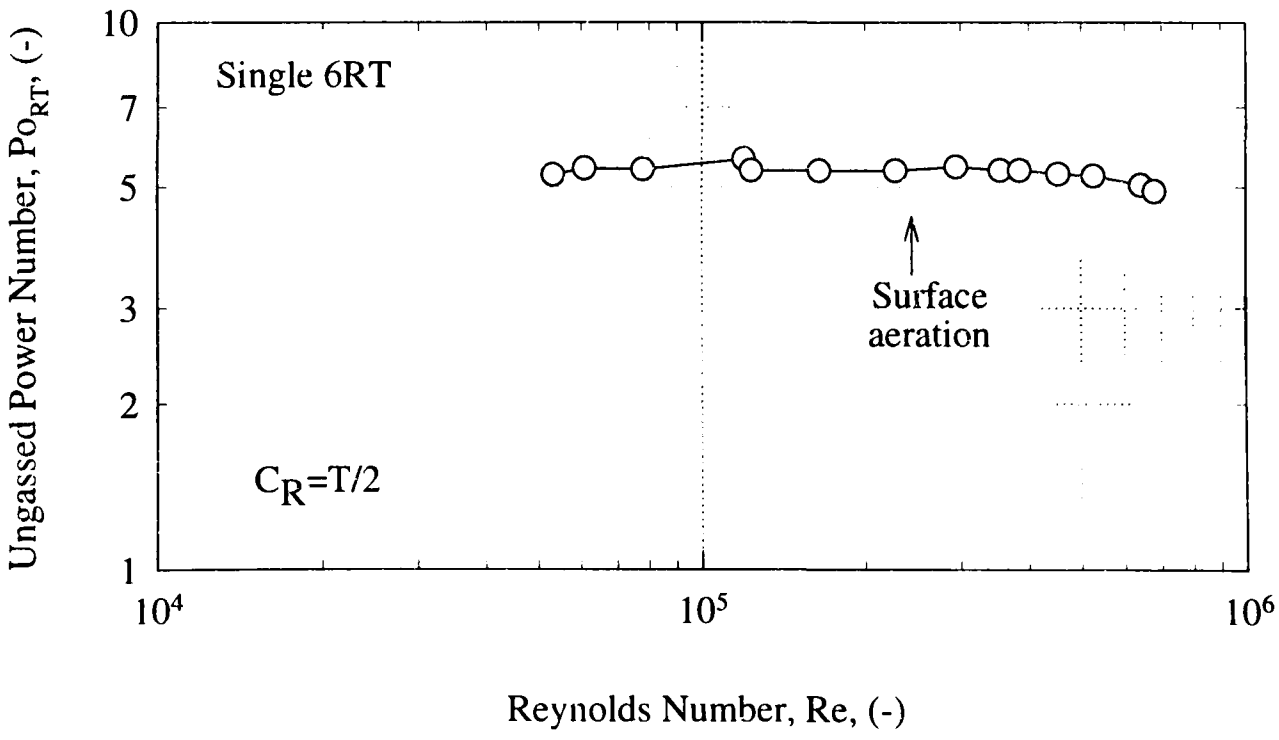

Figure 4.3-1 Ungassed power number for the 6RT (D=T/3) in water; draft tube

4.3.1.2 Single 3SHP1

Power measurements for the 3SHP1 impeller gave an unaerated power number of 0.42 (Figure 4.3-2) which is about 10% greater than the value obtained without the draft tube present (0.38)[29]. Again this increase was probably due to the close proximity of the draft tube wall to the edge of the impeller and the drag on the fluid restricting its flow as it is pumped down the draft tube. Surface aeration occurred at a relatively low impeller speed of 75 rpm but did not effect the power draw until speeds in excess of 300 rpm were reached. Since this was greater than the maximum agitator speed used (240 rpm) in most of the work (see above) the resulting trend was not studied.

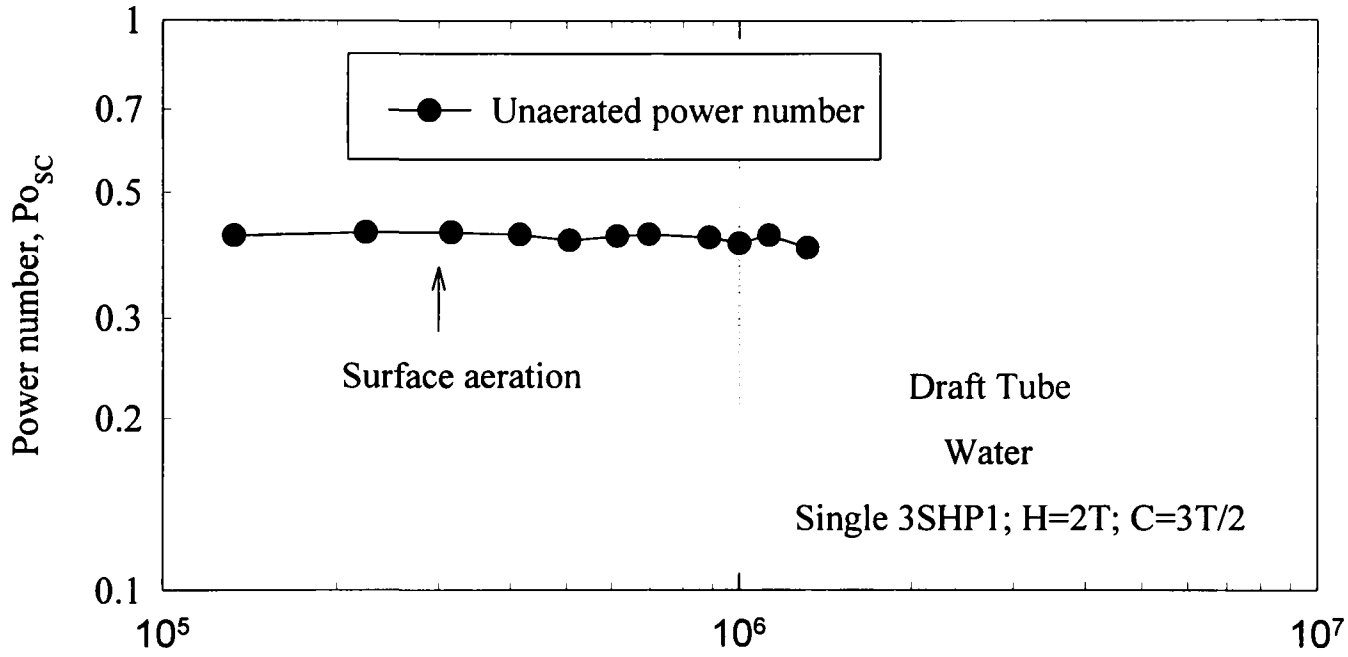

Figure 4.3-2 Ungassed power number for the single 3SHP1 in water.

4.3.1.3 Dual impellers with draft tube present

Figure 4.3-3 shows the influence of the impellers on each other when run simultaneously in the same direction. at the same speed, *i.e.* the single shaft simulation. It can be seen that the action of the upper impeller resulted in a drop in the power number, from 5.35 to 4.2, for the 6RT. This drop in power number was attributable to the absence of baffles inside the draft tube resulting a swirling motion of the downward flowing liquid. Since the swirl was in the same direction as the rotation of the 6RT, resistance to its motion was lowered and therefore

so was the power required. However when operating the 6RT in the reverse direction, no change in power number was observed, *i.e.,* it was still 5.4.

It is also clearly shown that the 6RT does not influence the power drawn by the 3SHP1 at any speeds, *i.e.*, Po_{SC}.= 0.42.

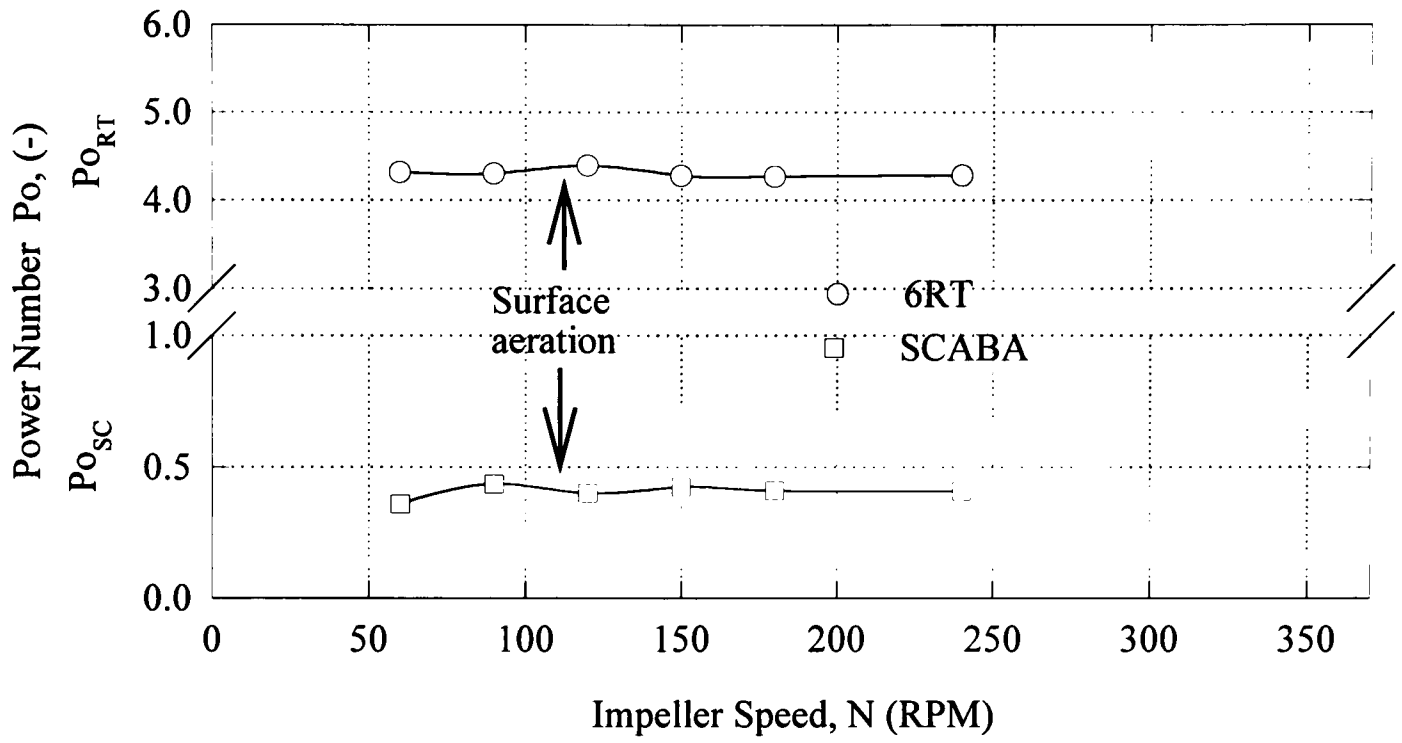

Figure 4.3-3 Ungassed power numbers for the dual impellers running at the same speed and in the same direction; draft tube

4.3.2 Gassed power draw

4.3.2.1 Single 6RT with draft tube

Figure 4.3-4 shows the power number as a function of flow number for constant impeller speeds of 150, 180, 240 and 320 rpm. As expected increasing the air flow rate resulted in a decrease of power number; the ratio of aerated to unaerated power number (Pog/Po) was reduced to 0.6 (40% reduction) for a gas flow rate of 0.5 vvm. This was due to the development of gas cavities behind the impeller blades reducing the power drawn. At an impeller speed of 150 rpm and a gas flow rate of 125 l/min ($Fl_G \sim 0.05$) the impeller became flooded and the power number decreased rapidly. This was because increasing the air flow rate increased the size of the cavities until they became too large for the agitation conditions, the air flow dominated the bulk flow pattern and the air was poorly dispersed. Reducing the air flow rate back from 125 l/min resulted in the air becoming re-dispersed at 80 l/min, but the

power number remained lower throughout the reduction, (*i.e.* for the same air flow rate, depending on the initial agitation conditions it was possible for the impeller to be either loaded or flooded with either a high or low power number) and finally returned to its original value, displaying a certain degree of hysterisis. A similar trend was observed for 180 rpm except that the impeller did not become flooded until a gas flow rate of 195 l/min ($Fl_G \sim 0.08$). It must be noted that flooding occurred at significantly lower gas flow rates than

- predicted by equation (4.5) and
- that observed for the configuration without the draft tube (Figure 4.3-13).

The most probable explanation, is that the restricting action of the draft tube hampered the formation of the upper circulation loop and hence reduced the liquid down flow into the impeller region. Therefore, it is possible that either

- the trailing vortex on the upper part of the blade did not become fully formed, or
- the rising gas bubbles did not undergo vortex capture, as the buoyancy force was greater than downward force of liquid required to trap them.

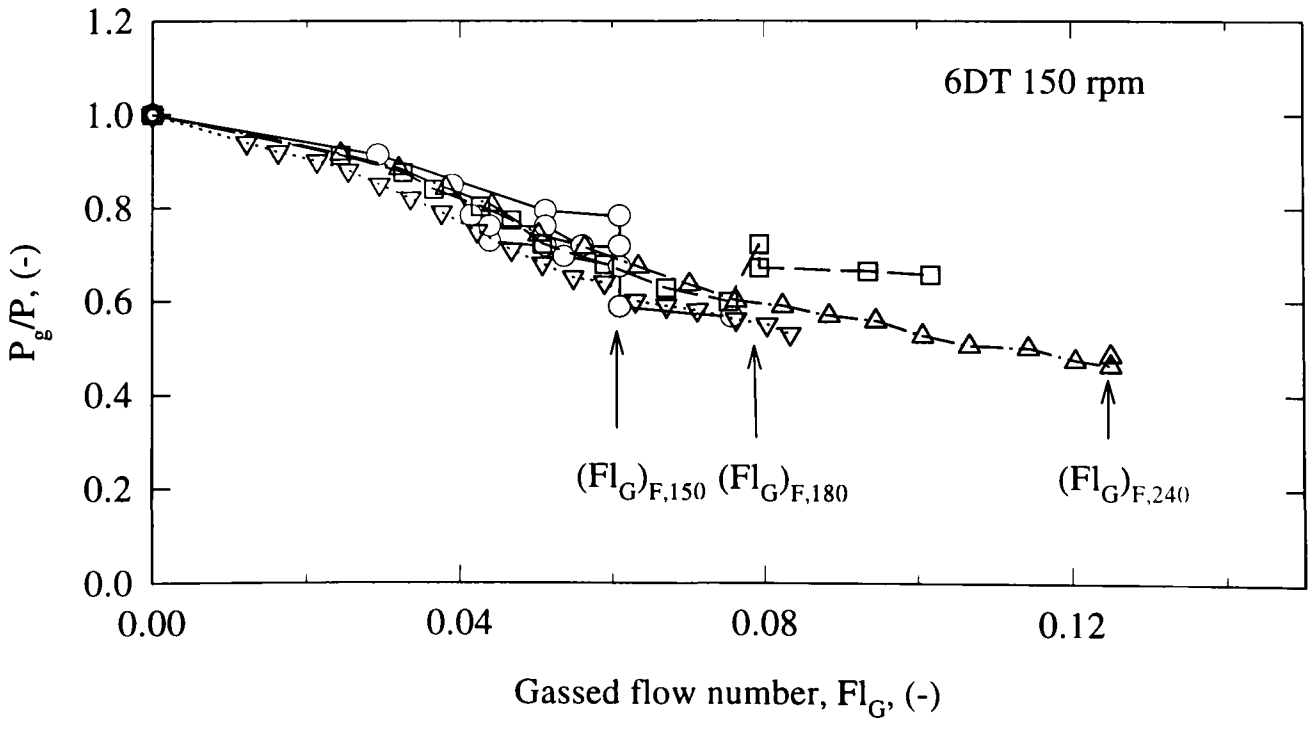

Figure 4.3-4 Gassed power drawn by a single Rushton Turbine (D=T/3) at a constant impeller speed of 150, 180, 240 and 320 rpm with an increasing gas flow rate; draft tube

For a constant gas flow rate of 0.25 vvm there is an initial drop in power is encountered upon aeration, but as the impeller speed is increased above that required for flooding the power number also increases until the power draw is slightly lower than unaerated value (Figure 4.3-5). In contrast to previous work[9], the minima in the curve occurred at the flood point as apposed to the point of complete dispersion. The two regimes, however, were very close together. Nienow *et al.*[9] suggested that the minima at complete dispersion was due to liquid flow from the top and lower half of the blades forming gas filled cavities in both positions. At impeller speeds below the minima / complete dispersion point, Nienow *et al.*[9] reported that gas cavities were formed on the upper part of the blade only. As previously explained, the inclusion of the draft tube interfered with the upper circulation loop possibly leading to a delay in the formation of the vortex on the upper part of the blade. Therefore, the flooding point and complete dispersion point (represented by gas trapped in upper and lower vortices respectively) occurred almost simultaneously. This also explains the presence of one elongated minima, for both dispersion and flooding, compared with two minima reported previously[15].

For constant gas flow rates of 0.5 and 0.62 vvm a similar trend is observed but due to the larger cavity sizes formed the initial fall in power draw is greater and the rise after complete dispersion is reduced.

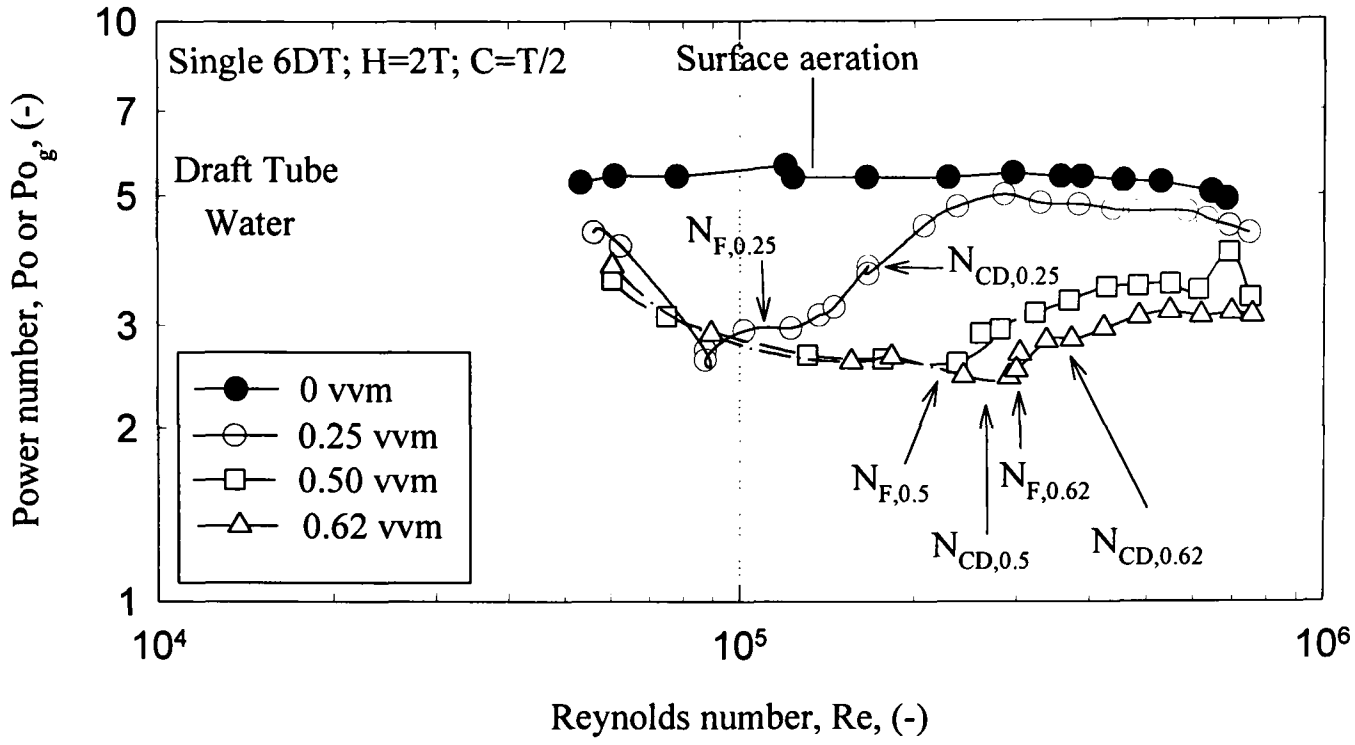

Figure 4.3-5 Gassed power drawn by a single Rushton turbine (D=T/3) for constant gas flow rates and increasing impeller speeds

4.3.2.2 Single 3SHP1 with draft tube

In agreement with Chapman *et al.*[1], for axial flow impellers pumping down, the 3SHP1 impeller gave values of $Po_g/Po>1$ at low speeds (Figure 4.3-6 ($Re < 5.5 \times 10^5$) and Figure 4.3-7). However this was because of the buoyancy force produced on the impeller blades by the bubbles rising in the draft tube and not thought to be due to small bubbles attaching to the rear face of the blade and altering the flow around the blade. This force increased the torque on the impeller and is of similar magnitude to that imposed by the impeller, so was therefore detected by the upper torque meter. As the gas flow is increased (to 0.5 and 0.62 vvm) the buoyancy force produced by the bubbles was greater, therefore the torque increased and hence did the power number. As impeller speed was increased there was a steady drop in the power number, the rate of which was greater for higher gas flow rates, until at approximately 130 rpm ($Re \sim 6x10^5$) the lines seem to converge and the reduction in power number was independent of gassing rate. At these higher impeller speeds the action of the impeller controls the bulk blending and power number is reduced due to the formation of cavities behind the blades

reducing the drag. It is also noted at the lower speeds that very little bulk flow occurs with only small amounts of gas passing below the base of the draft tube.

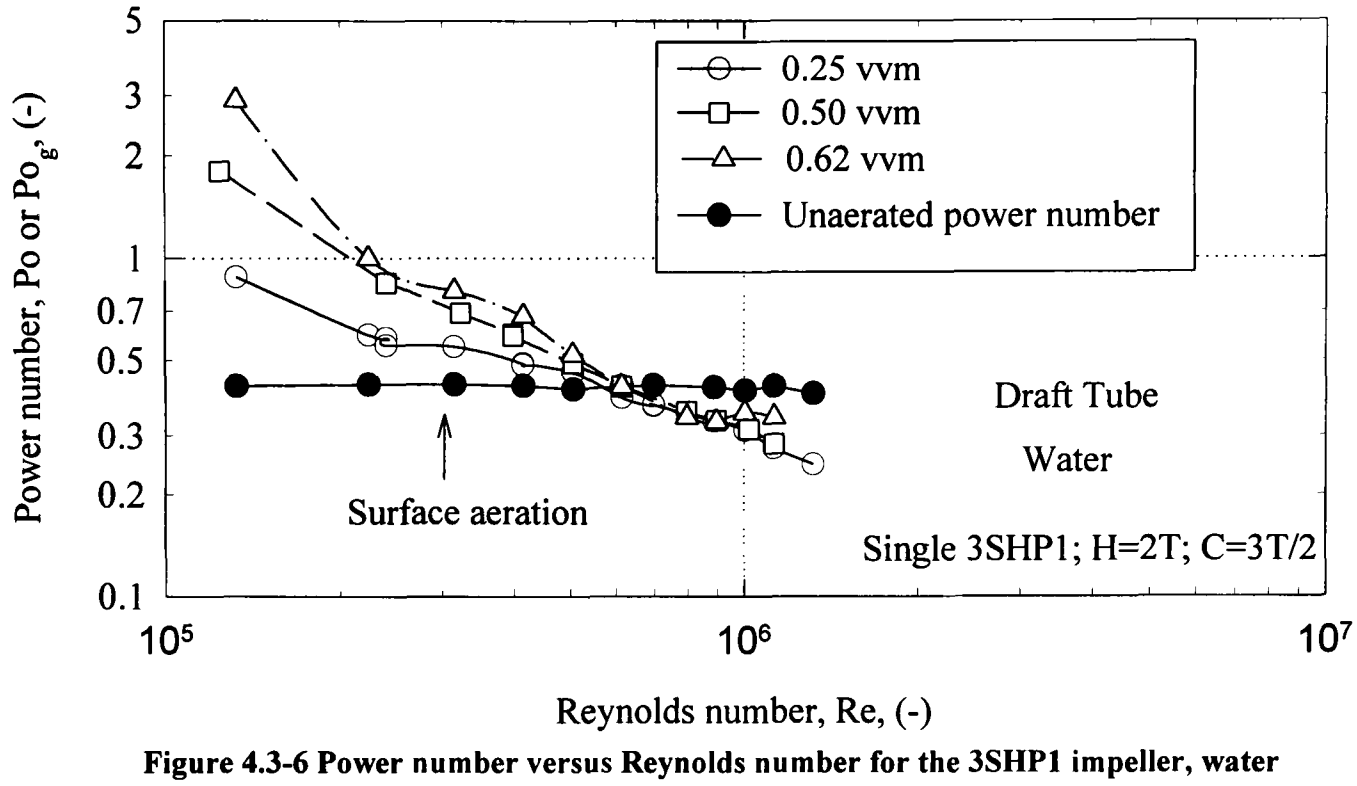

Figure 4.3-6 Power number versus Reynolds number for the 3SHP1 impeller, water

The situation was different however at higher impeller speeds (150 to 240 rpm). In this case the force produced by the impeller blades were of greater magnitude than the buoyancy force of the bubbles and the trend can be split into two distinct phases (Figure 4.3-8(i) and Figure 4.3-8(ii)):

(i) Indirect loading - at low gas flow rates the gas did not enter vortices formed by the impeller, but was forced back by the action of the fluid passing down from the blades. There is a large amount of gas passing below the draft tube and bulk flow. Any gas passing through the blades (*i.e.* downward from the upper region of the annulus) would produce small less developed cavities and there is a slight drop in power number.

(ii) Direct Loading - as the gas flow rate was increased the bubbles contacted directly with the vortices formed by the blades creating a different cavity structure. These cavities play a predominant role in the flow and lead to a decrease in the power drawn by the impeller. As the flow rate is increased further there is a gradual increase in Po_g due to the increased

buoyancy force exerted by the bubbles. At high gas flow rates the impeller was seen to flood with gas swirling out of the top of the draft tube.

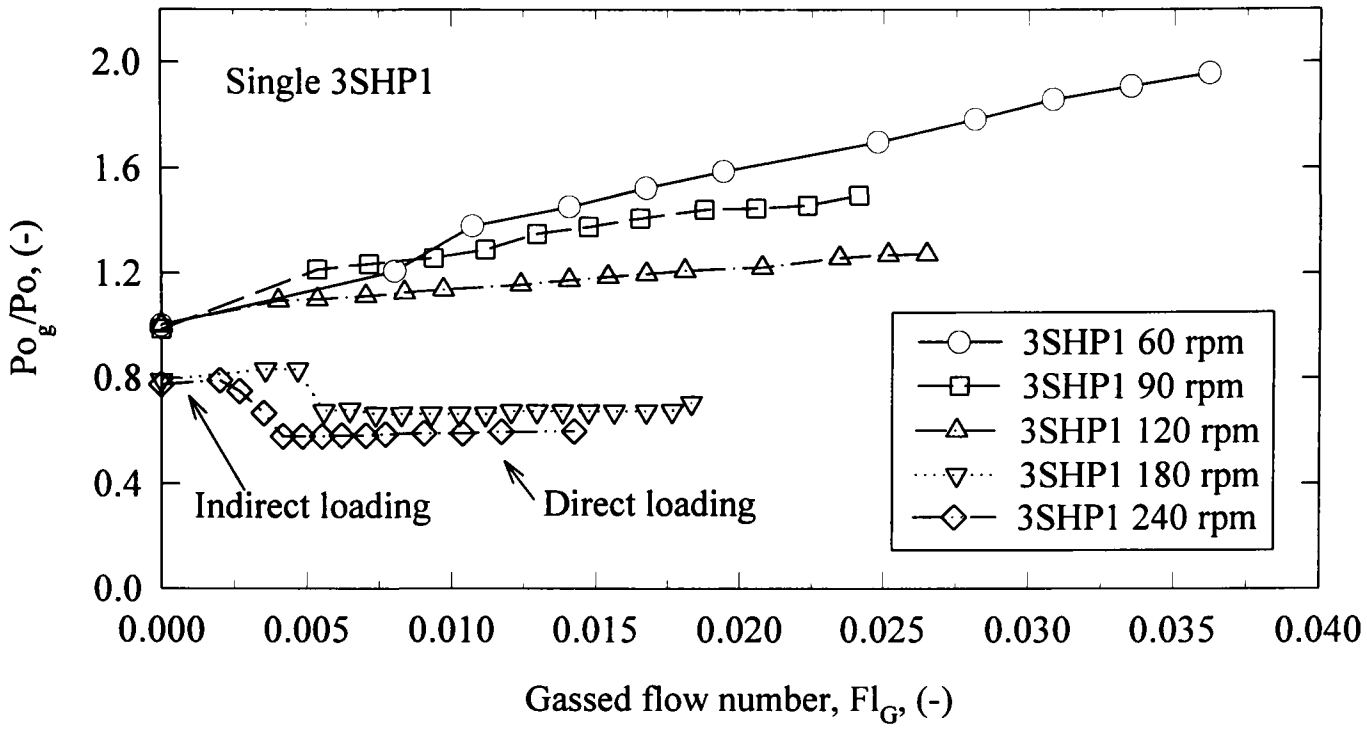

Figure 4.3-7 Ratio of gassed to ungassed power number for the 3SHP1 impeller for a constant impeller speed and increasing gas flow rate

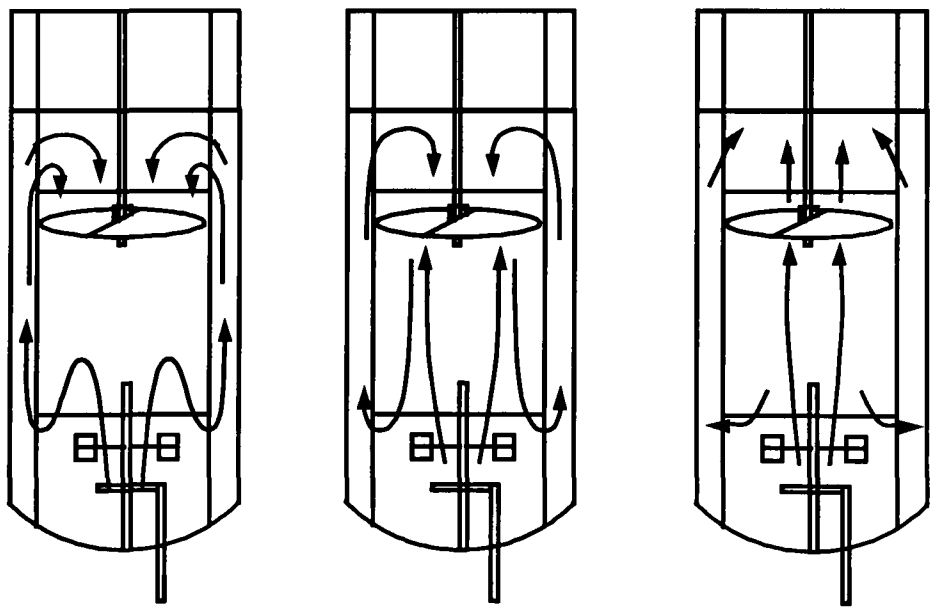

(i) Indirect Loading (ii) Direct Loading (iii) Flooding

Figure 4.3-8- Bulk flow characteristics of the SCABA Axial 3SPH1 without the 6RT running (arrows represent the direction of gas flow); Increasing N, Left to right.

4.3.2.3 Dual Impellers

Figure 4.3-9 to Figure 4.3-12 show Po_g/Po as a function of Q_G for constant 6RT speeds (120, 150, 180 and 240 rpm) and a range of 3SHP1 speeds (90, 120, 180, 240 rpm). Again, there is

little influence of the upper impeller speed on the power drawn by the 6RT impeller and the behaviour overall is much like that without a draft-tube except for certain instabilities as set out below [20,27,30].

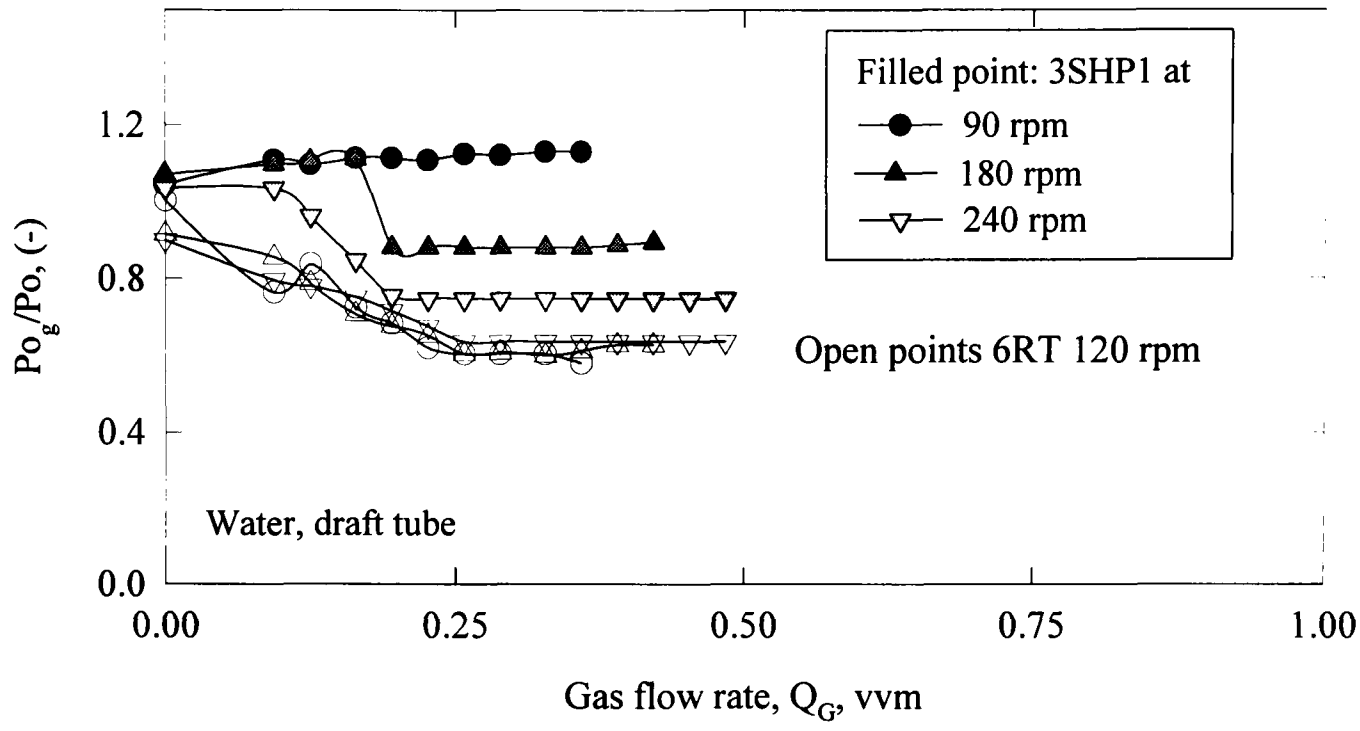

Figure 4.3-9 Po_g/Po for each impeller with the 6RT at 120 rpm and with the 3SHP1 at various speeds as a function of gas flow rate

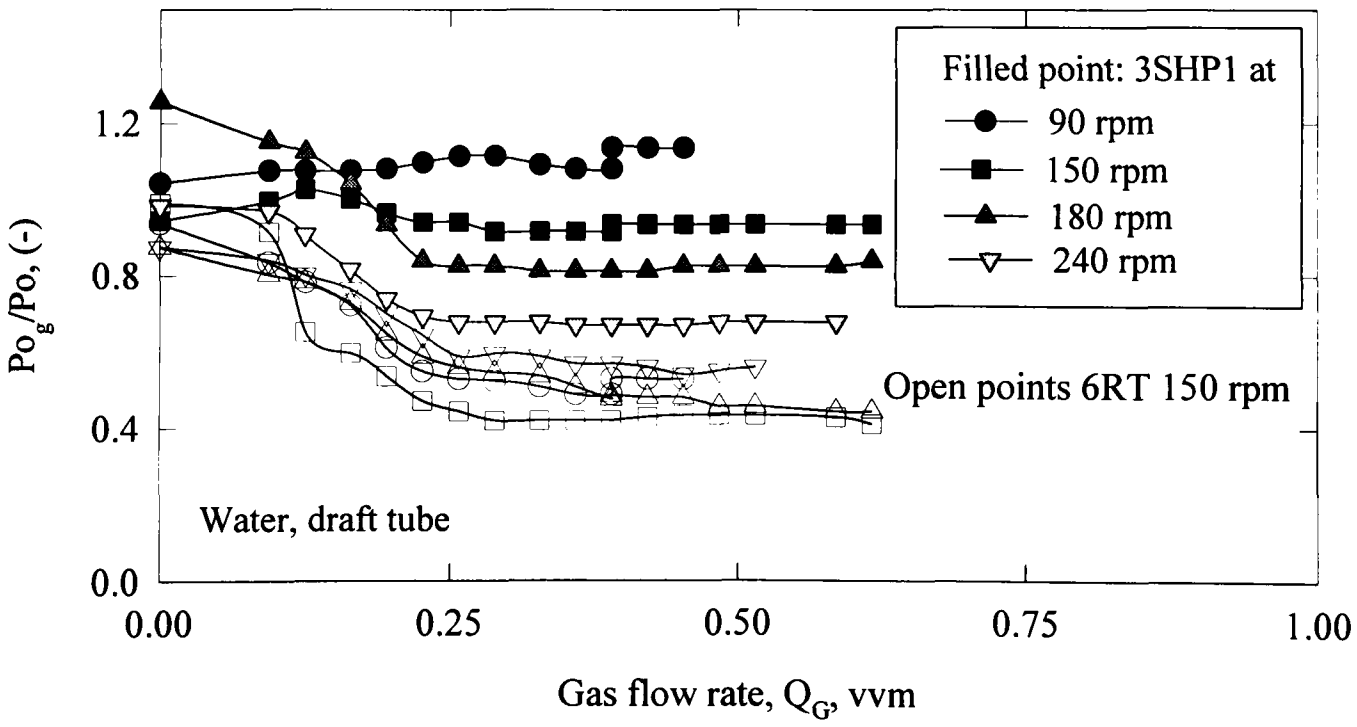

Figure 4.3-10 Po_g/Po for each impeller with the 6RT at 150 rpm and with the 3SHP1 at various speeds as a function of gas flow rate

UNIVERSITY OF BIRMINGHAM LIBRARY

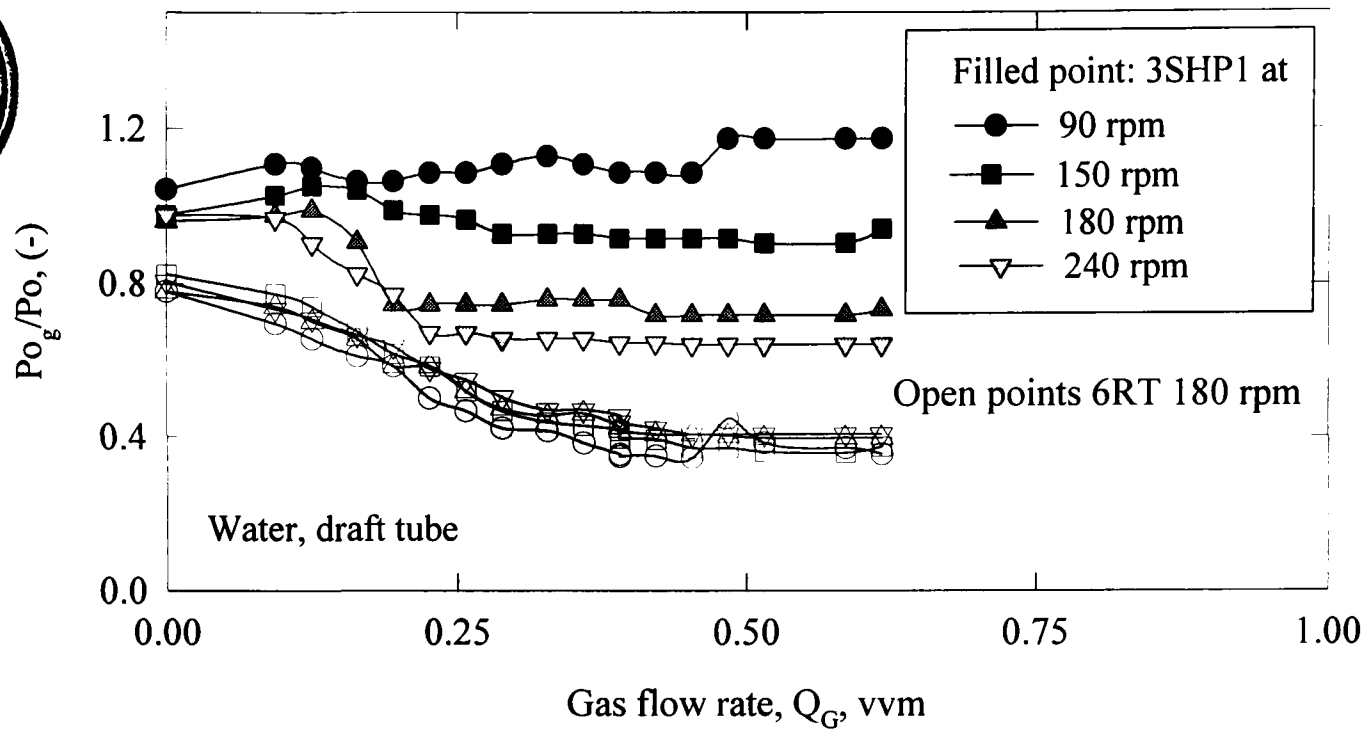

Figure 4.3-11 Po_g/Po for each impeller with the 6RT at 180 rpm and with the 3SHP1 at various speeds as a function of gas flow rate

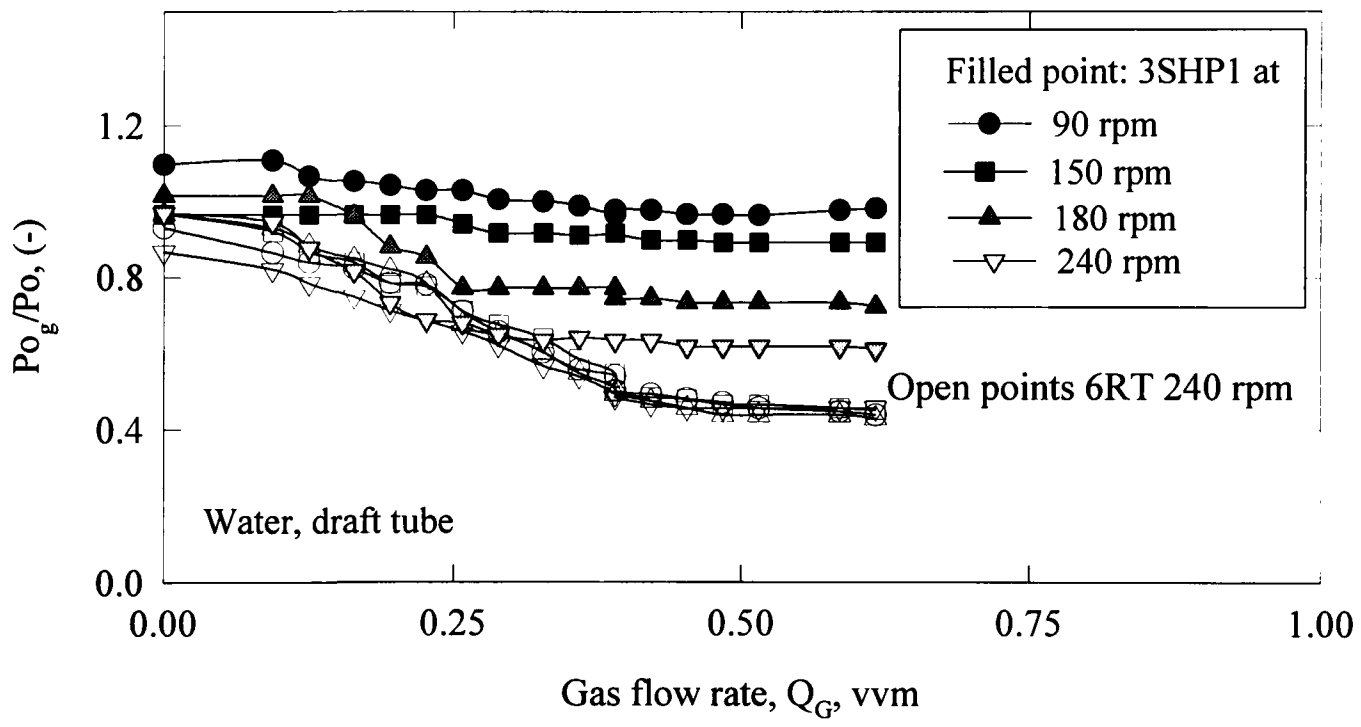

Figure 4.3-12 Po_g/P ofor each impeller with the 6RT at 240 rpm and with the 3SHP1 at various speeds as a function of gas flow rate

In general, the power drawn by the 3SHP1 again has a strong dependence on the impeller speeds. For low 3SHP1 speeds (90 & 120 rpm), Po_g/Po remained in the range 0.9 to 1.1. As described above, values above 1 were due to the torque imparted on the impeller by the buoyancy force of the rising gas-liquid plume (Section 4.3.2.2). Thus, at low 3SHP1 speeds and when the 6RT was flooded, the proto-fermenter acted in a similar manner to a bubble

column with draft tube. All the sparged gas travelled up the tube and the resulting local density difference produced bulk flow throughout the vessel, *i.e.*, liquid flows up through the tube and down through the annulus. When the 6RT became loaded, the gas was dispersed into the annulus and liquid flowed up through the annulus and down the tube. This bulk flow was further enhanced by the action of the 3SHP1 axial flow agitator. At higher 3SHP1 speeds, the fluid hydrodynamics became very complicated, with either a high or low pumping capacity for the 3SHP1 occurring under certain conditions. This situation will be discussed in the next section (System Instabilities).

It was also noticable that the gas dispersion by the 6RT was aided by the axial pumping action of the 3SHP1. At 6RT impeller speeds just lower than N_F, introducing the 3SHP1 produced a downward liquid flow and the gas was dispersed. It can be seen that the flooding-loading transition is equal to a single impeller without draft tube and can be predicted by equation (4.6). In fact, for the same 6RT speed, the gas dispersion was improved by increasing the 3SHP1 speed, *i.e.* the loading zone becomes narrower (Figure 4.3-13). It is evident therefore, that the downward liquid flow produced by the 3SHP1, or the upper circulation loop in a standard configuration, is imperative for either the creation of the upper blade vortex or the balance of the buoyancy force of the bubbles. Abradi *et al.*[14] have also reported that the influence of the upper impeller, in a dual impeller system, generally tends to decrease N_{CD}. The operating characteristics for efficient hydrodynamic design can be displayed in a flow regime map (Figure 4.3-13).

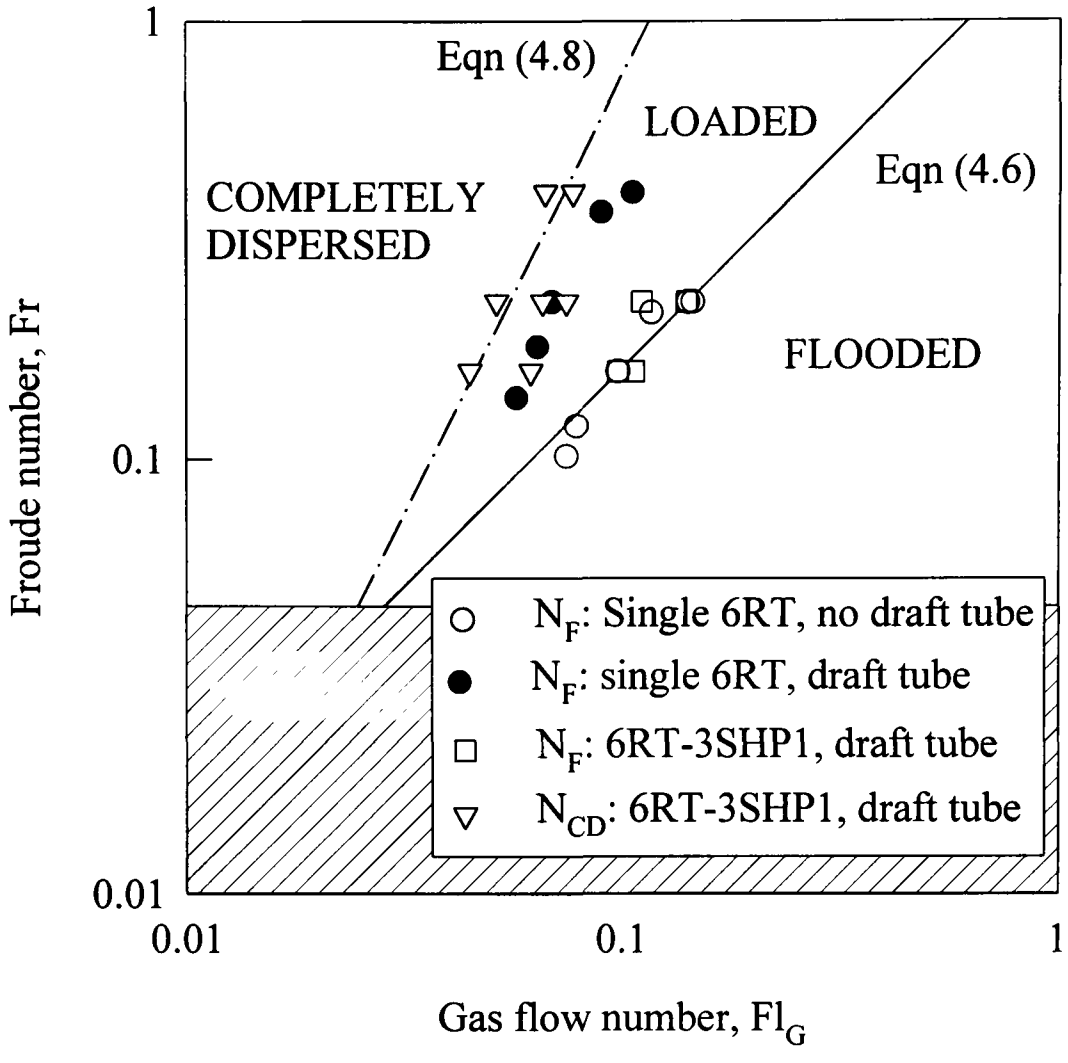

Figure 4.3-13 Flow regime map for the 6RT

4.3.2.3.1 System instabilities

Draft tube absent: Under certain circumstances, *e.g.* an impeller speed for the 6RT just above that required to prevent it flooding, $(N_F)_{RT}$, significant instabilities were noted. The situation has been described by John *et al.*[29] (Appendix VII).

Draft tube present. The inclusion of the draft tube results in a more stable configuration, although small instabilities in the power drawn by the 3SHP1 were observed in particular circumstances e.g. between gas flow rates of 0.3 to 0.4 vvm with the 6RT at 240 rpm and the 3SHP1 at 180 or 240 rpm. These instabilities are indicated in rapid changes in Po_g/Po with Q_G (Figure 4.3-9 to Figure 4.3-12). These instabilities arise as follows. If the 6RT was operating at a speed just below $(N_F)_{RT}$ and the 3SHP1 speed was increased until it was no longer flooded, the flow downward from the 3SHP1 aided the gas dispersion and the 6RT impeller became loaded (Figure 4.3-14 (a→b)). At this point, large stable cavities were

formed behind the 3SHP1 blades and the impeller was operating in what is called here the "low pumping capacity regime" (Figure 4.3-14 (b)). As the 3SHP1 speed was increased further, these cavities were reduced in size, forming smaller clinging cavities, and consequently the pumping capacity of the impeller was increased. Since there was an increased pumping capacity, more gas is drawn into the draft tube from the annulus (Figure 4.3-14 (b→c)) and the cavities once again grew in size, reducing the pumping capacity once more. The cycle continued until the 3SHP1 speed was great enough to form small stable cavities behind the blades and the impeller was then operating in the "high pumping capacity regime" (Figure 4.3-14 (c)). The situation is very similar to the competitive regime reported previously[17].

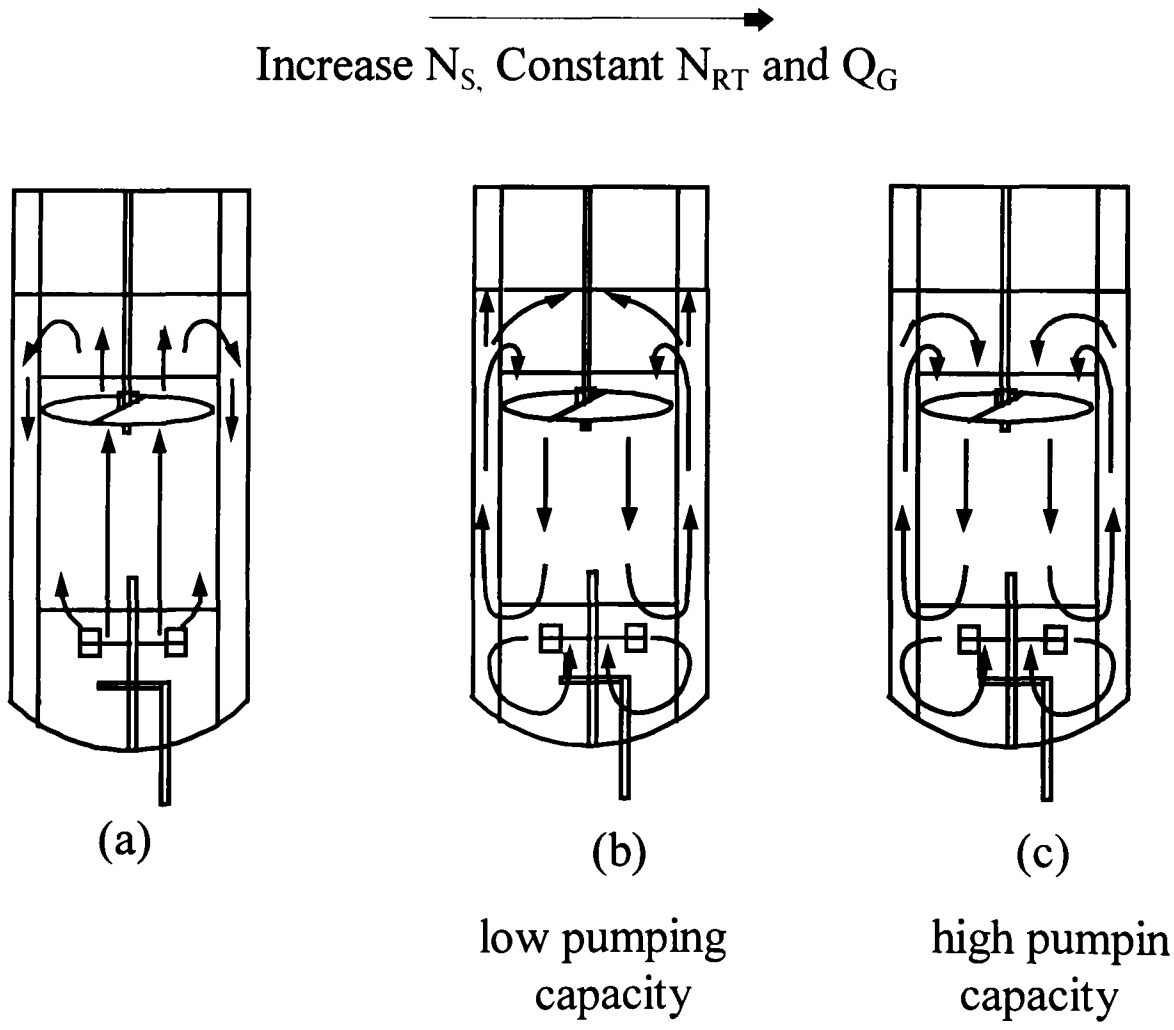

Figure 4.3-14 Flow patterns in the system with the draft tube

Figure 4.3-14 can also be related to conditions of constant 6RT and 3SHP1 speeds and an increasing air flow rate and related to the power characteristic indicated by Figure 4.3-9 to Figure 4.3-12. At low air flow rates (0.125 vvm), the majority of the gas was drawn into the draft tube and small stable cavities were present behind the 3SHP1 impeller blades when it was operating in the "high pumping capacity regime" (Figure 4.3-14 (c)). On increasing the air flow rate further (0.3 to 0.4 vvm) these cavities grew in size and the pumping capacity of the impeller is reduced so that it enters the "lower pumping capacity regime". Since there is a reduction in pumping capacity, less gas was drawn into the draft tube from the annulus, the cavities behind the blades fell in size and the impeller regained its higher pumping capacity, therefore drawing more gas from the annulus once again. This cycle continued until the air flow rate was high enough to form large stable cavities behind the blades of the 3SHP1. After that, the 3SHP1 operated stability in the "lower pumping capacity regime" (Figure 4.3-14 (b)).

The described changes in the structure of cavities were looked into during the experiment under the conditions where observation was physically possible (*i.e.* moderate impeller speeds and gas flow rates). The sequence of changes is consistent with experience with similar type impellers investigated in a single impeller rig, where direct observations of cavity structure were possible throughout the whole range of experimental conditions[17]. The “lower pumping capacity regime” and “higher pumping capacity regime” are analogous to the radial flow regime and axial flow regime respectively.

The torque fluctuations in the competitive regime were in the order of 10 to 20 % (±5-10%) compared to between 5 and 9% (±2.5 - 4.5%) when operating stably.

4.3.3 Effect of viscosity

4.3.3.1 Unaerated power numbers

Figure 4.3-15 shows the unaerated power characteristics of the 6RT and the 3SHP1 over the transitional and turbulent regimes using water, two CMC solutions and three *A.niger* broths of differing biomass concentrations. The agreement between low speed, Po's in water and high speed Pos in viscous systems confirms the accuracy of the measurement.

The results for the Rushton turbine are consistent with earlier work [6,7,24,25,27] for viscous non-Newtonian and Newtonain fluids. Po_{RT} rose with increasing speed, from 3.5, in the transitional regime, to 5.35, in the turbulent regime, after which it remained approximately constant.

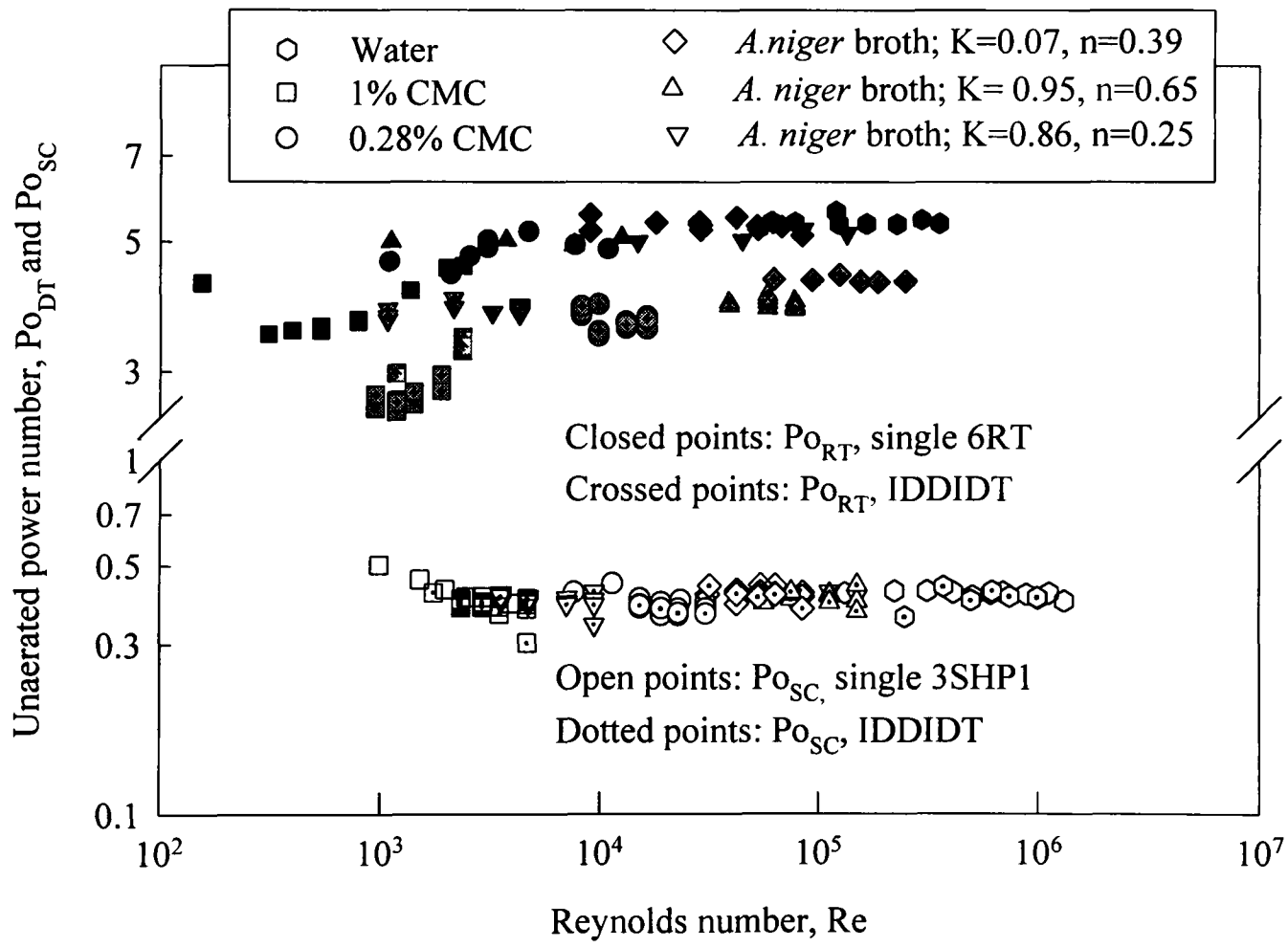

Figure 4.3-15 Po as a function of Re for the 6RT and the 3SHP1 in water, CMC and fermentation broths

The power number for the 3SHP1 was constant at 0.42 from the turbulent regime down to Re~2000 where it increased with decreasing speed up to a value of 0.503 at Re = 985. The phenomena has been reported for other axial flow impellers [6,16,17,20,31] and is probably due to a combination of increased drag on the impeller and decreased velocity of fluid entering the impeller, resulting in an increase in the effective angle of attack of the fluid to the blade[17].

As with water, when both impellers where operational the action of the 3SHP1 once again lowered the Po of the 6RT. Increasing the viscosity produced a similar trend to that seen for the single 6RT, with Po_{RT} increasing from 2.5, in the transitional regime, to 4.2, in the turbulent regime, after which it remained approximately constant. Once again there was no influence of the 6RT speed on the power drawn by the 3SHP1.

For the 3SHP1, similar power curves were seen for CMC solutions and fermentation broths, regardless of fluid type. However, in the transitional regime, Po_{RT} tended to be larger in the fermentation broths than the CMC solutions. The differences in the power numbers at similar *Re* values questions the validity of the Metzner and Otto[32] shear rate concept for the calculation of the apparent viscosity for fermentation broths and has been reported previously for Rushton turbines in *Penicilium chrysogenum*[33]. Patel[33] cited various authors who suggested k_s was dependent on the flow behaviour of the fluid [34,35] and not just impeller type. The value of k_s for the 3SHP1 may be less sensitive to the fluid characteristics, due to different flow patterns over the blades. Only a small amount of power data were collected for the fermentation broths so further work is suggested to verify this phenomenon.

4.3.3.2 Aerated flow and power characteristics

Observation of the flow patterns in CMC solution, under aerated conditions, was difficult as small trapped bubbles rendered the fluid opaque. The overall mechanism of the flow occurring was deduced from the flow observed at the walls of the vessel and power characteristics.

A bi-model distribution of bubbles was apparent in both the CMC solutions and the fermentation broths. A large quantity of small bubbles followed the movement of the liquid and a few large, often spherical cap shaped bubbles were seen rapidly channeling to the surface. Figure 4.3-16 shows the effect of viscosity on the power drawn by the single 6RT and the single 3SHP1. Figure 4.3-17, Figure 4.3-18 and Figure 4.3-19 show the gassed to ungassed power ratio, for IDDIDT, at constant impeller speeds and increasing air flow rates for fermentation broths and the 0.28% CMC, 1% CMC respectively. For all solutions, it is evident that drop in power on aeration is independent of aeration rate for the 3SHP1 and only a weak function of it for the 6RT, suggesting that large, stable, equally sized cavities were formed behind the agitator blades[2]. Such cavities have been reported to be independent of the gassing rate[2]. It was noticable that, there was no sudden drop in power between 0.1 - 0.25 vvm and that the torque fluctuations were consequently reduced. It is likely that the 3SHP1 was operating only in the "low pumping capacity" regime as large cavities were always present. However, the relative drop in power was similar for all the non-Newtonian fluids and water. At Reynolds numbers greater than 1000 this is to be expected[24].

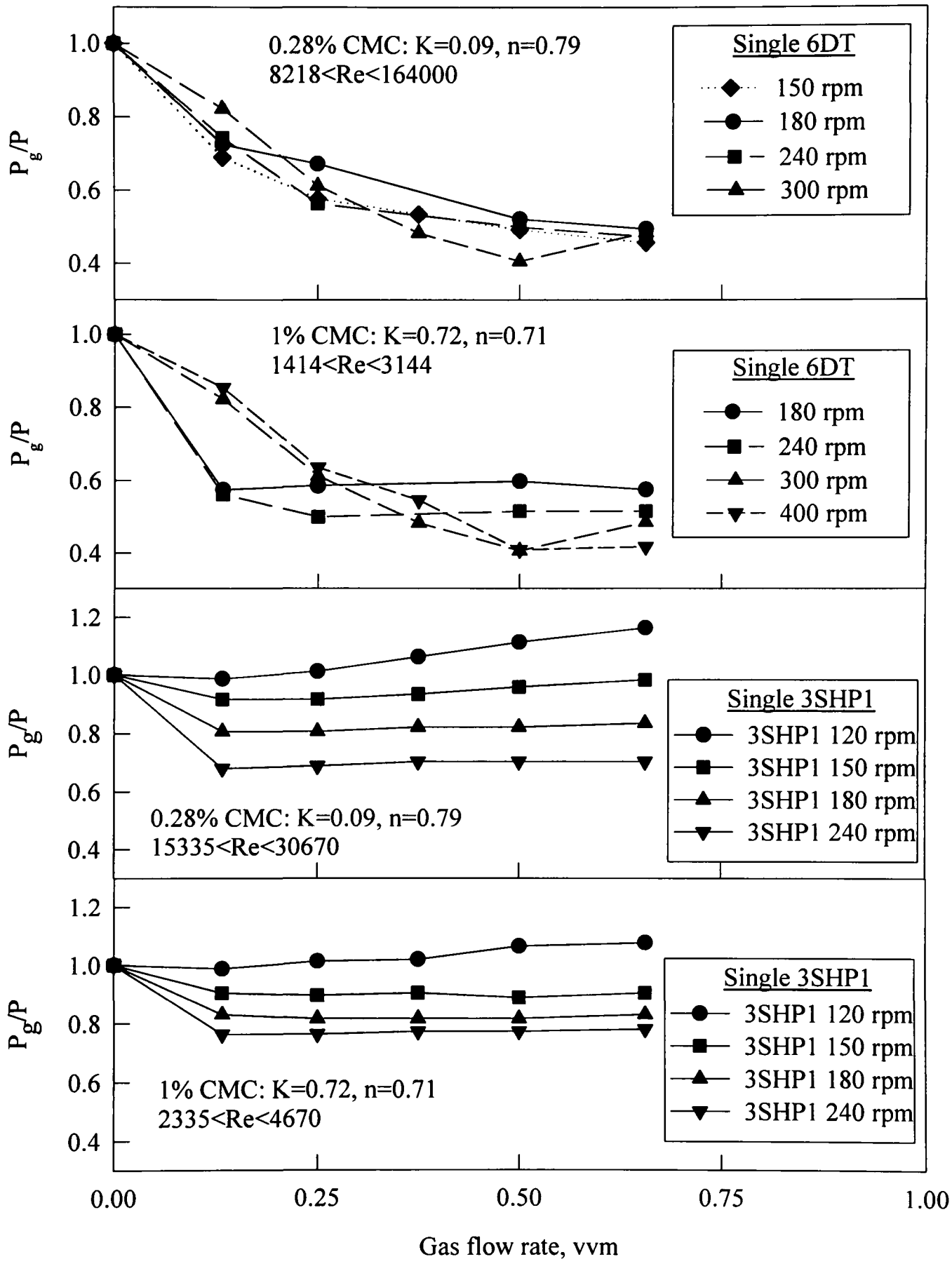

Figure 4.3-16 P_g/P for single impellers in CMC solutions

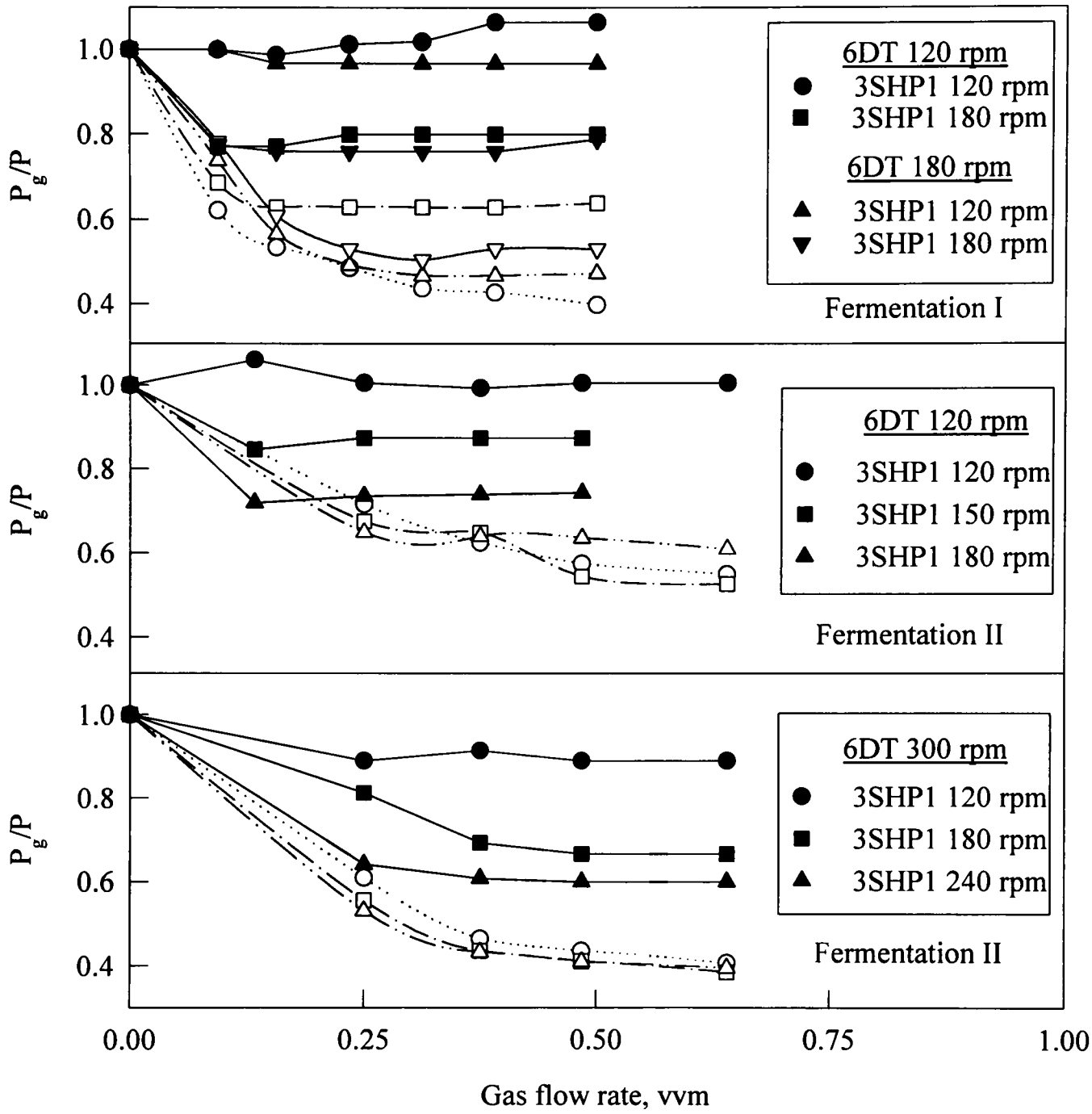

Figure 4.3-17 P_g/P at constant N and increasing Q_G , in *A.niger* fermentation broths; open points-6RT, closed points-3SHP1

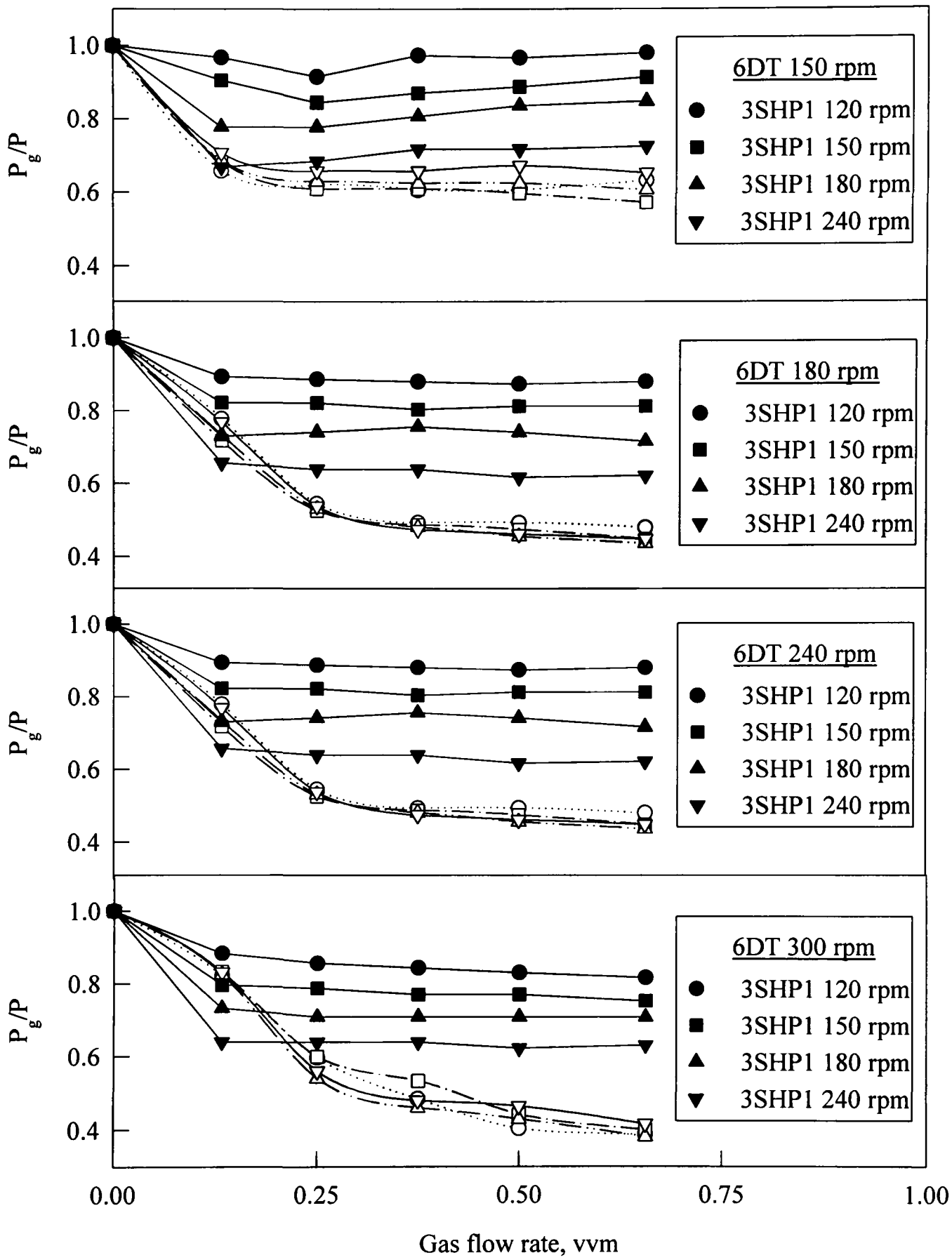

Figure 4.3-18 P_g/P for constant N and increasing Q_G, in 0.28% CMC; open points-6RT, closed points-3SHP1

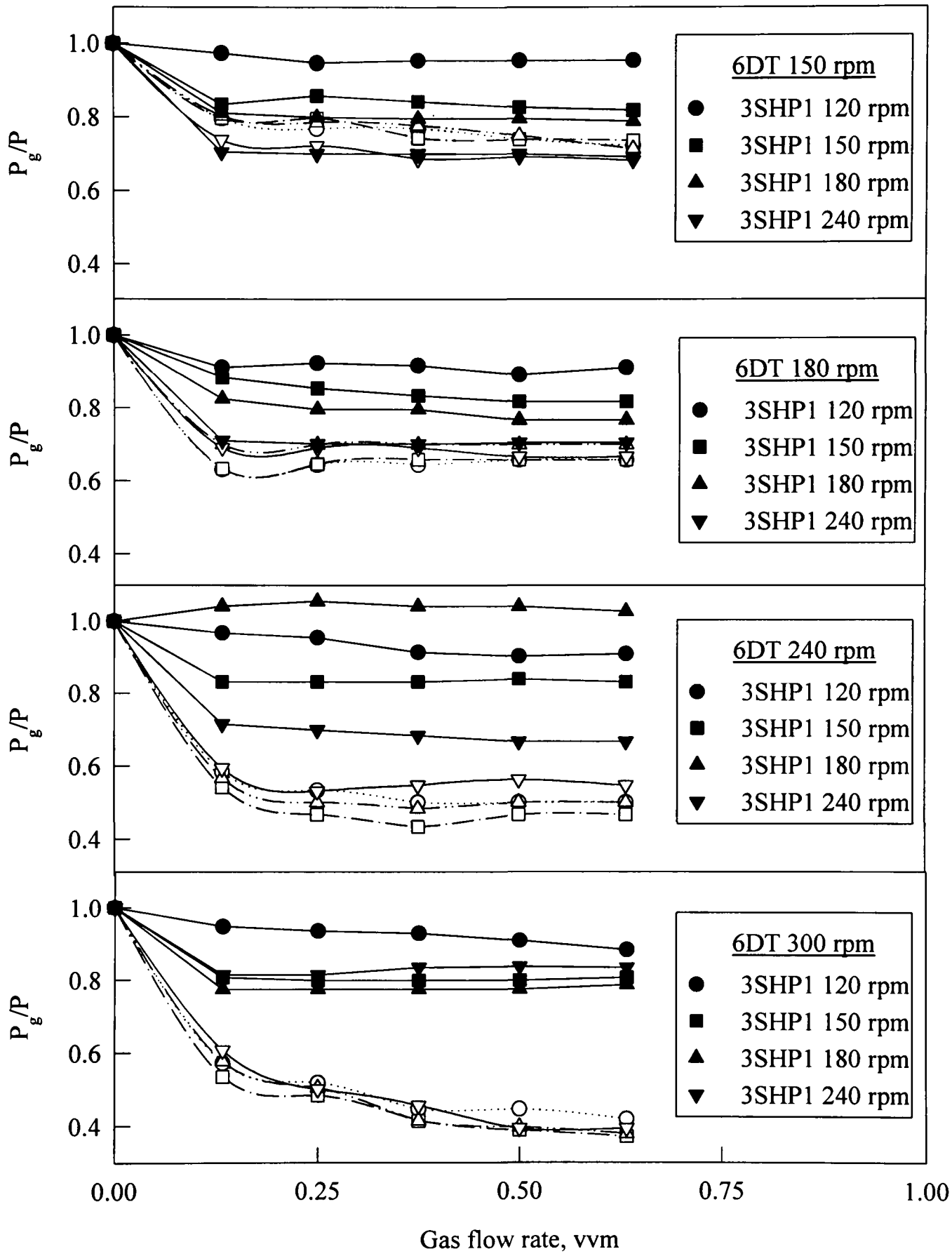

Figure 4.3-19 P_g/P at constant N and increasing Q_G , in 1% CMC; open points-6RT, closed points-3SHP1

4.4 Conclusions

The unaerated and aerated power characteristics of a independently-driven dual impeller reactor, fitted with draft tube, have been investigated in water, CMC and *Aspergillus niger* fermentation broths. Each impeller has been studied alone, in addition to them operated simultaneously. The two-phase bulk flow characteristics have been linked to the subsequent changes in power draw. The following conclusions can be drawn:

1. The unaerated power numbers for the 6RT (Po_{RT}=5.4) and the 3SHP1 (Po_{SC}=0.42) were approximately constant in the turbulent regime. However when operated simultaneously the action of the 3SHP1 lowered the power number of the 6RT to a constant value of 4.2.

2. The single 6RT, with draft tube, flooded at relatively low gas flow rates unless aided by the action of the 3SHP1.

3. The flow instabilities associated with single hydrofoils were reduced by the presence of the lower Rushton turbine and this improvement was most marked in the presence of the draft tube. The small torque instabilities were explained by observations of the flow patterns.

4. The standard correlation (equation (4.6)) is satisfactory for predicting $(N_F)_{RT}$ provided the 3SHP1 is operational. In addition, the loaded regime was narrowed by increasing the 3SHP1 speed. The speed required for complete dispersion can be calculated from equation (4.8), however this will be a slight over-prediction for the higher 3SHP1 speeds.

In aerated non-Newtonian viscous systems, large stable cavities formed behind the impeller blades and the power draw was independent of the gas flow rate. In this situation, the 3SHP1 operated in the "low pumping capacity regime".

4.5 References

1. Chapman, C.M., Nienow, A.W., Cooke, M. and Middleton J.C., 1983, "Particle-gas-liquid mixing in stirred vessels Part II: Gas-liquid mixing", *Chem.Eng.Res.Des.*, 61: 82-95

2. Nienow, A.W., 1990, "Gas dispersion performance in fermenter operation", *Chem.Eng.Progress.*, Feb: 61-71

3. Schmitz, R., 1997, "Circulation time studies in Newtonian and non-Newtonian fluids in stirred tanks", *Ph.D. thesis*, University of Birmingham, UK

4. Van der Molen, K. and van Maanen, H.R.E., 1978, "Laser-doppler measurements of the turbulent flow in stirred vessels to establish scaling rules", *Chem.Eng.Sci.*, 33: 1161-1168

5. Rushton, J.H., Costich, E.W. and Everett, H.J., 1950, "Power characteristics of mixing impellers: Part I", *Chem.Eng.Progress.*, 46, No.8: 395; 1959, "Power characteristics of mixing impellers: Part II", *Chem.Eng.Progress.*, 46, No.9: 467

6. Bates, R.L., Fondy, P.L. and Corpstein, R.R., 1963, "An examination of some geometric parameters of impeller power", *Ind.Chem.Eng.Proc.Des.Dev.*, 2, 310

7. Nienow, A.W., Wisdom, D.J. and Middleton, J.C., 1977, "The effect of scale and geometry on flooding, recirculation, and power in gassed stirred vessels", *Proc.2nd.Euro.Conf.Mixing.*: F1.1-F1.16

8. Bujalski, W., Nienow, A.W., Chatwin, S. and Cooke, M., 1987, "The dependency on scale of power numbers of Rushton disc turbines", *Chem.Eng.Sci.*, 42, No.2: 317-326

9. Nienow, A.W. and Wisdom, D.J., 1974, "Flow over disc turbine blades", *Chem.Eng.Sci.*, 29: 1994-1997

10. Van Suijdam, J.C. and Metz, B., 1981, "Influence of engineering variables upon the morphology of moulds", *Biotech.Bioeng*, 23: 111-148

11. Warmoeskerken, M.M.C.G. and Smith, J.M., 1985, "Flooding of disc turbines in gas-liquid dispersions: a new description of the phenomenon", *Chem.Eng.Sci.*, 40, No.11: 2063-2071

12. Nienow, A.W., Waroeskerken, M.M.C.G., Smith, J.M. and Konno, M., 1985, "On the flooding/loading transition dispersal condition in aerated vessels agitated by a Rushton turbine", *Proc.5th.Euro.Conf.Mixing.*, BHRA/Cranfield, U.K., paper 15: 143-154

13. Bakker, A., Smith, J.M. and Myers, K.J., 1994, "How to disperse gases in liquids", *Chem.Engng.*, Jan: 94-100

14. Abradi, V., Rovero, G., Baldi, G., Sicardi, S. and Conti, R., 1990, "Hydrodynamics of a gas-liquid reactor stirred with a multiple-impeller system", *Trans.I.Chem.E.*, 68, Part A: 516-522

15. Sharma, R.N., Howk, R.A. and Lally, K.S., 1992, "Flooding characteristics of impellers in stirred tanks", *Process.Mixing.Chem.Biochem.Appl.* A.I.Chem.E. Symposium series, Part 2, 89, No. 293: 85-89

16. Balmer, G.J., Moore, I.P.T. and Nienow, A.W., 1987, "Biotechnology processes; Scale-up and mixing", (C.S. Ho and J.Y. Oldshue, Eds.), A.I.Chem.E., New York: 117-127

17. McFarlane, C.M., 1991, "Gas-liquid mixing studies on hydrofoil impellers", *Ph.D. Thesis*, University of Birmingham, UK

18. Bujalski, W., 1986, "Three phase mixing: studies of geometry, viscosity and scale", *Ph.D. Thesis,* University of Birmingham, U.K.

19. Nienow, A.W., Hunt, G. and Buckland, B.C., 1996, "A fluid dynamic study using a simulated viscous, shear thinning broth of the retrofitting of large agitated bioreactors", *Biotech.Bioeng.*, 49:15-19

20. Bujalski, W., Sharpe, R., Sanchez, A., Torres, L., Galindo, E., Koutsakos, R. and Nienow, A.W., 1993, "Preliminary investigations into the mixing performance of an independently driven, dual impeller fermenter", *Proc.1993.I.Chem.E.Research.Event.*: 678-680

21. Bakker, A. and van den Akker, H.E.A., 1994, "Gas-liquid contacting with axial flow impellers", *Trans.I.Chem.E.*, Part A, 72, 583-594

22. Nienow, A.W., Hunt, G. and Buckland, B.C., 1994, "A fluid dynamic study of the retrofitting of large agitated bioreacotrs: turbulent flow", *Biotech.Bioeng.*, 44: 1177-1185

23. Cooke, M., Middleton, J.C. and Bush, J.R., 1988, "Mixing and mass transfer in filamentous fermentations", *Proc.2nd.Int.Conf.Bioreactor.Fluid.Dynamics.*, BHRA/Cranfield: 37-64

24. Nienow, A.W., Wisdom, D.J., Solomon, J., Machon, V. and Vlecek, J., 1983, "The effect of rheological complexities on power consumption in an aerated agitated vessel", *Chem.Eng.Commun.*, 19: 273-293

25. Valesco, D, Martínez, A. and Galindo, E., 1993, "Hydrodynamics of industrial fermentations: rheology and power draw in Rifamycin production", *Ind.Mixing.Tech.*, A.I.Chem.E. Symposium series, No299, 90: 157-165

26. Sensel, M.E., Myers, K.J. and Fasano, J.B., 1992 "Gas dispersion in high aeration rates in low to moderately viscous Newtonian liquids", *Process.Mixing.Chem.Biochem.Appl.*, Part 2, A.I.Chem.E.Symposium series, 89, No.293: 76-84

27. Bujalski, A.W., Nienow, A.W., Sánchez, A., Torres, L. and Galindo, E., 1992, "Hydrodynamics of an independently driven, dual impeller bioreactor for very large scale fermentations", *1st.Ind.Chem.Eng.Technol.Topical.Conf.*, A.I.Chem.E. Annual meeting, St. Louis, Nov 7-12: 25-30

28. Hudcova, V., Machon, V. and Nienow, A.W., 1989, "Gas-liquid dispersion with dual Rushton turbine impellers", *Biotech.Bioeng.*, 34:617-628

29. John, A.H., Bujalski, W., Nienow, A.W., Sánchez,A., Torres, L. and Galindo, E., "Studies of an independently driven dual impeller proto-fermenter with and without a draft tube: Power and hold-up, *Trans.I.Chem.E.*, 1995, 73, Part A, 535-541

30. John, A.H., Bujalski, W. and Nienow, A.W., 1997, "A novel reactor with independently-driven dual impellers for gas-liquid processing", *Proc.9th.Euro.Conf.Mixing*, Paris, France, 11, No. 52: 169-176

31. Bujalski, W., Priede, M.A., Viesturs, U.E., Cox, P.W., Thomas, C.R. and Nienow, A.W., 1997, "Mixing in fungal fermentations using dissimilar impeller systems", *Proc.4th.Int.Conf.Bioreactor.Bioprocess.Fluid.Dynamics.*, BHRA, Cranfield, Edinburgh, UK: 9-26

32. Metzner, A.B. and Otto, R.E., 1957, "Agitation of non-Newtonian fluids", *A.I.Chem.E.*, 3, No.1: 3-10

33. Patel, D, 1997, "Mixing and rheological studies of real and simulated fermentation broths", *Ph.D. Thesis*, University of Birmigham, UK.

34. Brito De La Fuente, E., Leuliet, J.C., Choplin, L. and Tanguy, A., 1991, "On the effect of shear thinning behaviour on mixing with a helical ribbon impeller", *A.I.Chem.E. Symposium series*, No. 286, 88: 28-32

35. Ducla, J.M., Desplanches, H. and Chevalier, J.L., 1983, "Effective viscosity of non-Newtonian fluids in a mechanically agitated stirred tank", *Chem.Eng.Comm.*, 21: 29-36

CHAPTER 5

GASSED HOLD-UP

5.1 Introduction

In fermentation processes, a major functions of the agitator is to break-up and disperse the sparged gas in order to provide an interfacial area, a, for mass transfer. Improvements in gas-liquid mass transfer evolve from optimising the interfacial area available against the resultant costs due to increasing impeller speed or gas flow rate, or changing a reactor configuration. However, a, is difficult to determine experimentally, so gas hold-up is often used as an estimation of reactor performance. Gas hold-up, ε_T, can be linked to $k_L a$, the mass transfer coefficient, since

$$d_B = 6\frac{\varepsilon_G}{a} \times \frac{1}{100} \tag{5.1}$$

where d_B is the Sauter mean bubble size. Over the limited range of impeller speeds studied and assuming the same hydrodynamic regime, k_L, the mass transfer coefficient in the liquid phase, and d_B are very weak functions of agitation and aeration rate. Therefore:

$$k_L a \propto \varepsilon_G$$

However, it is also important to realise that high hold-up can be a problem since productivity goes down as hold-up increases.

Hold-up is defined as

$$\varepsilon_G = \frac{gas\ volume}{gas\ volume + liquid\ volume}$$

and is calculated, as a fraction or percentage, from the change in liquid height on gassing, *i.e.*

$$\varepsilon_G = \frac{H_G - H}{H_G} \times 100\% \qquad (5.2)$$

where H is the unaerated liquid level and H_G is the level of the gas-liquid dispersion.

Traditionally, estimation of hold-up for comparative and scale-up purposes has been based on an empirical correlation incorporating the specific gassed power input and the superficial gas velocity and is of the form

$$\varepsilon_G = k\left(\frac{P_T}{V}\right)^{\alpha}(u_s)^{\beta} \qquad (5.3)$$

Generally, many workers have reported that the values of k, α and β are independent of impeller type[1,2,3,4,5] although the absolute values depend on the fluid and thus can vary between workers (Table 5.1-1(a,b)). In contrast, when using water, significantly different hold-up values for hydrofoils compared to Rushton turbines at similar power inputs and superficial gas velocities have been observed[6,7]. However, at high gas flow rates in water, or when using CMC solutions, the hold-up values were broadly similar for both hydrofoil and Rushton turbine impeller types [6].

Greaves and Barigou[8] reviewed a number of correlations and suggested an improvement could be achieved by choosing a model based on system independent parameters, *i.e.* N, Q_G and D/T coupled with the type cavity present. Higher hold-up values were reported in the presence of vortex-clinging cavities compared to large cavities. This was due to the reduced pumping capacity resulting in a lower bulk flow and a decrease in recirculation when large cavities are present. Similarly, Bujalski *et al.*[3] expressed hold-up in terms of N and Q_G, with a different ratio for each impeller type, allowing mixer design without the need for inferring the gassed

power draw. The correlation of hold-up in terms of geometric parameters is suitable for the examination of similar impeller types on differing scales. However, its use for comparing impeller types is questionable.

5.1.1 Multiple impellers

Multi-impeller systems, commonplace in the fermentation industries, have been shown to exhibit similar hold-up characteristics to single impeller systems. Nocentini *et al.*[9], Pinelli *et al.*[10], Abradi *et al.*[11] and Whitton and Nienow[12] reported similar gassed hold-ups for multiple and single Rushton turbines provided the specific power input and gas flow rates were equal. Similarly, Cooke *et al.*[2] successfully correlated hold-up with total power input and superficial gas velocity for a variety of single and dual impeller types and combinations, at scales from 0.02 m^3 to 4.3 m^3. However, it was noted that the exponent on the specific power function (0.15) was lower than previously quoted for single impeller systems (~0.33) (Table 5.1-1(b)). On the large scale (14 m^3), Nienow *et al.*[5] also found that a single correlation was satisfactory for the prediction of hold-ups using multiple hydrofoils or Rushton turbines and the exponent on P/V (0.13) was lower than the usual value. On the other hand, Bujalski *et al.*[7] reported higher hold up values, at similar energy dissipation rates and gas flow rates, for an independently-driven dual-impeller configuration compared to single impeller systems.

5.1.2 Non-Newtonian viscous liquids

In non-Newtonian viscous fluids, the bubble size distribution becomes bi-modal with many small bubbles following the fluid flow and a few large bubbles in the plug flow[13]. Due to their increased size and buoyancy, the large bubbles tend to rise rapidly and have a very short residence time. Therefore, viscous fluids exhibit reduced hold-up compared to the water for the same operating conditions. For Rushton turbines and hydrofoils, McFarlane[6] found the exponents on power input in equation 5.3 were smaller in CMC solutions compared to water.

Alternatively, the inclusion of a viscosity term into equation (5.3) has proved successful for predicting hold-up in viscous solutions [2,9,14] (Table 5.1-1(b)). A close relationship between k_La and hold-up is not always found[9,14,15]. Therefore, care must be taken when using hold-up as a basis for assessing the mass transfer performance in viscous non-Newtonian liquids. Allen and Robinson[14] observed very little effect of *Aspergillus niger* broth rheology (5 - 20 g/l) on hold-up values. However k_La was significantly affected.

5.1.3 Bubble columns

Bubble columns and airlift bioreactors have become widely developed for two and three phase industrial processes. Their design and applications have been extensively reviewed[16] however there remains much controversy over the possible improvements in hold up/mass transfer due to the inclusion of a draft tube. Christi and Moo-Young[16] concluded from their review that the addition of a draft tube has no influence on the overall hold-up for bubble columns. It was noted, however, that bubble columns with or without draft tubes produced higher hold-ups compared to external loop reactors. In contrast, enhanced hold-ups have been reported, by other authors, for bubble columns with draft tubes compared to those without[17,18,19,20].

Table 5.1-1 Empirical hold-up correlations reported in the literature

$$\varepsilon_G = k\left(\frac{P_T}{V}\right)^{\alpha}(u_s)^{\beta}$$; ε_G in %, (P/V) in W/m^3 and u_s in m/s;

RT - Disc Turbine, UPM/DPM - Up/Down Pumping Mixed flow impeller, A315 - hydrofoil, PMT - Prochem Maxflo T hydrofoil, CBRT - Curved Blade Disc Turbine

(a) Water

Author	Equipment	Outcome	K	α	β
van't Riet[21]	Several types of RT	Independent of RT shape	9.6	1/3	2/3
Chapman *et al.*[1]	RT, UPM, DPM	Independent of impeller type	19.7	0.31	0.67
Bujalski *et al.*[3]	RT, UPM, DPM	Independent of impeller type	21.74	0.326	0.776
Nienow *et al.*[5]	4 -RT, 3-A315, 4-PMT	Independent of impeller type	-	0.13	0.55
Pinelli *et al.*[10]	3-RT, 3-A315, RT-2 A310	Broadly independent of impeller type	-	0.21-0.24	0.56-0.69
Bakker *et al.*[22]	RT, CBRT	Broadly independent of impeller type. CBRT gives higher hold-up than 6RT	0.16	0.33	0.67

(b) Effect of viscosity, μ^{δ}

Author	Equipment	Outcome	k	α	β	δ
Nocentini *et al.*[9]	Multiple RT	Inclusion of viscosity term gives satisfactory correlation				
		Water	8.35	0.375	0.62	
		Water + Glycerol	8.35	0.375	0.62	-1/3
Cooke *et al.*[2]	Combination of multiple RT's and hydrofoils	Filamentous suspensions	10.92	0.15	0.54	-0.42
Saito *et al.*[4]	RT, CBRT	Independent of impeller type. Increased viscosity reduced k and β				
		Water	9.6	1/3	0.68	-
		CMC	5.7	1/3	0.6	-
McFarlane[6]	Single A315, PMT,RT.	Hold-up dependent on impeller type. Exponents reduced with increasing viscosity.				
		Water: A315	32.81	0.38	0.96	-
		RT	86.46	0.26	1.0	-
		CMC: A315	47.80	0.26	0.90	-
		RT	26.37	0.20	0.68	-
Dawson[23]	Single A315, RT, Intermigs	Similar hold-ups for A315 and RT, different for the Intermigs.	16.9	0.3	0.6	-
		Water: A315	12.07	0.28	0.47	-
		RT				
		CMC: A315	6.78	0.25	0.58	-0.25
		RT	10.04	0.15	0.43	-0.17

5.2 Results and Discussion

Hold-up was measured under the experimental conditions described in Chapter 4 using the technique explained in Chapter 3. Firstly, the hold-up characteristics of the single 6RT, single 3SHP1 and IDDIDT configuration, operating in water have been made (Section 5.2.1). Secondly, a comparison between these configurations and a single shaft dual Rushton turbine system (RT-RT) were drawn in Section 5.2.2. Finally, hold-ups in CMC and *Aspergillus niger* solutions have been presented and explained in Section 5.2.3.

5.2.1 Hold-up in Water

5.2.1.1 Single 6RT with the draft tube

Hold-up was found to increase with gas flow rate and impeller speed when the air was loaded or completely dispersed.

Figure 5.2-1 clearly shows, for 6RT speeds of 150 and 180 rpm, a definite drops in gassed hold-up which could be coupled with a subsequent increase in Po (Chapter 4, Figure 4.3-4), when the impeller became flooded at 125 l/min (Fl_G= 0.06) and 195 l/min (Fl_G=0.08) respectively.

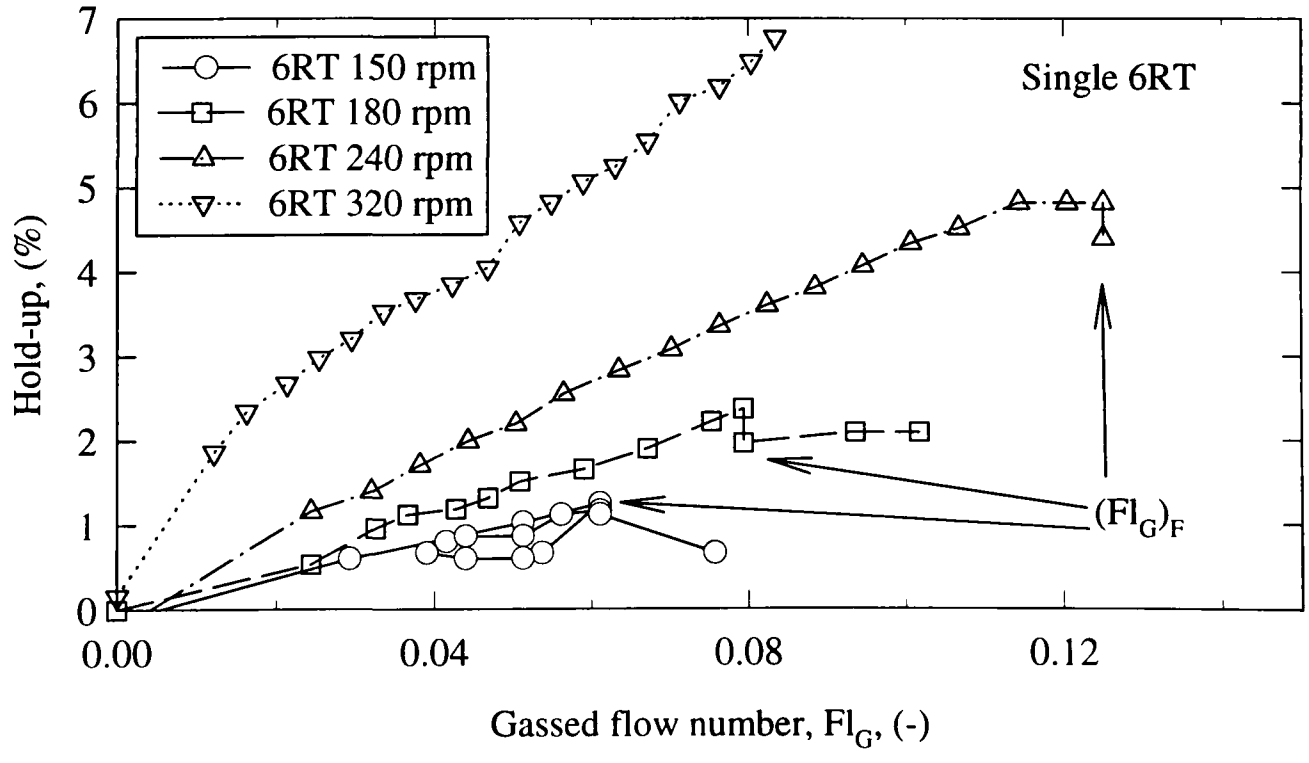

Figure 5.2-1 Hold-up as a function of gassed flow number for the single 6RT at various speeds (D=T/3)

A more common manner to describe hold-up is as a function of specific power input and superficial velocity (equation (5.3)). In agreement with other researchers hold-up was found to correlate very well with these variables. Experimental values of 0.26 and 0.86 compared well with the values compiled by Greaves and Barigou[8] and others (Table 5.1-1) in which α and β vary from 0.26 to 0.8 and 0.36 to 1.0 respectively.

5.2.1.2 Single 3SPH1 with the draft tube

For impeller speeds of 60, 90 and 120 rpm the impeller is essentially flooded and hold-up can be seen to increase linearly with increasing gas flow rate (Figure 5.2-2).

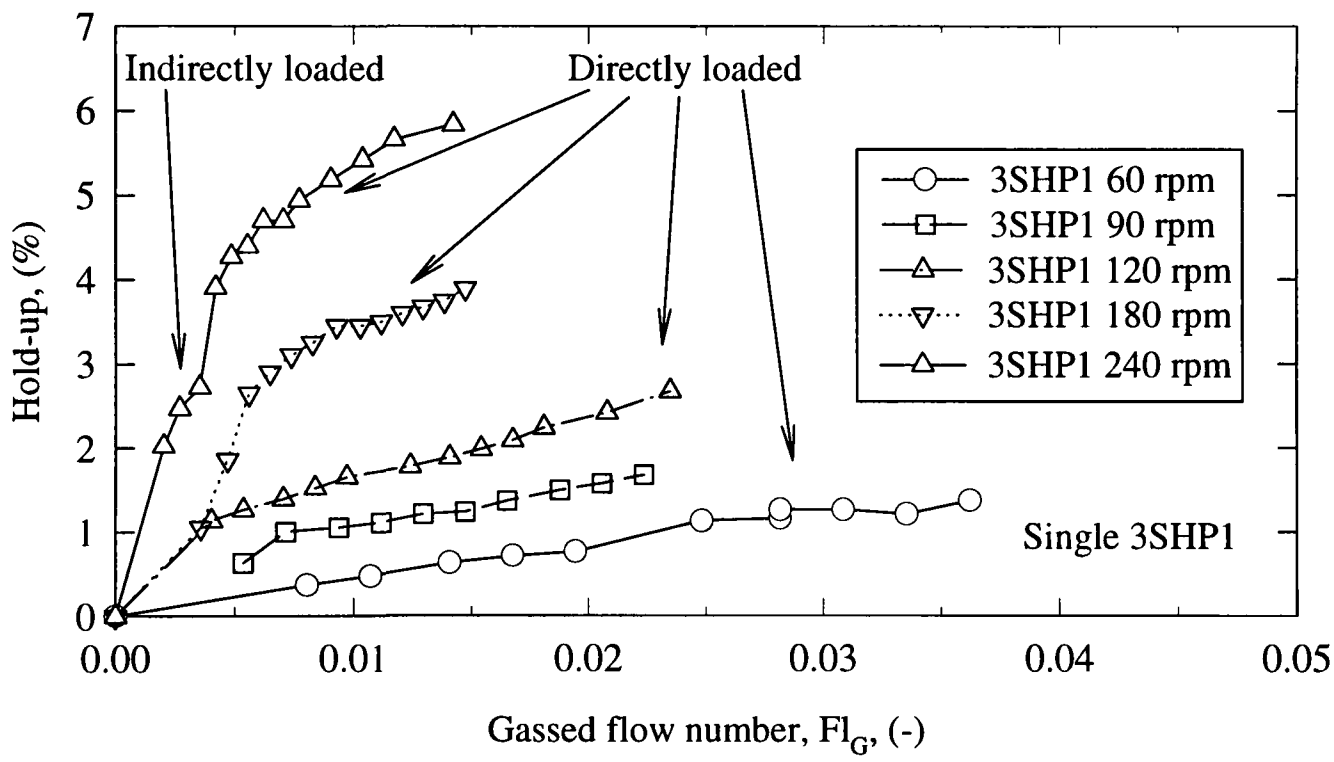

Figure 5.2-2 Hold-up versus gas flow rate for the single 3SHP1 at a variety of speeds

For higher impeller speeds which posses enough energy to disperse the gas (180 and 240 rpm) hydrodynamic conditions can once again be split into distinct regions (Section 4.3.2.2).

(i) Indirect Loading - Initially the rate of change of hold up was high when gas flow rate was increased. Most of the energy from the blades was utilised by the fluid, the impeller was operating in the "high pumping capacity regime" (Chapter 4), with large amounts of gas being drawn from the annulus into the draft tube. There was a large amount of bulk recirculation and an even distribution of bubble sizes.

(ii) Direct Loading - There was a sudden increase in hold up, which linked directly to a drop in power draw (Figure 5.2-2 and Figure 4.3-7), as the flow changed from indirect to direct loading. Similar observations were made by McFarlane for hydrofoil impellers when they entered the radial flow regime[6]. However, the large increase was due to gas becoming trapped in large cavities formed behind the impeller blades rather than an increase in specific surface area due to increased recirculation. In addition, the increase in hold-up was not a definite advantage since some bubbles did not posses enough downward momentum to clear the bottom of the draft tube. Consequently, due to buoyancy forces, they returned to the impeller region. In a microbial systems, this could be considered a disadvantage since the oxygen inside such bubbles would soon become exhausted and therefore their contribution to the increased hold-up would contain no improvements for mass transfer. Also due to the influence of the large cavities the pumping capacity of the impeller was reduced and the rate of change of hold up with increasing gas flow rate was lower compared to when indirectly loaded.

(iii) Increasing Q_G passed the point of direct loading resulted in a decrease in the quantity of draft tube dispersion and recirculation until the flooding point was reached. At the flooding point the rate of change of hold up was once again reduced and gas could be seen swirling out of the top of the draft tube.

It was only possible to obtain a reliable correlation for hold-up in the directly loaded regime since very little data was obtained for the indirectly loaded regime (Table 5.2-1).

It is noticeable that the hold-up for the directly loaded single 3SHP1 was more dependent on power input and less dependent on gas flow rate, in comparison to the single 6RT. This was most probably because the 3SHP1 was operating in the "low pumping capacity regime" and therefore less gas was recirculated into the draft tube on increasing gas flow rate. However,

the exponents on power (0.49) and superficial gas velocity (0.36) fall into the expected range and are similar to those reported by Dawson [23]. A best fit correlation for the few points obtained in the indirectly loaded regime produced exponents of 0.26 and 1.0 for the specific power and superficial gas velocity respectively, very similar to those observed with the 6RT. In the indirectly loaded regime, when the 3SHP1 is pumping at high capacity, a large quantity of gas was recirculated back into the draft tube hence explaining the large exponent on the superficial gas velocity term. McFarlane[6] also reported high exponents on the superficial gas velocity term. However, it was noted that the correlation covered both "axial" and "radial" flow regimes encountered with hydrofoil impellers. It is evident, therefore, that a knowledge of the two phase bulk flow is essential if realistic correlations are to be produced for design and scale up purposes. The majority of workers, however, state a single correlation covering a range of flow regimes which has possibly led to the discrepancies reported.

5.2.1.3 Dual impeller system (IDDIDT)

The trends observed in hold up are directly comparable to the simultaneous changes in power draw described in Section 4.3.2.3. Decreases in power draw and instabilities when the flow changed from "high pumping" to "low pumping" could be coupled to hold up fluctuations and a decrease in the rate of change of hold up with air flow rate. Figures 5.2-3 to 5.2-6 show the increase in hold-up with increasing air flow rate for some typical operating conditions. At low air flow rates, the hold-up increased rapidly and this region of the plot, designated (c), corresponds to the "high pumping capacity regime" of Figure 4.3-14(c), with the change in slope occurring at higher air flow rates as the speed increased. The region designated (b), corresponding to Figure 4.3-14(b), is the "low pumping capacity regime" and here the rate of increase of hold-up with aeration rate is markedly lower. At higher gas flow rates the 6RT impeller becomes flooded and there is a drop in the hold-up (designated (a)).

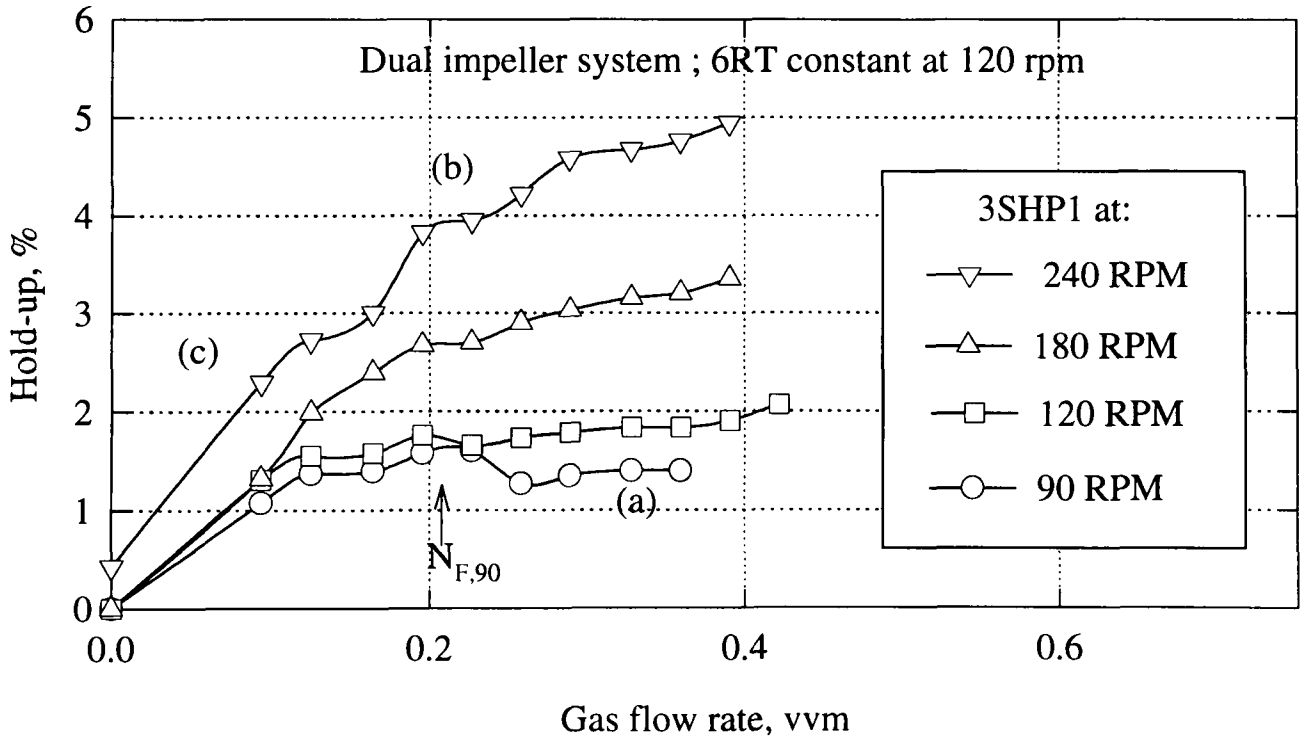

Figure 5.2-3 Hold-up versus gas flow rate, in water, for IDDIDT with 6RT constant at 120 rpm

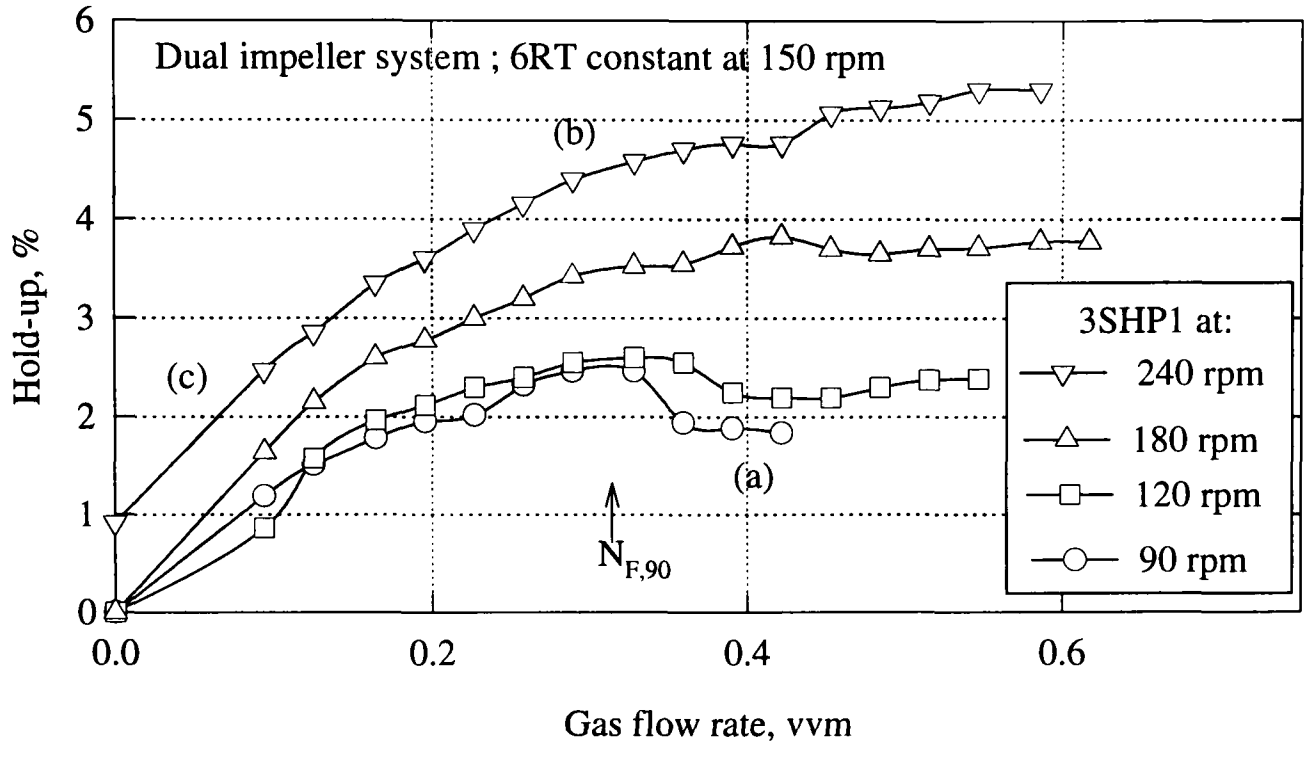

Figure 5.2-4 Hold-up versus gas flow rate, in water, for IDDIDT with 6RT constant at 150 rpm

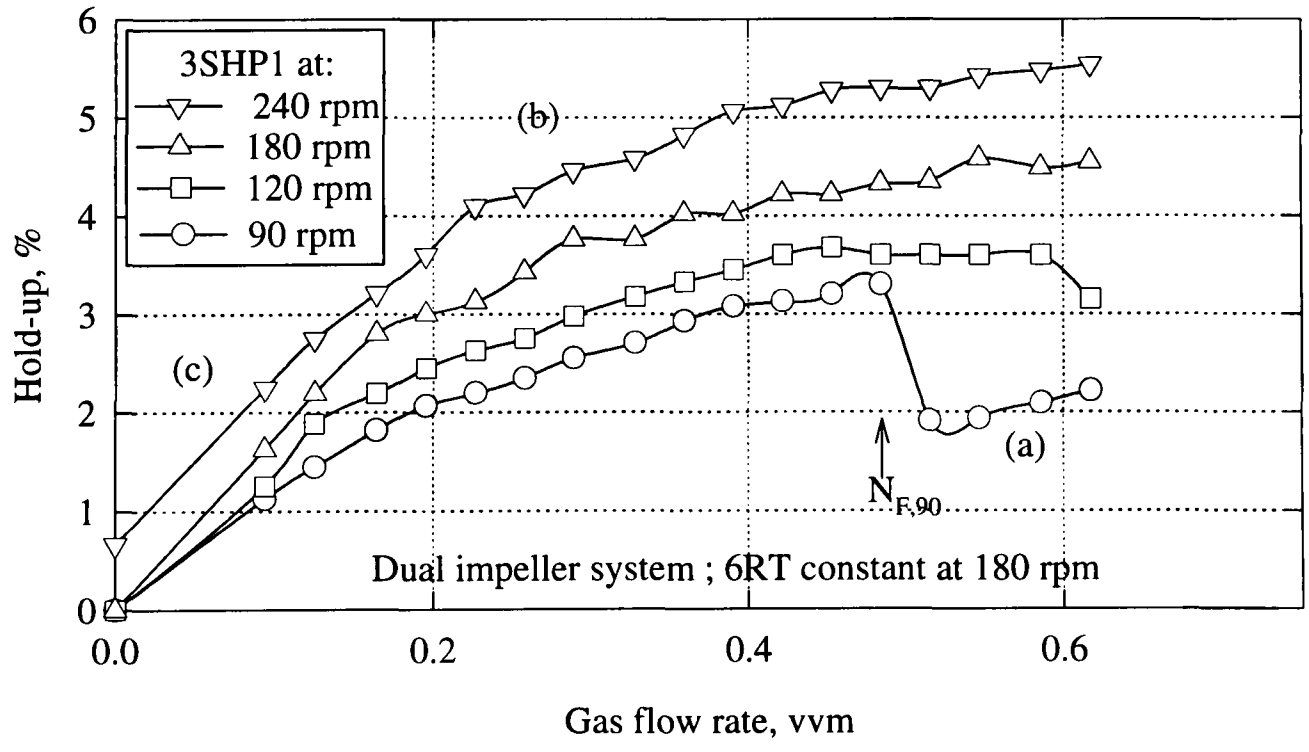

Figure 5.2-5 Hold-up versus gas flow rate, in water, for IDDIDT with 6RT constant at 180 rpm

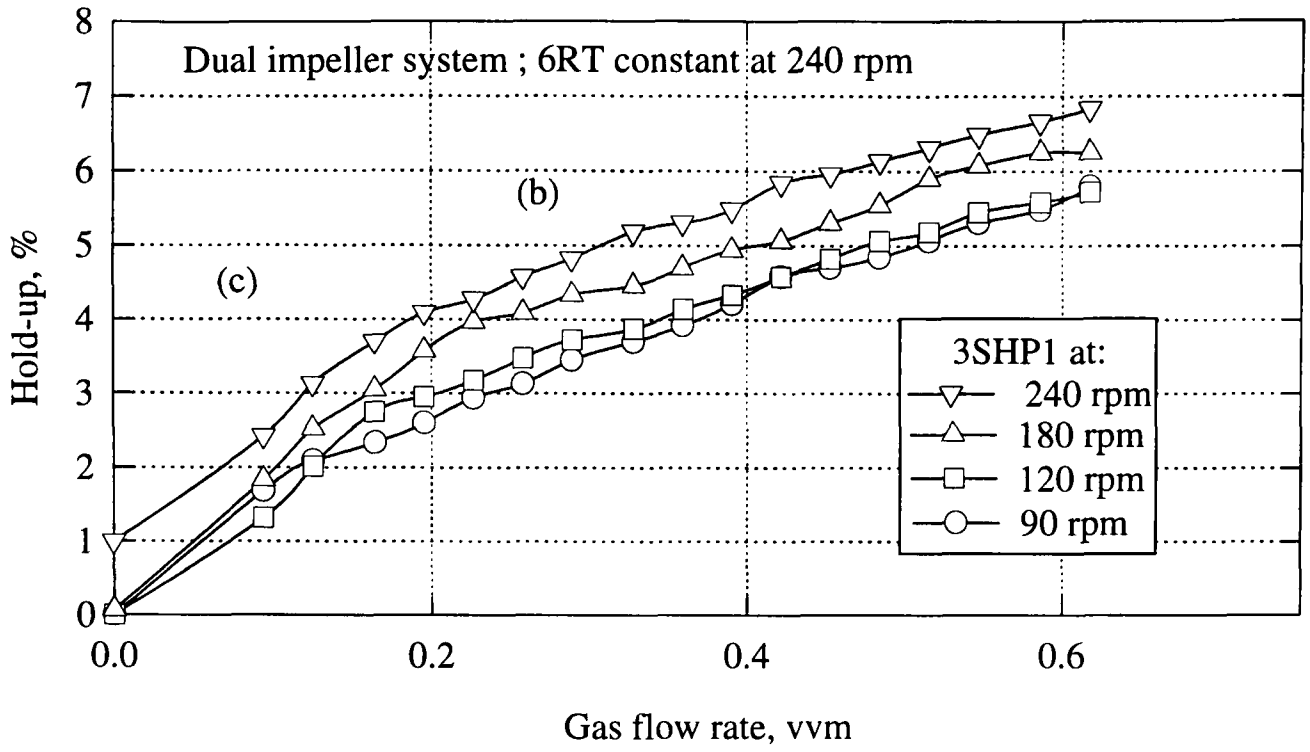

Figure 5.2-6 Hold-up versus gas flow rate, in water, for IDDIDT with 6RT constant at 240 rpm

The best fit curve obtained for IDDIDT produced exponents very similar to those previously reported (Table 5.2-2). This was most likely due to an averaging effect of the different impeller types present in the configuration.

Table 5.2-1 Hold-up correlations in water

$$\varepsilon_G = k\left(\frac{P_T}{V}\right)^{\alpha}(u_s)^{\beta}$$; ε_G in %, (P/V) in W/m^3 and u_s in m/s.

System	Test Fluid	No. of points	k	a	b	r^2	Eqn.
Single 6RT: draft tube	Water	47	44.0	0.26	0.86	0.98	5.4
Single 3SHP1: draft tube,	Water directly loaded	53	1.0	0.48	0.37	0.98	5.5
	indirectly loaded	6	123.0	0.26	1.0	0.81	5.6
RT-RT no draft tube	Water	18	80.6	0.25	0.95	0.99	5.7
IDDI draft tube	Water	153	17.9	0.30	0.70	0.97	5.8
All combined	Water	278	12.07	0.37	0.72	0.91	5.9

5.2.2 Effect of geometry/impeller type

Four geometries were tested at gas flow rates of 0.1, 0.25, and 0.5 vvm. For the configuration with the draft tube, a single 6RT, a single 3SHP1 and two, independently-driven, impellers (IDDIDT) were investigated. Without the draft tube a dual Rushton turbine (RT-RT) was studied. To obtain a full picture, hold-up data for an independently driven dual impeller system with no draft tube (IDDINT) were also obtained (personal communication with W. Bujalski). Initial hold-up measurements for IDDINT were done using visual observations due to the lack of appropriate instrumentation on the rig at that stage. Later, parallel measurements made using the ultrasonic echo gauge showed a consistent offset (about 10%) between the two techniques. Therefore, data from the IDDINT were "updated" to enable a direct comparison to be made.

Figure 5.2-7, Figure 5.2-8 and Figure 5.2-9 show hold-up at increasing energy inputs for constant gas flow rates of 0.1, 0.25 and 0.5 vvm respectively. It is evident that, at low gas flow rates of 0.1 and 0.25 vvm, hold-up was geometry dependent. For similar specific power inputs, the draft tube configurations, incorporating the 3SHP1, gave enhanced hold-up compared to the RT-RT without the draft tube. For example, at 0.25 vvm and 1 W/kg (Figure 5.2-8) the 3SHP1 and IDDIDT gave 62% and 45 % higher hold-up values respectively, compared to the RT-RT. In fact, at 0.1 vvm enhancements of approximately 80 % were common (Figure 5.2-7). Increased hold-up values were attributable to increased gas recirculation into the draft tube. At 0.1 vvm the 6RT performed similarly to the RT-RT, however, at 0.25 vvm the 6RT gave higher hold-ups at similar power inputs, probably due to the increased circulation caused by the density difference in liquid between the annulus and the draft tube. Provided gas dispersion was satisfied, low 6RT coupled with high 3SHP1 speeds gave the most efficient operating conditions on basis of total power input. However, the rate

of change of hold-up with increasing specific power input was more rapid at the higher 6RT speeds.

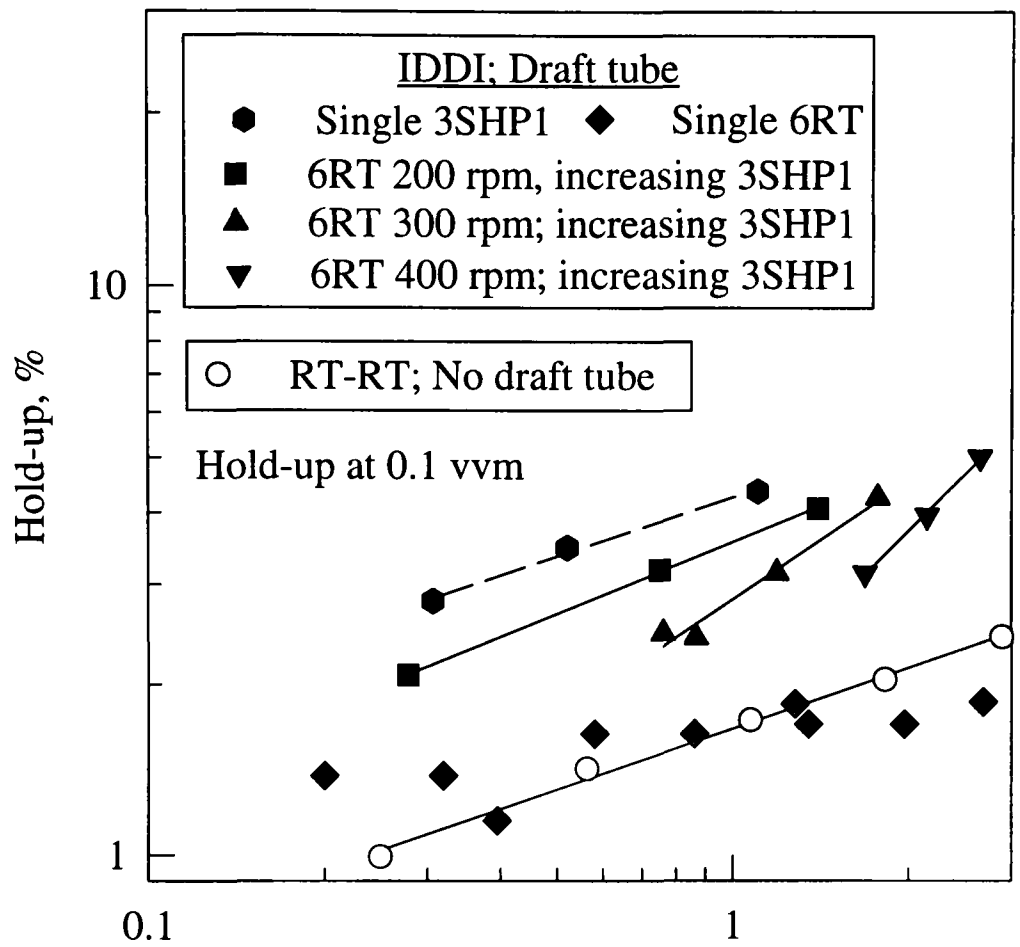

Figure 5.2-7 Hold-up as a function of specific power input; 0.1 vvm, various geometries

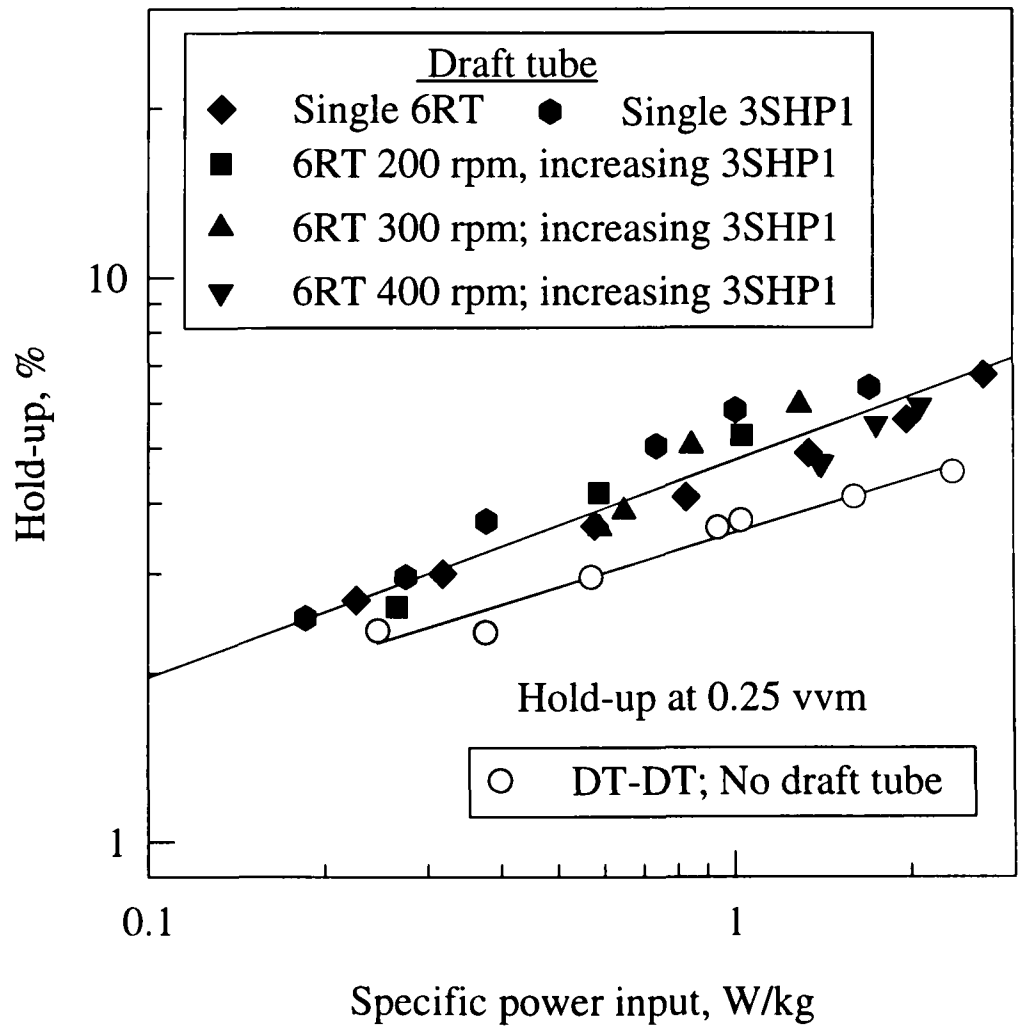

Figure 5.2-8 Hold-up as a function of specific power input; 0.25 vvm, various geometries

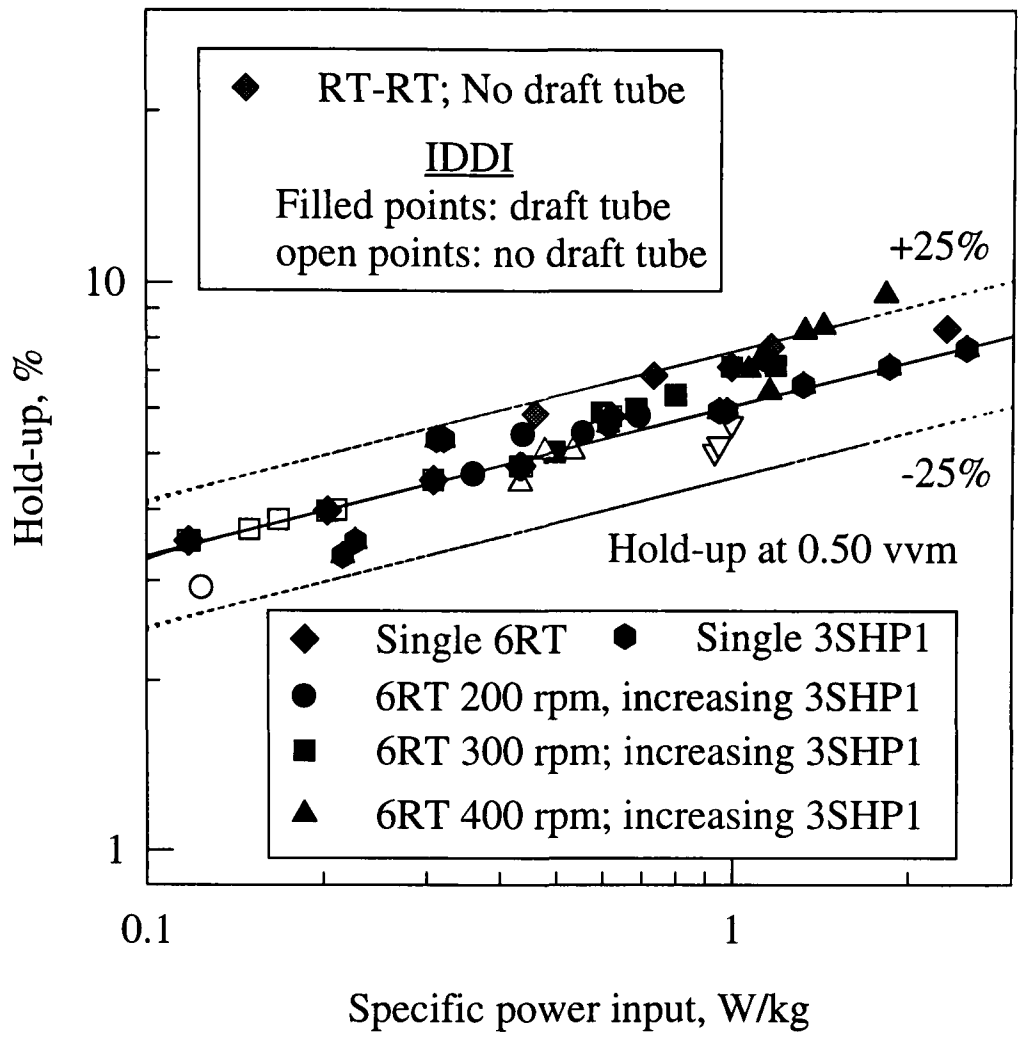

Figure 5.2-9 Hold-up as a function of specific power input; 0.5 vvm, various geometries

In agreement with McFarlane[6] a reduced dependency on impeller type was discovered with increasing gas flow rate. Generally, there was little difference between the configurations at a gas flow rate of 0.5 vvm. The similarity between the systems was most likely due to a reduction in the amount of gas recirculation resulting from the reduced pumping capacity of the 3SHP1 at the higher gas flow rates. Over the power range studied, $0.1<P/V<2.0$ W/kg, hold-up values for all geometries were predictable to within about $\pm$ 25%.

At all gas flow rates, for a constant 6RT speed, increasing the 3SHP1 significantly improved hold-up with only a marginal increase in power draw. The general trend suggested further increases in 3SHP1 speed (P/V) would enhance hold-up values at a greater rate than any increases in 6RT speed (P/V). Unfortunately, the range of 3SHP1 speeds studied only permitted a comparison on the basis of overall (6RT + 3SHP1) power input.

The empirical constants obtained for equation (5.3) using all impeller types and geometries are shown in Table 5.2-1. In general the values obtained are in good agreement with those reported in the literature (Table 5.2-2). The P/V exponent, α, was circa 0.25 for the single 6RT, RT-RT and 3SHP1 in the indirectly loaded regime. A higher value (0.48) was found for the 3SHP1 when directly loaded. Similarly, the value of the u_s exponent, β, lay between 0.86 and 1.0 for the 6RT, RT-RT, indirectly loaded 3SHP1, whereas a much lower value (0.37) was achieved with the 3SHP1 when directly loaded. The differences between the exponents was probably due to the effect of gas on the pumping capacity of the 3SHP1.

As expected, when using IDDIDT the values of k, α and β lie between the two extremes described above and are in excellent agreement with those reported by Chapman *et al.*[1], Saito *et al.*[4] , van't Riet[21] and Bakker *et al.*[22] (Table 5.2-2). In addition, an overall correlation was created by combining all the data obtained from each geometry and impeller type. However, the overall correlation was statistically different from the individual correlations, due to the significant differences at the lower gas flow rates (Appendix III).

Table 5.2-2 Comparison of empirical constants obtained with correlations from the literature

Author	k	α	β
van't Riet[21]	14.3	0.33	0.67
Chapman *et al.*[1]	19.7	0.31	0.67
Saito *et al.*[4]	9.6	0.31	0.68
This work, IDDIDT	17.9	0.30	0.70
This work, All configurations	12.07	0.37	0.72

The advantages of the flexibility of the IDDIDT system can be explained in terms of flow regime maps, similar to those used by Bakker *et al.* [22]. The comparison has been made on a purely hypothetical basis in order to give a broad idea as to the possible improvements gained

by using the IDDIDT system. Therefore, it must be stressed that the following assumptions have been made:

1. The empirical correlations (Table 5.2-1) are valid over a wide range of power inputs and superficial gas velocities.

2. Identical correlations for calculating N_{CD} and N_F (equations 4.5 and 4.7) have been used, irrespective of geometrical set-up. It is believed the correlations produce a good estimate for the single 6RT, RT-RT and IDDIDT configurations (Chapter 4). However, for a single shaft RT-3SHP1 system it is possible that, at higher gas flow rates, lower speeds may be required due to the action of the 3SHP1 impeller. This was noted in Chapter 4.

3. The power draw for the upper RT in the RT-RT configuration was estimated from the design criteria set out by Bakker *et al.*[22]. The power draw by the 3SHP1 was gauged through knowledge of the ungassed to gassed power ratio at differing gas flow rates and impeller speeds.

As an example it is assumed that a hold-up of ~ 5% is required for a process. The flow regime maps for a single 6RT, IDDIDT, RT-RT and RT-3SHP1 are shown in Figure 5.2-10. Each map contains: an operating line, calculated from the respective hold-up correlations; a loading line and a flooding line. The operating lines, $P_{5\%}$, (dotted line) for all configurations are very similar, as would be expected from the correlations presented in Section 5.2.1. However, the hold-up correlations, created from loaded or completely dispersed data, take no account of the flow regime and thus would produce invalid results if the impeller became flooded/loaded. Therefore, superimposed onto the operating lines are the complete dispersion/loading, P_{CD}, and flooding/loading, P_F, curves (dash and dash-dot respectively).

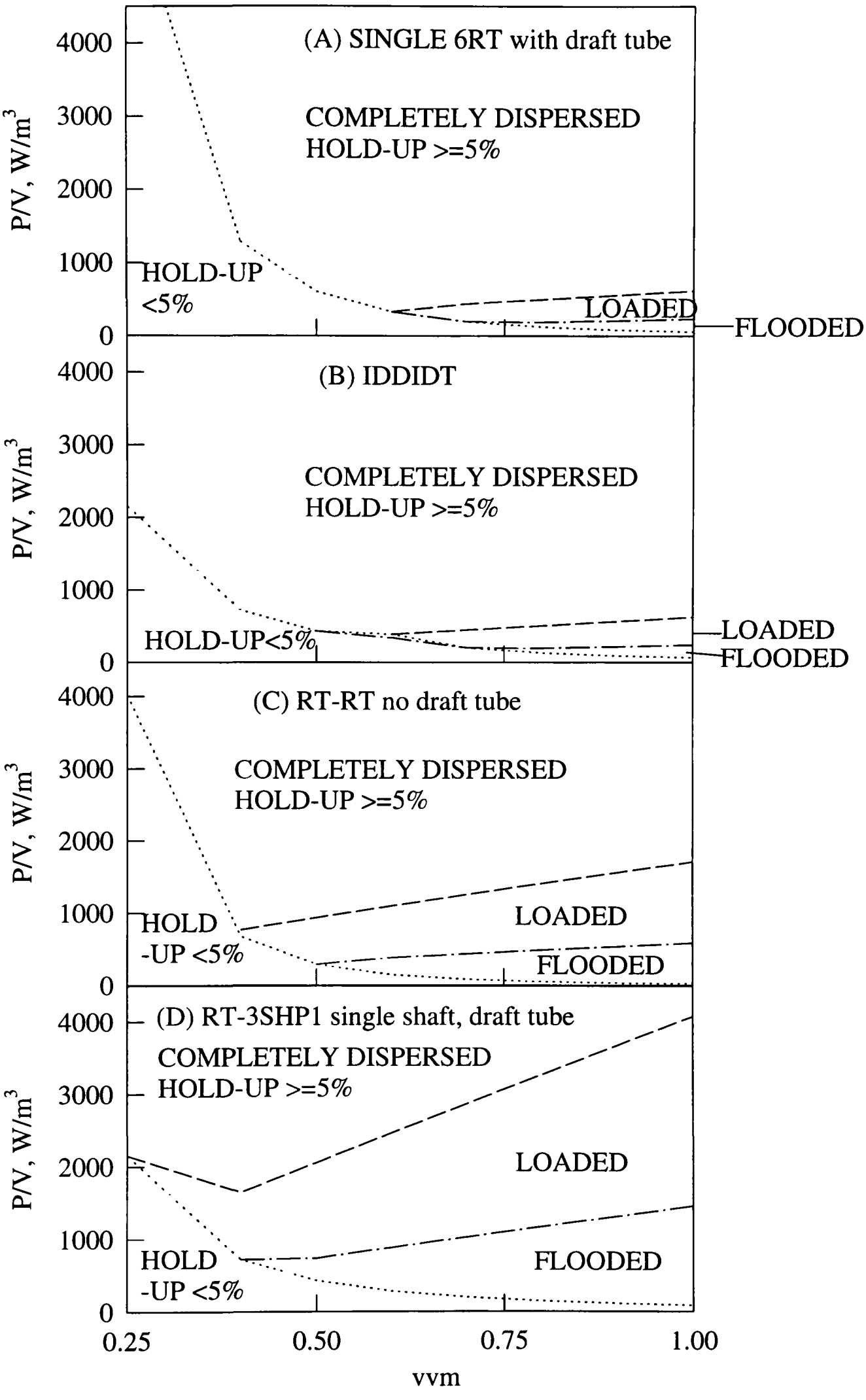

Figure 5.2-10 Flow regime maps for various configurations and a hold-up requirement of 5%

Taking Figure 5.2-10 (C) as an example, at low gas flow rates (0-0.3 vvm) the gas is completely dispersed at the impeller speed that is required to produce a hold-up of 5%. Increasing the gas flow rate passed 0.3 vvm results in the impeller becoming loaded at $P_{5\%}$, so the impeller speed must be increased if complete dispersion is required. Similarly, above 0.5 vvm the impeller will become flooded at $P_{5\%}$, and the speed must be increased so that $P>P_F$. This will also result in a possibly undesired increased hold-up consequently reducing productivity. It is clear that P_{CD} and P_F for the dual impeller systems is much greater compared to the single impellers. This is due to the equal N_{CD} and N_F requirements irrespective of the number of impellers attached to the shaft. Therefore the single 6RT impeller configuration tends to perform better when flooding/loading is a problem, but is inferior at lower gas rates due to poor recirculation. At lower gassing rates initiating the 3SHP1 in the IDDIDT configuration can reduce the power requirement for a specific hold-up. In addition, as a single Rushton turbine is not noted for its blending efficiency in tall vessels, multiple impellers are commonplace. It is evident however, that a 6RT and 3SHP1 on a common shaft will result in much higher power requirements for gas dispersion and so a separately driven 3SHP1 would prove advantageous. Alternatively, a smaller diameter 3SHP1 could be used at the expense of the improved blending efficiency outlined in Chapter 7.

Using specific power as a basis, the minimum in the curve (point at which $P_{5\%}$ and P_{CD} cross) represents the ideal operating conditions. At gas flow rates where $P_{5\%}<P_F$ energy savings of at least 50% (up to 87%) can be gained by using the IDDIDT compared to the RT-RT or the RT-3SHP1. At gas flow rates where $P_{5\%}>P_F$ the results of IDDIDT and RT-3SHP1 are similar.

5.2.3 Effect of rheology

The influence of rheology was determined using 0.28% CMC, 1% CMC and *Aspergillus niger* fermentation broths. The solutions enabled studies between Reynolds numbers of 1179 and 3.78×10^4, covering an apparent viscosities from 15 to 281 centipoise (mPas).

In contrast to water, a bi-modal bubble distribution was observed in the CMC solutions and fermentation broths. Under flooded conditions, very large spherical cap bubbles, circa 10-20 cm accelerated rapidly towards the surface. On loading, bubble break up occurred creating smaller bubbles of between approximately 1-7 cm diameter. At all times very small bubbles (~1mm) were superimposed on the bulk liquid flow. These small bubbles present a potential error in the measurement of hold-up due to their low rise velocity causing gas retention in the fluid, even after the termination of aeration and agitation. Complete gas disengagement could take up to 16 hours. As CMC solutions degraded with time it was not practical to leave 16 hours between experiments and subsequent experiments were undertaken with the residual bubbles in the fluid.

5.2.3.1 Single impellers

Figure 5.2-11 and Figure 5.2-12 show hold-up as a function of gas flow rate, measured in 0.28% and 1% CMC, for the 6RT and 3SHP1 respectively. The hold-up values in 0.28% CMC were of similar size to those achieved in water. However, the majority of the entrained gas was due to the retention of small bubbles. For the 6RT, increases in gas flow rate or impeller speed had a much lesser effect on hold-up compared to similar changes undertaken with water as the test fluid. Reduced values of the exponents (Table 5.2-3), similar to those reported by Dawson[23] for CMC solutions and Cooke *et al.*[2] for fibre suspensions, support the trends observed. In 1% CMC, increasing the specific power input of a single 6RT had little or no effect on the overall hold-up. The exponent on P_T/V was reduced to 0.04 in this case. Such a phenomena has been reported previously [2,23]. In contrast, the 3SHP1 displayed no change in

the value of α and only a small reduction in the value of β. Similarly, Dawson[23] reported matching P_T/V exponents in water and CMC when using A315 hydrofoil impellers.

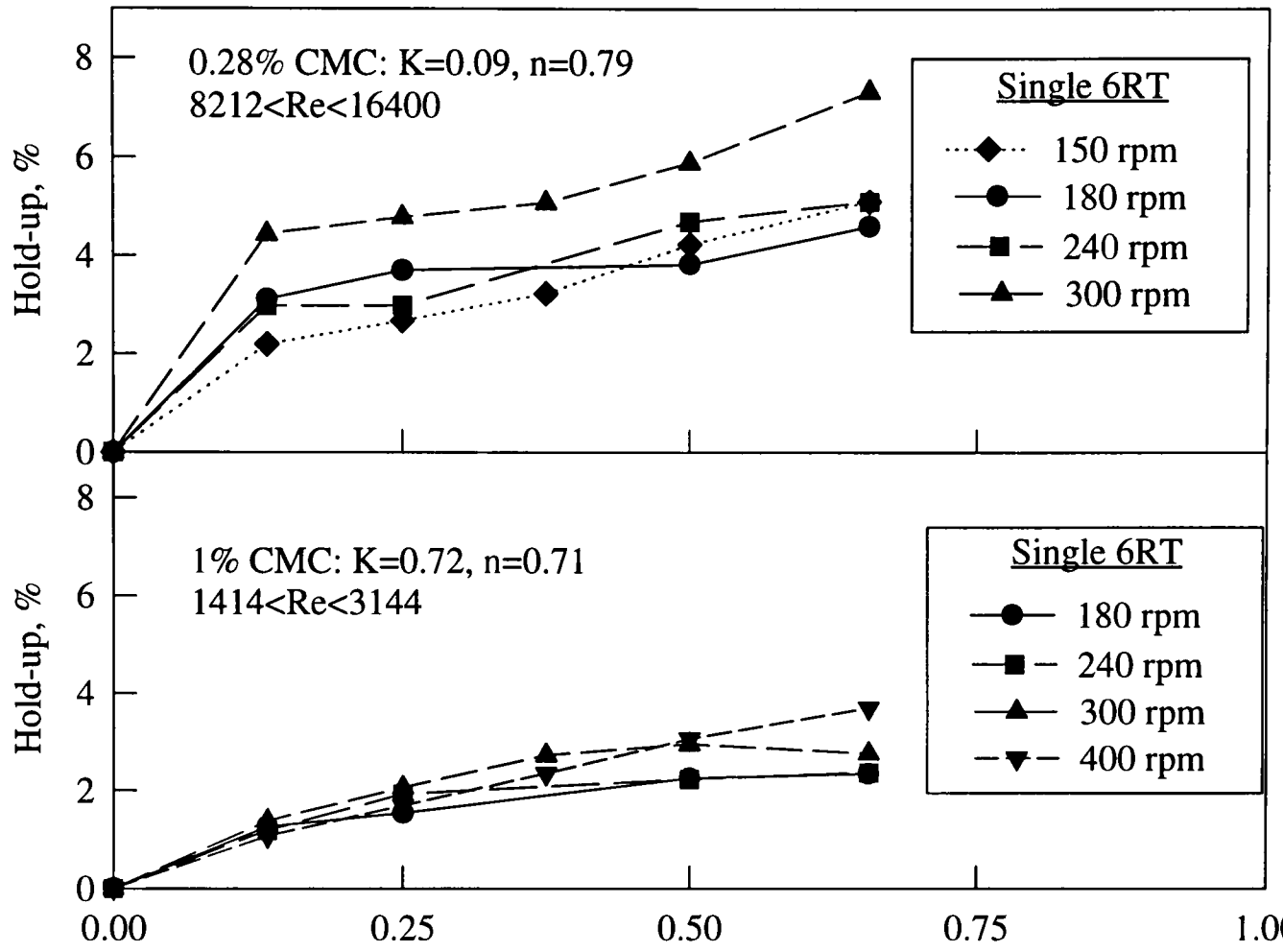

Figure 5.2-11 Effect of viscosity on hold-up; 0.25vvm, 0.5 vvm, single 6RT

Reliable correlations created by combing hold-up data measured using the two CMC solutions were not possible unless an additional viscosity term was included (Table 5.2-3). Inclusion of the viscosity term yielded a statistical improvement of the combined correlation while remaining statistically insignificant compared to the separate equations at each CMC concentration (Appendix III). However, as only two CMC concentrations were used it is not recommended that the correlation be employed as a reliable scale-up criteria. The more negative exponents on viscosity for the 6RT compared to the 3SHP1 were indicative of the greater relative hold-ups achieved by the 3SHP1 when viscosity was increased. Values of δ between -0.25 and -0.44 are in agreement with those reported in the literature (Table 5.1-1(b))

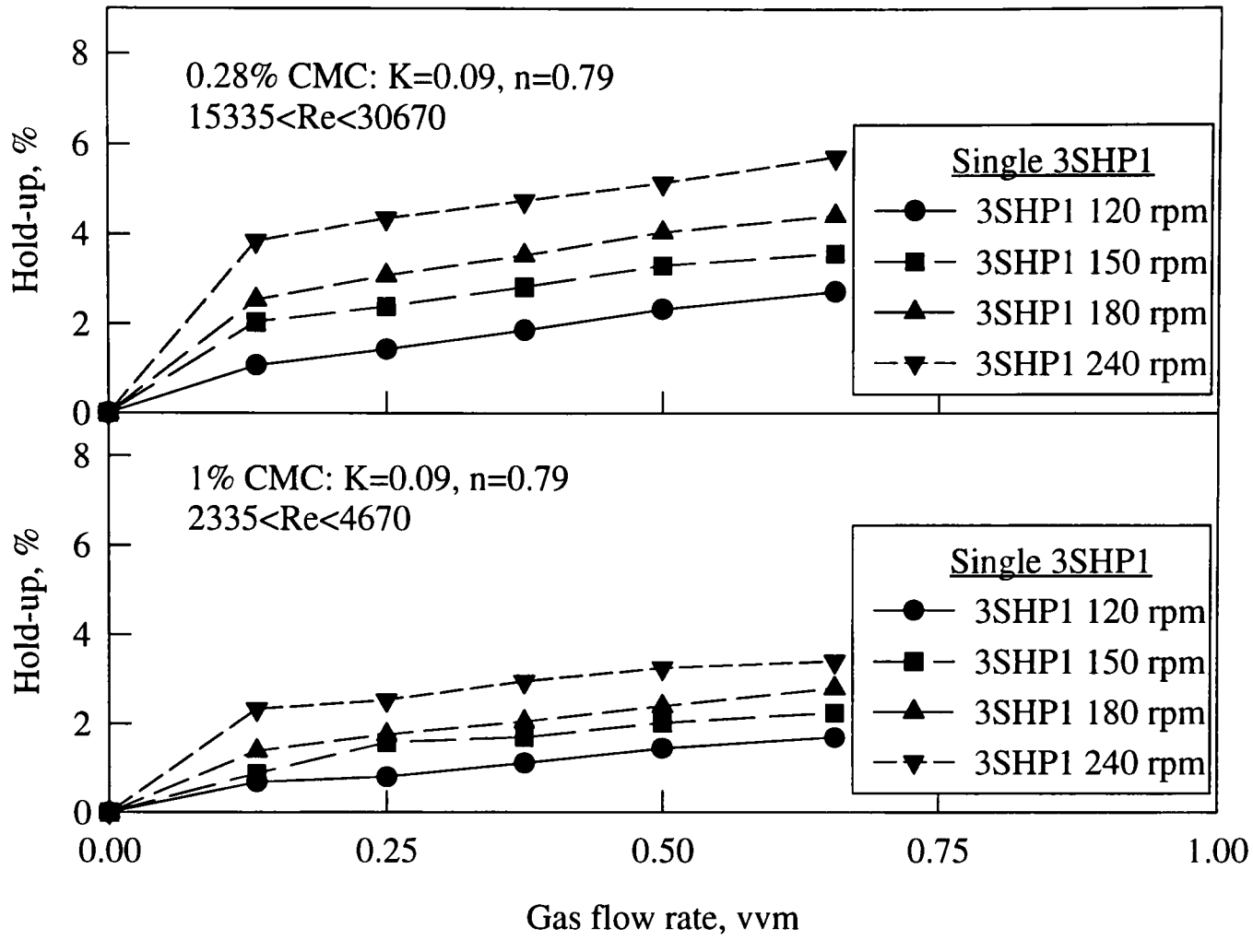

Figure 5.2-12 Effect of viscosity on hold-up; 0.25vvm, 0.5 vvm, single 3SHP1

5.2.3.2 Dual impellers with draft tube (IDDIDT)

Rheology had a similar impact on the performance of the IDDIDT as on the single 6RT and 3SHP1. Figure 5.2-13 shows that broadly similar hold-ups were achieved in 0.28 % CMC in comparison to water, although for the former, the rate of change with increasing gas flow rate or power input was significantly lower and this was reflected in the α and β exponents. As expected, the exponents for IDDIDT lie between the values quoted for the single 6RT and 3SHP1 impellers. Increasing the viscosity further (1% CMC, Figure 5.2-14), resulted in a significant reduction in the hold-up values at similar gas flow rates and impeller speeds. However, in like manner to the single 3SHP1, there was little change in the values of the α and β exponents.

Table 5.2-3 Gas hold-up correlations in non-Newtonian viscous fluids

System	Test Fluid	No. of points	k	a	b	d	r^2	Eqn.
Single 6RT draft tube	0.28%CMC 40-49 mPas	28	14.11	0.14	0.39	-	0.93	5.10
	1.0% CMC 204-257 mPas	23	37.33	0.04	0.65	-	0.97	5.11
	0.28%, 1% CMC	49	42.56	-0.01	0.51	-	0.72	5.12
	0.28%, 1% CMC	49	4.54	0.103	0.41	-0.44	0.94	5.13
Single 3SHP1 draft tube	0.28% CMC 42-49 mPas	24	0.65	0.49	0.29	-	0.97	5.14
	1.0% CMC 290-345 mPas	24	0.52	0.49	0.34	-	0.95	5.15
	0.28%, 1% CMC	48	0.58	0.49	0.32	-	0.66	5.16
	0.28%, 1% CMC	48	0.37	0.47	0.31	-0.26	0.93	5.17
IDDIDT draft tube	0.28%, 1% CMC $41<\mu_a<281$ mPas	205	40.0	0.20	0.30	-	0.93	5.18
	0.28%, 1% CMC $41<\mu_a<281$ mPas	205	2.07	0.20	0.35	-0.39	0.93	5.19
IDDIDT draft tube	*A. niger broths* $15<\mu_a<38$ mPas	54	11.1	0.15	0.20	-	0.53	5.20

The hold-up results recorded using fermentation broths are plotted in Figure 5.2-15. It is evident that hold-up is higher than for water and CMC solutions. This is in agreement with other workers[9,23] when operating at impellers speeds which gave apparent viscosities from 0.8 to 3.7 mPas. The main effect of the increased viscosity was to inhibit coalescence, producing many very small bubbles, thus increasing *a* and hold-up[9,23]. In addition, the fermentation broth contained salts (NH_4SO_4, $MgSO_4$, KH_2PO_4, $MnSO_4$, $FeSO_4$), from the initial medium, and

possibly proteins, produced during the growth phase, which promote coalescence inhibition.

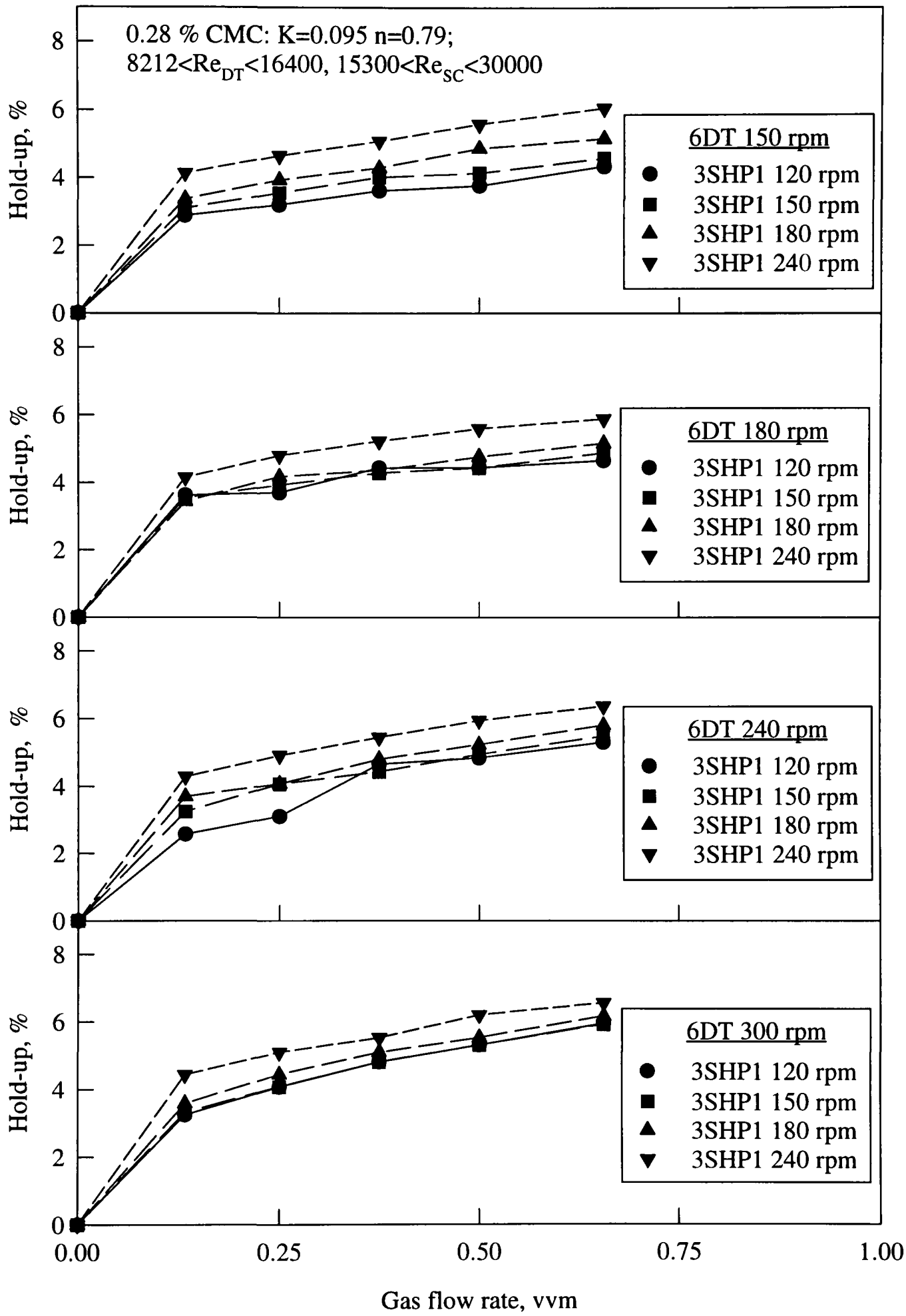

Figure 5.2-13 IDDIDT hold-up in 0.28% CMC solution

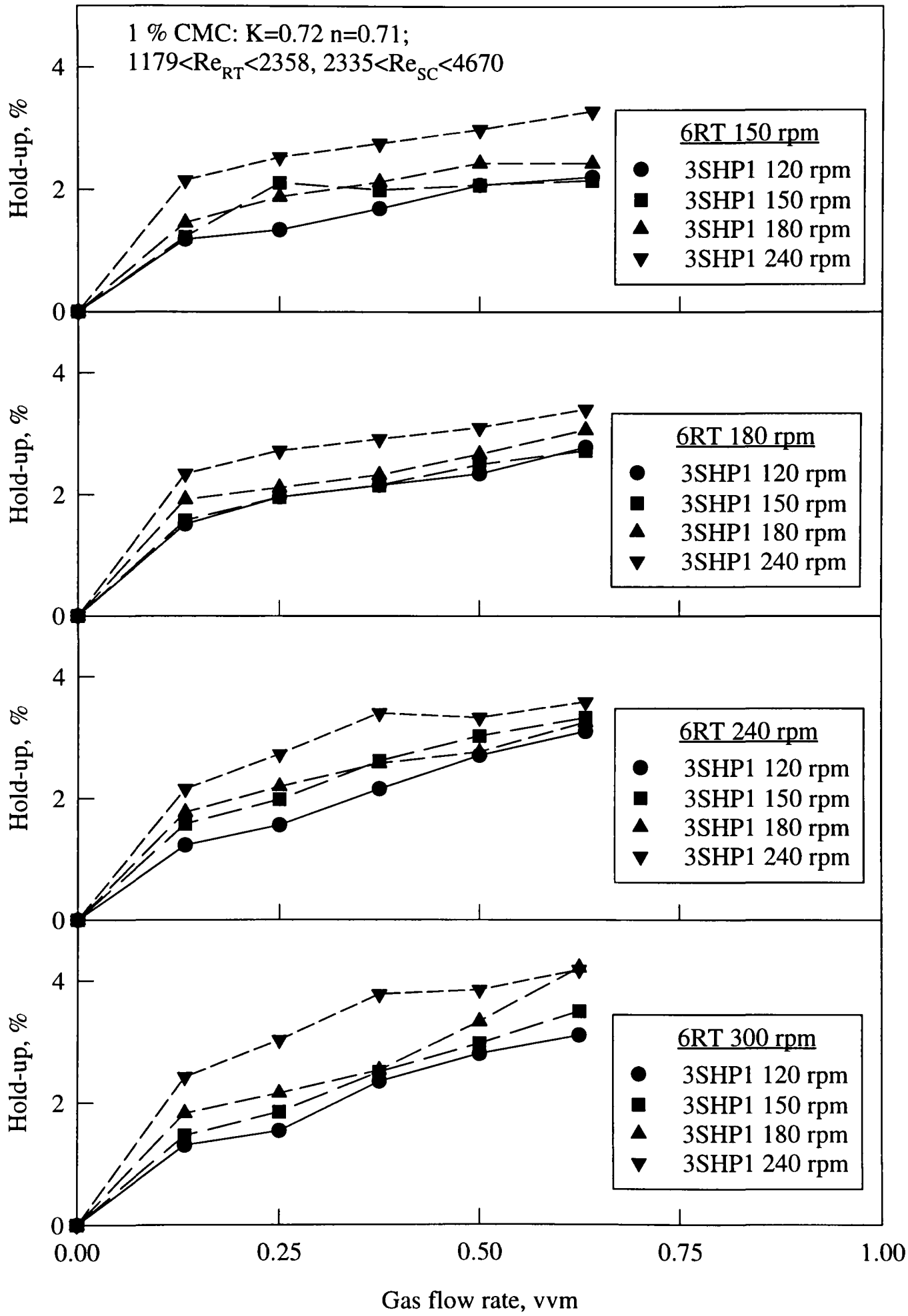

Figure 5.2-14 IDDIDT hold-up in 1% CMC solution

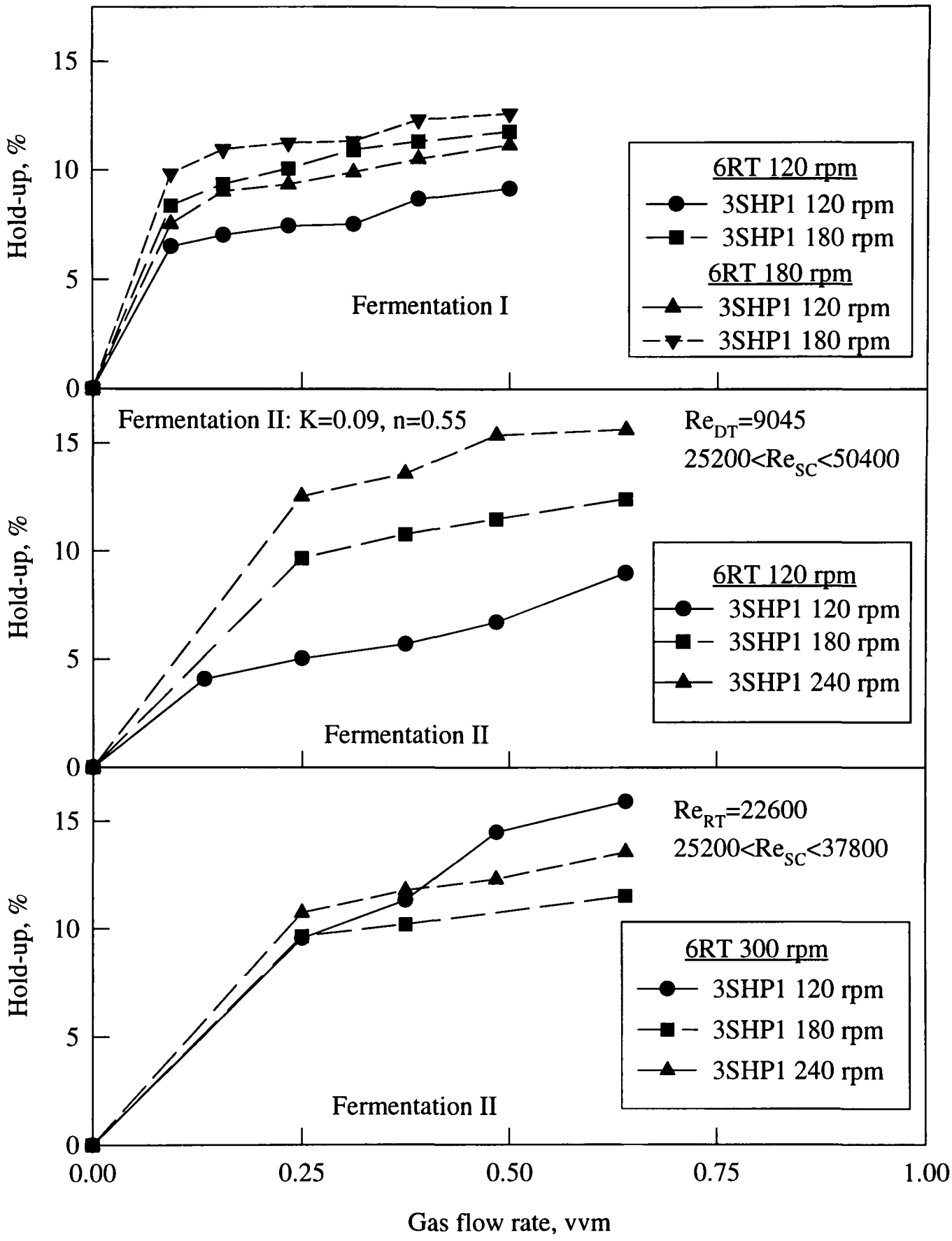

Figure 5.2-15 IDDIDT hold-up in *A.niger* fermentation broths

Under these conditions, a lower proportion of large bubbles were present compared to the 0.28% and 1.0% CMC solutions and consequently the reduction in hold-up encountered with the latter was not apparent. However, the exponents on P_T/V and u_s (Table 5.2-3) were reduced in a similar manner as with the CMC solutions indicating a reduction effect of increasing viscosity. Although CMC solutions provided a good model fluid for the prediction

of the gassed power in fermentation broths (Chapter 4) they were a poor predicter of the gassed hold-up. It is evident that in addition to broth viscocity, the coalescence properties of the fluid must be considered in order to provide a satisfactory imitation. Hence care must be taken when using test fluids to mimic fermentation broth behaviour.

For CMC solutions, a comparison was also made, on a basis of increasing P_T/V, at constant gas flow rates (0.25 vvm, 0.5 vvm), between the single impellers (6RT and 3SHP1) and the IDDIDT configuration (Figure 5.2-16). Firstly, as with water, differences between geometries were most noticeable at the lower gas flow rate. Secondly, over the P_T/V range studied, at 0.5 vvm there was generally little influence of geometry/impeller type on the hold-up achieved at similar specific power inputs. However, proceeding about 0.3W/kg, 6RT hold-up remained constant, whereas the 3SHP1 hold-up continued to rise, suggesting possible improvements, for the latter, at higher specific power inputs. In both CMC solutions at 0.25 vvm and 0.5 vvm distinct trends are apparent. As previously reported for Rushton turbines[24,25], at all gas flow rates and CMC solutions, increasing specific power input led to an initial increase in hold-up which then remained relatively constant. Using the IDDIDT, experiments were undertaken with the 3SHP1 initially redundant and then incrementally increasing the 3SHP1 speed whilst keeping the 6RT speed constant. The first point in each curve corresponded to the value achieved when operating the 6RT singularly and confirmed the reproducibility of the experiments. Switching on the 3SHP1 resulted in a drop in hold-up, to a value similar to that encountered by the single 3SHP1, for the same P_T/V. Any further increases in 3SHP1 speed resulted in a continuation of the trend exhibited by the single 3SHP1. Enhanced hold-up with increasing power input from the 3SHP1 was due to the break up of large spherical cap bubbles (circa 10 cm) to produce smaller more uniform bubbles (circa 6 cm).

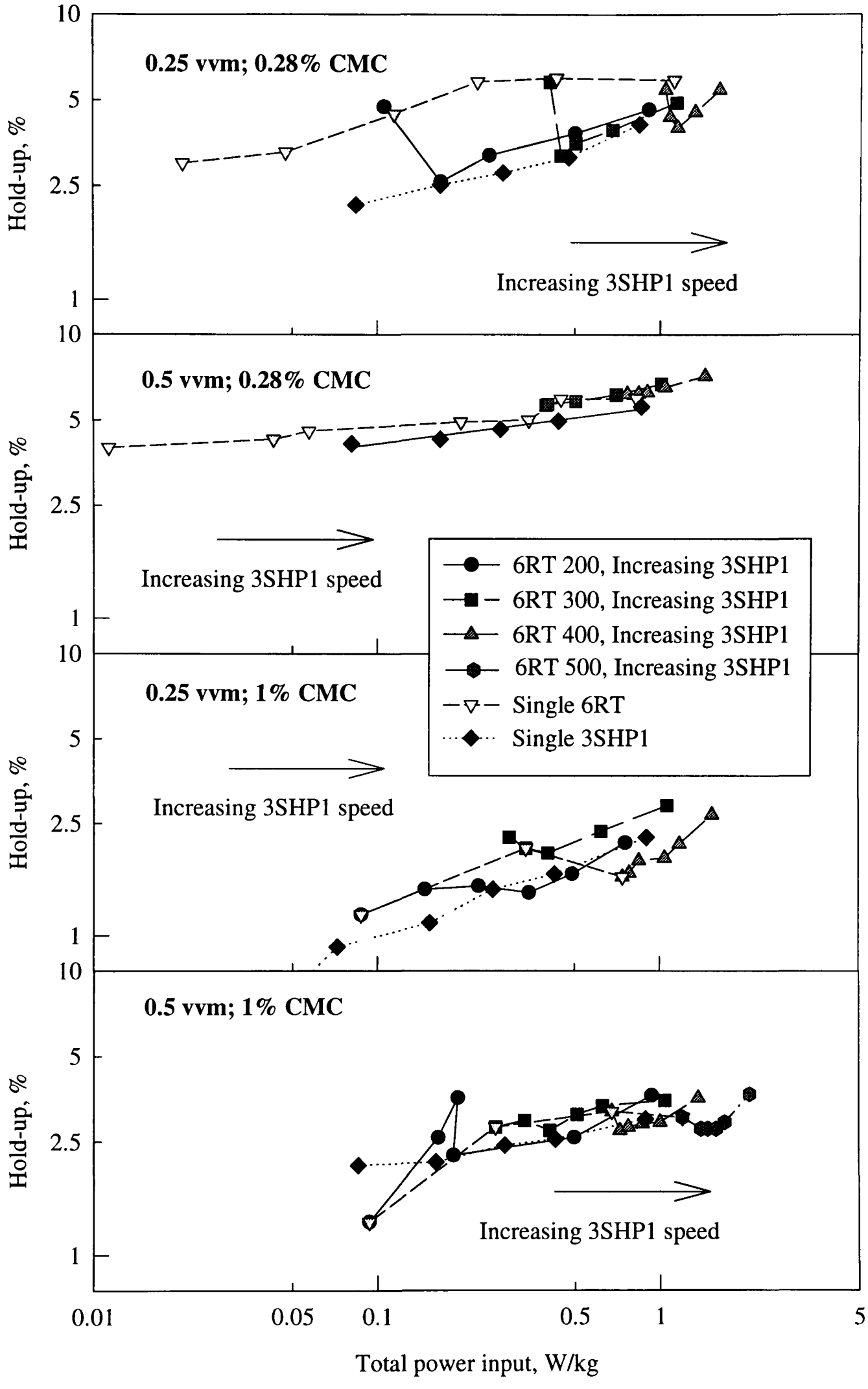

Figure 5.2-16 Hold-up as a function of P/V at 0.25vvm and 0.5vvm; 0.28% and 1.0% CMC

5.3 Conclusions

The hold-up characteristics of the IDDIDT, single 6RT and single 3SHP1 have been coupled to flow patterns and changes in power draw, from which the following can be concluded:

1. Provided gas was dispersed, different impeller types and geometries gave similar hold-ups at 0.5 vvm. However, at lower gas flow rates large discrepancies occurred. Under all conditions the configurations with the draft tube gave the highest hold-ups and the improvement was most marked with the 3SHP1 operational.

2. Increasing viscosity tended to lower hold-up due to the greater amount of large bubbles present. This was reflected in the empirical values of k, α and β. The dependency on viscosity was found to be $-0.26<\delta<-0.44$

3. The hold-up results in water gave exponents which agreed well with the literature values and for the IDDIDT could be satisfactorily predicted from:

$$\varepsilon_G = 17.9\left(\frac{P_T}{V}\right)^{0.30}(u_s)^{0.70}$$

Using two solutions of CMC the following correlation was generated:

$$\varepsilon_G = 2.07\left(\frac{P_T}{V}\right)^{0.20}(u_s)^{0.35}(\mu_a)^{-0.39}$$

however, the equation was not intended for design purposes because only a small range of viscosities was studied.

A less reliable prediction for *Aspergillus niger* fermentation was in the form

$$\varepsilon_G = 11.1\left(\frac{P_T}{V}\right)^{0.15}(u_s)^{0.20}$$

With P_T/V in W/m^3 , u_s in m/s and μ_a in Pas.

4. The flexibility of the IDDIDT system allowed the provision of a required hold-up without the necessity of running the upper impeller at inefficiently high speeds.

5.4 References

1. Chapman, C.M., Nienow, A.W., Cooke, M. and Middleton, J.C., 1983, "Particle-gas-liquid mixing in stirred vessels Part II: Gas-liquid mixing", *Chem.Eng.Res.Des*, 61, 82-89

2. Cooke, M., Middleton, J.C. and Bush, J.R., 1988, "Mixing and mass transfer in filametnous fermentations", *Proc.2nd.Int.Conf.Bioreactor.Fluid.Dynamics.*, BHRA: 37-64

3. Bujalski, W., Konno, M. and Nienow, A.W., 1988, "Scale-up of 45° pitch blade agitators for gas dispersion and solid suspension", *Proc.6th.Euro.Conf.Mixing.*, BHRA:389-398

4. Saito, F., Nienow, A.W., Chatwin, S. and Moore, I.P.T., 1992, Power, gas dispersion and homogenisation characteristics of scaba SRGT and Rushton turbine impellers", *J.Chem.Eng.Japan.*, 25, No.3: 281-287

5. Nienow, A.W., Hunt, G. and Buckland, B.C., 1994, "A fluid dynamic study of the retrofitting of large agitated bioreactors: turbulent flow", *Biotech.BioEng.*, 44: 1177-1185

6. McFarlane, 1991, "Gas-liquid mixing studies on hydrofoil impellers", *PhD thesis*, University of Birmingham, UK

7. Bujalski, W., Nienow, A.W., Sánchez, A., Torres,L. and Galindo, E., 1993 "Hydrodynamics of an independently driven, dual impeller bioreactor for very large scale fermentations", *Industrial Mixing and Scale-up, A.I.Chem.E.Annual meeting*, St. Louis, USA:25-30

8. Greaves, M. and Barigou, M., 1988, "Estimation of gas hold-up and impeller power in a stirred vessel reactor", *Proc.Fluid.Mixing.3. I.Chem.E.Symp.Series.*, No. 108: 235-256

9. Nocentini, M., Fajner, D., Pasquali, G. and Magelli, F., 1993, "Gas-liquid mass transfer and hold-up in vessels stirred with multiple Rushton turbines: water and water-glycerol solutions", *Ind.Eng.Chem.Res.* 32: 19-26

10. Pinelli, D., Nocentini, M. and Magelli, F., 1994, "Hold-up in low viscosity gas-liquid systems stirred with multiple impellers. Comparison of different agitators types and sets", *Proc.8th.Euro.Conf.Mixing.*: 81-88

11. Abradi, V., Rovero, G., Sicardi, S., Baldi, G. and Conti, R., 1988, "Sparged vessels agitated by multiple turbines", *Proc.6th.Euro.Conf.Mixing.*, BHRA, Cranfield: 329-333

12. Whitton, M.J. and Nienow, A.W., 1993, "Scale up correlations for gas hold-up and mass transfer coefficients in stirred tank reactors", *3rd.Int.Conf on Bioreactor.Bioprocess.Fluid.Dynamics.*, BHRG, Cranfield, September: 135-149

13. Nienow, A.W., 1990, "Gas dispersion performance in fermenter operation", *Chem.Eng.Progress.*, Feb: 61-71

14. Allen, D.G. and Robinson, W.R., 1989, "Hydrodynamics and mass transfer in *Aspergillus niger* fermentations in bubble column and loop bioreactors", *Biotech.BioEng.*, 34: 731-740

15. Nienow, A.W. and Elson, T.P., 1988, "Aspects of mixing in rheologically complex fluids", *Chem.Eng.Res.Des.*, 66, Jan: 5-15

16. Christi, M.Y. and Moo-Young, M., 1987, "Airlift reactors: characteristics, applications and design considerations", *Chem.Eng.Comm.*, 60: 195-242

17. Kawase, Y. and Moo-Young, M., 1986, "Influence of non-Newtonian flow behaviour on mass transfer in bubble columns with and without draft tubes", *Chem.Eng.Comm.*, 40: 67-83

18. Koide, K., Horibe, K., Kawabata, H. and Ito, S., "Gas hold-up and volumetric liquid phase mass transfer coefficient in solid suspended bubble column with draught tube", *J.Chem.Eng.Japan.*, 18, No.3: 248-254

19. Margaritis, A. and Sheppard, J.D., 1981, "Mixing time and oxygen transfer characteristics of a double draft tube air lift fermenter", *Biotech.Bioeng.*, 23: 2117-2135

20. Pandit, A.B. and Joshi, J.B., 1983, "Mixing in mechanically agitated gas-liquid contactors, bubble columns and modified bubble columns", *Chem.Eng.Sci.*, 38, No.8: 1189-1215

21. van't Riet, K, 1975, *Ph.D. Thesis*, University of Delft

22. Bakker, A., Smith, J.M. and Myers, K.J, 1994, "How to disperse gases in liquids", *Chem.Eng.*, Dec.

23. Dawson, M.K., 1992, "The influence of agitator type on fluid dynamics and oxygen mass transfer in a pilot scale mixing vessel", *Ph.D. Thesis*, University of Birmingaham, U.K.

24. Solomon, J., Nienow,A.W. and Pace, G.W., 1981, "Flow patterns in agitated plastic and pseudoplastic viscoelastic fluids", Fluid mixing, *I.Chem.E.Symp.Series.,* No. 64: A1-A13

25. Nienow, A.W., 1984, "Mixing Studies on high viscosity fermentation processes - xanthan gums", In: *World.Biotech.Report*, On line publication (London, U.K.), Europe, 1: 293-304

CHAPTER 6

MASS TRANSFER

6.1 Introduction

As mentioned in Chapter 5, mass transfer from one phase to another is of great importance for a number of industrial applications. Dissolved oxygen is an essential substrate for the growth of (and product formation by) micro-organisms in submerged culture processes, and the transfer of oxygen from the gas phase to the liquid phase is therefore of particular interest. This chapter seeks to explain the fundamental theory behind gas-liquid mass transfer, and outline the measurement techniques available.

Results from the previous chapter suggests that, if hold-up can be related to $k_L a$, improved mass transfer performance is achievable using IDDIDT compared to more conventional systems. Therefore, the interdependence between gas hold-up and the volumetric mass transfer coefficient, $k_L a$, has been investigated. In addition, the mass transfer characteristics of the IDDIDT and a dual Rushton turbine (RT-RT) were assessed and compared. In this study, the accuracy, reliability and simplicity of the hydrogen peroxide reduction technique made it the obvious choice for $k_L a$ measurement. In addition, during fermentations "live culture" mass transfer experiments were undertaken to assess mass transfer performance in realistic process fluids.

6.1.1 Theory

The rate of mass transfer, r, across a gas-liquid interface is given by (Treybal, 1968)[1]:

$$r = k_g A\left(p_g - p_i\right) = k_L A\left(C_i - C_L\right) \qquad (6.1)$$

where

k_g is the mass transfer coefficient in the gas phase

k_L is the mass transfer coefficient in the liquid phase

A is the area of contact between the gas and liquid phase

p_g is the partial pressure of transferring species in the gas phase

p_i is the partial pressure of transferring species at the gas/liquid interface

C_L is the concentration of transferring species in the bulk liquid

C_i is the concentration of transferring species at the gas/liquid interface

The interfacial concentrations can be assumed to be in equilibrium and are related by:

$$p_i = H' C_i \qquad (6.2)$$

H' is Henry's Law constant

substituting and re-arranging generates:

$$r = \frac{A\left(\frac{p_g}{H} - C_L\right)}{\left(\frac{1}{Hk_g} + \frac{1}{k_L}\right)} \qquad (6.3)$$

The liquid phase concentration of oxygen which is in equilibrium with the gas phase can be described by:

$$C_L^* = \frac{p_g}{H} \qquad (6.4)$$

Since the diffusion coefficient in the gas phase is much larger than in the liquid phase[1] then,

$$k_g \rangle\rangle k_L$$

$$\frac{1}{Hk_g} \langle\langle \frac{1}{k_L}$$

and equation (6.3) becomes

$$r = k_L A\left(C_L^* - C_L\right) \qquad (6.5)$$

The overall mass flux can be defined as

$$N_A = k_L a\left(C_L^* - C_L\right) \qquad (6.6)$$

where N_A is the amount of transferred species per unit time per unit liquid volume = r/V

a is the specific interfacial area = A/V.

The above equation assumes that all mass transfer resistance lies on the liquid film side and is termed the film theory[2]. Although more complex models, such as the penetration theory[3] and the surface renewal model[4] have been developed, the film theory is used for agitated aerated vessels involving chemical/biochemical reactions because of its simplicity. In fact, all the models have an indirect dependency of k_L on turbulence[34] due to a change in film thickness, particle velocity or renewal rate.

The concentration driving force, $(C_L^*-C_L)$, is influenced by the bulk mixing characteristics, *i.e.* C_L^* and C_L depend on the gas phase and the liquid phase mixing respectively. Liquid phase mixing is controlled by the agitation intensity (P/V), provided the impeller is not flooded. In the completely-dispersed regime, aeration has little effect on the mixing time (Chapter 7). Therefore, it is usually assumed that a well-mixed liquid phase is achieved under all the experimental conditions, *i.e.* C_L is constant spatially throughout the fermenter.

Gas phase mixing is dependent on the residence time distribution (RTD) of bubbles within the reactor. This is affected by impeller type and gas flow rate. Typically, three basic models have been used to describe the RTD:

(i) No-depletion model. Historically, the most common model, it assumes that all the gas bubbles have the same concentration as those in the inlet stream. Thus,

$$C_{Li}^* = \frac{p_{in}}{H'} \qquad (6.7)$$

Its application is satisfactory for small scale, low $k_L a$ systems[5]

(ii) The fully backmixed model. This assumes a perfectly mixed gas phase, *i.e.* all the bubbles in the vessel have the same concentration as those in the exit stream. Therefore,

$$C^*_{Lo} = \frac{p_{out}}{H'} \tag{6.8}$$

and is applicable to small scale, high k_La systems[5].

(iii)Plug flow model. Here the bubbles are considered to flow through the vessel as in a steady state co-current process. As the bubbles travel through the reactor the transferring species (oxygen in this case) diffuse into the liquid. Consequently, the oxygen concentration in the exit is lower than the inlet and the driving force is calculated from the log-mean average of the inlet and outlet concentrations:

$$\Delta C_{LMCD} = \frac{\left(C^*_{Li} - C_L\right) - \left(C^*_{Lo} - C_L\right)}{\ln\left[\frac{\left(C^*_{Li} - C_L\right)}{\left(C^*_{Lo} - C_L\right)}\right]} \tag{6.9}$$

This model is generally the most reliable for large scale mixing processes where poor gas phase mixing occurs.

A two probe technique developed by Chapman *et al.*[6] enabled the calculation of k_La without knowing the gas phase mixing patterns. Using this double response method, Bujalski *et al.*[7] discovered that the no-depletion model over-estimated the driving force and hence under-estimated k_La. The discrepancy was predominant at higher impeller speeds, or power inputs, due to the large amount of recirculation occurring. Similarly, Davies[8] found an under-estimation of k_La when applying the no-depletion model, compared to values obtained using an initial response technique. In addition, Davies[8] discovered that the fully backmixed model produced an over-estimation of k_La. Once again, the deviations from the double response

method were much greater at higher power inputs. A best fit was achieved when applying the plug flow model.

6.1.2 Bubble columns

As previously mentioned (Chapter 4 and 5), the inclusion of a draft tube into bubble columns can significantly effect the hydrodynamics and hold-up characteristics.

Koide *et al.*[9,10] have carried out a significant amount of research into the use of draft tubes. They discovered that inclusion of a draft tube will increase gas hold-up and mass transfer coefficients ($k_L a$) where gas is injected into either the tube or annulus. Conversely, for Newtonian systems, researchers have reported significantly reduced $k_L a$ values when incorporating a draft tube into a bubble column[11,12,13]. Zhao *et al.*[13] suggested that the reduction was due to an increase in circulation rate lowering the gassed hold-up. However, Kawase and Moo-Young[11] observed an increased gassed hold-up coupled with the lower $k_L a$ values and proposed that a combination of effects between the sparger and draft tube was responsible. Dependency of $k_L a$ on the interaction between the gas distribution system and the draft tube was reported by Goto *et al.*[14].

Higher mass transfer coefficients were achieved for bubble columns fitted with a draft tube than for those without. It was proposed that enhanced shear rates due to the introduction of the draft tube yielded a lower apparent viscosity and hence caused the $k_L a$ to increase [11,13].

Kawase and Moo-Young[11] investigated the effect of mechanical agitation in a bubble column with a draft tube. It was found that the introduction of an impeller was effective in improving mass transfer between the gas and non-Newtonian fluids. This was considered to be due to the break up of bubbles rather than an improvement in bulk blending.

6.1.3 Mechanically agitated vessels

The mass transfer performance of stirred vessels has been reviewed previously[15,16]. The majority of workers correlate mass transfer data using the empirical equation:

$$k_L a = C'\left(\frac{P_g}{V}\right)^{\alpha}\left(u_s\right)^{\beta} \qquad (6.10)$$

where $0.3 < \alpha,\beta < 0.8$ for coalescing (water) systems (Table 6.1.3-1). When examining non-Newtonian systems, an apparent viscosity term is usually included:

$$k_L a \propto \left(\frac{\mu_a}{\mu_w}\right)^{\delta} \qquad (6.11)$$

where μ_a is the apparent viscosity (Section 2.1.1.2), μ_w is the viscosity of water and the constant δ lies between -0.33 and -1.17.

This correlation is particularly useful for comparing the mass transfer efficiency of different configurations. There still remains much controversy in the literature regarding the possible increase in mass transfer performance due to changes in system geometry, *e.g.* impeller type, impeller dimensions, inclusion of draft tube (Table 6.1.3-1).

Blakebrough and Sambamurthy[17] reported that, for two phase systems, mass transfer was proportional to the total power input and independent of geometric considerations. However, in three phase systems (air dispersion/paper pulp), $k_L a$ was influenced by the impeller geometry and speed[17]. Nocentini *et al.*[18] found that $k_L a$ values in water were dependent on total power input, and superficial gas velocity irrespective of the number and position of Rushton turbines. In addition, it has been reported that impeller type has no influence on the mass transfer performance, provided similar power inputs and gas superficial velocities are used[7,19]. Conversely, Oldshue *et al.*[20] have shown that, for low viscosity systems, hydrofoils (Lightnin

Table 6.1.3-1 Selection of correlations used to predict mass transfer coefficients

$$k_L a = C'\left(\frac{P_T}{V}\right)^{\alpha} u_s^{\beta}\left(\frac{\mu_a}{\mu_w}\right)^{\delta}$$; ***P/V*** **in W/m^3, u_s in m/s, μ in Pas; F -flat D-dished BV bottomed vessel**

Author	Method	Equipment	Outcome	Correlation constants			
				C'	α	β	δ
van't Riet [31]	Dynamic	6RT	Water	0.026	0.4	0.5	-
Cooke *et al.*[27]	Live culture: Steady state Pseudo steady state Transient	FBV, DBV Single impellers; multiple impellers with combinations of flat/curved blades and hydrofoils	Water, paper pulp and fermentation broth: k_La can be predicted by the correlation to ± 30%	1:1 0.013 3:1 0.0115	0.56 0.50	0.3 0.3	-1 -1
Bakker *et al.*[30]	Not stated	Air-water Single impellers	k_La impeller dependent k_La predicted to ± 30%	0.015	0.6	0.6	
Nocentini *et al.*[18]	Dynamic oxygen electrode	FBV Multiple Rushton turbines (3 and 4)	Overall k_La independent of geometry Water or Water-glycerol	0.015 0.0055 -	0.59 0.62 0.62	0.55 0.4 0.4	-1.17
Pandit *et al.*[25]	Dynamic gassing out	FBV Rushton Turbine, convex bladed mixed flow impeller (CBMF)	k_La impeller dependent Water CBMF RT	0.01 0.025	0.6 0.42	0.57 0.54	
Hickman[21]	Hydrogen peroxide reduction	FBV Rushton turbine	Technique works Water CMC	0.046	0.47 -	0.67 -	-0.6
Cooke *et al.*[22]	Hydrogen peroxide reduction	DBV Rushton turbine, variety of test fluids	Technique works Water	0.00191	0.7	0.3	-

A315) can achieve up to 35% higher $k_L a$ values compared to Rushton turbines at equal energy inputs. Likewise, Zhao *et al.*[23] found mass transfer performance dependent on geometric configurations. In water, for reactors with a draft tube, they found enhanced mass transfer efficiency for turbine/axial combinations compared to axial-axial systems. However, in viscous solutions (CMC) the converse was true[23]. Mass transfer coefficients in non-Newtonian fluids tend to be higher when using axial/mixed flow impellers (as apposed to radial) due to the dependency of $k_L a$ on liquid phase mixing in highly viscous systems[24,25,26]. The increased $k_L a$ performance in these systems has been attributed to lower apparent viscosities [25,26,27], producing larger micromixing regions[26] (the micromixer is defined as the impeller cavern region where high shear rates produce a low viscosity[28]). This can be explained[27]: when retrofitting and scaling up at constant power input, impeller diameter and gas flow rate:

$$k_L a \propto \mu_a^{-\delta} \tag{6.12}$$

and

$$\mu_a \propto \gamma^{(n-1)} \propto N^{(n-1)} \quad and \quad N \propto Po^{-1/3}$$

therefore

$$\frac{k_L a_1}{k_L a_2} = \left(\frac{Po_1}{Po_2} \right)^{-[\delta(n-1)/3]} \tag{6.13}$$

Since δ is negative and n is less than one (for shear thinning fluids as found in fermentations), an inverse relationship between $k_L a$ and Power number (Po) exists. Hydrofoils, axial flow and mixed flow impellers have much lower Power numbers (up to 90% lower) than Rushton turbines and so achieve higher mass transfer coefficients in non-Newtonian viscous solutions, at similar power inputs, gas flow rates and impeller diameters.

However, Bujalski *et al.*[29] observed lower k_La values, at similar energy dissipation rates and gas flow rates, for a counter flow mixing system compared to Rushton turbines despite the former exhibiting a lower apparent viscosity. This questions the possibility of an additional mechanism influencing the mass transfer characteristics, *e.g.* nature of gas dispersion, bulk flow patterns etc..

Design and scale-up correlations have been proposed by Cooke *et al*[27] and Bakker *et al.*[30] claiming k_La prediction to within ±30% for a wide range of scales (0.6 m^3 to 20 m^3) and impeller types (Table 6.1.3-1). However it was stated that, at high gas flow rates, concave-blade impellers give mass transfer rates at least 20% higher than flat-blade turbines[30].

6.2 Mass transfer measurement techniques

As previously explained, the transfer of oxygen between the gas and liquid phases is governed by:

$$\text{Oxygen Transfer Rate } (OTR) = k_L a \, \Delta C$$

Since it is more difficult to measure k_L and a separately they are generally combined and measured as the overall mass transfer coefficient, $k_L a$. Techniques used to determine $k_L a$ can be divided into two categories, dynamic and steady state. The methods have been critically reviewed,[31,32,33,34] and are summarised here.

6.2.1 Dynamic Methods

Dynamic, or transient, methods mostly involve continuous measurement of the liquid phase oxygen concentration after a step-change in the gas concentration. Most frequently, a step-change from nitrogen to air ("gassing out") is employed [12,14,18,25,31,35,36,37]. However, poor estimates of $k_L a$ are encountered due to assumptions about the gas phase mixing. Mathematical models incorporating the gas phase dynamics and oxygen electrode response[32,37,38,39,40] are obligatory for the calculation; their incorrect use can lead to gross errors.

Assumptions of a simultaneous and homogenous change in gas phase concentration throughout the reactor can be satisfied by forcing a global step-change in oxygen concentration (instead of changing feed concentration) due to a small pressure change in the vessel[41,42]. Alternatively, gas phase mixing patterns can be disregarded when using a double response (two probe) technique involving measurement of the exit gas concentration in addition to the liquid concentration [6,7,27,43]. However, in viscous solutions errors still occur due to the presence of small bubbles.

6.2.2 Steady State Methods

In the steady state technique, the dissolved oxygen concentration remains constant while oxygen continuously transfers between the phases. At steady state, the rate of oxygen removal from one phase must equal the rate of generation in the other. In order to remove oxygen from the gas phase the bulk liquid must act as an oxygen sink; or vice-versa. This can be achieved by chemical or biochemical means.

The most widely documented technique is the sodium sulphite oxidation method[17,20,23]. Here, the sulphite reacts with oxygen in the presence of a catalyst to produce sodium sulphate. However, the reagents can alter the physical properties of the liquid, changing the mass transfer characteristics of the fluid under examination. In addition, the reaction rate for the process is difficult to determine, making valid comparisons between systems difficult.

Hickman and Nienow[44] introduced a method using a biochemical oxygen sink whereby oxygen was removed from the liquid phase by respiring yeast. Similarly, Cooke *et al.*[27] used "live culture" mass transfer measurements in addition to transient techniques to form a correlation for scale-up criteria. The $k_L a$ data from both techniques could be predicted to within $\pm 30\%$ by the reported equation (Table 6.1.3-1). More recently, Bujalski *et al.*[29] assessed mass transfer performance for differing impeller systems using *Aspergillus niger* as an oxygen sink. Although these biological systems provide mass transfer data for a realistic process environment, the reproducibility of the fermentations causes a problem. In addition, the costs associated with running a large scale fermentation are rather high.

Other steady state techniques, including absorption of CO_2 [13,45] and oxidation of hydrazine[46] or glucose[47], encounter errors due to unknown reaction rates or because of changing fluid properties during experimentation.

Recently, Hickman[21] has developed a novel technique which eliminates many of the problems encountered by the techniques previously discussed. Here, the bulk liquid contains an oxygen source produced by the continual catalytic decomposition of hydrogen peroxide into O_2 and H_2O. Mass transfer occurs in the reverse direction, *i.e.* from the liquid to the gas phase, but is assumed not to influence the k_La values. Cooke *et al.*[22] have assessed this technique and made suggestions for the optimal experimental conditions needed to accomplish the most accurate k_La measurement. Apart from a slight increase in volume, due to water production, the chemicals have very little effect on the physical properties, and hence, the mass transfer characteristics of the system. However, the activity of the enzyme catalyst (catalase) is reduced by various salt solutions producing an error in the estimation of k_La[22]. Substitution of the catalase with a chemical catalyst (activated manganese dioxide) permitted reproducible results in salt solutions[34].

In this study, the hydrogen peroxide decomposition technique was employed for mass transfer measurements due to its simplistic and reliable nature. In addition, "live culture" k_La measurements were made during fermentations.

6.3 Materials and Methods

The overall mass transfer coefficient, $k_L a$, was measured by the well developed H_2O_2 decomposition technique [25,21,22,34,48]. The theory, materials and method are described in this section.

6.3.1 Theory

The catalytic degradation of hydrogen peroxide produces oxygen and water according to:

$$2\ H_2O_2 \longrightarrow 2\ H_2O + O_2$$

The presence of the catalyst aids the rapid decomposition of H_2O_2. The reaction is first order with respect to peroxide concentration, and independent of catalyst concentration over a wide range, *i.e.*,

$$r = k\left[H_2O_2\right]^1\left[MnO_2\right]^0 \qquad (6.14)$$

Oxygen supersaturation of a previously saturated (aerated) liquid occurs due to the production and dissolution of the molecular oxygen produced by the above reaction. The over-saturation acts as the driving force for mass transfer of oxygen from the liquid into the gas phase. The continuous addition of peroxide to the vessel produces a steady supply of oxygen to the liquid phase. This oxygen is stripped from the liquid by a continuous flow of air through the vessel. After an initial period of hydrogen peroxide and oxygen accumulation steady state is reached. At steady state the rate at which oxygen is produced is balanced by the rate of oxygen transfer from the liquid to the gas phase. Hence,

$$r_d = \frac{Q_{H_2O_2}\left[H_2O_2\right]}{V} \qquad (6.15)$$

and

$$\frac{r_d}{2} = OTR = k_L a \, \Delta C \qquad (6.16)$$

(see Appendix IV for further details).

The oxygen concentration driving force, ΔC, is calculated from the dissolved oxygen concentration in the liquid, C_L, the gas phase concentration, C_G, and the Henrys Law constant, H' (Appendix IV). The value attributed to C_G depends on the mixing model used to describe the gas behaviour (Section 6.1.1). Since oxygen solubility and Henrys constant are temperature dependent and 98.3 kJ/mol of energy is generated from the decomposition of H_2O_2, temperature control is obligatory. Using a simple stainless steel U-tube, with mains water as cooling fluid, it was possible to maintain the temperature at 25.0 ± 0.1°C.

The inlet and exit gas streams from the vessel were linked to an on-line mass spectrometer making it possible to determine $k_L a$ from a mass balance across the reactor, in addition to the method described above (Appendix IV).

6.3.2 Hydrogen Peroxide

Hydrogen Peroxide (BDH Ltd., U.K., 30% w/v) was continuously pumped into the vessel by a peristaltic pump (Watson Marlow) through 4.8 mm bore silicon tubing. The peroxide was discharged into a well mixed zone above the 3SHP1 via a stainless steel tube. Initially the feed rate was calculated by placing the H_2O_2 aspirator on a digital balance (Oertling) and recording the reduction in weight with time. However, under high agitation and aeration conditions more H_2O_2 (and hence a larger aspirator) was necessary, and the flow rate was determined from a pump calibration.

For each set of experiments, a batch of H_2O_2 was made by combining several bottles of peroxide. For each batch, the concentration determined by separate titrations with potassium

permanganate[49] gave a value with an error of ± 0.5%. However, the concentration varied by ± 4.7 % (standard deviation, ± 1.6 % standard error) between batches.

6.3.3 Catalyst

The decomposition of H_2O_2 requires a catalyst. Previously used catalysts include the enzyme catalase[21,33,34] and manganese(IV)dioxide [25,34,48]. In water, under identical operating conditions, k_La was found to be virtually independent of catalyst type[34]. Since the rate of activity deterioration, in electrolyte solutions, with activated manganese (IV) dioxide was much slower than with catalase, MnO_2 was applied as the catalyst. The activity of the catalyst was checked at the start and end of each experiment (Section 6.3.5). A concentration of 0.8 g/l provided sufficient activity for experiments lasting several days[34].

6.3.4 Dissolved oxygen probes

A polarographic probe (Ingold, Mettler Toledo, U.K,) was used to measure the dissolved oxygen concentration. The vertical probe was positioned 1.0 m below the liquid surface, 0.18 m from the vessel wall. Dissolved oxygen concentration was monitored via a control unit (Electrolab, U.K.) connected to a chart recorder. The reading was obtained as a percentage of the saturation value, dissolved oxygen tension (DOT), at the operating conditions. The absolute concentration (mg/l) was found from theoretical saturation values calculated at the operating temperature and pressure (Appendix IV). The flow pattern achieved with the IDDIDT configuration (Chapter 7) ensured that the probe membranes were generally well swept by liquid. However, for a single Rushton turbine, with a less developed flow pattern, anomalies did occur.

For calibration, the probe was initially zeroed (Zeroing gel, Mettler, Toledo, U.K.). Then, it was placed in the vessel and spanned to 100% for the experimental agitation and aeration

conditions. Between each set of experiments, the probe was removed from the vessel and the membrane and electrolyte checked for damage and air bubbles respectively.

6.3.5 Typical experimental procedure

All experiments were undertaken with de-ionised water as the test fluid. Before each experiment, the probe was left to soak in a beaker of aerated water, to moisten and check the membrane. It was then zeroed using the gel and rechecked. Once the temperature of the vessel had reached 25°C, the probe was mounted and spanned to 100%. A typical experiment followed a similar sequence of steps to those described by Dawson[33] and Thomas[34] and is outlined below (Figure 6.3-1):

1. Set experimental agitation and aeration conditions; allow dO_2 to reach equilibrium; and span probes (100%) for at least 5 minutes.
2. Add 0.8 g/l of MnO_2. Stop aeration.
3. Prime pump and pipelines with H_2O_2. dO_2 rises sharply, cease pumping. dO_2 continues to increase until all peroxide is broken down and then the value falls slowly.
4. Start aeration. dO_2 drops rapidly to 100%. Respan probe if necessary.
5. Start timer and peroxide pump. dO_2 increases until a suitable peroxide induced value is reached ($130\% < dO_2\% < 300\%$). Allow between 15 minutes (0.5 vvm) and 25 minutes (0.1 vvm) to get a steady state value.
6. Cease pumping. Record aspirator weight and time, adjust N, Q_G and/or pump speed.
7. Repeat steps 5 and 6 for the range of experimental conditions.
8. Adjust N, Q_G and pump speed to initial conditions. dO_2 should reach the same equilibrium value.

9. Cease pumping. dO_2 drops to saturation value (100%).

Adding MnO_2 (at step 2) allowed a check of the catalyst activity. This was essential if experiments were conducted over a long time period. Re-running the initial experiment (step 8) checked for a drop in catalytic activity over the time course of the experimentation. The peroxide induced equilibrium should attain the same value as the first experiment. If a similar value is not obtained, catalyst activity has dropped and the set of experiments (steps 2 to 8) should be repeated.

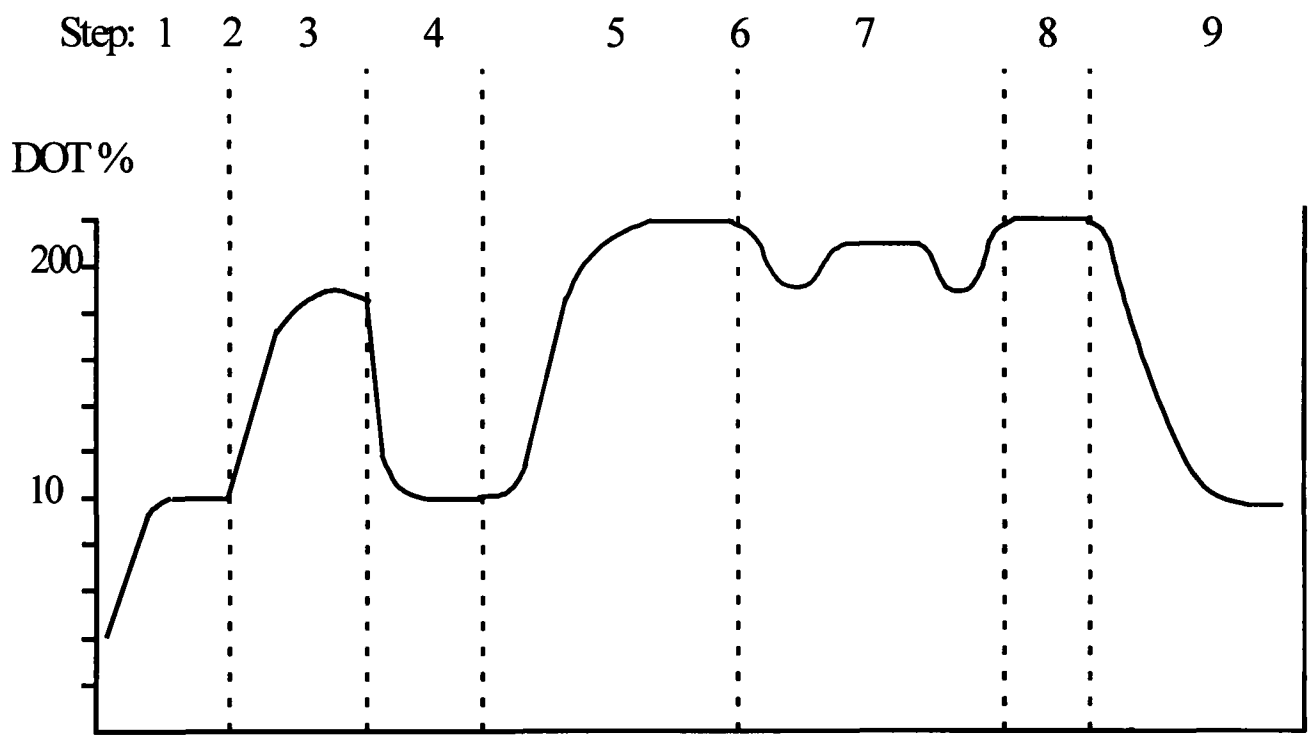

Figure 6.3-1 Schematic transient of the dissolved oxygen concentration for a typical experiment

6.4 RESULTS and DISCUSSION

6.4.1 Results in water

6.4.1.1 Dual Rushton turbines; no draft tube

The volumetric mass transfer coefficients for constant gas flow rates (0.1 vvm, 0.25 vvm and 0.5 vvm) and increasing impeller speeds (and power inputs) are shown in Figure 6.4-1. For each condition the $k_L a$ was calculated using the fully back mixed model (FBM) and the plug flow model (PFM). In addition, results obtained from the oxygen balance over the reactor and those evaluated from the peroxide pumping rate are compared. The agreement between the $k_L a$ values obtained from the gas phase mass balance and the pumping rate verified the accuracy of the technique for determining the oxygen production rate. During experimentation, continuous analysis was made between the two methods of calculation, and any discrepancies highlighted possible problems occurring. A check of the equipment and procedures could then be made and any problematic experimental conditions rectified and repeated. Data was also collected for a constant power input of ~ 1W/kg and an increasing gas flow rate (Figure 6.4-3).

6.4.1.1.1 Gas-phase mixing model

The mass balance across the reactor showed that the oxygen concentration in the exit stream was considerably higher than in the inlet. Therefore, the no-depletion (strictly the "no-enhancement") model would severely under-estimate $k_L a$ and so has not been considered here. Figure 6.4-1 shows $k_L a$ values determined from the fully backmixed model (FBM) and the plug flow model (PFM). As expected, the FBM generally produced higher values compared to the PFM. At low energy inputs both models give similar results with significant deviations occurring at higher power inputs. The deviation was especially noticeable at the lower gas

flow rate. In fact, over the power range investigated the results were almost identical to Davies[8], suggesting that any further increase in power input would result in a change in functionality when using the FBM. Since the PFM matched the results from the double response method most closely in the work of Davies, it is assumed that the PFM will give the best representation of the gas phase mixing in this work also. Therefore, any further results or comparisons in $k_L a$ were calculated from a driving force based on a plug flow model of the gas phase mixing.

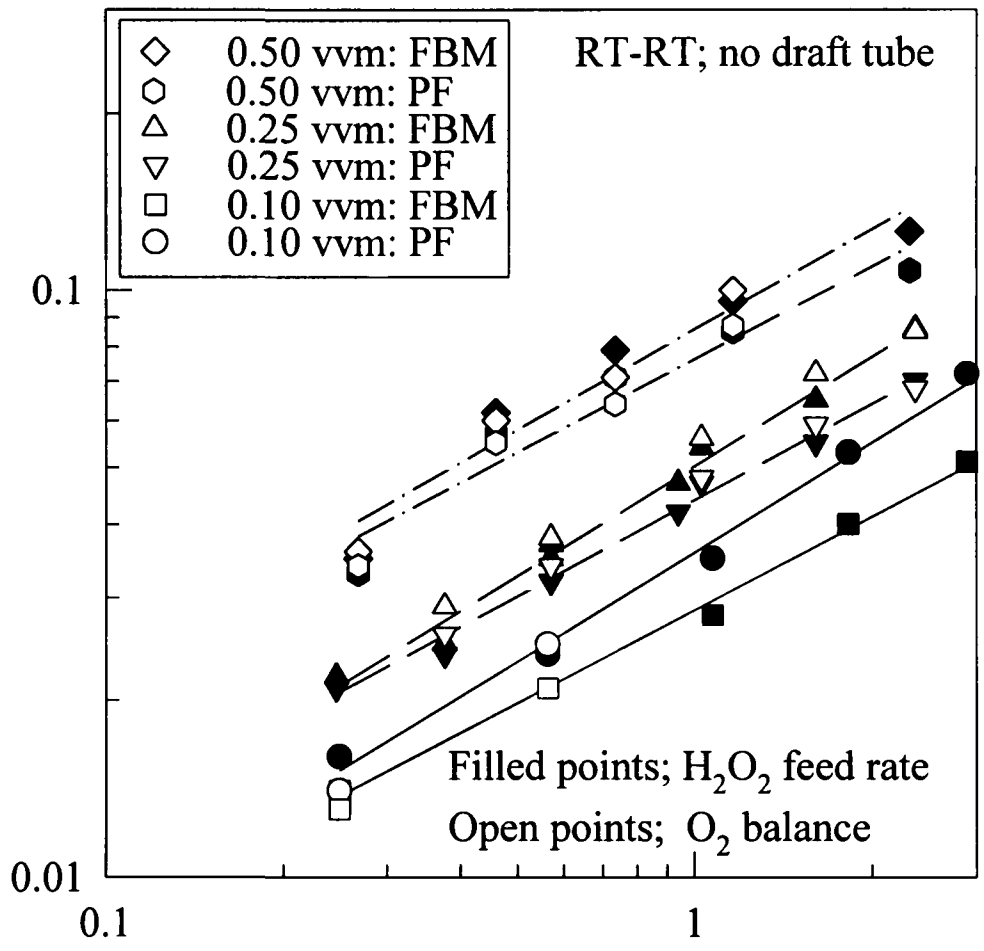

Figure 6.4-1 Mass transfer coefficient as a function of power input in water for RT-RT configuration

6.4.1.1.2 Mass transfer coefficients for RT-RT

It can be seen that the $k_L a$ values increase with increasing power input and gas flow rate (Figure 6.4-1). The best fit for the data was and is shown in (Figure 6.4-2):

$$k_L a = 0.040\left(\frac{P_T}{V}\right)^{0.50}\left(u_s\right)^{0.64} \qquad (6.17)$$

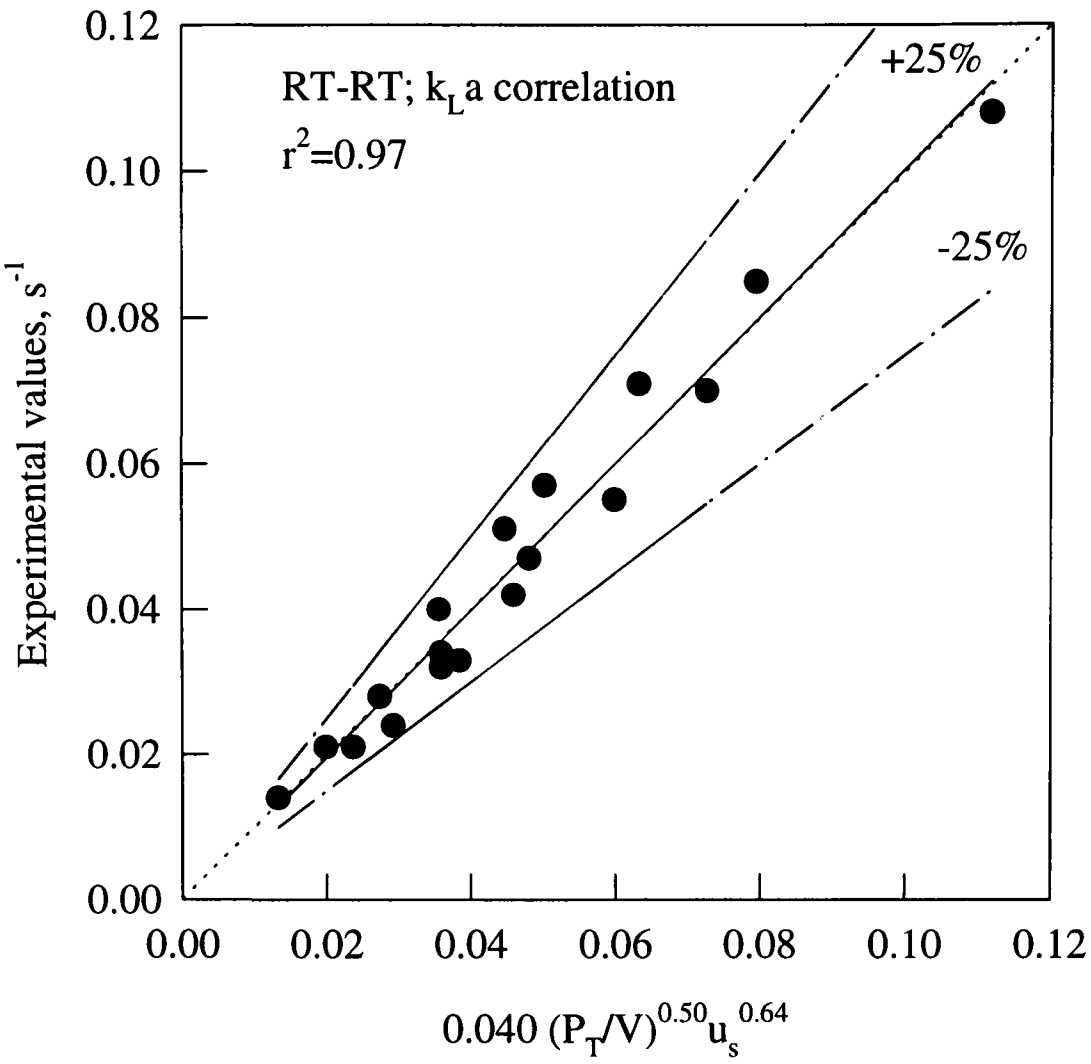

Figure 6.4-2 Mass transfer correlation (Equation (6.17)) for RT-RT in water

which compares favourably with many of the correlations published in the literature (Table 6.1.3-1). A regression coefficient, r^2, of 0.967 confirms a good fit of the experimental data to the correlation (average error = 8.9%). It is evident that the rate of change of $k_L a$ with changing power input is independent of the gas flow rate (Figure 6.4-1).

Hold-up experiments conducted simultaneously, described in Section 5.2.2, show very similar trends to those observed for mass transfer. Although hold-up and mass transfer were both dependent on power input and gas velocity, the relative proportionalities differed. Superficial gas velocity, u_s, had a much greater effect on hold-up compared to $k_L a$, *i.e.* $\varepsilon_H \propto (u_s)^{0.95}$ whereas $k_L a \propto (u_s)^{0.64}$. Conversely power input had a greater impact on the mass transfer compared to the hold-up, *i.e.* $\varepsilon_H \propto (P_T/V)^{0.25}$ whereas $k_L a \propto (P_T/V)^{0.50}$. This can be hypothetically explained through bubble size distributions. Hold-up and a are related by[18]

$$a = 6\frac{\varepsilon_G}{d_B} \times \frac{1}{100} \tag{6.18}$$

where d_B is the mean volume to surface area bubble size (*i.e.* Sauter mean diameter). Since a must be equal under specific operating conditions, the differences in the functionality between hold-up and $k_L a$ must stem from a difference in k_L which in turn depends on d_B. Therefore,

$$\frac{k_L}{d_B} \propto \frac{k_L a}{\varepsilon_H} \propto \left(\frac{P_T}{V}\right)^{0.25} (u_s)^{-0.31}$$

Assuming the the liquid film coefficient is unaffected by the gas flow rate then it follows that $d_B \propto u_s^{0.31}$, *i.e.* increasing the gas flow rate at constant energy inputs produces bubbles with higher volume to area ratios. Similarly, $k_L/d_B \propto (P_T/V)^{0.25}$ and assuming that for a given system[50] d_B is approximately proportional $(P_T/V)^{-0.4}$, then k_L is a weak function of specific power input ($\propto (P_T/V)^{-0.15}$), *i.e.* increasing the impeller speed / power input slightly reduces the liquid film coefficient. Such a phenomena has been reported previously[18,34].

6.4.1.2 IDDIDT

Mass transfer for IDDIDT was assessed for gas flow rates from 0.1 to 0.5 vvm and power inputs between 0.1 and 1.3 W/kg. For clarity data calculated from the backmixed model have been excluded. As expected, the FBM gave higher $k_L a$ values than the PFM (data not shown) and so, as previously mentioned (Section 6.4.1.1.1), the PFM was used for all the calculations.

6.4.1.2.1 Mass transfer coefficients for IDDIDT

Figure 6.4-3 shows $k_L a$ as a function of gas flow rate for a constant power input of approximately 1W/kg.

$$a = 6\frac{\varepsilon_H}{d_B} \tag{6.18}$$

where d_B is the mean volume to surface area bubble size (*i.e.* Sauter mean diameter). Since a must be equal under specific operating conditions, the differences in the functionality between hold-up and $k_L a$ must stem from a difference in k_L which in turn depends on d_B. Therefore,

$$\frac{k_L}{d_B} \propto \frac{k_L a}{\varepsilon_H} \propto \left(\frac{P_T}{V}\right)^{0.25} (u_s)^{-0.31}$$

Assuming the the liquid film coefficient is unaffected by the gas flow rate then it follows that $d_B \propto u_S^{0.31}$, *i.e.* increasing the gas flow rate at constant energy inputs produces bubbles with higher volume to area ratios. Similarly, $k_L/d_B \propto (P_T/V)^{0.25}$ and assuming that for a given system[50] d_B is approximately proportional $(P_T/V)^{-0.4}$, then k_L is a weak function of specific power input ($\propto (P_T/V)^{-0.15}$), *i.e.* increasing the impeller speed / power input slightly reduces the liquid film coefficient. Such a phenomena has been reported previously[18,34].

6.4.1.2 IDDIDT

Mass transfer for IDDIDT was assessed for gas flow rates from 0.1 to 0.5 vvm and power inputs between 0.1 and 1.3 W/kg. For clarity data calculated from the backmixed model have been excluded. As expected, the FBM gave higher $k_L a$ values than the PFM (data not shown) and so, as previously mentioned (Section 6.4.1.1.1), the PFM was used for all the calculations.

6.4.1.2.1 Mass transfer coefficients for IDDIDT

Figure 6.4-3 shows $k_L a$ as a function of gas flow rate for a constant power input of approximately 1W/kg.

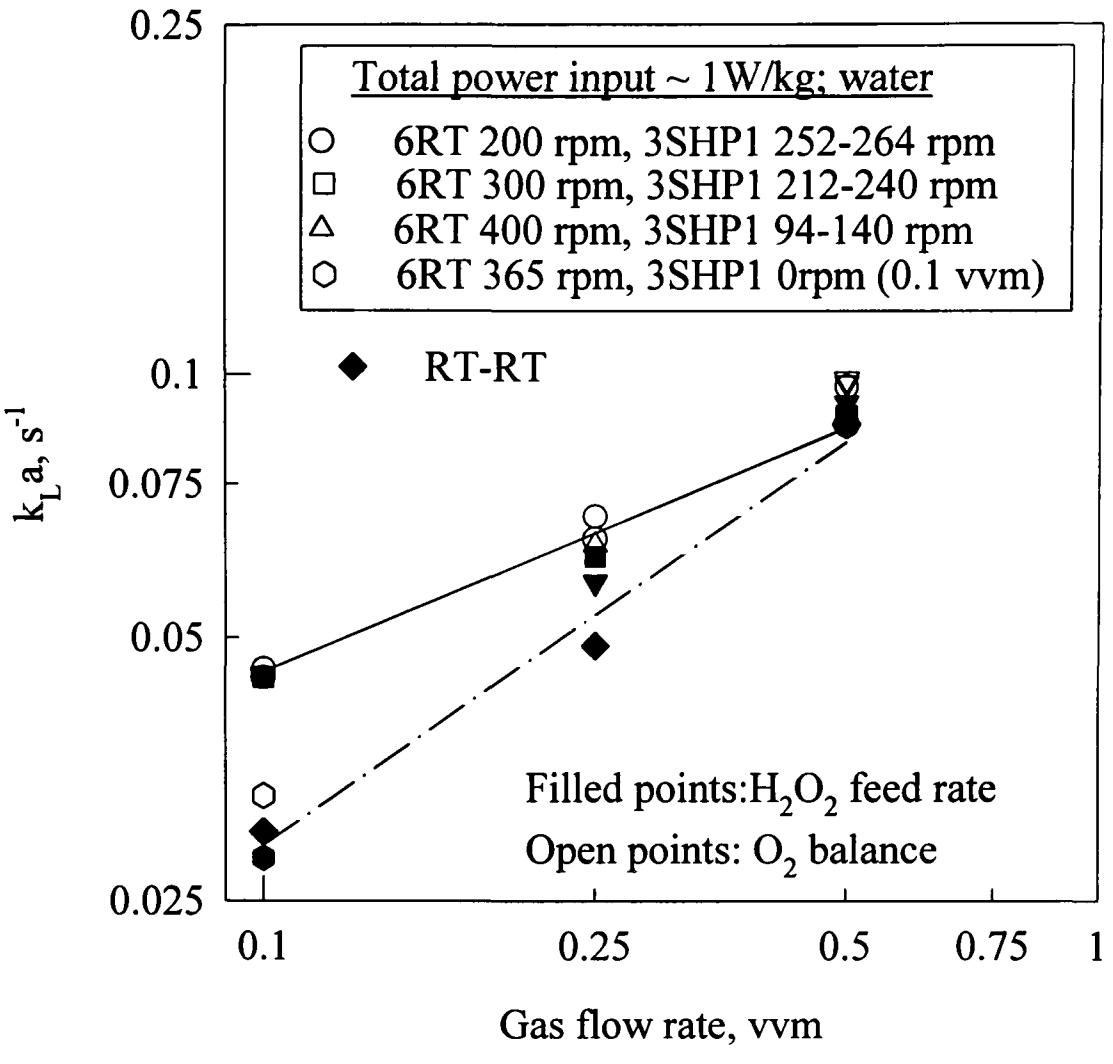

Figure 6.4-3 Mass transfer coefficients, in water, at increasing gas flow rate and constant power input of 1W/kg

At each gas flow rate, the 6RT speed was maintained at either 200, 300 or 400 rpm and the 3SHP1 speed altered so that the total power input was 1 W/kg. In addition one run was done with the 3SHP1 off and the 6RT at 365 rpm and 0.1 vvm to give an equal P/V value of 1W/kg. In agreement with Bujalski *et al.*[7], Nocentini *et al.*[18] and Martin *et al.*[19], it is clear that, for IDDIDT, the mass transfer performance is proportional to the total power input to the system regardless of which impeller type is inputting the majority of the power. However, the single 6RT gives lower k_La values, similar to those encountered for the RT-RT configuration. This implies that gas recirculation due to the action of the 3SHP1 is of paramount importance. In addition, scattered data obtained at constant gas flow rates and various impeller speeds (Figure 6.4-5 to Figure 6.4-7) suggested that there may be some dependency of k_La on impeller type. Mass transfer and hold-up values were affected similarly when changing the power input from

the 3SHP1 at constant 6RT impeller speeds, *i.e.*, the slope for a constant 6RT speed of 400 rpm and increasing 3SHP1 speed was greater than that for 200 rpm and increasing 3SHP1 impeller speed, for both the $k_L a$ and the hold-up. However, for the experimental range studied, this dependency was not statistically significant (F-test) therefore the data was correlated in the traditional manner (Figure 6.4-4), *i.e.*,

$$k_L a = 0.0038\left(\frac{P_T}{V}\right)^{0.7}\left(u_s\right)^{0.4} \qquad (6.19)$$

giving a regression coefficient of $r^2 = 0.81$ (average error = 14.8%) and values of α and β in agreement with those found in the literature (Table 6.1.3-1).

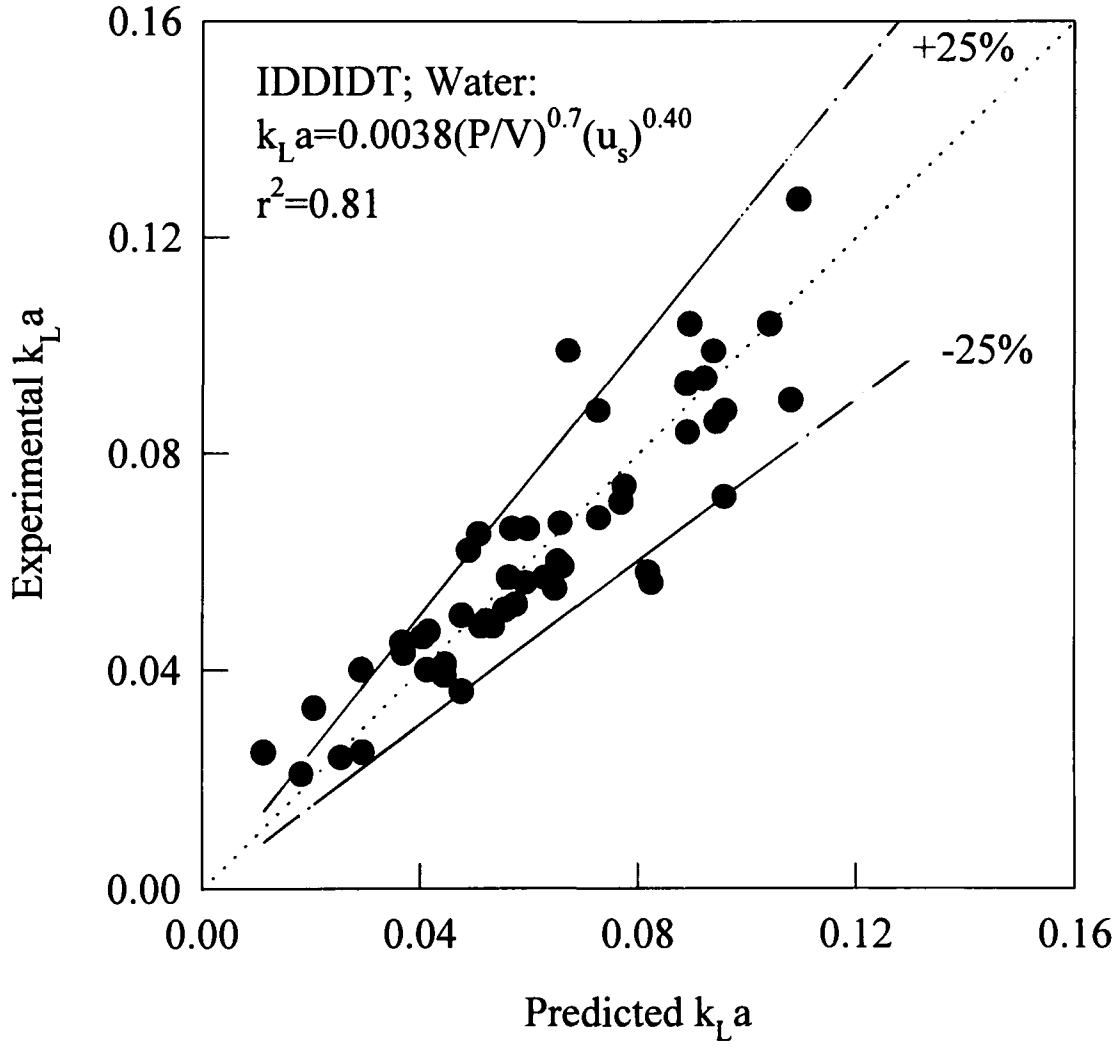

Figure 6.4-4 Mass transfer correlation for IDDI in water

As with the dual Rushton turbines, $k_L a$ was affected to a lesser degree compared to hold-up for any changes in superficial gas and to a greater degree for any changes in power input. In fact,

comparison of Figure 6.4-5 and Figure 6.4-6 shows that there is very little difference between the k_La's obtained with IDDIDT at 0.1 vvm and those obtained at 0.25 vvm. As described earlier, the discrepancy between k_La and hold up can be described by bubble size distributions (Section 6.4.1.1.2). Thus, for the IDDIDT

$$\frac{k_L}{d_B} \propto \frac{k_L a}{\varepsilon_H} \propto \left(\frac{P_T}{V}\right)^{0.40} (u_s)^{-0.3}$$

As with the RT-RT configuration, assuming no effect of gas flow rate on k_L, the mean area-volume ratio, d_B, is proportional to $u_S^{0.3}$. However, in contrast to the RT-RT configuration, changing the power input apparently has little effect on k_L (if $d_B \propto (P_T/V)^{-0.4}$).

6.4.1.3 Comparison between k_La values for RT-RT and IDDIDT

The mass transfer measurements in water for the RT-RT and IDDIDT are compared in Figures 6.4-3 to 6.4-7. In addition, comparisons with literature correlations have been made.

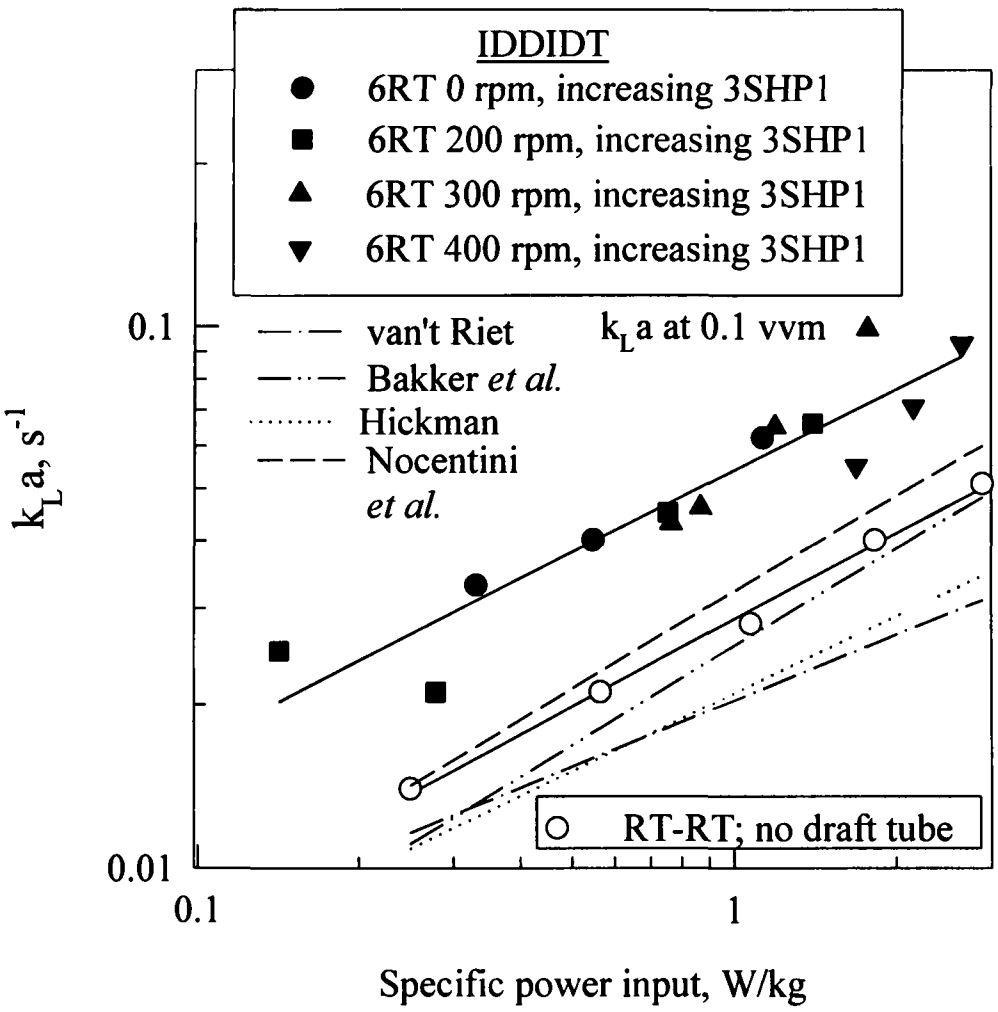

Figure 6.4-5 k_La, at 0.1 vvm, as a function of power input for the RT-RT and IDDIDT; Refs- Table 6.1.3-1

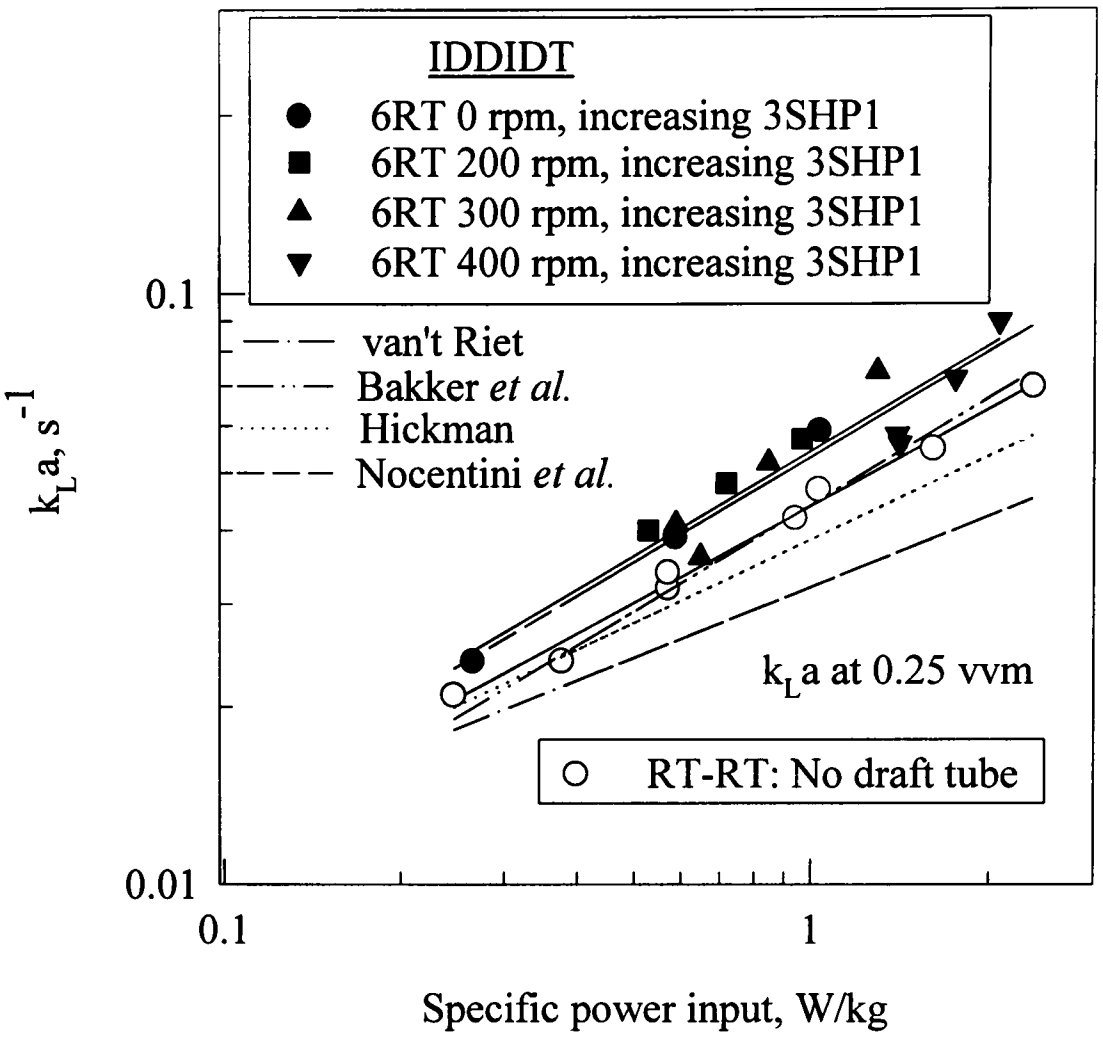

Figure 6.4-6 k_La, at 0.25 vvm, as a function of power input for the RT-RT and IDDIDT; References as Table 6.1.3-1

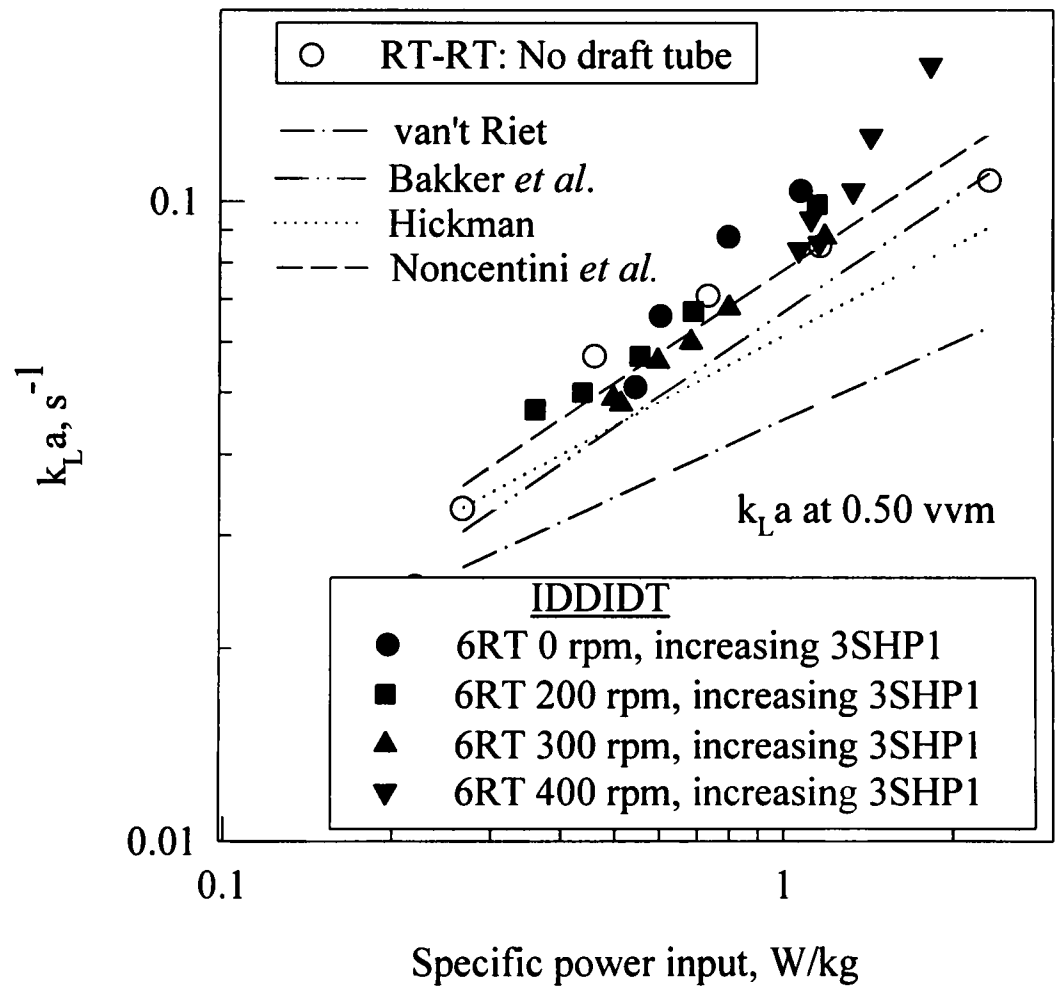

Figure 6.4-7 k_La, at 0.5 vvm, as a function of power input for the RT-RT and IDDIDT; References as Table 6.1.3-1

It has already been shown that k_La is a function of power input and superficial gas velocity for both the RT-RT and the IDDIDT configurations (Section 6.4.1.2.1 and Section 6.4.1.1.2). However, it is evident that the P_T/V exponent is dependent on the geometry of the system. The RT-RT configuration exhibits $k_La \propto (P_T/V)^{0.50}$ whereas for the IDDIDT $k_La \propto (P_T/V)^{0.7}$. This is in agreement with Dawson[33] who reported an exponent of 0.51 for a single Rushton turbine compared to 0.7 for a single hydrofoil. The difference could be explained by the dependency of k_L on power input for the RT-RT configuration ($\propto (P_T/V)_{RT}^{-0.15}$). In addition, since $(\varepsilon_H)_{RT} \propto (P_{RTRT}/V)^{0.25}$ and $(\varepsilon_H)_{IDDIDT} \propto (P_{IDDIDT}/V)^{0.30}$ the remaining difference was possibly due to a higher rate of change of interfacial area, a, with increasing power input for the IDDIDT.

At gas flow rates of 0.1 vvm and 0.25 vvm, for similar energy inputs, the k_La values are significantly higher for the IDDIDT compared to the RT-RT system and the majority of literature based correlations. In addition, the increase in k_La values were of similar magnitude to the increase in hold-up values recorded under the same conditions. This implies that the enhanced mass transfer (for the IDDIDT) is due to an increase in interfacial area, possibly caused by increased bubble recirculation into the draft tube by the action of the 3SHP1 impeller. At higher gas flow rates (0.5 vvm) the values of k_La and ε_H obtained with the IDDIDT were similar to those for RT-RT configuration. This suggests that the interfacial area was equal for both systems. The inefficiency of the IDDIDT is not unexpected, since it has been reported [51] (Chapter 4) that between gas flow rates of 0.3 to 0.4 vvm the 3SHP1 enters the "low pumping capacity regime" and consequently draws less gas into the draft tube, hence lowering a.

Combining the data obtained from both configurations produced a best fit of:

$$k_L a = 0.0102\left(\frac{P_T}{V}\right)^{0.587}(u_s)^{0.447} \qquad (6.20)$$

In comparison with equation (6.17) for the RT-RT, equation (6.20) over-predicts $k_L a$ by 20% on average. In fact, equation (6.17) is statistically different (and better than) equation (6.20) at the 99.5% significance level (Appendix III). Therefore, $k_L a$ was not conclusively independent of geometry. However, due to the scattered data obtained for the IDDIDT, there is no statistical difference between equation (6.20) and equation (6.19), although, on average, $k_L a$ was under-predicted by about 10%.

Generally, at low gassing rates, experimental $k_L a$ values for the IDDIDT configuration were higher than those predicted by the literature correlations, suggesting improved mass transfer performance. The correlation of van't Riet severely underestimated $k_L a$ because gas phase O_2 depeletion was not assumed by the dynamic technique. However, the correlation of Noncentini *et al.*[18] produced a reasonable fit at gas flow rates of 0.25 and 0.5 vvm.

6.4.2 "Live culture" mass transfer experiments

In order to determine whether the improvements in mass transfer would be realised in viscous fermentation systems it was decided to undertake "live culture" experiments using *Aspergillus niger* broths. Since fermentation broths tend to be highly viscous and non-Newtonian in behaviour, $k_L a$ is dependent upon the liquid phase mixing[24,25,26]. In addition to the increased $k_L a$'s in water, the well defined flow patterns of the IDDIDT, provide good bulk blending, (Chapter 6) and hence suggests possible improvements in mass transfer efficiency[26].

The rheological and biological properties of the *A.niger* fermentation broths have been described elsewhere (Chapter 9). The final biomass concentrations and rheological properties of the two fermentations (RT-RT and IDDIDT) differed. Therefore a comparison has been

drawn between the experimental k_La values for the IDDIDT and the predicted k_La values evaluated from correlations for the RT-RT (see below).

6.4.2.1 Dual Rushton turbines (RT-RT)

It can be seen from Figure 6.4-8 that, as with water, k_La was a function of the gas flow rate and total power input to the system. However, due to the increased viscosity, the absolute values were at least 50% lower than encountered in water.

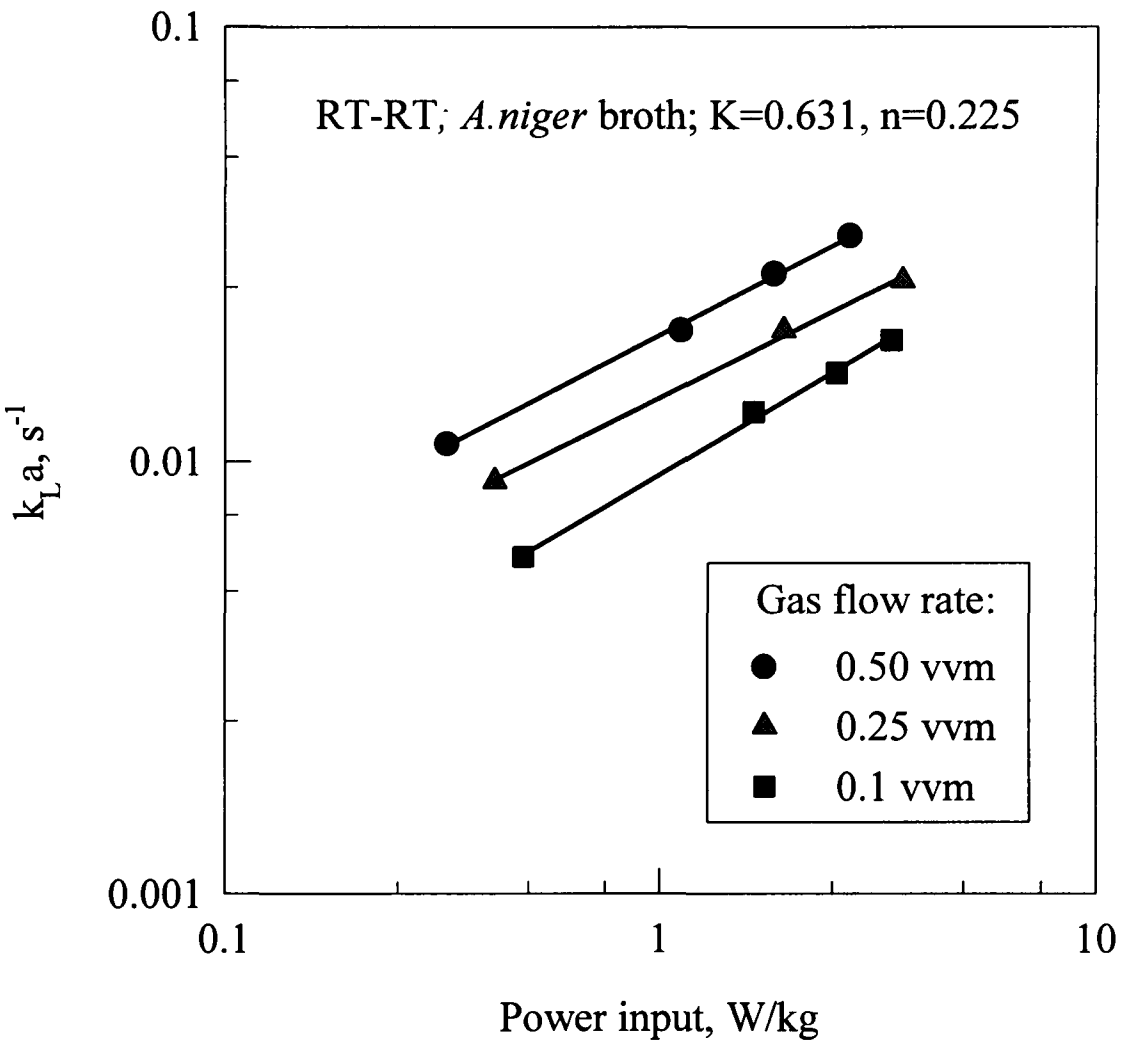

Figure 6.4-8 Live culture k_La values for RT-RT

The data was correlated in two ways. Firstly an extremely good fit (r^2=0.99, average error 3.42%) was provided by the correlation:

$$k_La = 0.0025\left(\frac{P_T}{V}\right)^{0.55}(u_s)^{0.41} \qquad (6.21)$$

However, the equation is system specific and doesn't permit the prediction of k_La's in fluids of differing viscosities. It appeared more reasonable to update the original correlation, made with water as the test fluid, by including an apparent viscosity term (Figure 6.4-9). It was found that adjusting for viscosity such that

$$k_L a \propto \mu_a^{-0.4}$$

produced only a marginal reduction in the regression coefficient (r^2=0.97) and the change was statistically insignificant (Appendix III), *i.e.*,

$$k_L a = 0.0025\left(\frac{P_T}{V}\right)^{0.50}(u_s)^{0.64}(\mu_a)^{-0.40} \qquad (6.22)$$

As the effect of viscosity was not studied in depth, the use of the correlation for scale-up is not justified. However, it was useful for comparing the performance of then RT-RT and the IDDIDT configurations (see later).

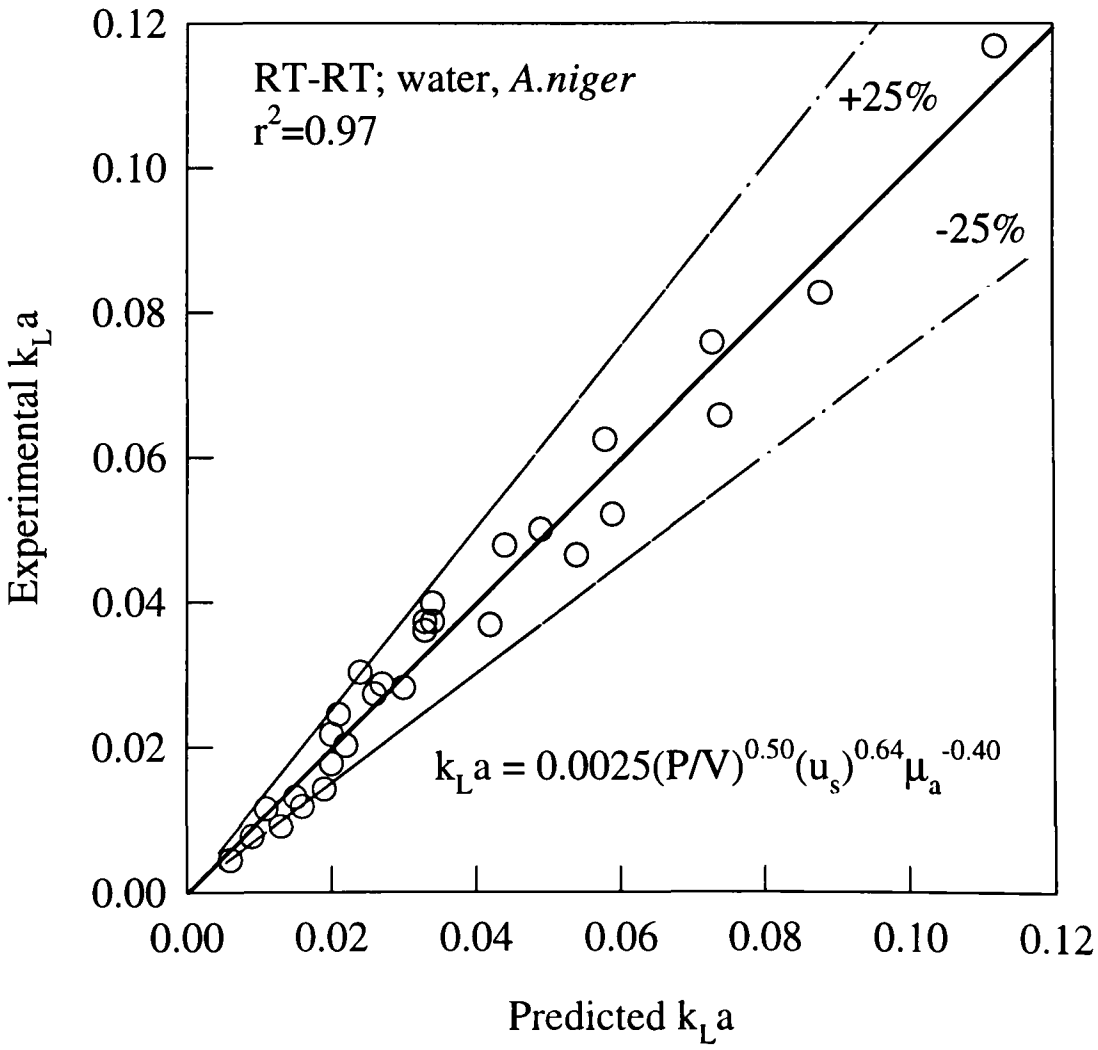

Figure 6.4-9 Updated RT-RT correlation to include apparent viscosity term

6.4.2.2 IDDIDT

The mass transfer coefficients evaluated using *A.niger* fermentation broth (K=0.22, n=0.20) were found to be proportional to the gas flow rate and the power input irrespective of which impeller was inputting the majority of the power (Figure 6.4-11). However, in contrast to the results using water, the single 6RT gave similar k_La values to IDDIDT (based on Equation (6.22)). This implies that, in viscous solutions, the 3SHP1 impeller may be in the "low pumping capacity regime" due a change in gas cavity structure behind the blades. Once again, an apparent viscosity term was added to the original correlation, giving

$$k_La = 0.00029\left(\frac{P_T}{V}\right)^{0.70}(u_s)^{0.4}(\mu_a)^{-0.4} \qquad (6.23)$$

and producing a slightly improved regression coefficient of 0.87 compared to Equation (6.19). Once again, the addition of the viscosity term was form comparative purposes only and was not intended for scale-up criteria.

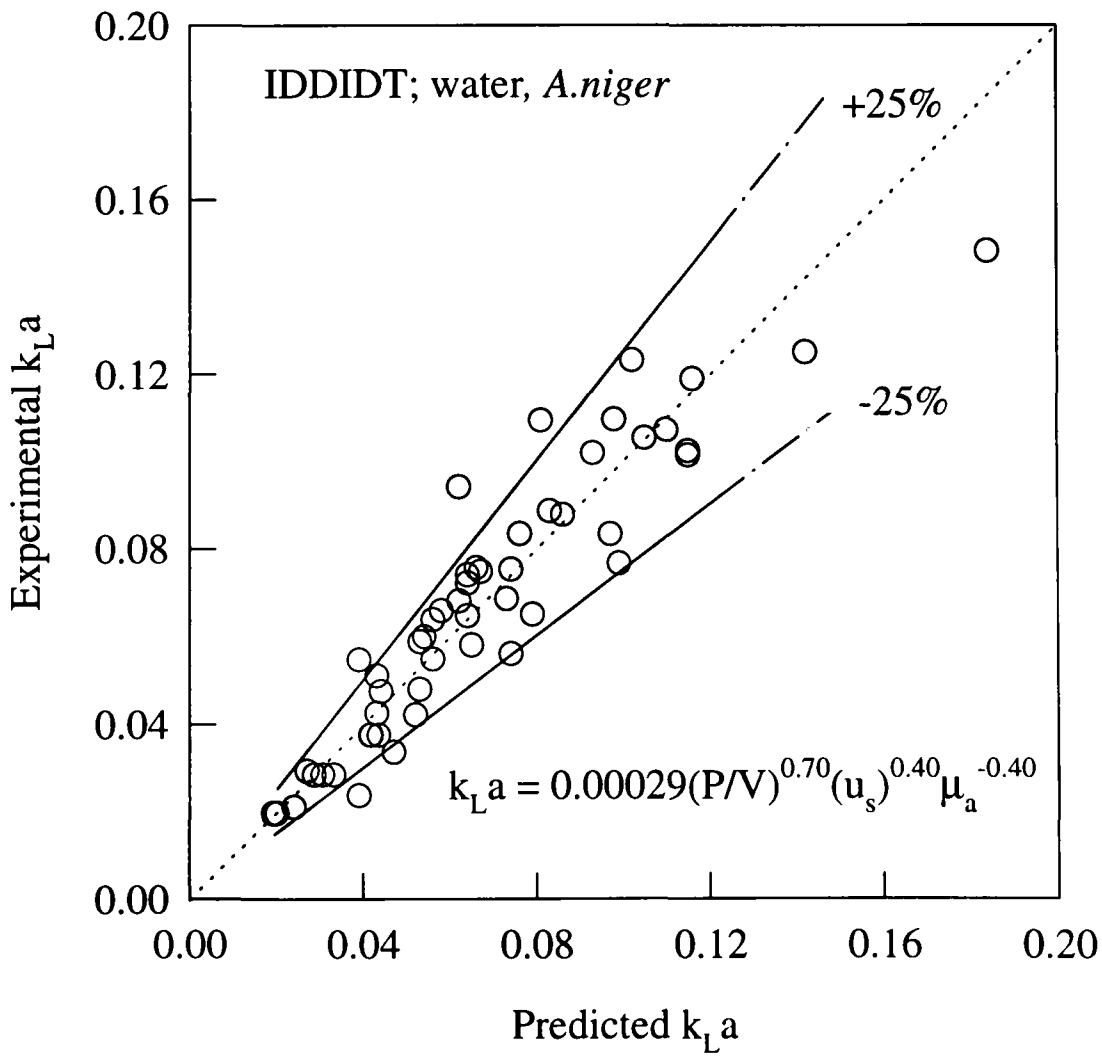

Figure 6.4-10 Updated correlation for IDDIDT including apparent viscosity term

6.4.2.3 Comparison between RT-RT and IDDIDT in A.niger fermentation broths

The mass transfer measurements, made in *A.niger* fermentation broths, are compared in Figure 6.4-11. The experimental k_La values for the RT-RT configuration were lower then in the IDDIDT system. However, the final viscosity of the RT-RT fermentation was approximately 3 times that of the IDDI fermentation. The k_La values for the RT-RT, in the lower viscosity fermentation broth, were therefore predicted by adjusting the experimental values accounting for the change in apparent viscosity ($k_La \propto \mu_a^{-0.4}$). This enabled a direct comparison to be made.

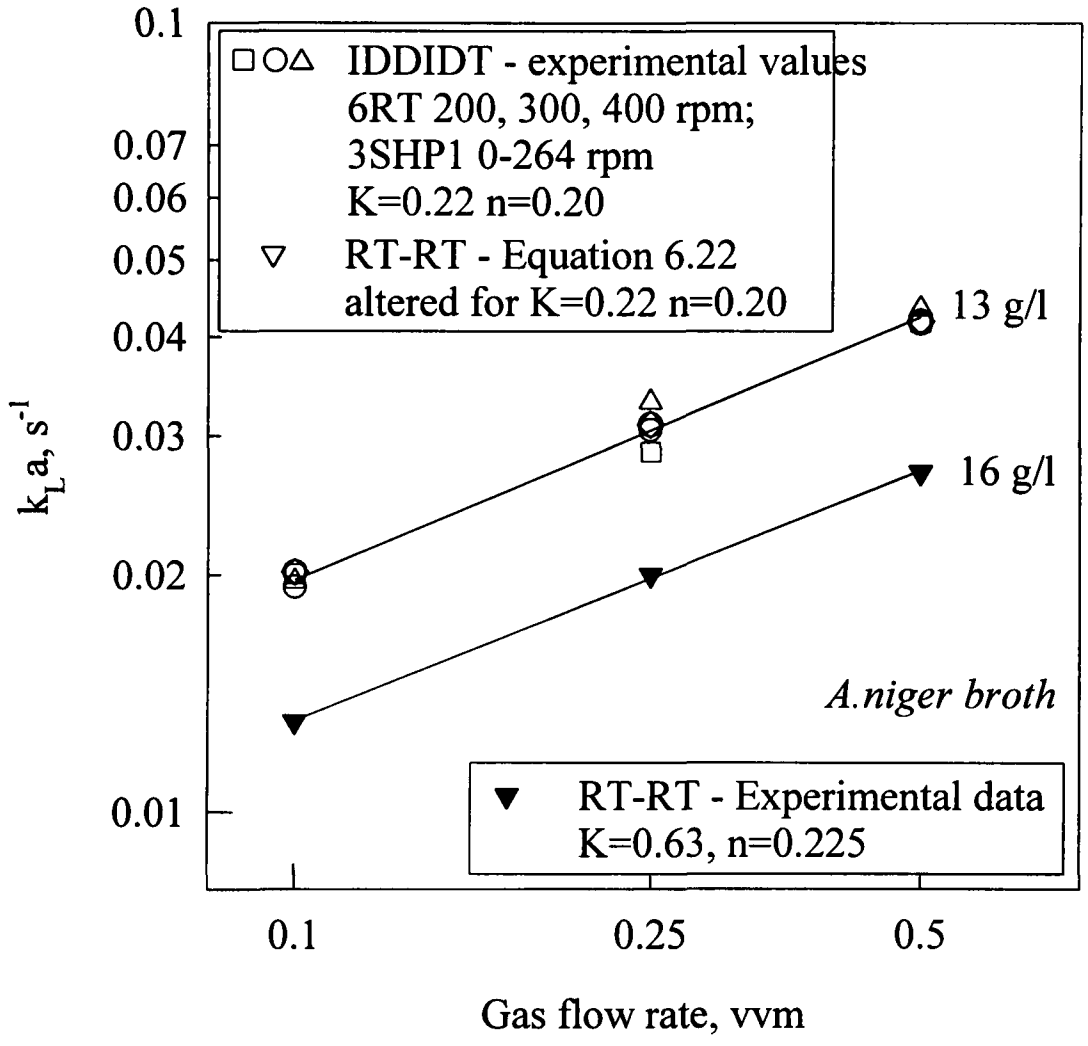

Figure 6.4-11 Comparison of k_La's between RT-RT and IDDIDT in *A.niger* fermentation broth.

It is evident that, in viscous *A.niger* fermentation broths, k_La was independent of impeller type and system geometry. Mass transfer data for all geometric configurations and test fluids can be correlated with the equation:

$$k_L a = 0.0006\left(\frac{P_T}{V}\right)^{0.57}(u_s)^{0.44}(\mu_a)^{-0.43} \qquad (6.24)$$

although, in comparison with individual equations, a lower regression coefficient is generally achieved (r^2=0.79). In addition, Equation (6.24) is statistically different from Equation (6.22) for the RT-RT configuration (Appendix III). However, the best-fit correlation for IDDIDT (Equation 6.23) is not statistically different from Equation (6.24) (also Appendix III). It is once again noted that as only a limited range of viscosities was studied the above correlation should not be used for design or scale-up.

6.5 Conclusions

Experiments in water suggest an improved mass transfer performance when using a dual mixed flow impeller system with draft tube compared to:

1. a single Rushton turbine with draft tube,

2. a dual Rushton turbine system with no draft tube.

Most researchers [7,8,16,27,22,32,33] have reported that k_La is independent of geometry but evidence from this study suggests that, at low gassing rates, k_La in water is very much dependent on the geometry of the system. However, for the IDDIDT, the k_La was not influenced by the impeller type as long as similar power inputs and gas flow rates were achieved. The increased efficiency of IDDIDT was due to the 3SHP1 drawing a large quantity of gas into the draft tube, hence increasing the specific interfacial area. The improvement only occurred when the 3SHP1 was operating in the "high pumping capacity regime" and was not realised in *Aspergillus niger* fermentation broths. In this case k_La was dependent upon the gas flow rate and the total power input to the system in a similar way irrespective of impeller type or system geometry.

6.6 References

1. Treybal, R.E., 1968, "Mass transfer operations", 2nd Ed., McGraw-Hill Kogakusha Ltd.
2. Lewis, W.K., and Whitman, W.G., 1924, "Principles of gas absorption", *Ind.Chem.Eng.*, 16: 1215
3. Higbie, R., 1935, "The rate of absorption of a pure gas into a still liquid during short periods of exposure", *Trans.A.I.Chem.E.,* 31: 365
4. Danckwerts, P.V., 1951, "Significance of liquid-film coefficients in gas absorption", *Ind.Chem.Eng*, 43, No 6: 1460-1467
5. Nienow, A.W., 1992, EFB Course, *Bioreactor Engineering, Euro.Federation.Biotechnol.Working.Party. and on measurement and control.*, Isle of Alberalla, Italy, Boris Kidric, Ljubijana, Slovanja: 209-229
6. Chapman, C.M., Gibilaro, L.G. and Nienow, A.W., 1982, "A dynamic response technique for the estimation of gas-liquid mass transfer coefficients in a stirred vessel", *Chem.Eng.Sci.*, 37: 891-896
7. Bujalski, W., Nienow, A.W. and Huoxing, L., 1990, "The use of upward pumping 45^0 PBT impellers in 3 phase reactors", *Chem.Eng.Sci.*, 45, No 2: 415-421
8. Davies, S.N., 1986, "The evaluation of gas-liquid mass transfer coefficients in gas sparged agitated vessels", *PhD Thesis,* University College London, UK
9. Koide, K., Horibe, K., Kawabata, H. and Ito, S., 1985, "Gas hold-up and volumetric liquid phase mass transfer coefficient in solid suspended bubble column with draught tube", *J.Chem.Eng.Japan.*, 18, No.3: 248-254
10. Koide, K, Horibe, K., Kitaguchi, H. and Suzuki, N., 1984, "Contributions of annulus and draught tube to gas-liquid mass transfer in bubble column with draught tube", *J.Chem.Eng.Japan.*, 17, No.5: 547-549
11. Kawase , M. and Moo-Young, M., 1986, "Influence of non-Newtonian flow behaviour on mass transfer in bubble columns with and without draft tubes" *Chem.Eng.Commun.*, 40: 67-83
12. Wu, W. and Wu, J., 1990, "Airlift reactor with net draft tube", *J.Ferment.BioEng.*, 70, No. 5: 359-361

13. Zhao, M., Niranjan, K. and Davidson, J.F., 1994, "Mass transfer to viscous liquids in bubble columns and air lift reactors: Influence of baffles", *Chem.Eng.Sci.*, 49, No 14: 2359-2369

14. Goto, S., Matsumoto, Y. and Gaspillo, P., 1989, "Mass transfer and reaction in bubble column with draft tube", *Chem.Eng.Commun.*, 85: 181-191

15. Pandit, A.B. and Joshi, J.B., 1983, "Mixing in mechanically agitated gas-liquid contactors, bubble columns and modified bubble columns", *Chem.Eng.Sci.*, 38, No.8: 1189-1215

16. Chapman, C.M., Nienow, A.W., Cooke, M. and Middleton, J.C., 1983, "Particle-gas-liquid mixing in stirred vessels Part IV: Gas-liquid mixing", *Chem.Eng.Res.Des*, 61. 182-185

17. Blakebrough, N. and Sambamurthy, K., 1966, " Mass transfer rates in fermentation vessels", *Biotech.Bioeng.*, 8: 23-42

18. Nocentini, M., Fajner, D., Pasquali, G. and Magelli, F., 1993, "Gas-liquid mass transfer and hold-up in vessels stirred with multiple Rushton turbines: Water and water-glycerol solutions", *Ind.Eng.Chem.Res.*, 32: 19-26

19. Martin, T., McFarlane, C.M. and Nienow, A.W., 1994, "The influence of liquid properties and impeller type on bubble coalescence behaviour and mass transfer in sparged, agitated reactors", *8th Euro.Conf.Mixing*, No 136: 57-64.

20. Oldshue, J.Y., Post, T.A., Wetman, R.J. and Coyle, K., 1988, "Comparison of mass transfer characteristics of radial and axial flow impellers", *6th Euro.Conf.Mixing*, Pavia, BHRA: 345-350

21. Hickman, A.D., 1988, "Gas-liquid oxygen transfer and scale-up. A novel experimental technique with results for mass transfer in aerated agitated vessels", *Proc.6th Euro.Conf.Mixing.*, BHRA, Pavia, May, 369-374

22. Cooke, M., Dawson, M.K., Nienow, A.W., Moody, G. and Whitton, M.J., 1991, "Mass transfer in aerated agitated vessels: Assessment of the NEL/Hickman steady state method", *Proc.7th Int.Euro.Conf.Mixing.*, Belgium, 409-416

23. Zhao, X.M., Gao, Y., Hu, Z.D. and Wang, D.Z., " Citric acid fermentations in bioreactors with different impeller combinations", 3rd *Int.conf.Bioreactor.Bioprocess.Fluid.Dynamics*, Cambridge, UK, Sept 14-16: 433-443

24. Nienow, A.W. and Elson, T.P., 1988, "Aspects of mixing in rheologically complex fluids", *Chem.Eng.Res.Des.*, 66, Jan: 5-15

25. Pandit, A.B., Reilly, C.D., Niranjan, K. and Davidson, J.F., 1989, "The convex bladed flow impeller: A multipurpose agitator", *Chem.Eng.Sci.*, 44, No 11: 2463-2474

26. Buckland, B.C., Gbewonyo, K., DiMasi, D., Westerfield, G. and Nienow, A.W., 1988, "Improved performance in viscous mycelial fermentations by agitator retrofitting", *Biotech.BioEng.*, 31: 737-742

27. Cooke, M., Middleton, J.C., and Bush, J.R., 1988, "Mixing and mass transfer in filamentous fermentations", *Proc.2nd.Int.Conf.Bioreactor.Fluid.Dynamics.*, BHRA/Elsevier, 37-64

28. Bajpai, R.K. and Reuss, M., 1982, "Coupling of mixing and microbial kinetics for evaluating the performance of bioreactors", *Can.J.Chem.Eng.*, 60: 384-392

29. Bujalski, W., Priede, M.A., Viestors, U.E., Cox, P.W., Thomas, C.R. and Nienow, A.W., 1997, "Mixing in fungal *A.niger* fermentations using dissimilar impeller systems", *Proc.4th.Int.Conf.Bioreactor.Bioprocess.Fluid. Dynamics*, July: 9-25

30. Bakker, A., Smith, J. and Myers, K.J., 1994, "How to disperse gases in liquids", *Chem.Eng.*, 101, No. 12: 98

31. van't Riet, K., 1979, "Review of measuring methods and results in nonviscous gas-liquid mass transfer in stirred vessels", *Ind.Eng.Chem.process.Des.Dev.*, 18, No.3: 357-364

32. Linek, V., Vacek, V. and Benes, P., 1987, "A critical review and experimental verification of the correct use of the dynamic method for the determination of oxygen transfer in aerated agitated vessels to water, electrolyte solutions and viscous liquids", *Chem.Eng.J.*, 34, 11-34

33. Dawson, M.K., 1992, "The influence of agitator type on fluid dynamics and oxygen mass transfer in a pilot plant scale mixing vessel", *PhD Thesis*, The University of Birmingham, UK

34. Martin, T., 1996, "Gas dispersion with radial and hydrofoil impellers in fluids with different coalescence characteristics", *PhD Thesis*, The University of Birmingham, UK

35. Spreit, J.A. and Botterman, J.H., "Correction factors for the dynamic measurement of the volumetric mass-transfer coefficient", *J.Chem.Technol.Biotech.*, *A-Chem.Technol.* 34: No.4: 137-153

36. Nocentini, M., 1990, "Mass transfer in gas-liquid, multiple-impeller stirred vessels: A discussion about experimental techniques for k_La measurement and models comparison", *Trans.I.Chem.E.*, 68, A, May: 287-294

37. Heineken, F.G., 1971, "Oxygen mass transfer and oxygen respiration rate measurements uitlizing fast responce oxygen electrodes", *Biotech.BioEng.*,13: 599-618

38. Dunn, I.J. and Einsele, A., 1975, "Oxygen transfer coefficients by the dynamic method, *J.appl.Chem.Biotech.*, 25: 707-720

39. Dang, N.D.P., Karrer, D.A. and Dunn, I.J., 1977, "Oxygen transfer coefficients by dynamic model moment analysis", *Biotech.BioEng.*, 14: 853-865

40. Linek, V., Benes, P., Vacek, V. and Hovorka, F., 1982, "Analysis of differences in k_La values determined by steady-state and dynamic methods in stirred tanks", *Chem.Eng.J.*, 25,:77-88

41. Linek,V., Benes, P., Sinkule, J. and Moucha, T., 1993, "Non-ideal pressure step method for k_La measurement", *Chem.Eng.Sci.*, 48, No.9: 1593-1599

42. Linek, V., Moucha, T., Dousová and Sinkule, K., 1994, "Measurement of k_La by dynamic pressure method in pilot-plant fermentor", *Biotech.BioEng.*, 43: 477-482

43. Davies, S.N., Gibilaro, L.G., Cooke, M. and Middleton J.C., 1985, "The application of two novel techniques for mass transfer determination to the scale-up of gas sparged agitated vessels", *5th.Euro.Conf.Mixing.*, Würzburg, D, BHRA: 27-33

44. Hickman, A.D. and Nienow, A.W., 1986, "Mass transfer and hold-up in an agitated simulated fermentation broth as a function of viscosity", *Int.Conf.Bioreactor.Fluid.Dynamics.*, Cambridge, BHRA: 301-316

45. Mehta, V.D. and Sharma, M.M., 1971, "Mass transfer in mechanically agitated gas-liquid contactors", *Chem.Eng.Sci.*, 26: 461-479

46. Zlokarnik, M., 1978, "Sorption characteristics for gas-liquid contacting in mixing vessels", *Adv.Biochem.Eng.* 8: 133

47. Rainer, B.W., 1990, "Determination methods of the volumetric oxygen transfer coefficient k_La in bioreactors", *Chem.Biochem.Eng.*, 4, 1990, 185-196

48. Muller, F.L. and Davidson, J.F., 1992, "On the contribution of small bubbles to mass transfer in bubble columns containing highly viscous liquids", *Chem.Eng.Sci.*, 47, No.13/14: 3525-3532

49. Vogel, A.I., 1978, "Textbook of quantitative inorganic analysis",4th Ed., Longman, London, UK: 355

50. Kawase, Y. and Moo-Young, M., 1990, "Mathematical models for design of bioreactors: application of Kolmogoroff's theory of isotropic turbulence", *Chem.Eng.J.*, 43: B19-B41

51. John, A.H., Bujalski, W., Nienow, A.W., Sánchez, A., Torres, L. and Galindo, E., 1995, "Studies of an independently-driven dual impeller protofermenter with and without a draft tube: Power and Hold-up", *Trans.I.Chem.E.*, 73, Part A: 535-541

CHAPTER 7

MIXING TIMES

7.1 Introduction

A major factor when considering the efficient design of mechanically agitated vessels or bubble columns is the degree of homogeneity attainable of the continuous liquid phase and the resultant impact on process productivity. Processes where optimum liquid phase mixing performance is of paramount importance include: two phase systems such as the blending of two immiscible liquids, chemical reactions or gas-liquid contactors, *e.g.* absorbers and strippers; and three phase systems *e.g.* gas-liquid-solid slurry reactors or fermentation vessels. In fermenters, the provision of a well defined homogeneous liquid environment is a pre-requisite for maximum biomass growth and yield of biosynthetic product. This is especially important with mycelial fermentations, of organisms such as *Penicillium chrysogenum* and *Aspergillus niger*, which produce highly viscous shear thinning broths, exhibiting probable poor bulk mixing and regions of stagnant fluid (dead zones), resulting in poor pH control, substrate feeding difficulties and possible heat transfer limitations. In addition, a reduction in mass transfer will be encountered since distribution of dissolved oxygen through the vessel will be limited. The importance of mixing quality has therefore received much attention in recent years and is frequently described in terms of mixing time (θ_m).

Mixing time can be defined as the time necessary to obtain a specified level of homogeneity of liquid within the vessel. It is dependent upon a number of parameters; fluid properties, vessel geometry, impeller type, impeller geometry, impeller speed and gas flow rate. The

inclusion of a draft tube in bubble columns has a profound effect on mixing. However, there is much controversy as to whether gas flow rate, or even impeller selection, have any impact on the blending performance in mechanically agitated vessels. To date, very little information has been published regarding the use of draft tubes in mechanically agitated vessels. These issues will be addressed in the following sections.

7.1.1 Bubble columns

Bubble columns and airlift bioreactors are being widely developed for the use in aerobic fermentations, wastewater treatment and other similar operations[1]. Their design and applications have been comprehensively reviewed by Chisti and Moo-Young (1987). Modifications in bubble column design have included additional inserts such as radial baffles[2], draft tubes [2,3,4,5,6,7,8,9,10,11,12,13] and ancillary impellers[14,15,16,17]. In this study, interest lies with the influence of the draft tube and the incorporation of mechanical agitation on blending performance. The inclusion of draft tubes within bubble columns increases mass transfer performance (Section 6.4) but has the tendency to reduce the blending efficiency.

Pandit and Joshi[12] found that mixing times initially decreased with increasing superficial gas velocity, then increased at higher gas velocities. They showed that mixing time increases with increasing height to diameter ratio, column diameter and the inclusion of a draft tube. Similarly, Magaritis and Sheppard[13] discovered that mixing times increase with the inclusion of a draft tube. Conversely, Zhao *et al.*[2] proposed that the decrease in $k_L a$ for Newtonian systems and increase in non-Newtonian systems was due to the increased circulation when incorporating a draft tube. The increase in $k_L a$ for the non-Newtonian system was due to the improved circulation resulting in a lower apparent viscosity. Allen and Robinson[8] assessed the influence of *Aspergillus niger* broth rheology and CMC on the performance of bubble column and loop reactors and concluded for both solutions that circulating liquid velocity

decreased and the k_La increased with apparent viscosity. Other investigators[1,8,9,11] have reported that increased apparent viscosity leads to an increase in circulation and mixing times.

Using the electrochemical method, Koide *et al*[11] found that the flow rate of the circulating liquid increased with increasing gas velocity, column diameter and draft tube length. The maximum flow rate was observed at a draft tube to column diameter ratio (D_{DT}/T) of about 0.6. This value was confirmed as giving minimum mixing times by Bando *et al.*[5] using the conductivity technique, and Koide *et al.*[9], using a heat pulse method. However, Jones[10] achieved the greatest circulation rate at D_{DT}/T equal to 0.5. Rousseau and Bu'lock[18] (for single phase flow) suggest using equal riser and downcomer cross-sectional areas (D_{RT}/T=0.71) for optimum circulation when designing bubble columns with draft tubes.

The inclusion of a draft tube within bubble columns has the tendency to increase hold-up and k_La and hence increase overall performance [9,11,12,17] although the increase in mixing times may represent a deterioration. This improvement might be further increased with the inclusion of mechanical agitation within the draft tube to improve bulk blending [17,19,20]. The effect of mechanical agitation in a column with draft tube will be addressed in Section 7.1.2.3.

7.1.2 Mechanically agitated vessels

Mechanically agitated vessels, especially unaerated single impeller systems, have been the subject of thorough investigation over the last 30 years. The effects of single impeller geometry and speed on mixing times are well documented, although there remains much controversy as to the blending characteristics under aerated conditions, especially with the utilisation of multiple impellers. Since the incorporation of multiple impellers in tall vessels is commonplace in the fermentation industries, the effect of aeration and multiple impeller configurations on the mixing time is of interest.

7.1.2.1 Single impellers

Traditionally data is correlated using dimensionless mixing time ($N\theta_m$), Reynolds number (Re) and Froudes number (Fr). Alternatively θ_m can be expressed as a function of power input (P) enabling a economic comparison between impeller types to be drawn. The majority of workers have found that for a given impeller in the turbulent regime, $N\theta_m$ is constant, independent of Re or Fr[21,22,23,24,25,26,27,28,29]. For this situation,

$$f\,(impeller\ geometry, vessel\ geometry) = Constant$$

However Biggs [30] and Norwood and Metzner[31] found $N\theta_m \propto N^a$, where a equals 0.16 and 0.34 respectively. Conversely Rielly and Britter[32] suggested that $N\theta_m \propto f(Re)$ and not Fr, hence accounting for longer mixing times on scale-up. Brennan and Lehrer[33] suggested wake effects caused a deviation from $N\theta_m = Constant$. Lundén *et al.*[34] observed an influence of N on $N\theta_m$ using three-dimensional CFD and experimental methods.

Substantial research has been carried out to assess the influence of different impellers on the blending efficiency within stirred tanks. Many workers [23,24,35,36,37] have reported that mixing time is determined by the total power input into the tank, independent of impeller type. Nienow[38] has shown that the experimental results of these resaerchers are in very good agreement with the correlation proposed by Ruszkowski[24] (Table 7.1-2). However, Shuie and Wong[22] showed higher mixing efficiency with axial flow impellers compared to radial flow. Similarly, Reilly and Burmester[39] discovered pitched-blade turbines require lower a power input to achieve the same degree of homogeneity as a Rushton turbine. Kramers *et al.*[28] stress that a Rushton turbine can give as rapid mixing as a propeller but require ten times as much energy. Recently developed high efficiency hydrofoil impellers (Lightin A315) give shorter mixing times than radial flow impellers (6RT, hollow bladed turbine) under the same operating conditions[40]. Fasano *et al.*[41] investigated the performance of a Chemineer high

efficiency impeller (HE3) and compared its blending performance to other impellers (6RT, 4RT, PBT). They suggested that blend times could be calculated from the following equation:

$$\theta_m = 4.605/k_m \text{ or } \theta_m = \frac{4.605}{aN\left(\frac{D}{T}\right)^b\left(\frac{T}{Z}\right)^{0.5}} \qquad (7.1)$$

where the constants *a* and *b* are a function of impeller style in the turbulent range (Table 7.1-1).

Table 7.1-1 The mixing rate constants for equation (7.1)

Impeller type	***a***	***b***
6RT	1.06	2.17
4RT	1.01	2.30
4-PBT	0.641	2.19
HE-3	0.272	1.67

This yields mixing times for the 6RT of approximately a quarter of that for HE3 at similar impeller speeds. However, for constant power inputs the blend times are approximately equal.

7.1.2.2 Dual impellers

Technological advances have led industry away from the use of single impeller mixing vessels towards taller thinner vessels agitated by multiple impellers for gas-liquid systems. For an equal batch volume, a multiple impeller system exhibits an increased heat transfer area/volume ratio, greater gas bubble residence time and occupies less space in a manufacturing plant, compared to single agitator configurations. However, whether mixing efficiency is improved when using multiple impellers is a question essentially unanswered.

A dual impeller system can be considered as two single impellers each having its own circulation loop with an equal and opposite mass exchange between them. Abradi *et al*[21] investigated the performance of three configurations (radial-radial; 2 x axial-radial) of dual

impellers and compared the results with mixing time values of single impeller systems predicted by Khang and Levenspiel[27] using:

$$N\theta_m = 0.5\left(\frac{T}{D}\right)^{2.3} \ln\frac{2}{M} \qquad (7.2)$$

where M represents the degree of homogenisation, *i.e.* for 98% M=0.02.

They discovered that single impeller systems (T/H=1) gave considerably lower mixing times than the dual impeller configurations, indicating that the rate of exchange between the circulation loops is lower than the flow rates induced by the impellers within the loops. The reduction in blending efficiency exhibited by dual impellers was minimised by using a mixed flow agitator (radial-axial) which probably increased the exchange flow rate between the upper and lower recirculation loops. Using decolorisation experiments it was discovered, at an aspect ratio of 2:1, that dual impeller configurations produced better blending than single impellers at similar speeds[42]. However, when comparing single impellers at 1:1 with dual impellers at 2:1 mixing was some 4 times better for the single impeller. At the aspect ratio of 2:1, with dual impellers, it was observed that 75% of the mixing time occurred in the upper section of the vessel[42]. Nienow and Elson[43] ranked different impeller configurations in order of efficiency when mixing rheologically complex fluids. They found that a mixed flow stirrer with high D/T ratios were generally most efficient, falling away with decreasing size and a reduction to a single impeller. Similarly, Cooke *et al.*[29] reported that for a dual impeller system incorporation of an axial flow impeller (rather than two disc turbines) can halve the mixing time for similar impeller speeds. Conversely, Kumori and Murakami[44,45] compared mixing efficiency in single and dual impeller systems and discovered that an improvement could be achieved by inducing large scale recirculation, hence reducing the number of

recircualtion loops in a tank. Mixing efficiency is increased with a single impeller configuration since it has fewer recirculating loops than a multi-impeller system.

Fasano *et al.*[41] estimated blend times for multiple impeller systems, within 30% accuracy, by substituting an effective mixing rate constant ($k_{m,eff}$) into Equation (7.1). $k_{m,eff}$ is obtained by the summation of $k_{m,i}$ for individual impellers (i) present in the agitation system, i.e.

$$k_{m,eff} \approx \sum_{i=1}^{n} k_{m,i} \qquad (7.3)$$

It is therefore evident that for multiple impeller systems the mixing time will be shorter (power input will be larger however). Similarly, Ando *et al.*[46] created a model for a horizontal vessel, stirred by multiple impellers, from a model using a single impeller. The model predicts the mixing time from adjacent well mixed zones where the exchange flow rate between two perfectly mixed cells controls the mixing. In this case, however, the mixing times are longer for multiple impeller configurations.

7.1.2.3 Draft tube

It is generally perceived that dual impeller systems produce lower quality mixing than single impellers, because of the increased number of circulation loops. However, incorporating a draft tube enhances bulk recirculation, i.e. top to bottom mixing, reduces the number of recirculation loops and should therefore improve mixing efficiency in both single and dual impeller systems.

Landau and Prochazka[19] made a comparative study of mixing vessels utilising either baffles or a conical draft tube. The inclusion of a draft tube had the advantage of increasing homogenisation efficiency especially in the transitional regime, i.e. *Re* from $2x10^3$ to $2x10^4$. Here $N\theta_m$ remained constant for the set-up with the draft tube, but increased with a reduction in *Re* for the baffled vessels. Hoogerdoorn and Hartog[20] investigated the effect of

incorporating a cylindrical draft tube on the mixing times of various mixers in the viscous flow region. The draft tube enhanced circulation and homogenisation resulting in a reduction of mixing times. Increasing the clearance between the tip of the impeller and the draft tube led to an increase in mixing times due to the formation of dead zones on the inside of the draft tube. Shuie and Wong[22] conducted similar experiments with similar results, *i.e.* mixers containing a draft tube may achieve equal mixing times at much lower power inputs than when the draft tube is excluded. This was especially the case when axial rather than radial flow impellers were used. Conversely, Pörtner *et al.* [47] showed, with Newtonian and CMC fluids, that paddle impellers and Intermigs gave better blending than a propeller with a draft tube.

7.1.2.4 Aerated mixing times

There exists much controversy as to whether mixing is enhanced or impaired by aeration. Discrepancies can evolve from the representation of mixing time data, *i.e.* should θ_m be described as a function of N or P_g?

Blakebrough and Sambamurthy[48] reported an increase in mixing times for similar agitation speeds on aeration, especially when the impeller became flooded. This was probably due to a lower pumping capacity caused by ventilated cavity formation. Cronin *et al.*[42] observed a general increase in mixing times on aeration, although at low power inputs the addition of gas aided the mixing process. Similarly, Arbardi *et al.*[21] defined two zones of mixing under gassed conditions. At high impeller speeds, when the gas is completely dispersed, mixing is controlled by the action of the impeller. Mixing time is still inversely proportional to N, although the absolute values increase as the gas flow rate is increased. When the impeller becomes flooded, the mixing time increases substantially and the bulk flow is controlled by the action of the bubbles. Combining these two effects allowed mixing times to be expressed

as a function of total power input to the system (including gas kinetic energy and energy of isothermal expansion of the gas). They found that all data fitted $\theta_m \propto \left(P_{tot}/V\right)^{-1/3}$. Cooke *et al.*[29] also made an allowance for the loss of pumping efficiency by using *P/V* instead of N, therefore:

$$\theta_m\left(\frac{P}{V}\right)^{1/3} = CONSTANT \text{ and hence, } \theta_m\left(Po_g\right)^{1/3} = CONSTANT$$

which fitted both gassed and ungassed mixing time data. Pandit and Joshi[12] also discovered distinct regions, for a variety of impellers, where either the gas flow or the impeller action dominated the mixing. At impeller speeds lower than that required to prevent flooding, mixing times shortened with increasing superficial gas velocity. However, when the gas was dispersed, mixing is controlled by the action of the impeller and increasing the superficial gas velocity resulted in longer mixing times.

For efficient mixed flow dual impeller agitators (axial-radial), in rheologically complex fluids, Nienow and Elson[43] found that mixing times increased on aeration. However, for inefficient mixers (single 6RT, angled blade impellers) blending was improved by the addition of gas, although the mixing was still considered poor. Similarly, Einsele and Finn[49] found that mixing times in aerated systems were greater than in ungassed systems. At constant power inputs no effect of aeration on the mixing times for radial impellers and only a slight reduction in mixing times for hydrofoils, was observed by Otomo[40]. The expected increase in performance when utilising a single Rushton (for gas distribution) and two hydrofoils (for top to bottom mixing) was not realised in experiments undertaken by Manikowski *et al.*[50]. Using an ultrasound Doppler probe, and by means of residence time studies, they found that compartmentalisation around each impeller occurred due to the gas

flow destroying the axial pumping capacity of the hydrofoils. Their observations were verified by mixing time experiments using the decolourisation technique.

Table 7.1-2 A selection of mixing time correlations for single and dual impeller systems

Author	Method	Equipment	Outcome	Correlation
Khang and Levenspeil Equation [27] (7.2)	Conductivity - pulse of NaCl	FBV Single Propeller and 6RT	Mixing dependent on impeller type	$N\theta_m = 0.5\left(\frac{T}{D}\right)^{2.3} \ln\frac{2}{M}$
Ruszkowski Equation [24] (7.4)	Conductivity-pulse of nitric acid	FBV Single 6RT, 4PTD, 6PTD, propellor.	Mixing time independent of impeller type	$\theta_m = 5.91T^{2/3}\left(\frac{\rho V}{P}\right)^{1/3}\left(\frac{T}{D}\right)^{1/3}$
Fasano *et al.* Equation [41] (7.1)	Not stated	Single/multiple impellers; 6RT, 4RT, 4PBT, HE-3	Mixing dependent on impeller type. θ_m decreases with multiple impellers	$\theta_m = \frac{4.605}{aN\left(\frac{D}{T}\right)^b\left(\frac{T}{Z}\right)^{0.5}}$
Cooke *et al.* Equation [29] (7.5)	Conductivity-pulse of KCl	FBV, DBV Single/multiple impellers with combinations of 6RT, 6GF, 6PRT, PHF	Aerated and unaerated mixing times can be predicted by the same equation. Axial-radial give θ_m ~ 1/2 of prediction.	$\theta_m Po_g^{1/3} N\left(\frac{D}{H}\right)^{2.43} = 3.3$

7.1.3 Mixing time measurement techniques

A variety of methods can be used to obtain mixing time measurements, which describe blending efficiency in a system. These include observation of an inert dye addition[47], pH [33,49], thermal[22,20,20,51], decolorisation[23,31,42,43,20,48,50] and, most frequently, conductivity techniques[12,21,25,28,27,29,30,39,40,44,45,46]. The diversity in techniques makes direct comparisons between different authors difficult. All of the methods which follow the progress of homogenisation after the injection of a small quantity of tracer have been reviewed previously[33,40,20] and are summarised in Table 7.1-3.

When comparing mixing times obtained using the conductivity and decolorisation techniques, Otomo[40] discovered consistent results for single impellers, but significantly differing results with dual impeller systems. However, a comparison could be made between

the shape of the conductivity transient and the progress of decolorisation in distinct parts of the vessel. Hoogendoorn and Hartog[20] found that decolorisation and thermal methods gave the same mixing times except when large dead zones were encountered.

Table 7.1-3 Review of different techniques for measuring mixing times

Method	Experimental procedure	Advantages	Disadvantages
Decolorisation	• The neutralisation of an iodine solution by sodium thiosulphate in the presence of a starch indicator. • Decolorisation of methyl red indicator with neutralisation of NaOH by HCl. The end point is the time at which the last wisp of colour disappears.	• Allows visual observation of the flow pattern occurring within the tank and identification of dead zones and poorly mixed regions. • The terminal mixing time is representative of the whole tank volume, i.e a global mixing time. • No probes are required therefore aeration poses less of a problem.	• Assessing the time at which decolorisation occurs is subjective. • pH decolorisation may alter the rheolgical characteristics of the fluid.
Colour addition	Addition of an inert coloured dye.	• As above.	• Very difficult to gauge the mixing time - nearing the end-point the whole vessel is coloured making any further changes difficult to see.
Conductivity	Concentration transient, measured by a conductivity probe, after the injection of ionic tracer e.g. NaCl, KCl. Mixing time is defined the time elapsed from the addition to reach 0.1-10% of the final concentration.	• Most popular and well understood technique • Reliable, cheap and simple • Fast probe response	• A local mixing time is obtained so dead zones may not be detected. • Bubble interference may cause problems under aerated conditions. • Background concentration must be considered and eventually the vessel contents need renewal.
pH	pH transient followed by probe after the addition of acid/alkali pulse.	• Little influence of air bubbles	• Local mixing time obtained • Slow response time • Effects rheology
Thermal	Temperature transient, measured by a thermocouple/thermistor, after the injection of a small quantity of heated liquid/steam	• Unlimited experimental repeats are possible • Negligible influence on rheology of Newtonian and non-Newtonian fluids *i.e.* heated tracer can be the same fluid.	• Large volumes of tracer required • Sensitive readout equipment required • Difficult for very high viscosity fluids

7.2 Material and Methods

Any advantage gained by utilising one mixing time measurement technique is usually offset by at least one distinct disadvantage (Table 7.1-3). Therefore, in order to obtain maximum benefit from mixing time measurements, two techniques were facilitated. Firstly, conductivity was favoured because[40]:

(i) it is a widely recognised technique, with a clear definition of the mixing time,

(ii)it is reliable, cheap and simple,

(iii) the conductivity probes have a fast and sensitive response.

However, conductivity does not readily provide information on the progress of mixing within the vessel but combining it with a visual technique does. Therefore, the decolorisation of an iodine solution by sodium thiosulphate was also used which allows:

(i) visual observation of the flow patterns occurring,

(ii) identification of dead zones and poorly mixed regions,

(iii) experimentation with polymer solutions to be undertaken (the reagents used have a minimal effect on rheology).

Using conductivity and decolorisation techniques, reproducible quantitative data could be obtained allowing a qualitative description of mixing progress. The conductivity and decolorisation techniques are described in Section 7.2.2 and Section 7.2.3 respectively. The experimental equipment has been previously described in Section 3.1.

7.2.1 Injection system

Both conductivity and decolorisation techniques use the pulse addition of a tracer and therefore require an injection system. When designing an injection system[52] the folowing pints were taken into account:

(i) The injection time must be much shorter than the mixing time,

(ii) Reproducible injection times must be obtainable.

An injection chamber similar to that used by Cronin[52] was fitted to the top of the proto-fermenter. The system has been fully described by Cronin and more recently Otomo[40] and only an outline of its operation will be discussed here.

To prime the system, the injection chamber and all associated pipe lines were filled with the required fluid. The chamber was then sealed and compressed air used to create a head pressure of 20/25 p.s.i.g.. A manual valve was opened to allow flow into the tank and an automatic solenoid valve, at the base of the chamber, controlled the amount injected. In addition, a small relief valve positioned on the end of the injection pipe ensured that a precise volume of tracer was injected. The injection system was calibrated to determine the injection times of predefined volumes under certain applied head pressures (Figure 7.2-1).

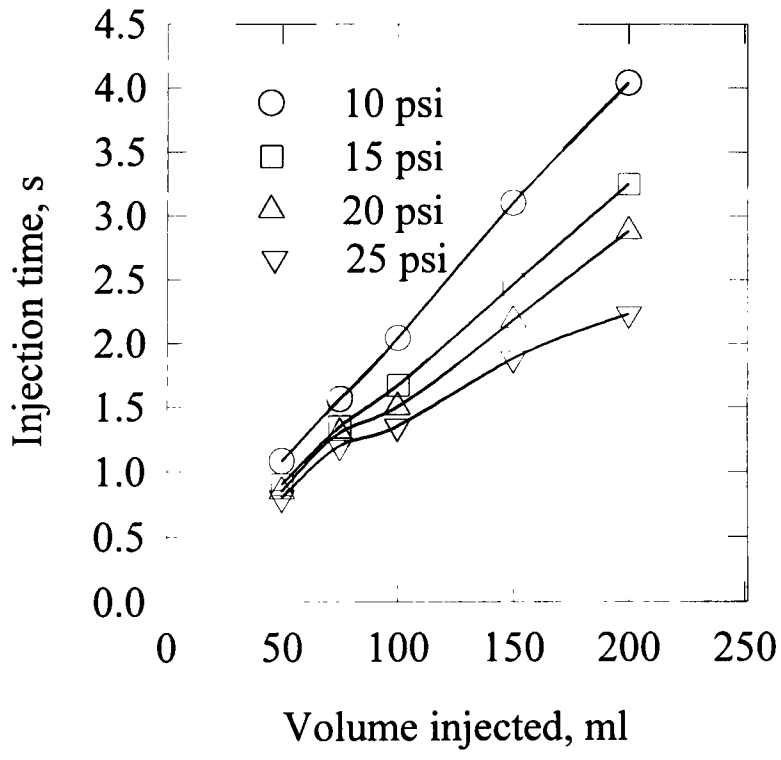

Figure 7.2-1 Calibration of injection chamber

7.2.2 Conductivity technique

The conductivity technique, first used by Landau and Procháka[53], has been described in detail by Otomo[40] and is summarised here. The mixing time was measured by examining the

concentration fluctuations after a small amount of ionic tracer was introduced to the vessel. The mixing time, θ_m, was defined as the time elapsed between the injection of the tracer and the readout value reaching within ± 5% of the final concentration (amplitude technique).

7.2.2.1 Methodology

The conductivity probes consisted of two tungsten wire electrodes attached to copper leads and protected by an outer glass casing. The whole probe and lead was water resistant. Although the tungsten wire conductivity probe is less accurate than a platinum coil conductivity probe (used by other workers), it is cheaper, easier to seal and is therefore considered the best option.

Previous problems arising from bubble interference under aerated conditions have been overcome by shielding the probes with a perforated cage[40]. The cage surrounds the tip of the probe ensuring that bubble contact with the electrodes is avoided, hence preventing signal loss under aerated conditions. Since the probes are horizontally mounted (rather than vertically as used by Otomo[40]) a modification of the design we employed was used as shown in Figure 7.2-2. Here, the perforated cage, constructed of a brass mesh sheet (0.5mm holes), had a solid base and an additional three holes (3mm) on the top plane. The three holes allowed the ready release of bubbles which may have become trapped in the cage. Otomo showed that such a cage did not effect the conductivity reading[40] and that was true here also.

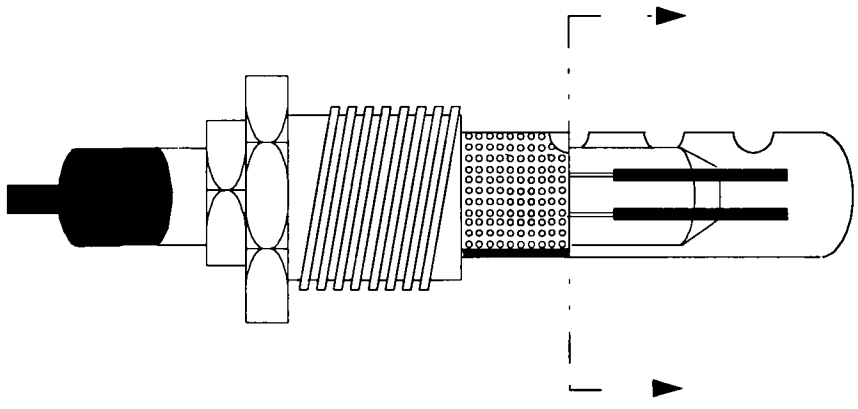

Figure 7.2-2 Conductivity probe and perforated cage

Changes in ionic concentration, and hence electrical resistance, within the vessel were detected by the conductivity probe, which acted as part of a resistance bridge. The probes were linked to a six channel conductivity meter (output 0-10V)[40], although only two channels were utilised simultaneously. Since the conductivity meter could not compensate for the background concentration only a limited number of experiments were possible before changing the liquid. Each experiment raised the output by approximately 0.2V. About 20 successive experiments could be performed (~4V) before the vessel was emptied, washed and refilled with de-ionised water. The conductivity meter and probes were calibrated over a 10 volt range through each channel with individual probes. Changes in voltage output were logged by a computer based data acquisition system (IBM® PS2 Model55SX with National Instruments® Multi-function I/O board AT-MIO-16) and transferred to Lotus 1-2-3® via software interfacing data (Measure V 2.2).

Table 7.2-1 Details for conductivity mixing times

Configuration	Impeller speeds rpm	Power range W/kg	Gas flow rates vvm
Single 3SHP1	60, 90, 120, 150, 180, 240	0.01-1.28	0, 0.25, 0.5
Common shaft simulation	60, 90, 120, 150, 180, 240	0.02-1.68	0, 0.25, 0.5
IDDI-6RT 200 rpm 3SHP1 varied	60, 90, 120, 150, 180, 240	0.11-1.58	0, 0.25, 0.5
IDDI-6RT 300 rpm 3SHP1 varied	60, 90, 120, 150, 180, 240	0.61-2.01	0, 0.25, 0.5
IDDI-6RT 300 rpm 3SHP1 varied	60, 90, 120, 150, 180, 240	1.50-2.90	0, 0.25, 0.5
Single 6RT	60, 120, 200, 300, 400	0.01-2.4	0, 0.25, 0.5

40 ml of 160g/l NaCl solution was injected into the vessel for each measurement, resulting in a concentration change of 0.001 wt% inside the vessel. This volume of tracer could be injected within 0.8 seconds at a head pressure of 20 p.s.i.g.

A comprehensive range of impeller speeds and gas flow rates were investigated (Table 7.2-1), producing reproducible quantitative data which could then be used to create correlations.

7.2.3 Decolorisation technique

Decolorisation was employed to visualise the progress of mixing within the vessel and to determine the flow patterns occurring at specific points of interest noted during the conductivity experiments. This method is fully described by Carreau *et al.*[54] and is based on the neutralisation of an iodine solution by sodium thiosulphate in the presence of a starch indicator. Iodine is only sparingly soluble in water so a solution of iodine in potassium iodide was used for the reaction:

$$I_3 + 2\ S_2O_3^{--} \longrightarrow 3\ I^- + S_4O_6^{--}$$

The dark brown iodine/iodide solution was rendered colourless on reduction with sodium thiosulphate. The end point (dark blue to colourless) was enhanced with the use of a starch indicator.

The iodine, sodium thiosulphate and starch indicator solutions were made up as described by Cronin[52] and the same procedure followed. The vessel has a working volume of 640 l and therefore 180 ml of sodium thiosulphate was injected. This is a scale up of Cronin's work in which a working volume of 586 l was utilised and 165 ml of sodium thiosulphate injected. Injection of 180ml takes 1.6 seconds with a head pressure of 25 p.s.i.g.. 100 ml of starch indicator was added at the beginning of a set of experiments.

(i) 180 ml of 2N sodium thiosulphate solution was injected just above the 3SHP1 impeller. The time elapsed between the initial injection and the point of total decolorisation was recorded (Figure 7.2-3).

(ii) The excess (25%) of sodium thiosulphate in the vessel was neutralised by the addition of 2N iodine solution until the light blue endpoint was reached (~15ml). The procedure may was then repeated for as many runs as required.

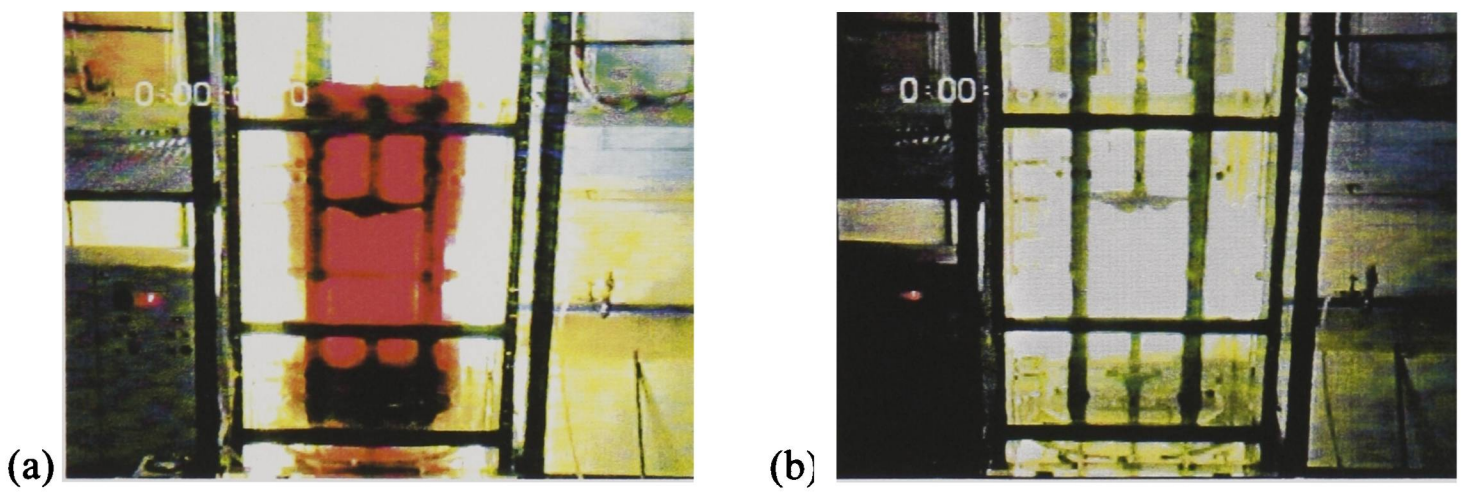

Figure 7.2-3 Progress of decolorisation (a) initial (b) final

The decolorisation experiments were recorded using a VTR system. This enabled the exact moment of decolorisation to be found. The tape is available at the School of Chemical Engineering, University of Birmingham.

The experimental conditions required for the verification of the conductivity method are shown in Table 7.2-2. In addition, CMC could also used as a test fluid since the reagents have very little effect on the fluid rheology.

Table 7.2-2 Experimental conditions for the decolorisation technique

Configuration	Impeller speeds rpm	Solution	Gas flow rates vvm
Single 3SHP1	60, 120, 240	Water, CMC*	0, 0.25, 0.5
Common shaft simulation	60, 120, 240*	Water CMC*	0, 0.25, 0.5
IDDI-6RT 200 rpm 3SHP1 varied	60, 120, 240	Water CMC*	0, 0.25, 0.5
IDDI-6RT 300 rpm 3SHP1 varied	60, 120, 240	Water CMC*	0, 0.25, 0.5
IDDI-6RT 400 rpm 3SHP1 varied	60, 120, 240	Water	0, 0.25, 0.5
Single 6RT	60, 120, 240	Water, CMC*	0, 0.25, 0.5

* CMC experimentation under ungassed conditions only

Throughout the results and discussion section, comparisons have been made with other researchers despite differing definitions (RMS or amplitude) for the calculation of the blend time.

7.3 Results and Discussion

Although the mixing time values obtained using both techniques are not quantitatively comparable the trends observed were similar (Figure 7.3-1). The decolorisation technique allowed visual characterisation of the trends occurring, whereas empirical correlations were created from values obtained via the conductivity technique.

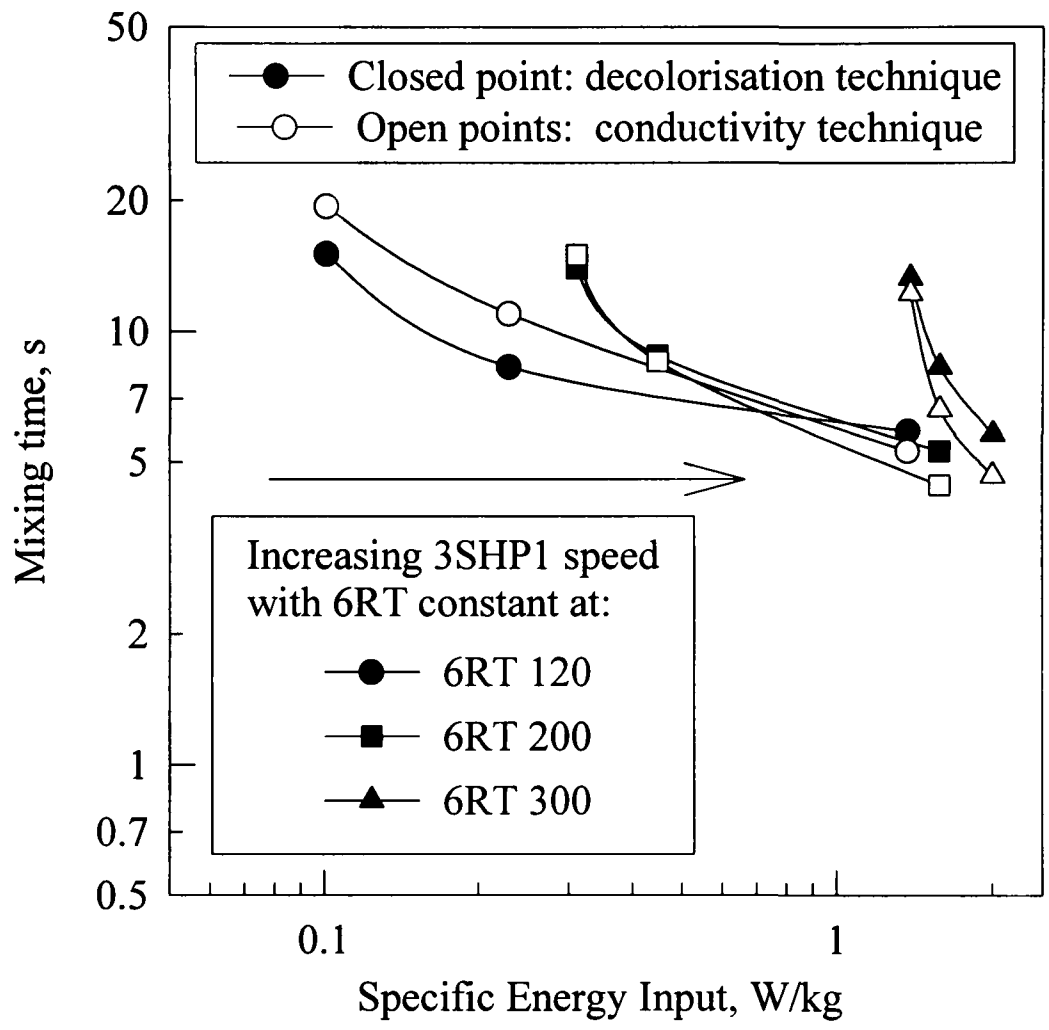

Figure 7.3-1 Comparison between decolorisation and conductivity techniques

7.3.1 Unaerated Mixing times: Conductivity technique

7.3.1.1 Single Impeller systems

Mixing time data have been represented in traditional manner, *i.e.* dimensionless mixing time ($N\theta_m$) as a function of Reynolds number (Re) (Figure 7.3-2)θ_m and as a function of specific power input (W/kg) (Figure 7.3-3, Figure 7.3-4).

The dimensionless constant $N\theta_m$ for the 6RT was found to be a strong function of impeller speed (statistically significant), although it is unknown whether this is attributable to the change in Reynolds or Froude's number. Regression analysis of the data gives $N\theta_m \propto N^{0.31}$

with a regression coefficient r^2 of 0.99 (Figure 7.3-2). An almost identical result was observed by Norwood and Metzner[31] for single six flat bladed turbines who expressed the dependency on N through the Froude number, Fr. However, this was difficult to clarify due to the inability to change g.

In agreement with the majority of other workers, $N\theta_m$ seems to be independent of impeller speed, Re or Fr, for the 3SHP1 impeller (Figure 7.3-2). An F test of the data gave a ratio of 5.303 , confirming the independence, since, for a 95% confidence level, F has to exceed 6.39 to show statistical significance (or exceed 15.98 for 99% significance).

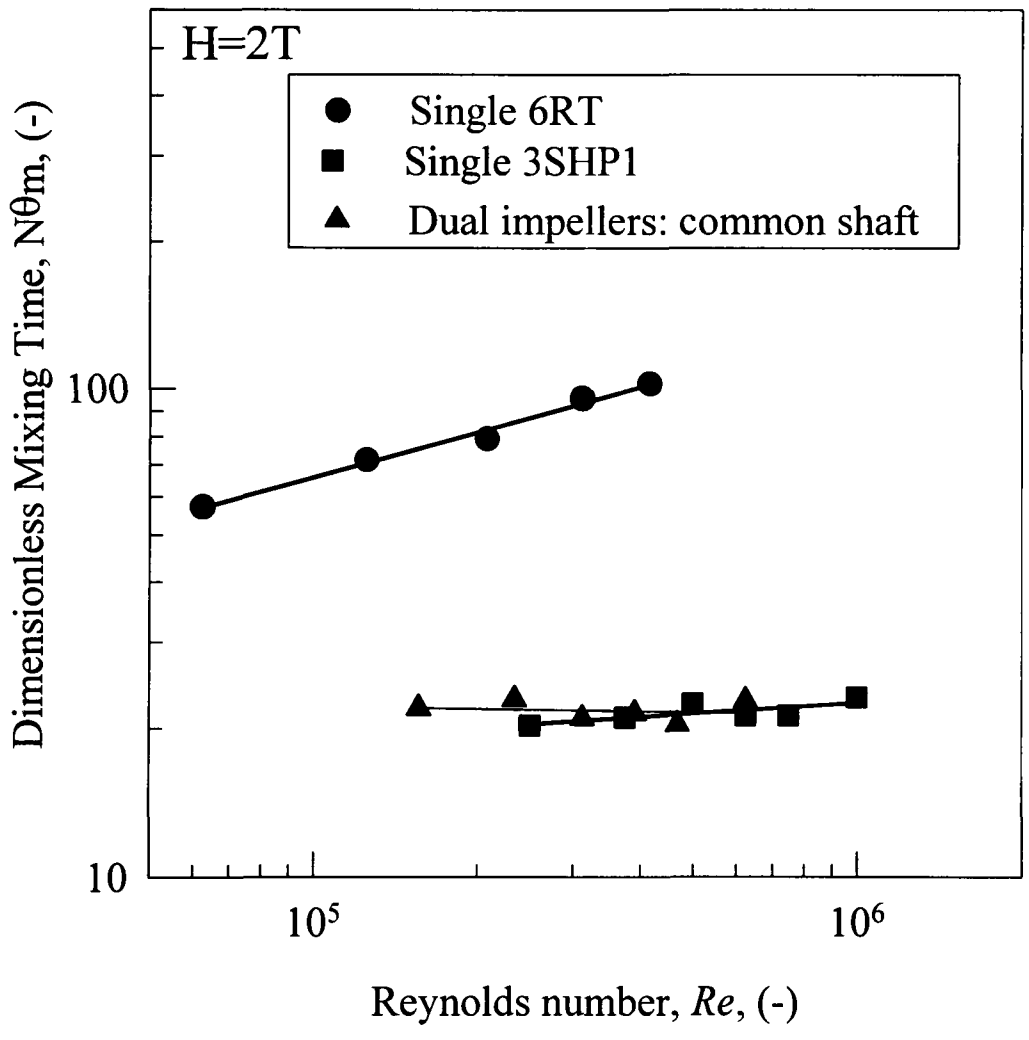

Figure 7.3-2 Dimensionless mixing time as a function of Reynolds number for the 6RT and 3SHP1 impellers

Figure 7.3-3 and Figure 7.3-4 show mixing times as a function of specific energy input for the single 6RT and 3SHP1 configurations respectively. Regression analysis of the plots yielded the correlations displayed in Table 7.3-1.

Table 7.3-1 Correlations produced for single impeller mixing times

P-1 was in the plane of the 6RT and P-2 was in the plane of the 3SHP1 (in annulus)

Impeller type	Probe	Correlation	Regression coefficient (r^2)	Equation number
6RT	Lower probe P-1	$\theta_m = 13.5\left(\frac{P_{RT}}{V}\right)^{-0.27}$	0.996	(7.6)
6RT	Upper probe P-2	$\theta_m = 18.6\left(\frac{P_{RT}}{V}\right)^{-0.2}$	0.983	(7.7)
3SHP1	Lower probe P-1	$_m = 5.01\left(\frac{P_{SC}}{V}\right)^{-0.33}$	0.996	(7.8)
3SHP1	Upper probe P-2	$_m = 5.12\left(\frac{P_{SC}}{V}\right)^{-0.31}$	0.957	(7.9)

As expected from the dimensionless mixing expression, θ_m (P-2) for the 6RT $\propto (P/V)^{0.23}$ since $\theta_m \propto N^{0.7}$ and $P \propto N^3$ then $\theta_m \propto P^{0.23}$.

It is evident that the terminal mixing time is dependent on probe positioning, *i.e.* the probe situated in the annulus gave slightly longer mixing times than the one positioned at the 6RT level. The effect was more prominent with the single 6RT which achieved mixing times, on average, 23.2% shorter for probe 1 (P-1) compared with probe 2 (P-2). This was due to the formation of a recirculation loop below the impeller entraining a small quantity of salt tracer, slowly releasing it into the annulus (see Chapter 8, Figure 8.3-7). As the impeller speed was increased the difference was enhanced due to the increased recirculation beneath the 6RT and subsequently 50% longer mixing times were observed by P-2 compared to P-1 (33.5% shorter if P-1 compared to P-2). With the 3SHP1 the slightly longer (10%) mixing times recorded by P-2 were due to the extra distance the tracer must travel before it reaches the probe.

Single 6RT. Cooke *et al.*[29] investigated blending performance with aspect ratios from 1:1 to 3:1 for multiple and single impellers systems. It is noted from Figure 7.3-3 that the experimental mixing times were some 50% faster (at low power inputs) than predicted by their correlation (Table 7.1-2, Equation (7.5)). Joshi *et al.*[26] proposed a correlation for θ_m based on the average circulation velocity and the maximum length of a circulation loop. The correlation fits reasonably well, although deviating considerably (approximately 50%) at lower impeller speeds (<120 rpm). Whereas the design equation of Fasano *et al.*[41] (Table 7.1-2, Equation (7.1)) predicted mixing times within 10% of either the P-1 or P-2 θ_m values. They suggested that the correlation is only reliable when designing a vessel with an aspect ratio less than 0.8 and any further increase in height would be at the detriment of the blending performance. Ruszkowski[24] based a correlation (Table 7.1-2, Equation (7.4)) for θ_m on theoretical analysis of the fluid dynamics of a system using various agitators at an aspect ratio of 1. Since mixing deteriorates as aspect ratios increase the correlation under-estimates θ_m by between 40% and 65% of those achieved at H/T=2.

Single 3SHP1. It is evident from Figure 7.3-4 that the 3SHP1 with draft tube produced mixing times at least 50% faster than predicted by the majority of previous researchers[26,29,41], for similar axial flow impellers, and also gave mixing times up to a third lower than were encountered for the 6RT at similar power inputs (Figure 7.3-3). Improved performance was due to the 3SHP1 promoting axial, not radial, flow. This increased the circulation flow rate and hence increased the probability of any single element of fluid passing through an intensely mixed region. Mixing times are fractionally shorter than predicted by Ruszkowski[24] even though the vessel is operated at an aspect ratio of 2:1. It is concluded that for single impeller configurations, at an aspect ratio of 2, mixing can be improved by the inclusion of a draft tube, especially when axial flow impellers are used.

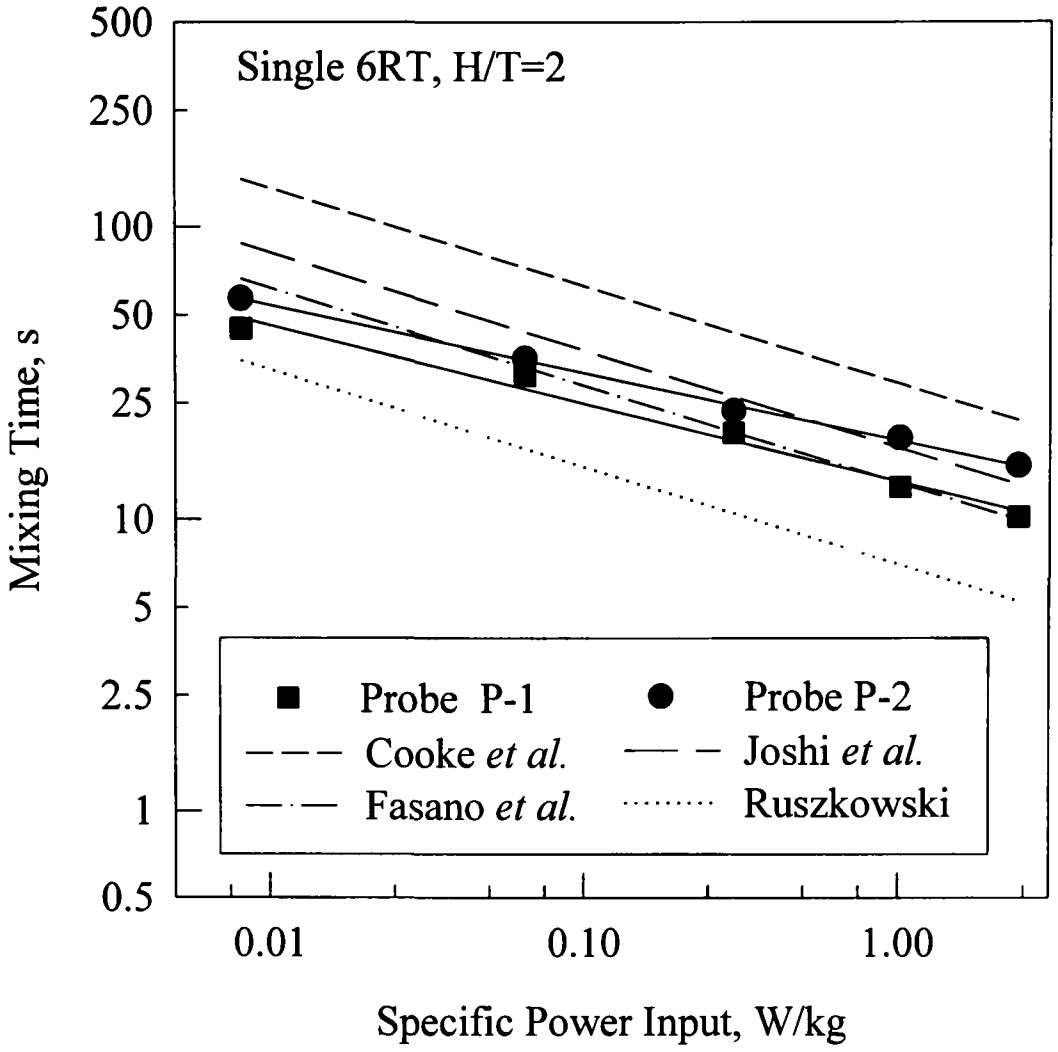

Figure 7.3-3 Mixing times for the single 6RT (DT) compared to the predictions of other workers

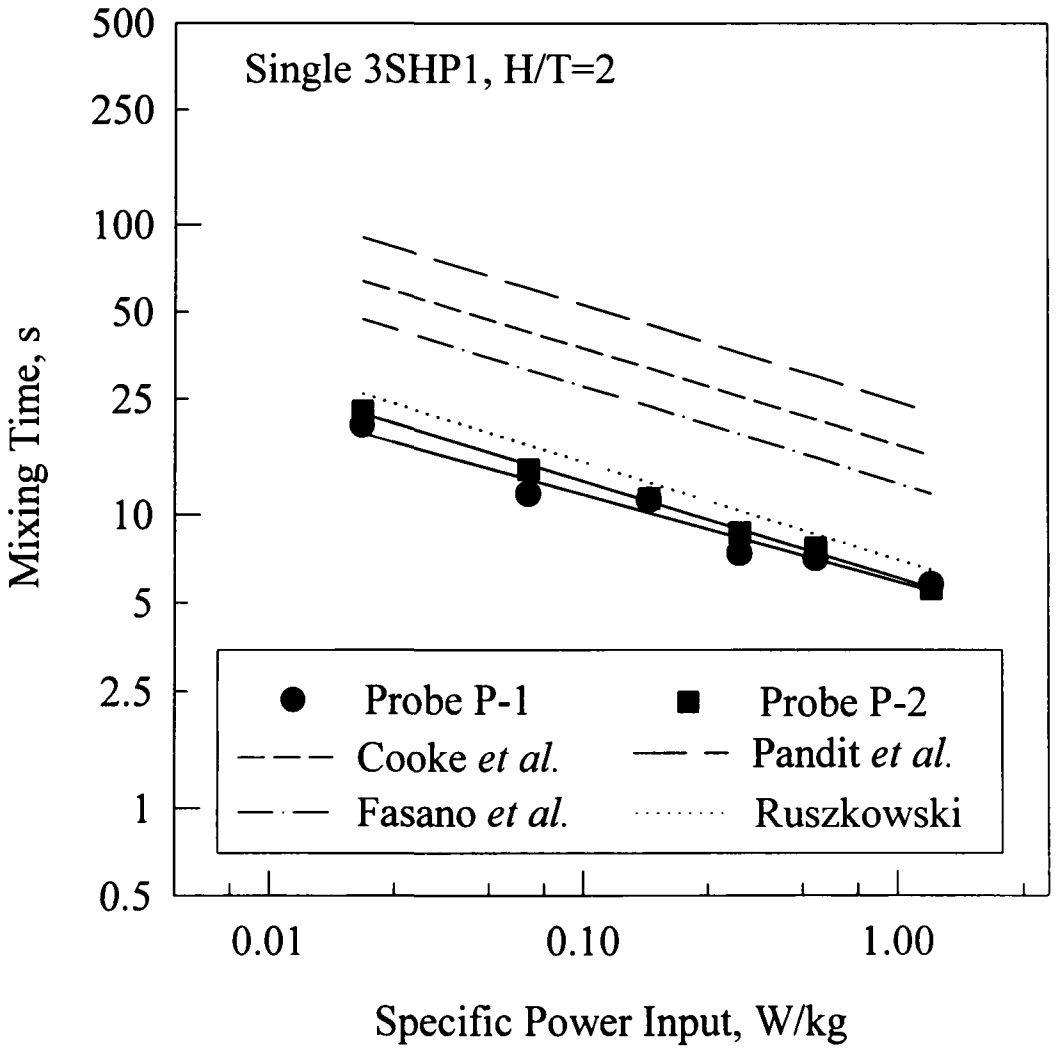

Figure 7.3-4 Mixing times for the single 3SHP1 (DT) compared to predictions of other workers

7.3.1.2 Dual impeller system

Figure 7.3-5 shows mixing times for the conductivity method as a function of specific energy input for the ungassed situation, with each plot representing a constant 6RT speed and range of 3SHP1 speeds. The initial "C" shape of the curve was due to the lower Po_{RT} when the 3SHP1 was operational. By comparing with Figure 7.3-4 and Figure 7.3-6 it can be seen that the mixing time for the single shaft simulation, *i.e.* both impellers running at the same speed, and those for the 3SHP1 running alone were almost identical for similar energy inputs and that both performed better than the independently-driven (IDDIDT) configuration, *i.e.* with each impeller operating at a different speed. Indeed, for similar energy inputs, high 6RT speeds had a detrimental effect on the mixing time, especially at lower 3SHP1 speeds. It is noticeable that increasing the 3SHP1 speed greatly reduced the mixing time, for example, at a 6RT speed of 200 rpm, increasing the 3SHP1 speed from 60 to 120 rpm reduced the mixing time by approximately 50% whilst only slightly increasing the total power drawn. In like manner to the single impeller configuration this was due to the 3SHP1 increasing the circulation flow rate and hence increasing the frequency of any single part of the fluid passing through an intensely mixed zone. Since the 6RT promotes radial, not axial flow, then any increased power input by the 6RT resulted in zoning around the 6RT impeller, not significantly increasing the circulation flow rate and hence can be considered redundant for blending. This theory is supported by visual observation experiments at high 6RT speeds and low 3SHP1 speeds (Section 7.3.3). Mixing times for the IDDIDT cannot be correlated with the sum of the specific energy input of both impellers since they were dependent upon which of the impellers is inputting the power to the system. Instead mixing times were found to be a function of the separate power inputs from the 6RT and 3SHP1 impellers respectively and the correlation becomes:

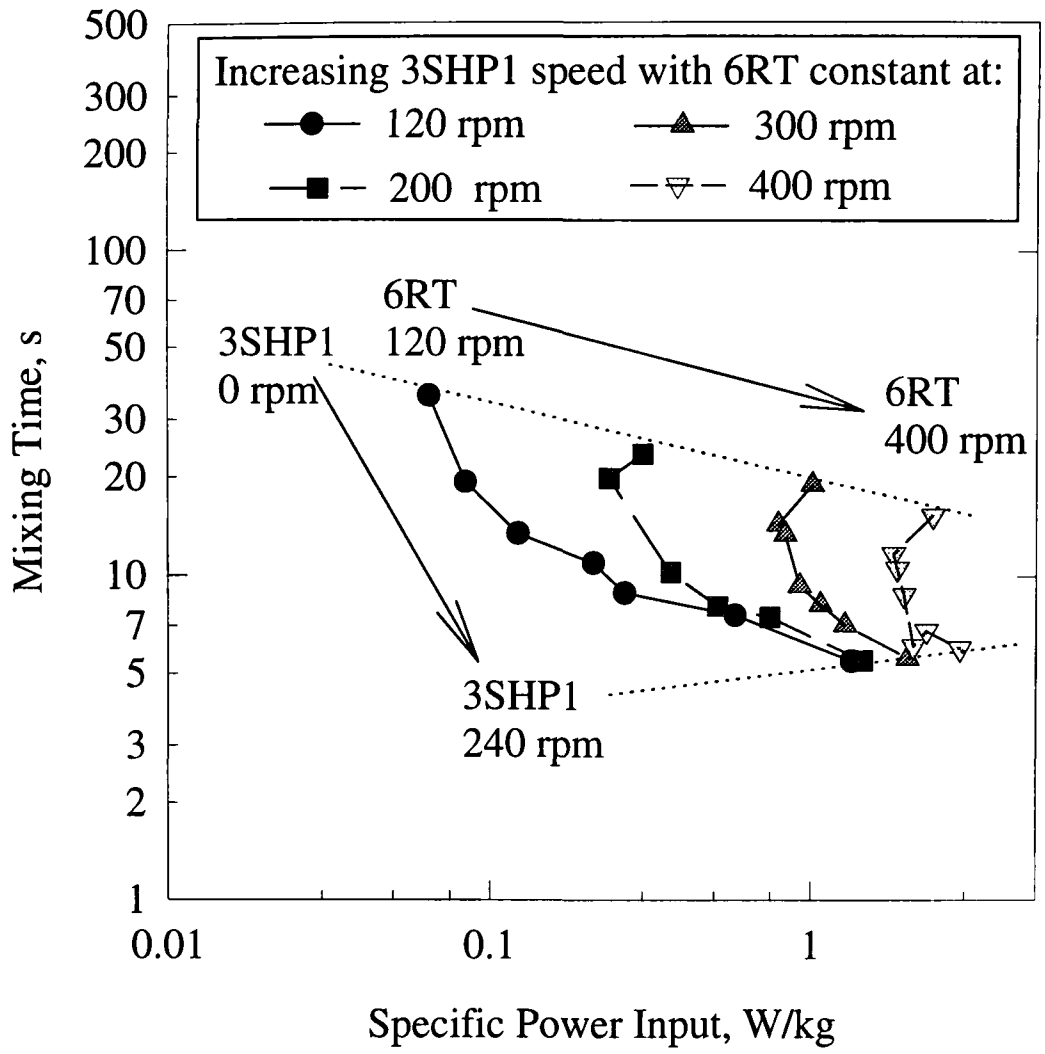

Figure 7.3-5 Mixing time as a function of power input for the IDDIDT

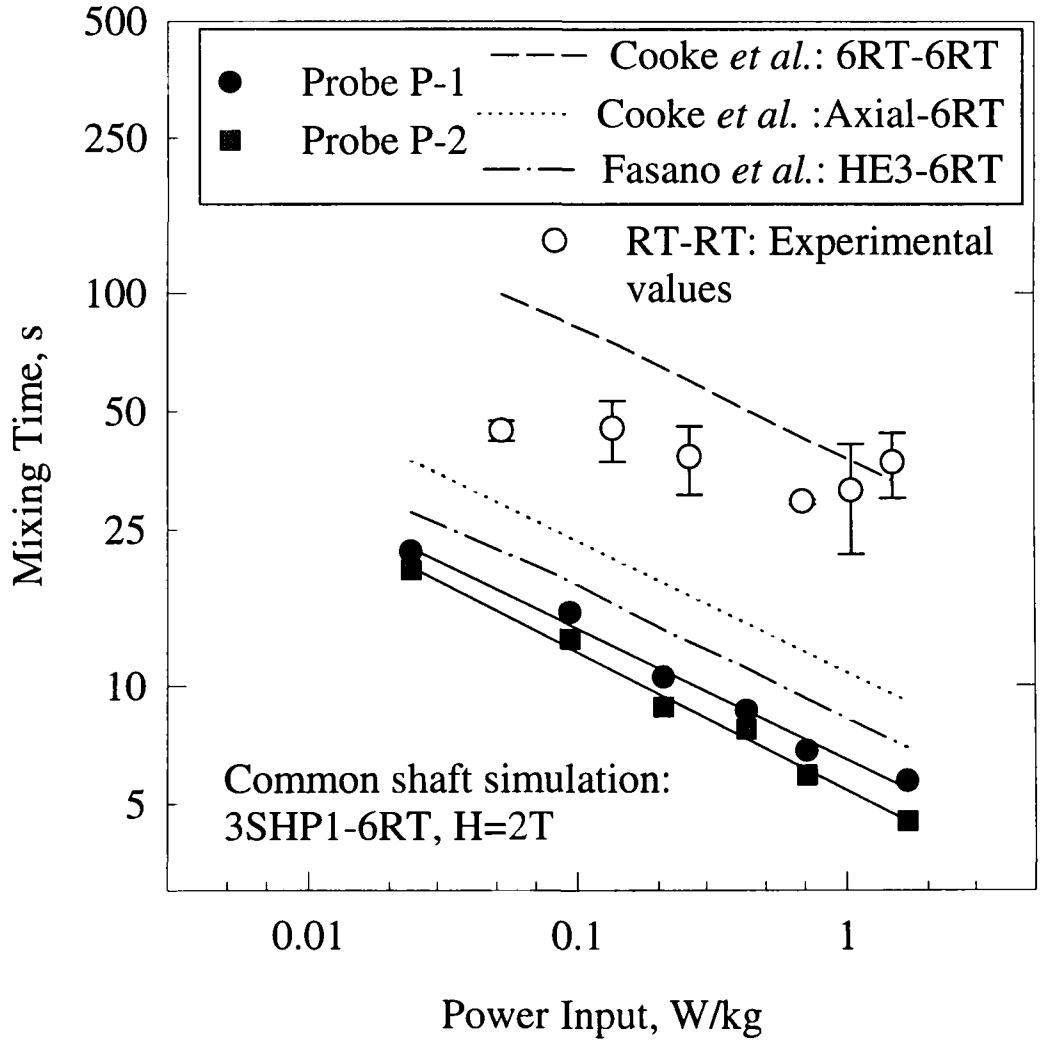

Figure 7.3-6 Mixing times for a mixed flow agitation system on a common shaft

$$\theta_m = 5.6\left(\frac{P_{SC}}{V}\right)^{-0.25}\left(\frac{P_{RT}}{V}\right)^{-0.08} \qquad (7.10)$$

This gives a regression coefficient r^2 of 0.95. A comparison of the predicted data from Equation 7.10 with those acquired experimentally can be seen in Figure 7.3-7.

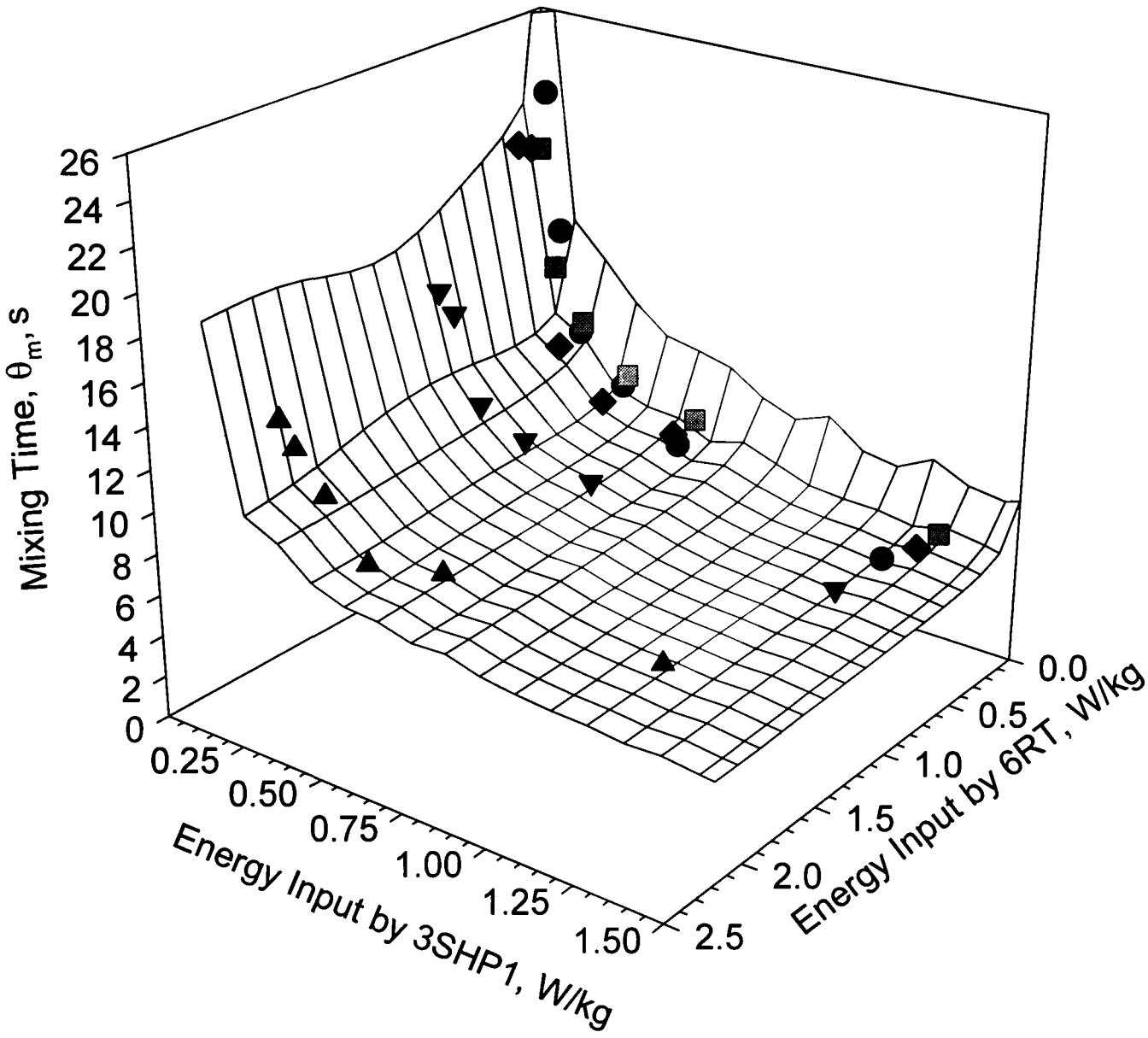

Figure 7.3-7 Comparison of experimental data with correlation

The similarity between the single 3SHP1 and the common shaft simulation can be explained since when both impellers are running at the same speed:

$$N_{SC}=N_{RT}$$

so,

$$\frac{P_{SC}}{P_{RT}} = \frac{Po_{SC} D_{SC}{}^{5}}{Po_{RT} D_{RT}{}^{5}} = \frac{0.42\left(\frac{2T}{3}\right)^{5}}{4.2\left(\frac{T}{3}\right)^{5}}$$

and therefore,

$$\frac{P_{SC}}{P_{RT}} = \frac{2.49}{1}$$

From Equation (7.10)

$$\theta_m = 5.6\left(\frac{P_{SC}}{V}\right)^{-0.25}\left(\frac{P_{SC}}{2.49V}\right)^{-0.08}$$

$$\theta_m = 6.02\left(\frac{P_{SC}}{V}\right)^{-0.33}$$

θ_m (common shaft) = 1.08 θ_m (single 3SHP1), for similar energy inputs.

That is mixing times are approximately 8% longer for the dual impeller common shaft configuration compared to the single 3SHP1 system for similar energy inputs. However, the blending remains more efficient in comparison to predictions for radial-radial (approx. 84% shorter) and axial-radial (about 40% shorter) configurations proposed by Cooke *et al.*[29]. For the radial-axial configuration the predictions using the Cooke *et al.* correlation were calculated using an average impeller diameter. Similarly, manipulation of the separate impeller speeds enabled mixing times approximately 50-80% faster to be achieved with the IDDIDT compared to the RT-RT. Inefficient blending in multi-impeller systems is often attributed to the onset of compartmentilisation around individual impellers, the poor

exchange flow rate between the well mixed compartments controlling the mixing process (Figure 7.3-8 (a)). Compartmentalisation is reduced for the situation with the draft tube, top to bottom mixing is enhanced and hence so is the blending efficiency (Figure 7.3-8 (b,c)).

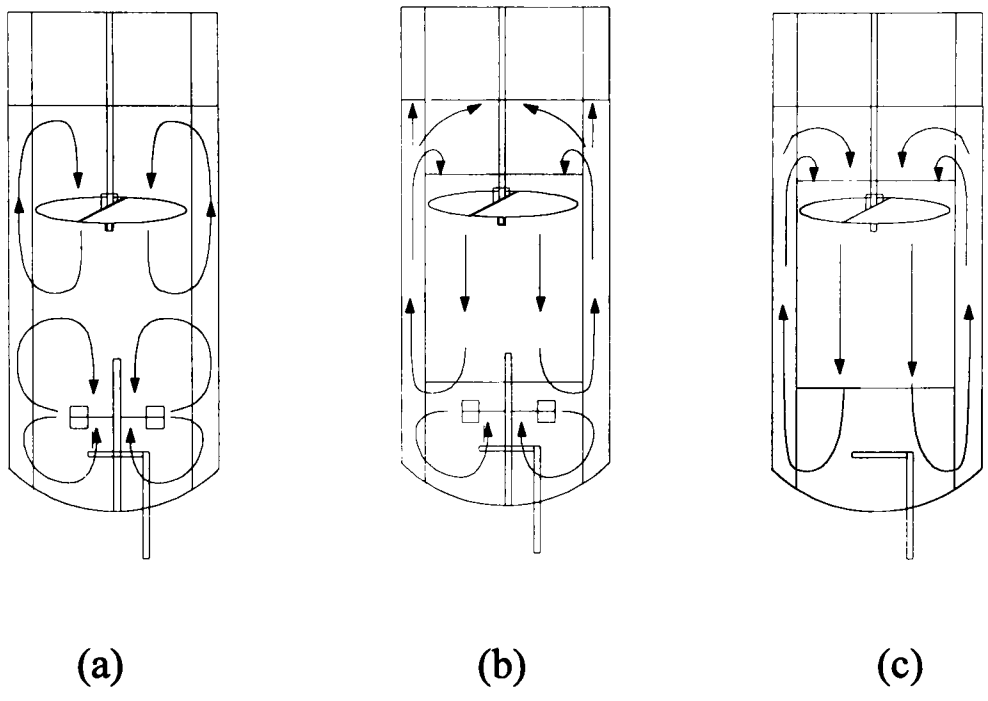

Figure 7.3-8 Flow patterns for (a) Dual impellers no draft tube; (b) dual impellers with draft tube; (c) single 3SHP1 with draft tube

The increased circulation rate achieved by the action of the 3SHP1 is demonstrated in Figure 7.3-9. Annular velocity (u_{an}) was calculated from the time elapsed between the initial responses of P-1 (θ_{R1}) and P-2 (θ_{R1}), *i.e.*

$$u_{an} = \frac{d_P}{\theta_{R2} - \theta_{R1}}$$

where d_p is the distance between the probes. It is evident that the circulation velocity is solely controlled by the speed of the 3SHP1 in the dual impeller configuration. In addition, the relatively poor mixing of the 6RT is explained by the low annular velocity in comparison to the 3SHP1 at similar impeller speeds.

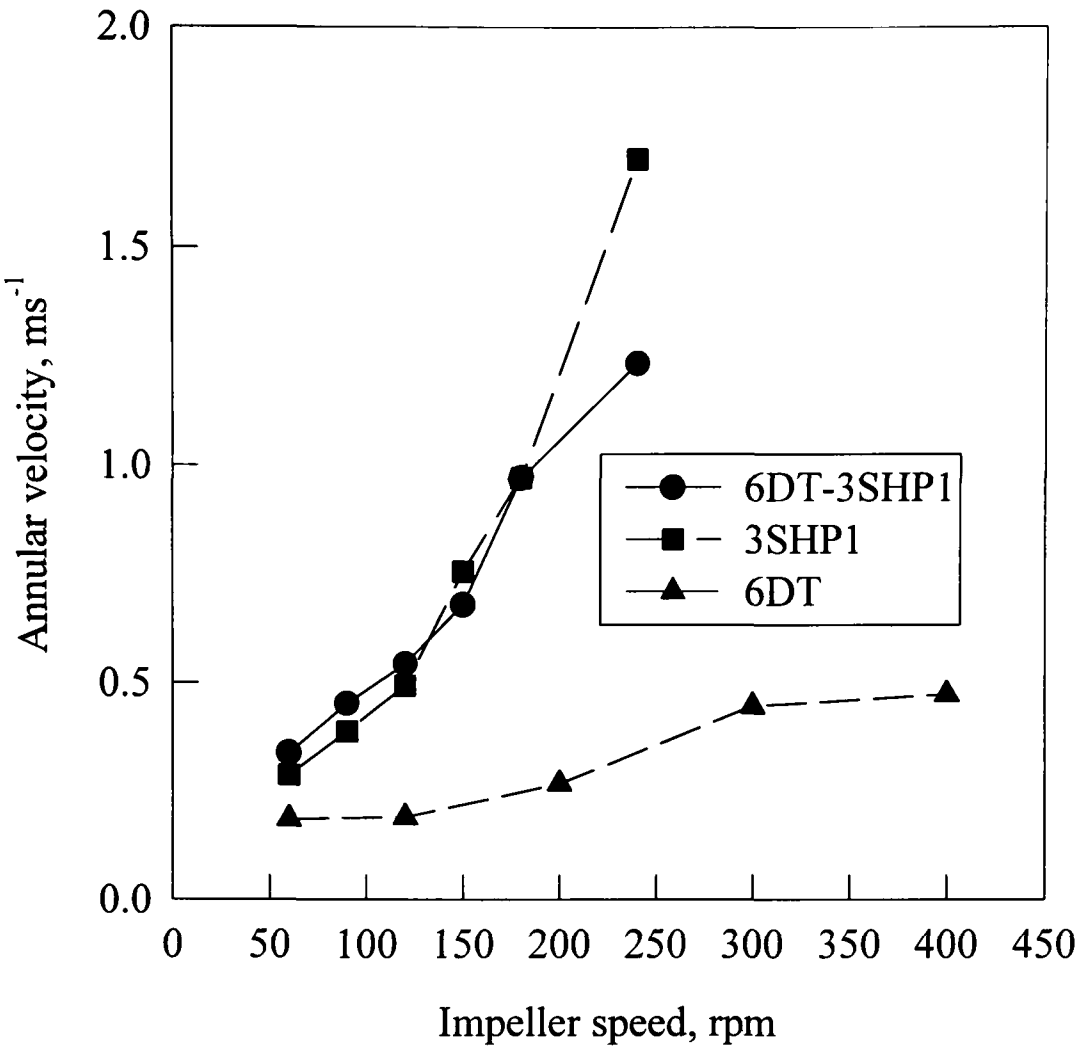

Figure 7.3-9 Annular velocity as a function of impeller speed.

7.3.1.3 Mixing efficiency of single and dual impeller systems

Mixing efficiency between single impellers, dual impeller common shaft systems and the IDDIDT are compared in Figure 7.3-10. The plot shows the power requirement, calculated from the proposed correlations, to achieve 95% homogeneity within a specified time. Clearly, the single 3SHP1 and the dual impeller common shaft configurations produce the necessary level of homogeneity with the minimum energy input. Blending efficiency then falls away with the use of IDDIDT configuration at low 6RT speeds, to the IDDIDT at high 6RT speeds and finally a single 6RT impeller is the least efficient (for set-ups with draft tube). Assuming a continuation of the trend seen for the RT-RT configuration (Figure 7.3-6) very high energy inputs (greater than an order of magnitude in comparison to IDDIDT) would be neccesary to achieve similar blend times. The dual Rushton turbine system, with no draft tube, is therefore the least efficient configuration.

Single 3SHP1	Common shaft	Independently-driven dual impellers			Single 6RT
(A)	(B)	(C) 6RT 200 rpm	(D) 6RT 300 rpm	(E) 6RT 400 rpm	(F)

Decreasing blending efficiency

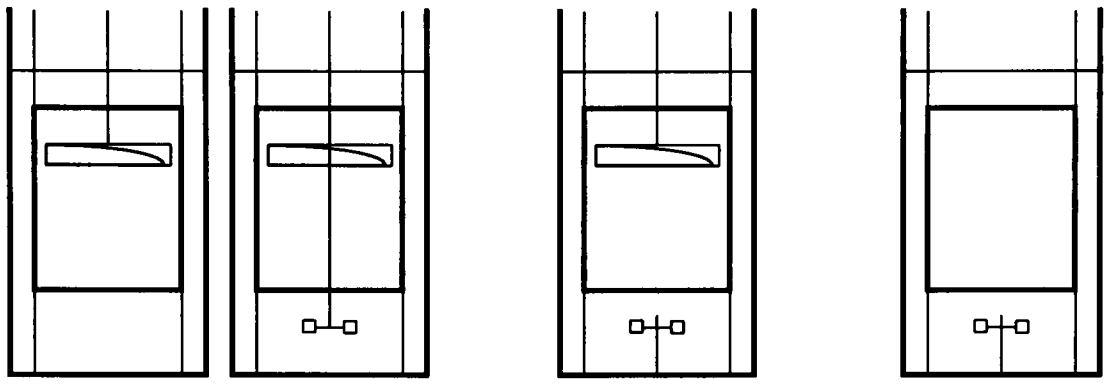

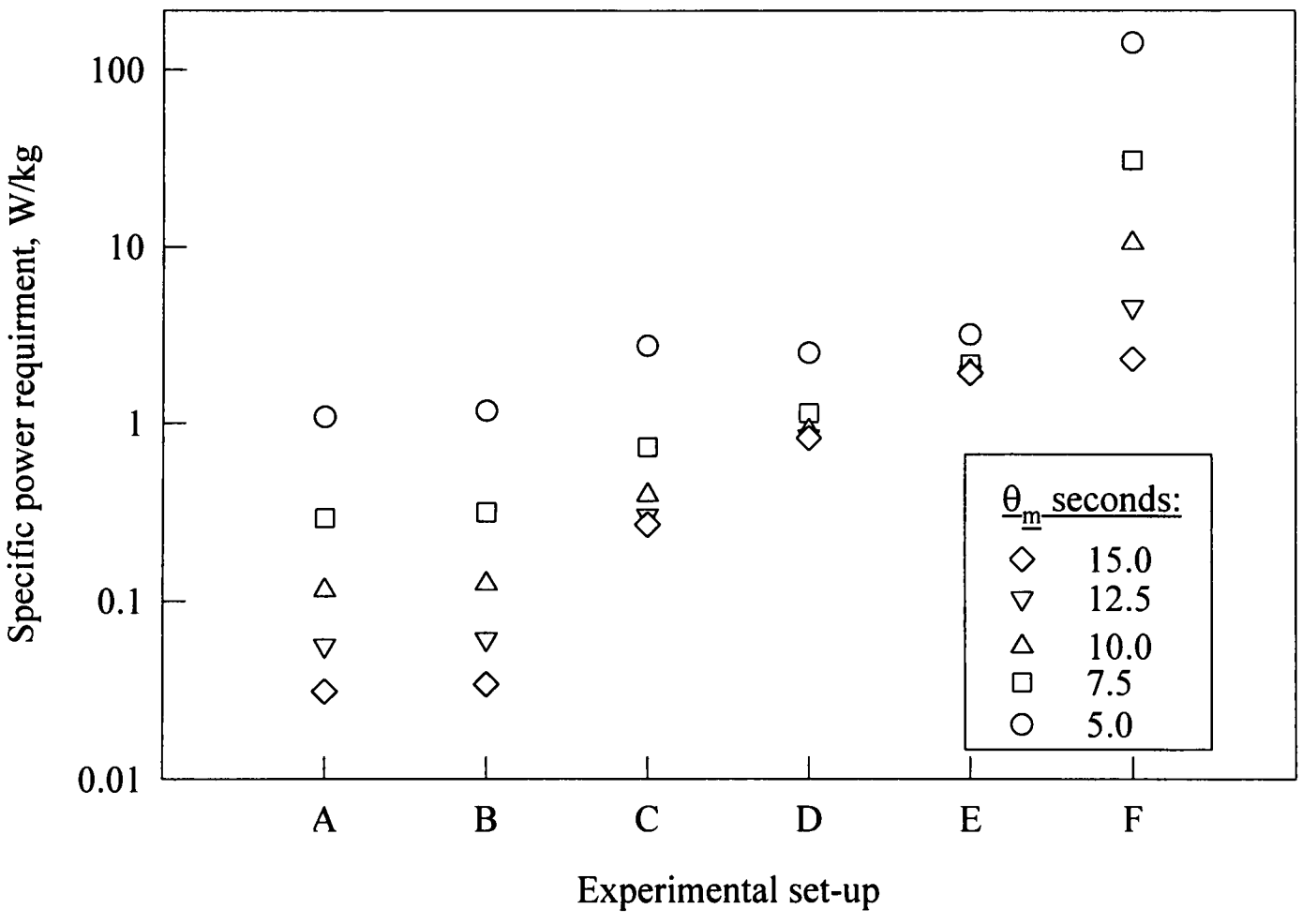

Figure 7.3-10 Minimum power requirements for bulk blending using various agitation systems

7.3.2 Aerated mixing time: Conductivity technique

7.3.2.1 Single impeller systems

Single 6RT. Under gassed conditions two distinct zones of mixing could be readily identified (Figure 7.3-11). At high power inputs, when the gas was completely dispersed, the impeller action controlled the mixing. Mixing time was still inversely proportional to N, although absolute values were incrementally higher than encountered in the unaerated situation. However, leveling off occurred at lower power inputs (0.2W/kg) and was attributable to the impeller becoming flooded. Here the gas controlled the blending and increasing gas flow rate shortened the mixing time. In fact, for similar energy inputs, blending was distinctly better when the impeller was flooded compared to when unaerated. The vessel is essentially acting as an airlift reactor with gas travelling up through the draft tube and down the annulus. The resultant density difference between the two-phase mixture in draft tube and annulus promoting liquid flow throughout the vessel. Probe responses offered evidence of the flow reversal, i.e. P-2 reacted fractionally faster than P-1 in the flooded regime, whereas the initial response of P-2 was slower than P-1 once the gas was dispersed (Figure 7.3-17). The reversal in annular velocity is displayed in Figure 7.3-16. Decolorisation experiments (Section 7.2.3) support the above explanation of the different two phase flows.

Single 3SHP1. Aeration has a more drastic effect on the blending performance of the 3SHP1 than the 6RT (Figure 7.3-12). Here aeration lengthened the mixing times considerably. This was probably due to the formation of gas cavities reducing the axial pumping capacity of the impeller. Increasing superficial gas velocity increases the mixing times, although to a lesser extent at higher impeller speeds. Flow reversal was apparent when the impeller became flooded (Figure 7.3-16).

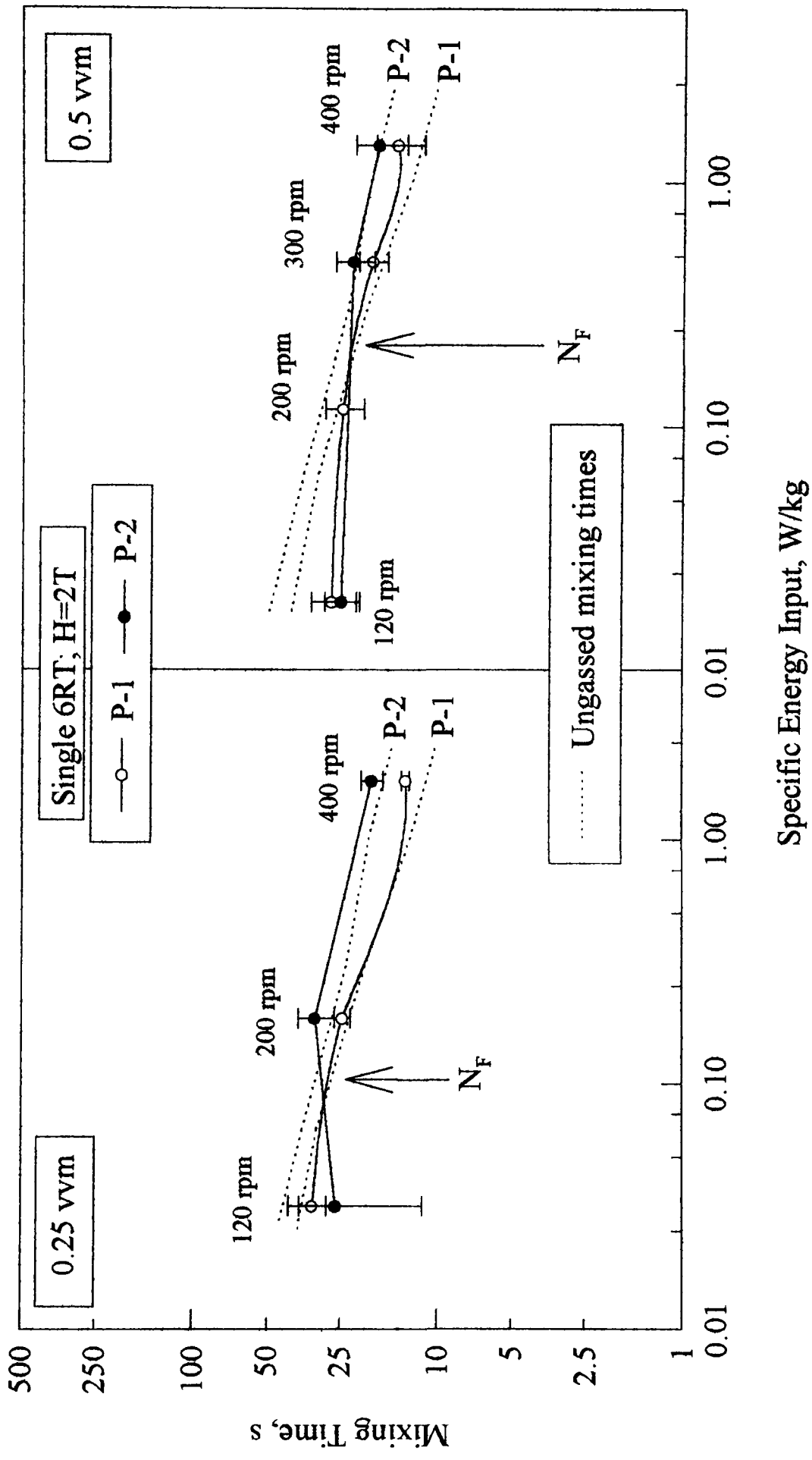

Figure 7.3-11 Aerated mixing times for single 6RT with draft tube

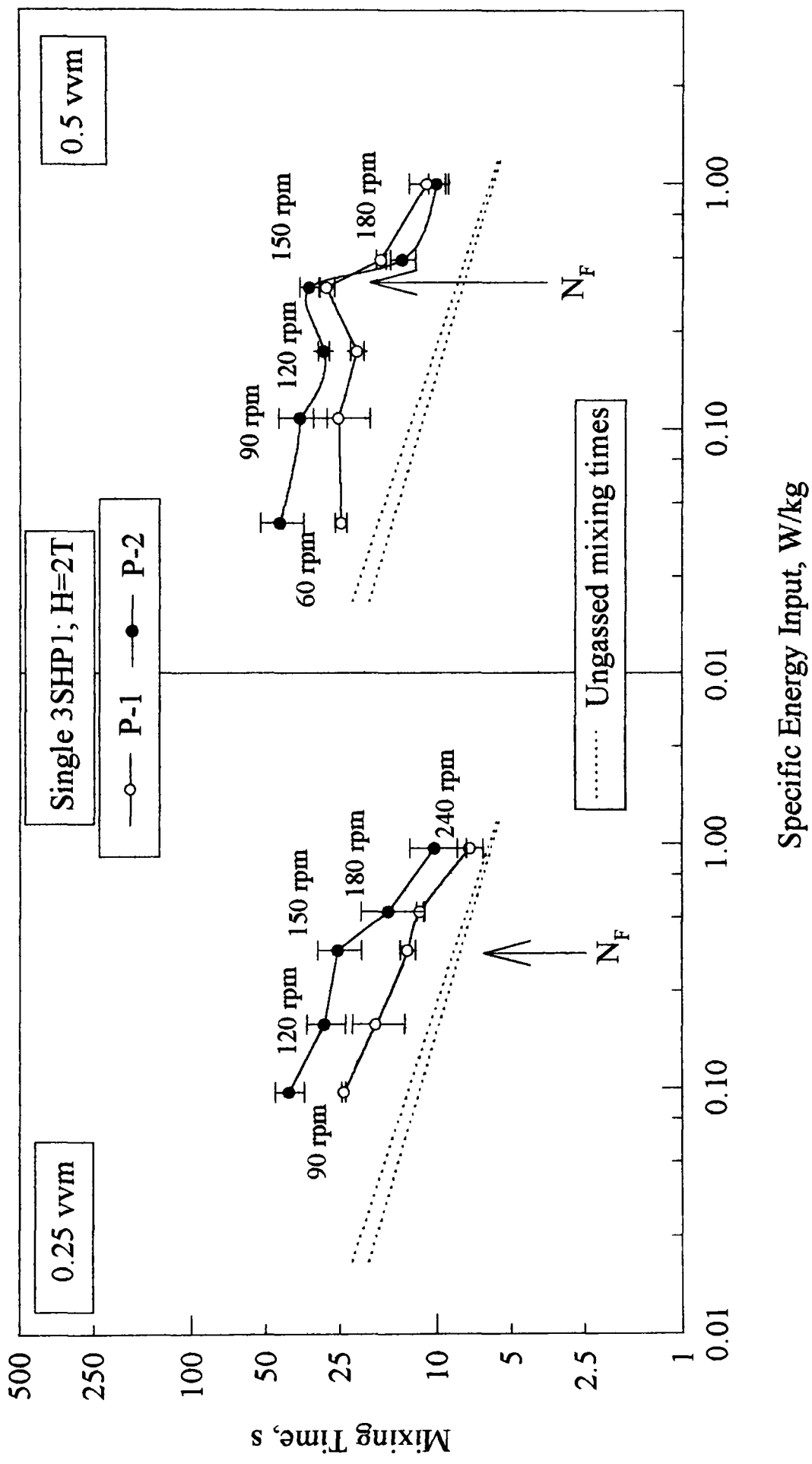

Figure 7.3-12 Aerated mixing times for the single 3SHP1 with draft tube

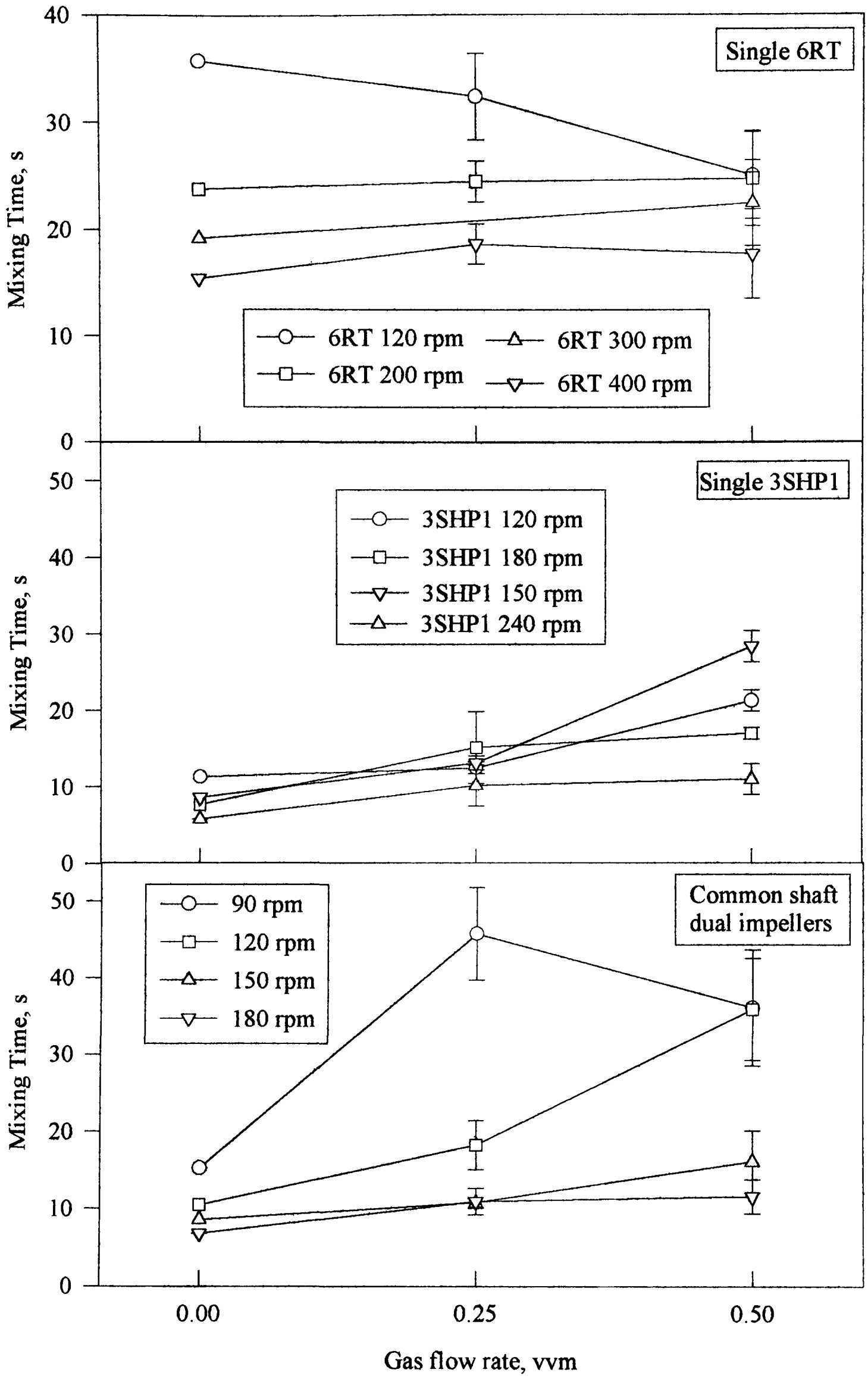

Figure 7.3-13 Effect of increasing gas flow rate on mixing times of single impeller and common shaft systems

7.3.2.2 Dual impeller systems

Common shaft. Two distinct regions of mixing, similar to those observed for the 6RT, were experienced by the dual impeller common shaft simulation (Figure 7.3-14). At impeller speeds lower than that required to prevent flooding (~120 rpm) mixing times were longer, for similar energy inputs, than when ungassed and shortened with increasing superficial gas velocity. For a constant gas flow rate, increasing impeller speed lengthened the mixing time until loading/dispersion occurred, at which point any further increase in speed reduced the mixing time. The initial increase in mixing time was due to the axial action of the 3SHP1 impeller opposing the flow promoted by the rising gas bubbles. This resulted in the formation of stagnant regions directly below the 3SHP1. Following gas dispersion the flow promoted by bubble action and that produced by the 3SHP1 is co-current and hence mixing times decreased rapidly with increasing impeller speeds. At high impeller speeds (>180 rpm) blending performance is similar to the ungassed situation. Once again the flow reversal is displayed in Figure 7.3-16 and verified by decolorisation experiments (Section 7.3.3).

IDDIDT. It was discovered that, for similar impeller speeds, mixing times increased on aeration, especially if the 6RT was flooded (Figure 7.3-15). If the gas was dispersed, increasing the aeration rate lengthened the mixing time whereas under flooded conditions any increase in aeration rate resulted in faster mixing times.

The influence of gas was found to be very dependent on the operating variables. At a gas flow rate of 0.5vvm and with high 6RT speeds (400 rpm) the increase in mixing times for similar agitation rates was offset by a large reduction in the power draw, seemingly producing similar mixing times at lower power inputs. However, at lower impeller speeds and lower gas flow rates the reduction in power drawn by the impellers was insignificant compared to the resultant increase in mixing times. Therefore for similar power inputs the

mixing time is seen to increase on aeration though at the higher speeds aerated and unaerated times were almost equal and much less than with standard dual impeller configurations.

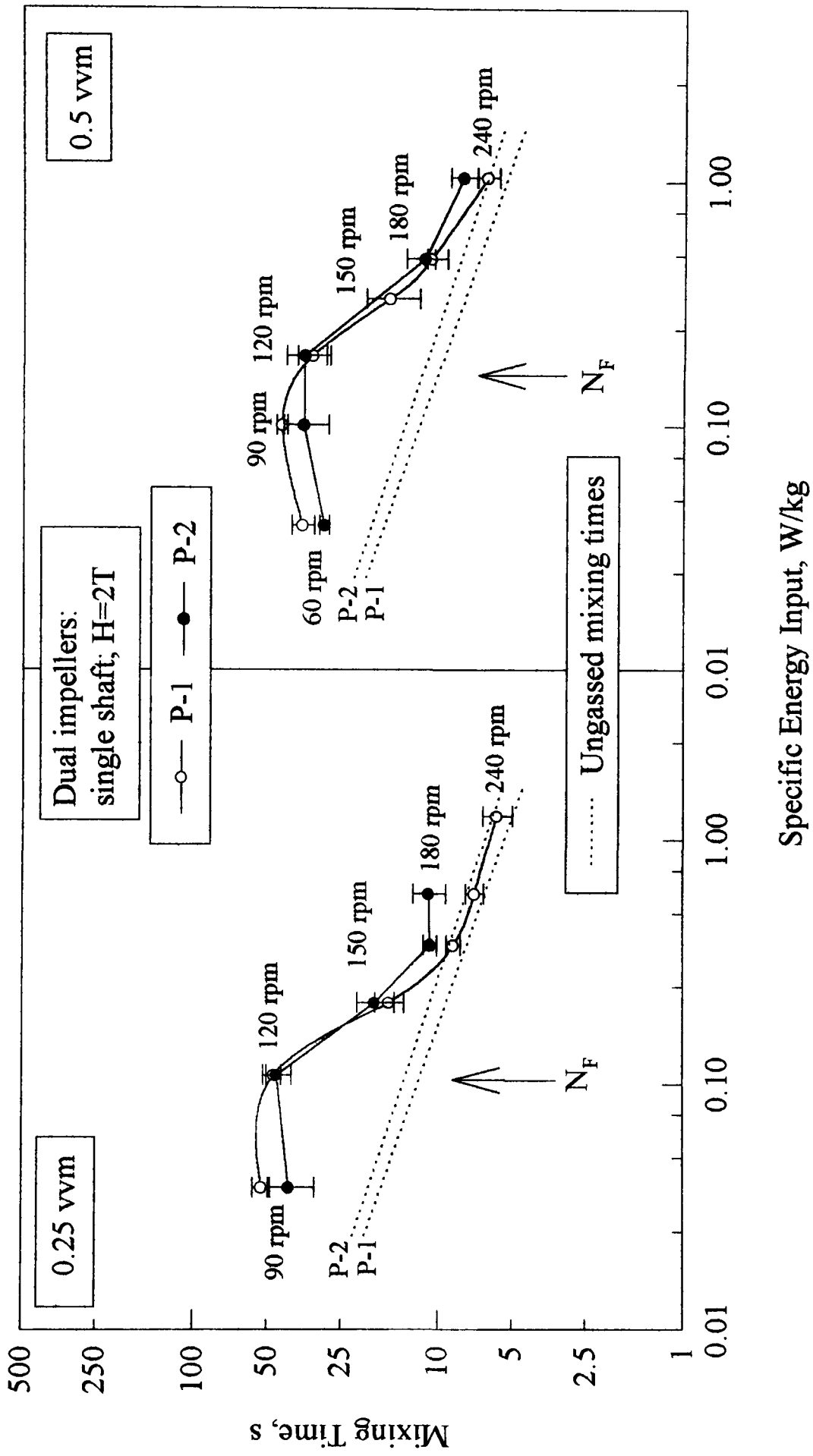

Figure 7.3-14 Aerated mixing times for the dual impeller common shaft simulation

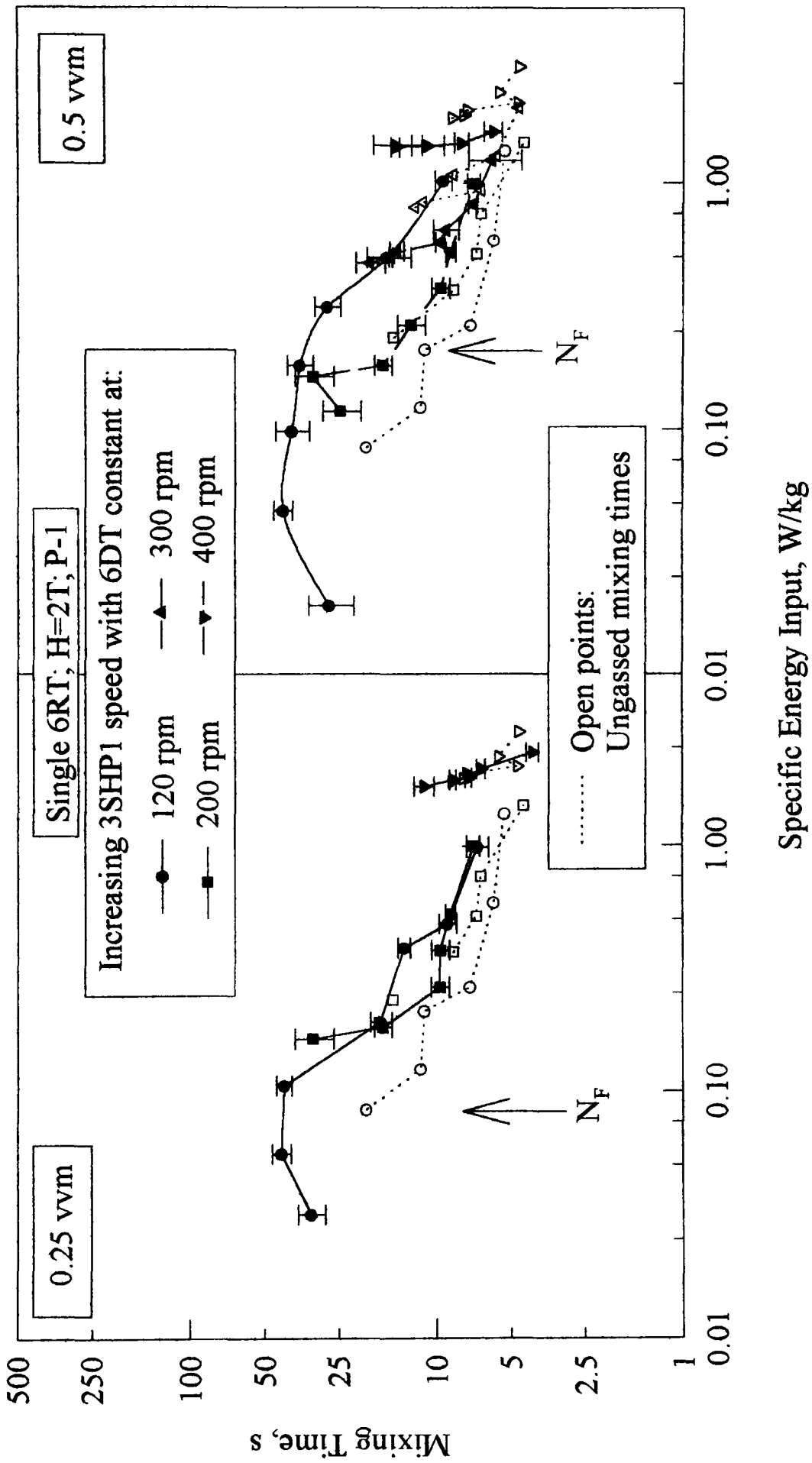

Figure 7.3-15 Aerated mixing times for the IDDIDT

7.3.2.3 Effect of aeration on annular velocity and flow patterns

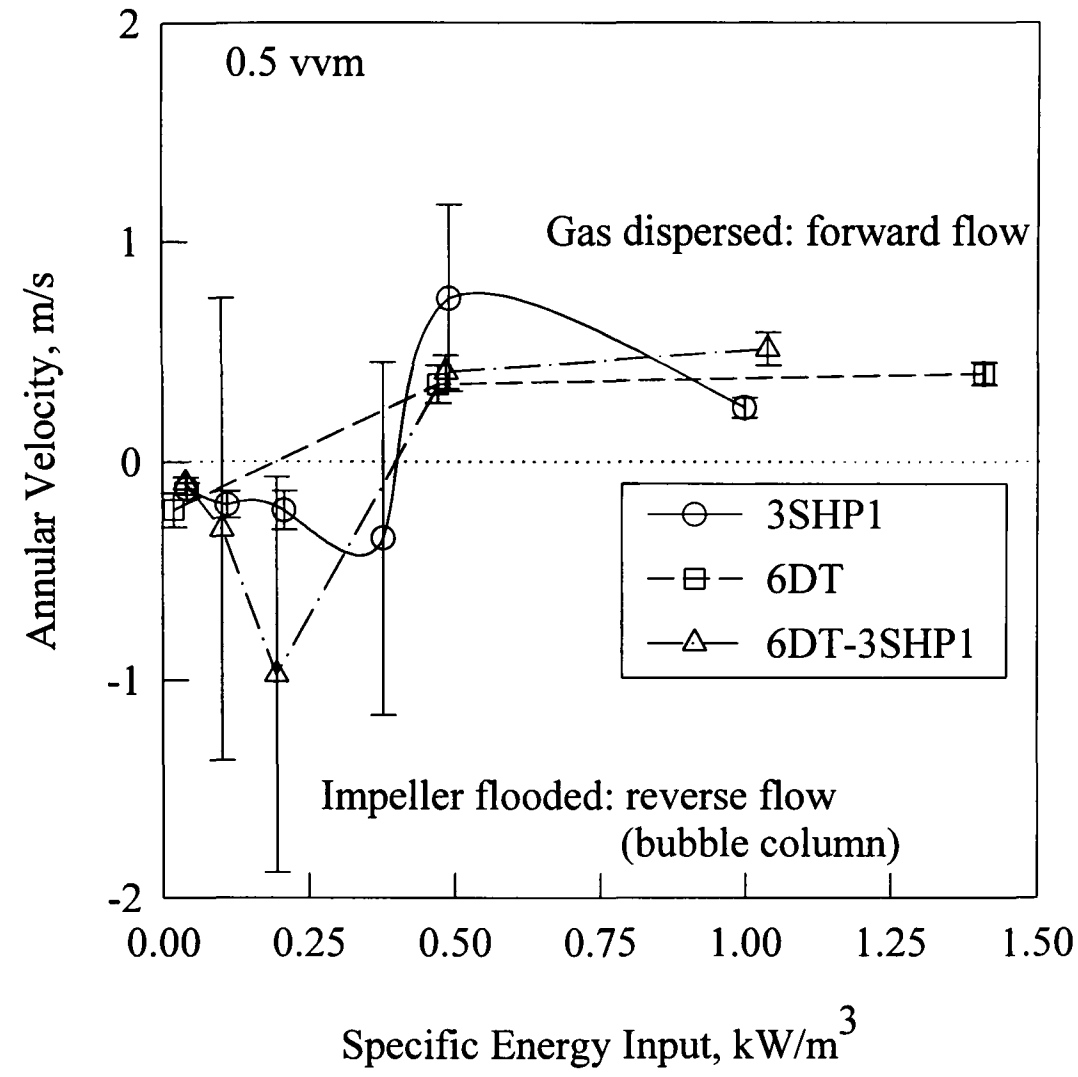

Figure 7.3-16 Effect of gas flow rate on annular velocity

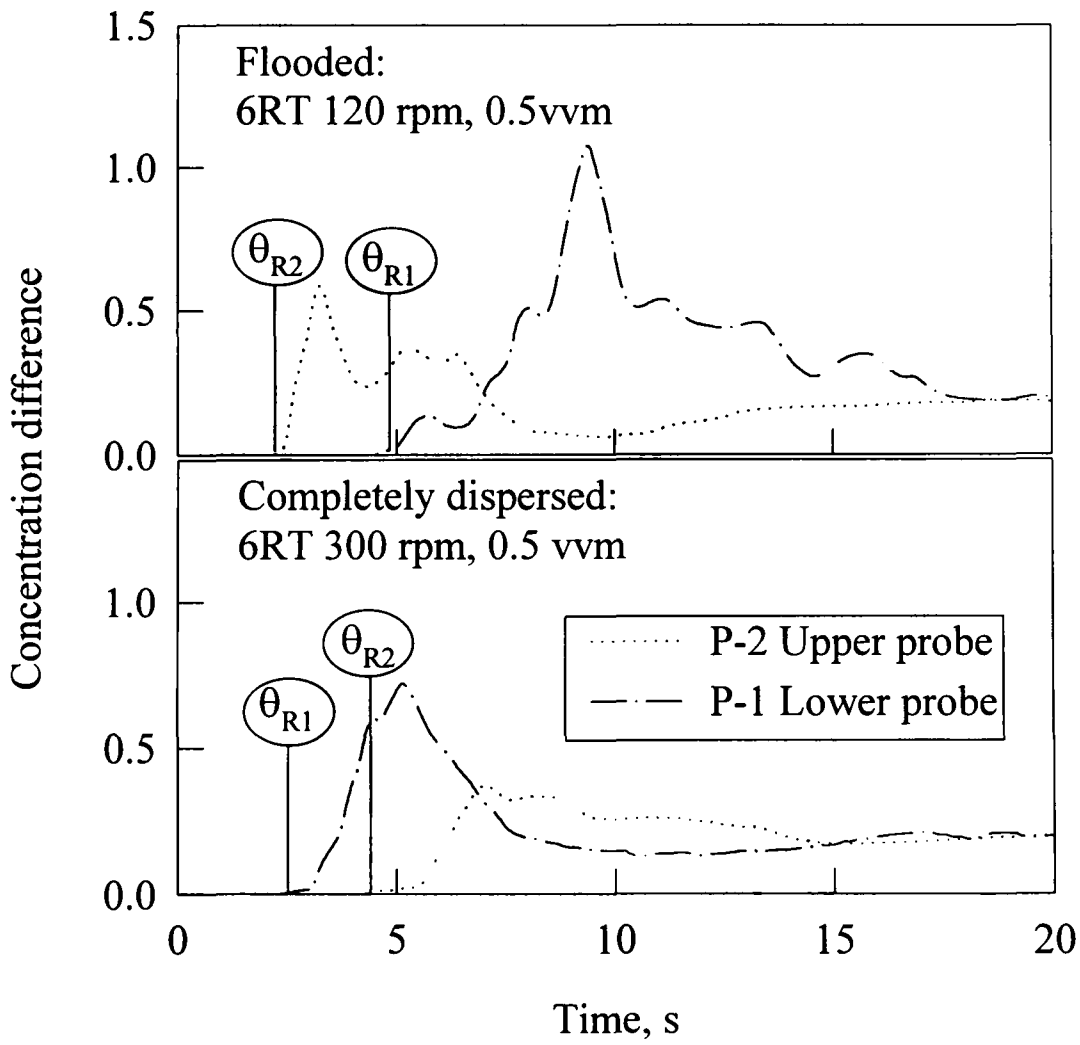

Figure 7.3-17 Probe response times under flooded and completely dispersed conditions

Flow patterns for differing hydrodynamic conditions, investigated in Section 4.3.2.3.1 and Section 7.3.3, were used to help explain the situation occurring when the 6RT was initially flooded (120 rpm) and the 3SHP1 speed is increased (Figure 7.3-14 and Figure 7.3-17). With the 6RT flooded and the 3SHP1 non-operational (a), gas flowed up into the draft tube creating a density difference and caused liquid to rise up the draft tube and flow back down through the annulus, in a similar manner as would be expected in a bubble column. Increasing the 3SHP1 speed from 0 to 60 rpm produced a downward axial flow opposing the upward force caused by the rising bubbles, resulted in a stagnant region in the draft tube ((a-b)) and hence increased the mixing time. Here the flow tended to fluctuate and gross errors are observed when calculating the annular velocity. At higher impeller speeds (*e.g.* greater than 90 rpm for the 3SHP1) the downward axial flow was greater than that of the rising bubbles and the direction of flow was reversed, *i.e.* liquid flows up the annulus and down through the draft tube (b) and the mixing time was reduced. However, it was noted that the pumping capacity of the 3SHP1 was also lowered compared to the unaerated case

7.3.3 Mixing Times: decolorisation technique

As explained previously the results from the decolorisation technique are used to qualitatively describe the process of mixing within the reactor.

7.3.3.1 Unaerated mixing times

Figure 7.3-18 shows the sequence of colour change for the unaerated IDDIDT system at a 6RT speed of 120 rpm and 3SHP1 speed of 60 rpm. The flow pattern observed here is similar for all unaerated dual impeller configurations. Initially the sodium thiosulphate is discharged into the draft tube and pumped downwards by the 3SHP1 into the well mixed zone surrounding the 6RT (3 seconds). After 6 seconds the lower half of the tank has decolorised and the $Na_2S_2O_3$ is clearly travelling up through the annulus. The unreacted

iodine is drawn from the annulus, by the axial pumping force of the 3SHP1, and has nearly filled the draft tube within approximately 9 seconds. Final decolorisation occurs near the 6RT after about 15 seconds.

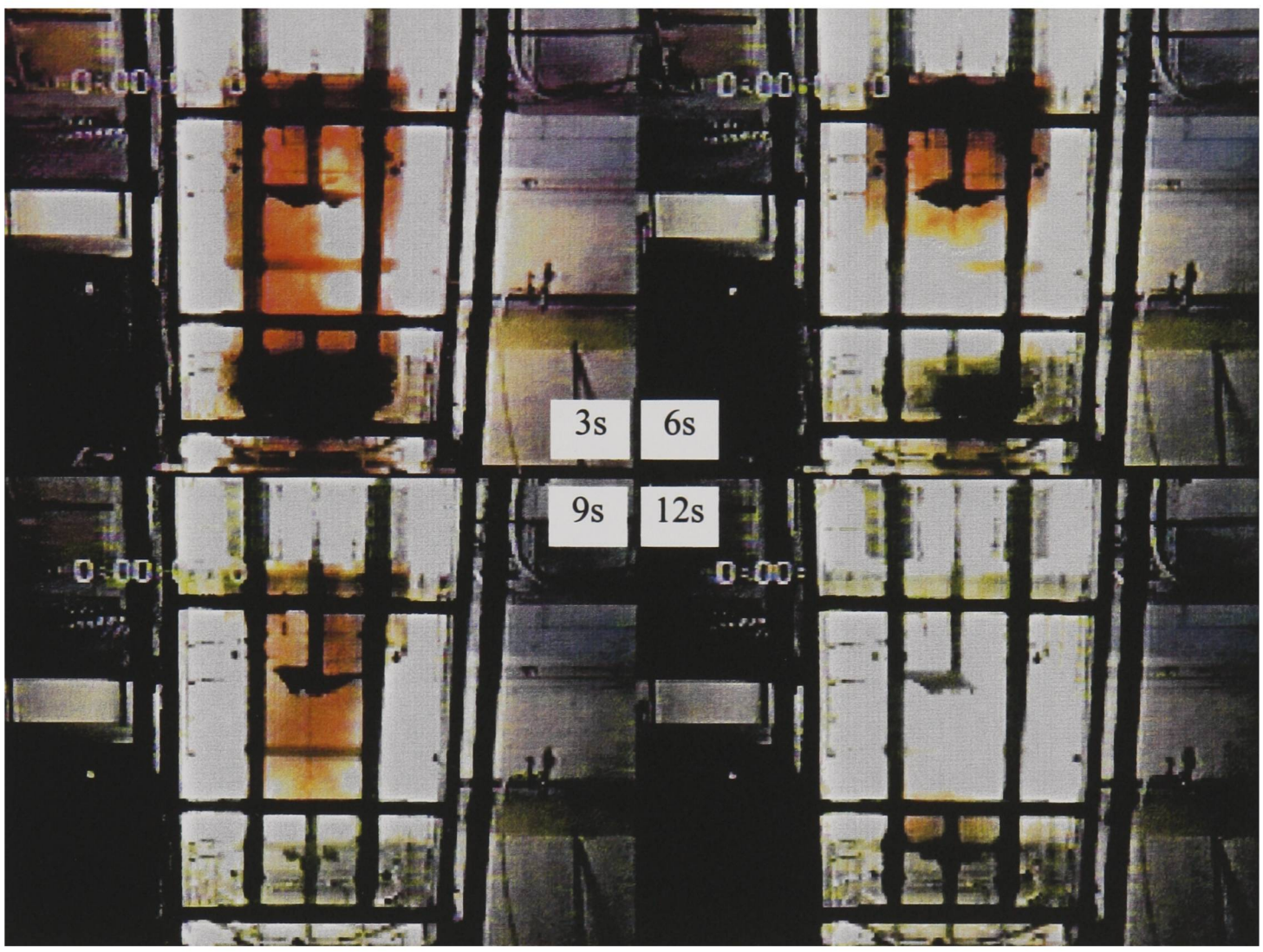

Figure 7.3-18 Mixing time for IDDI with 6RT at 120 rpm and 3SHP1 at 60 rpm using the conductivity technique

Figure 7.3-19 and Figure 7.3-20 show the progress of decolorisation for 6RT speeds of 200 and 300 rpm respectively with an increase in 3SHP1 speed from (a) 60 rpm to (b) 120 rpm and finally (c) 240 rpm. In all cases the progress of decolorisation is similar and occurs more rapidly for increased 3SHP1 speeds ((a) to (c)). However it is noticeable that increased 6RT impeller speed has little or no influence on the circulation rate of iodine and hence does not significantly improve the blending. The limiting factor is evidently the rate at which unreacted iodine contacts the highly mixed region surrounding the 6RT and is therefore dependent upon the axial pumping action of the 3SHP1.

a)

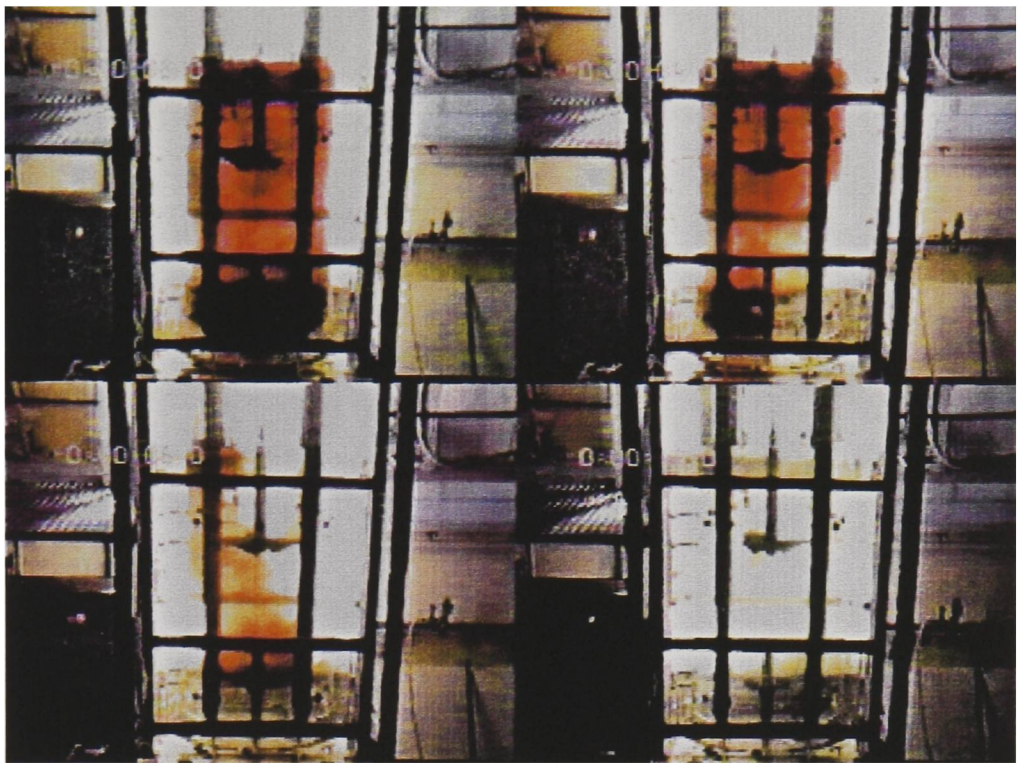

2 s	4 s
8 s	12 s

b)

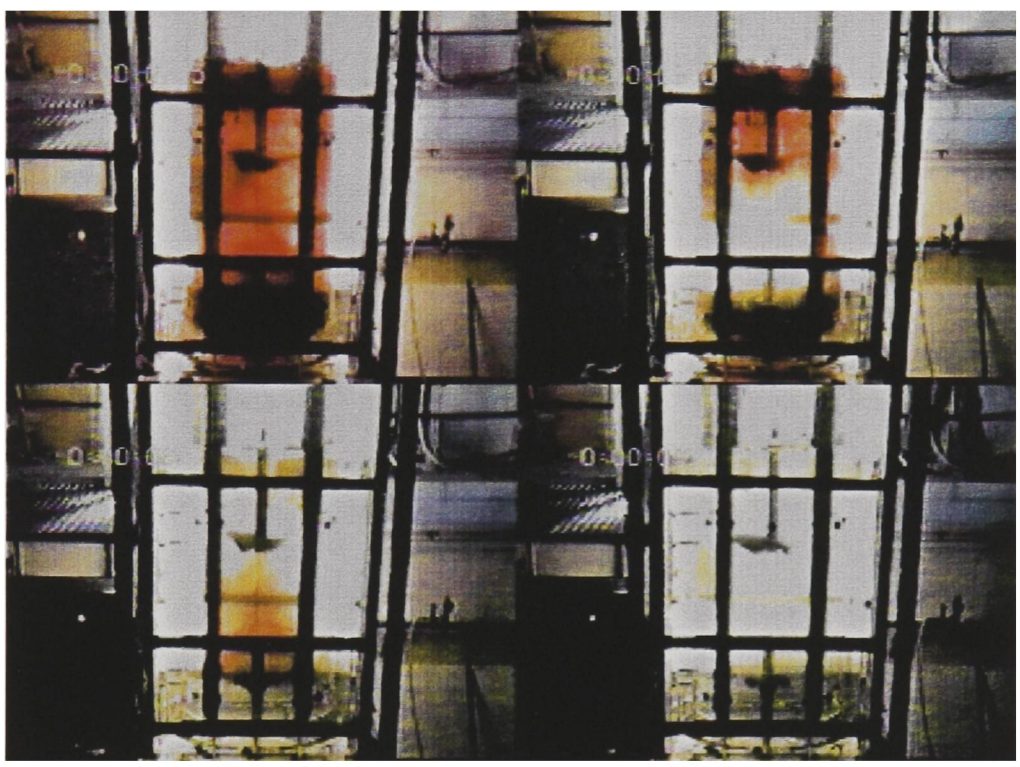

1.5s	3 s
6 s	8 s

c)

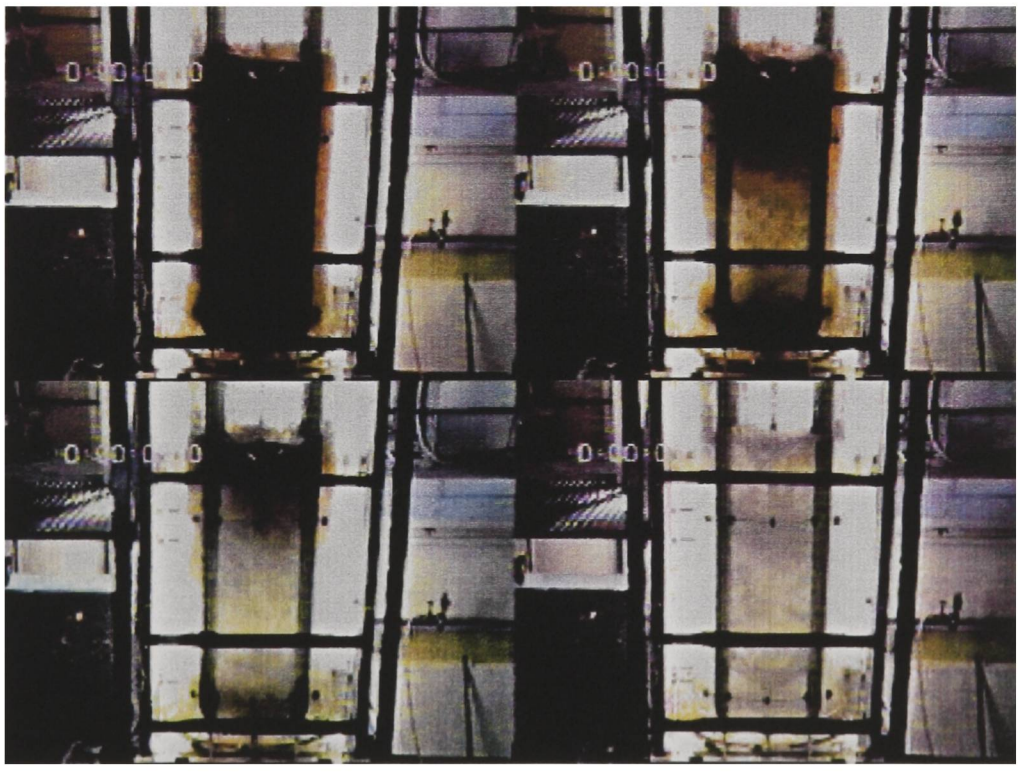

1 s	2 s
3 s	5 s

Figure 7.3-19 Unaerated mixing time fot the 6RT at 200 rpm and 3SHP1 at (a) 60 rpm (b) 120 rpm (c) 240 rpm

a)

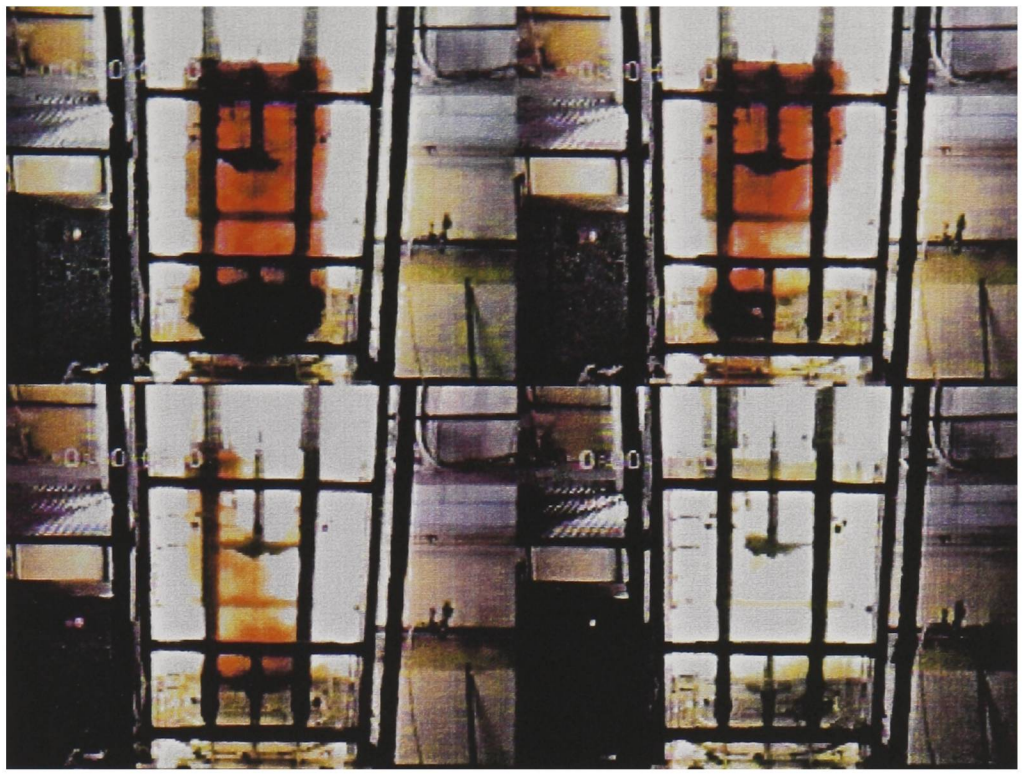

2 s	4 s
8 s	12 s

b)

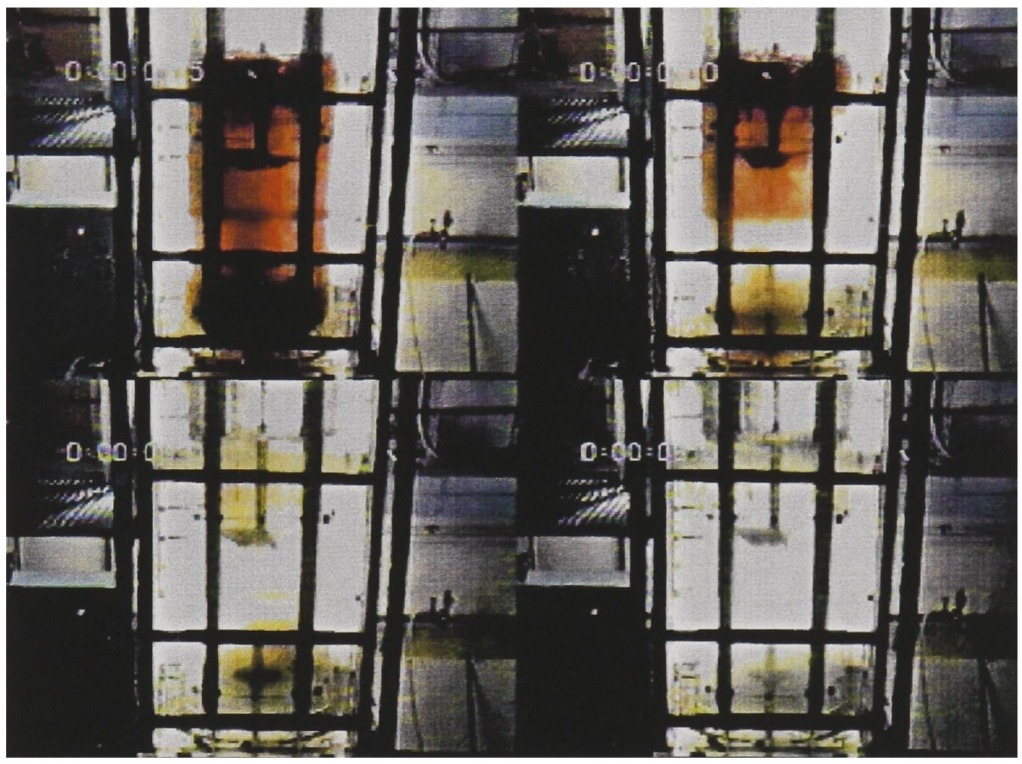

1.5s	3 s
6 s	8 s

c)

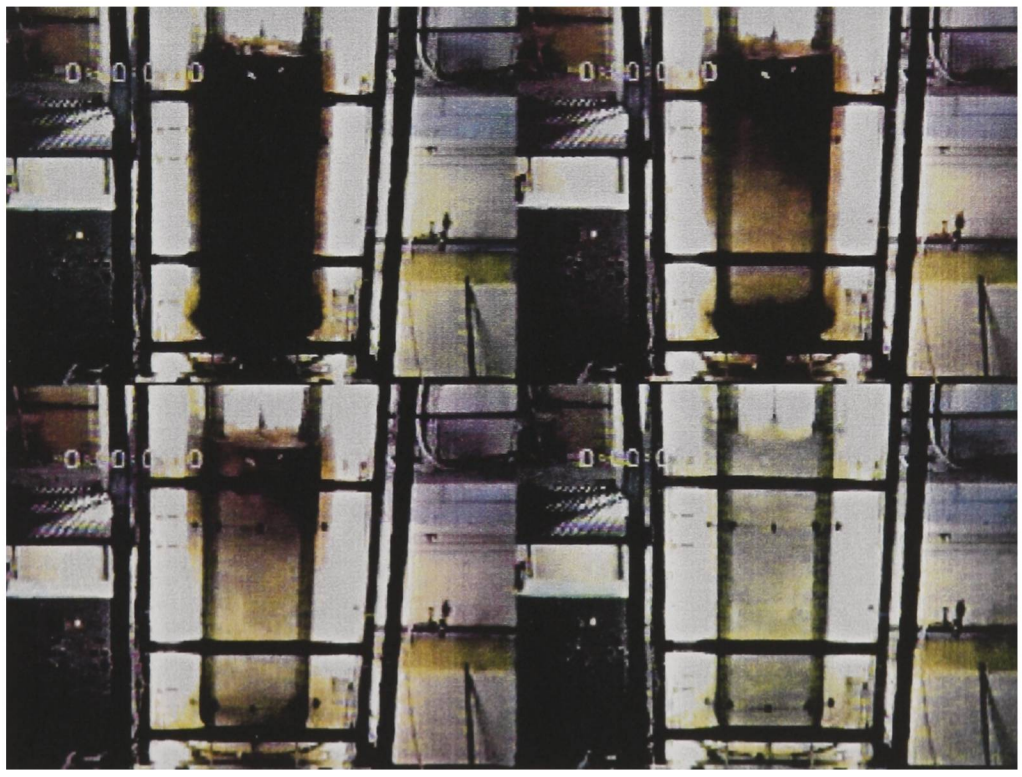

1 s	2 s
3 s	5 s

Figure 7.3-20 Unaerated mixing time fot the 6RT at 300 rpm and 3SHP1 at (a) 60 rpm (b) 120 rpm (c) 240rpm

7.3.3.2 Aerated mixing times

With 6RT impeller speeds lower than that required to prevent flooding, flow reversal was often observed. Figure 7.3-21 shows the sequence of colour change for the IDDI system at 0.25 vvm with a 6RT speed of 120 rpm and a 3SHP1 speed of 60 rpm. The flow pattern observed is opposite to that encountered under all unaerated conditions. Initially the sodium thiosulphate was discharged into the draft tube and moved upwards due to the flow promoted by the rising bubbles. After 10 seconds the upper half of the tank had decolorised and the $Na_2S_2O_3$ was clearly travelling down through the annulus. The unreacted iodine was drawn from the annulus by the rising bubbles and nearly filled the draft tube within approximately 17.5 seconds. Final decolorisation occurred near the 3SHP1 after about 25 seconds.

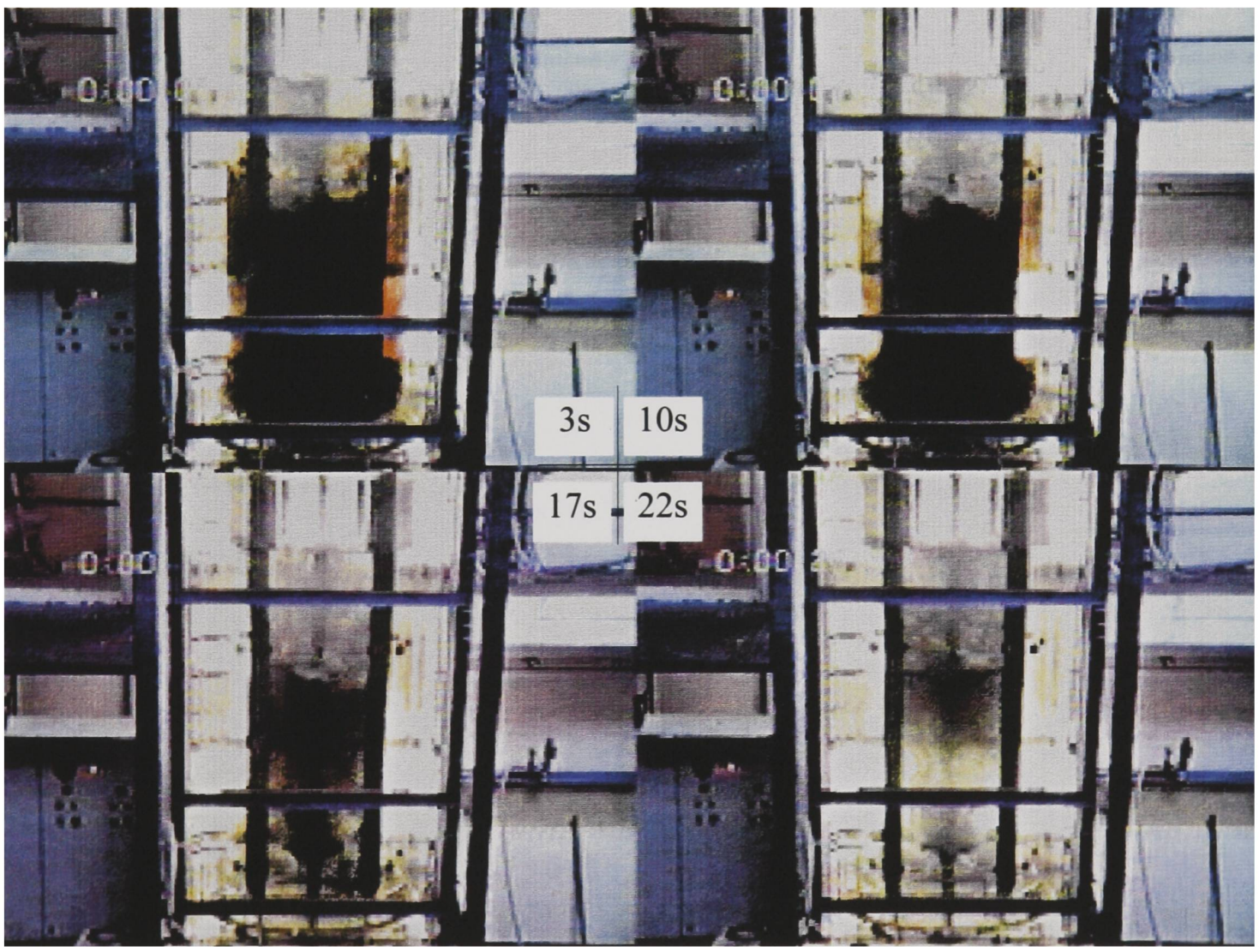

Figure 7.3-21 Mixing time using the decolorisation technique under flooded conditions

The visual observations for decolorisation when the gas was completely dispersed are shown in Figure 7.3-22 and Figure 7.3-23. The air flow rate was set at 0.25 vvm, the 6RT speed

constant at 200 rpm (Figure 7.3-22) or 300 rpm (Figure 7.3-23) and the 3SHP1 impeller speed increased from 60 rpm to 240 rpm, as with the unaerated case. For each set of conditions the process of decolorisation was essentially the same as the unaerated case although the observed mixing times were slightly longer. For example, at 6RT speed of 200 rpm and 3SHP1 speed of 120 rpm initial decolorisation of the lower half of the vessel (sodium thiosulphate travelling up annulus) took 6 seconds for the aerated case compared to approximately 3 seconds when unaerated. The difference however was less pronounced for higher 6RT speeds.

a)

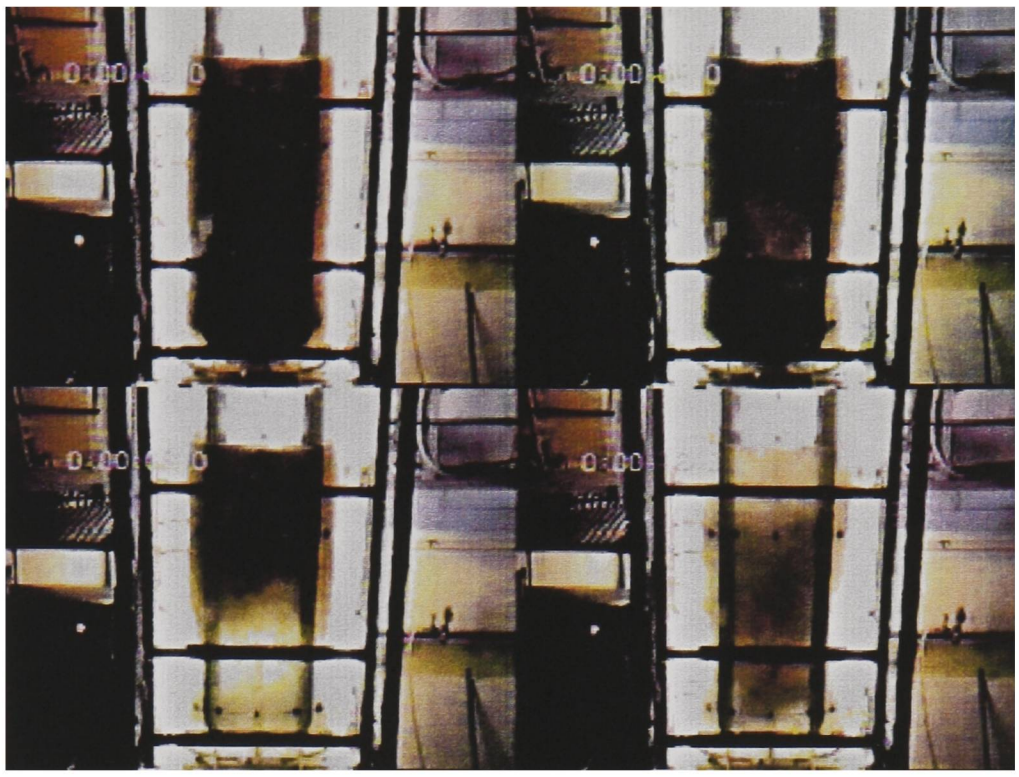

2 s	4 s
8 s	12 s

b)

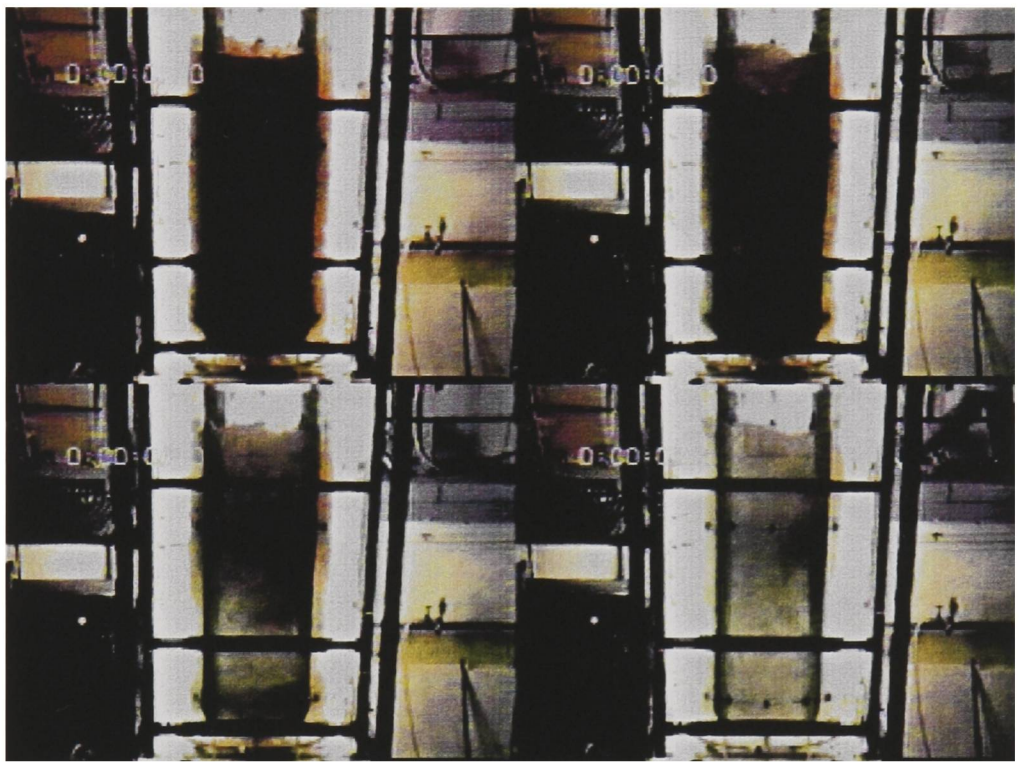

1.5s	3 s
6 s	8 s

c)

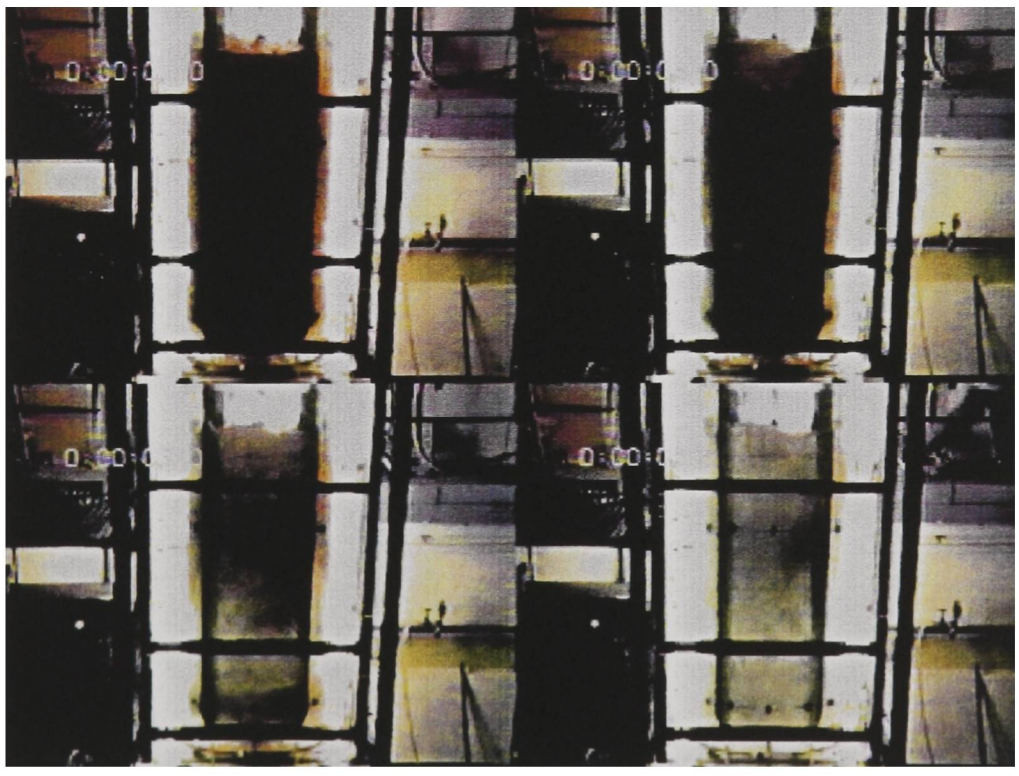

1 s	2 s
3 s	5 s

Figure 7.3-22 Aerated mixing time fot the 6RT at 200 rpm and 3SHP1 at (a) 60 rpm (b) 120 rpm (c) 240rpm

a)

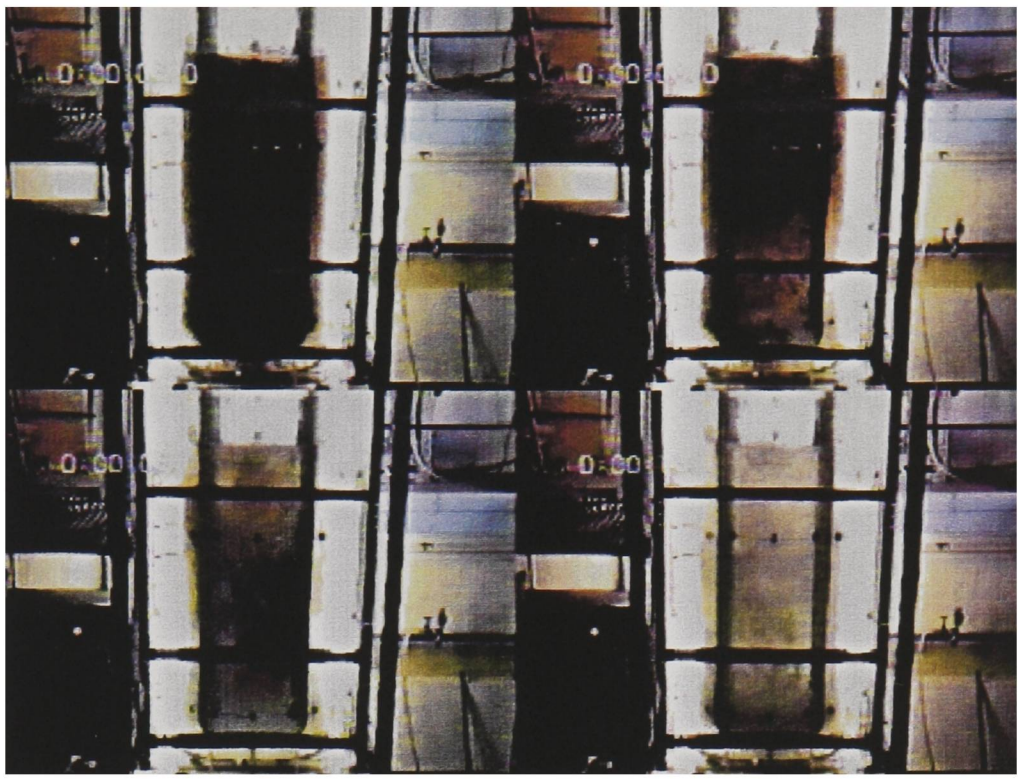

2 s	4 s
8 s	12 s

b)

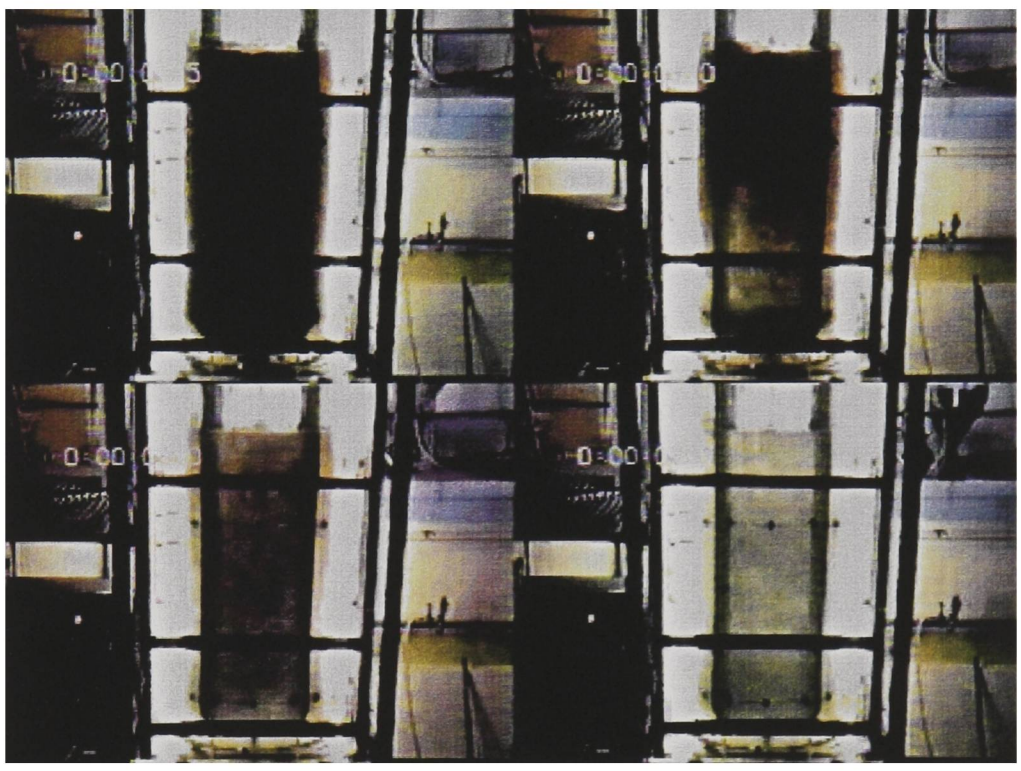

1.5s	3 s
6 s	8 s

c)

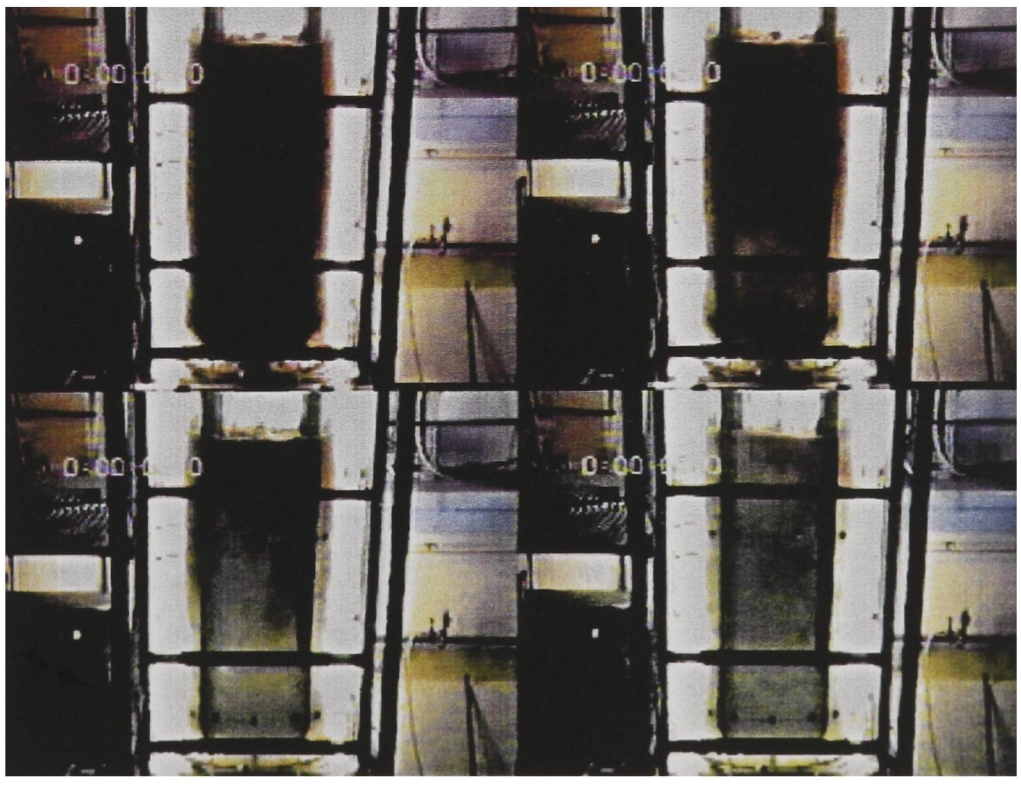

1 s	2 s
3 s	5 s

Figure 7.3-23 Aerated mixing time fot the 6RT at 300 rpm and 3SHP1 at (a) 60 rpm (b) 120 rpm (c) 240rpm

7.3.3.3 Effect of rheology on mixing times

The affect of rheology on the blending performance of ungassed agitation systems was investigated using 0.7% CMC solution in water. This enabled *Re's* in the transitional regime ($330<Re_{RT}<916$ and $477<Re_{SP}<3664$ (K=1.65, n=0.53)) to be studied. The mixing times are displayed in Table 7.3-2. It is noticeable that for the single 6RT mixing efficiency was significantly reduced with increasing broth viscosity, homogenisation taking minutes rather than seconds (Figure 7.3-24). For low 6RT speeds (<120 rpm) dead zones were visible below the liquid surface. These stagnant zones stayed coloured while the remaining vessel contents decoloured in about 2 minutes. However, for the single 3SHP1 and the dual impeller configurations, only a three fold increase, compared to water, was observed, *e.g.* with the 3SHP1 at 180 rpm decolourisation occurs within 5.3 seconds for water and 16.1 seconds for the CMC solution. The increased circulation resulting from the axial flow action of the 3SHP1 is shown in Figure 7.3-24. It is evident that a similar degree of homogeneity is achieved within 10 seconds for the situation when the 3SHP1 is operational compared to 1 minute when it is not.

Table 7.3-2 Unaerated mixing times in 0.7% CMC using the decolorisation technique

	6RT speed		
3SHP1 speed	0 rpm	120 rpm	240 rpm
0 rpm	-	120s*	50s*
120 rpm	28s	19s	17s
180 rpm	17s	-	-
240 rpm	12s	8s	8s

* Time for decolorisation excluding dead zones at top of vessel

a)

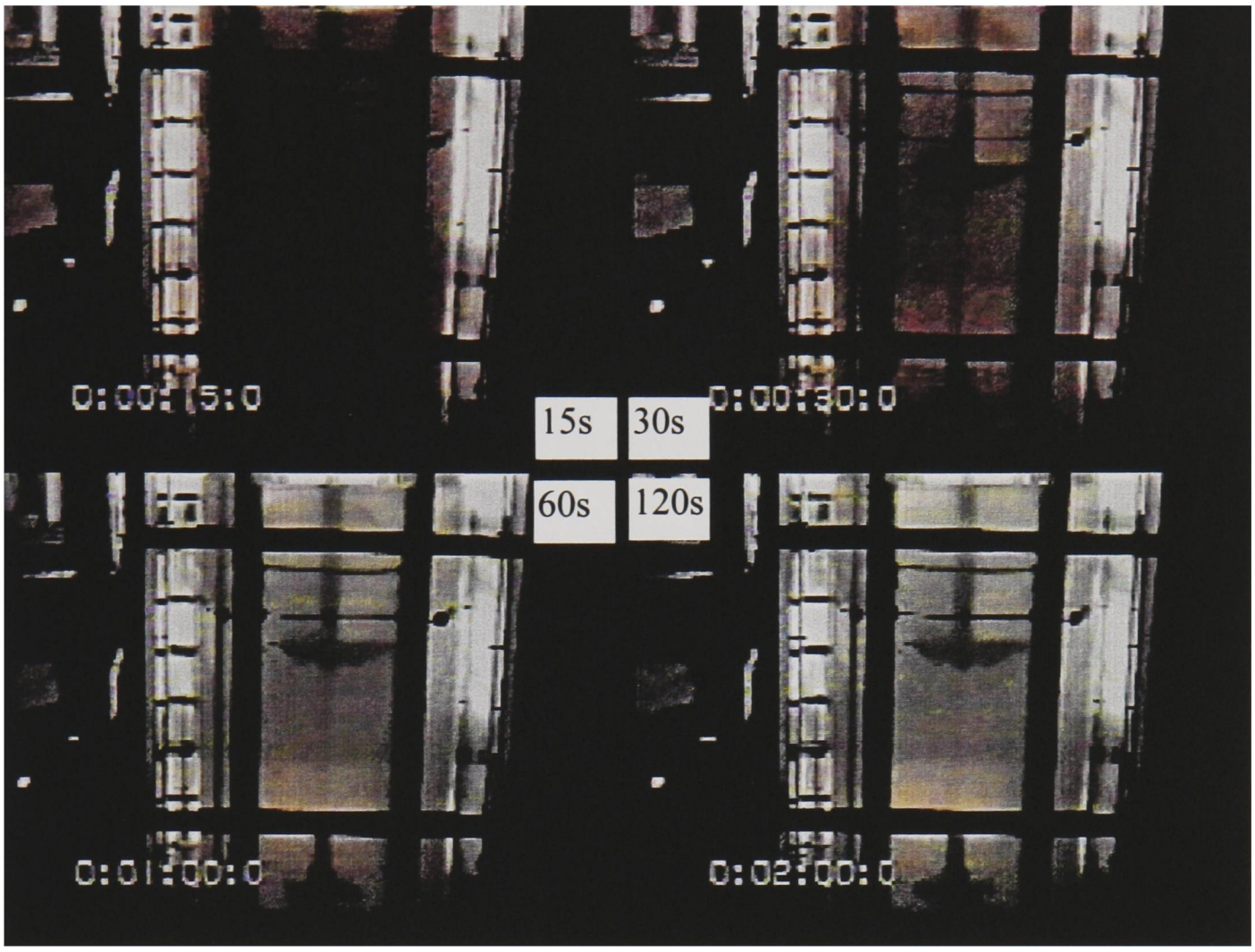

(b)

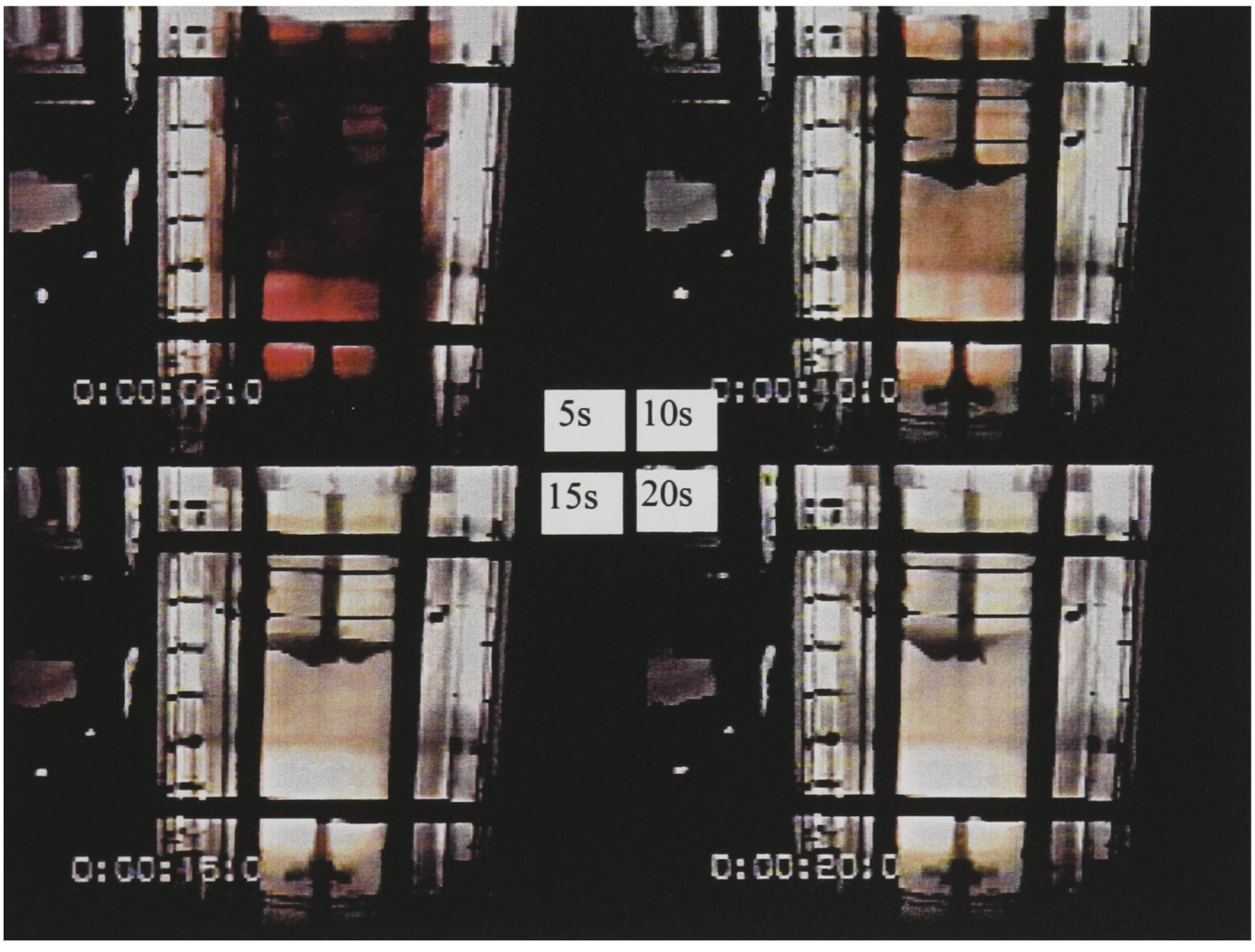

Figure 7.3-24 Unaerated mixing times in 0.7% CMC, using the declorisation technique (a) 6RT 120 rpm (b) IDDIDT 6RT-3SHP1 120 rpm

7.4 Conclusions

Mixing times for the independently-driven dual impeller proto-fermenter with draft tube have been studied using decolorisation and conductivity techniques from which the following conclusions can be drawn:

1. For the same operating conditions similar trends with mixing times in the same order of magnitude were obtained using both the decolorisation and conductivity techniques.

2. The dimensionless mixing time $N\theta_m$ was found to be constant for the single 3SHP1 and common shaft system, but a function of impeller speed for the single 6RT.

3. When operating the impellers independently (IDDIDT) the inverse dependency of mixing time on total power draw no longer holds and is instead described as a function of the power inputs from the separate impellers. The mixing times can be predicted well by:

$$\theta_m = 5.6\left(\frac{P_{SC}}{V}\right)^{-0.25}\left(\frac{P_{RT}}{V}\right)^{-0.08}$$

4. The blending efficiency achieved with IDDIDT was much higher compared to:

   - a dual Rushton system (upto 80% improvement),
   - predictions from the correlation proposed by Cooke *et al.* (40% lower mixing times).

   The increased efficiency was especially apparent in non-Newtonian viscous CMC solution where the axial action of the 3SHP1 was important.

5. Mixing times for the single 3SHP1 and common shaft system increase considerably on aeration, whereas there is little effect of gas on the mixing times observed with the 6RT, as long as the gas is dispersed (i.e. $N_{RT}>(N_{RT})_F$).

6. Gas flow rate effects the mixing times of the IDDIDT in a complex manner, either increasing or decreasing the mixing time for similar energy inputs depending on the specific circumstances. For the lower power inputs (i.e. low 6RT speeds) increasing the aeration rate increases the mixing time, whereas under higher energy circumstances (high 6RT speeds) mixing times are generally reduced.

Overall, rapid mixing times were observed which were directly controllable by altering the 3SHP1 speed. The configuration gives controllability of local energy inputs, increasing the flexibility of the system. Thus the 6RT can be used for gas dispersion and the 3SHP1 impeller speed can be altered to meet the other process mixing requirements such as bulk blending.

7.5 References

1. Christi, M.Y. and Moo-Young, M., 1987, "Airlift Reactors: Characteristics, applications and design considerations", *Chem.Eng.Comm.*, 60, 195-242
2. Zhao, M., Niranjan, K. and Davidson, J.F., 1994, "Mass transfer to viscous liquids in bubble columns and air-lift reactors: The influence of baffles", *Chem.Eng.Sci.*, 49, No 14, 2359-2369
3. Choi, K.H., Chisti, Y. and Moo-Young, M., 1996, "Comparitive-evaluation of hydrodynamic and gas-liquid mass transfer characteristics in bubble column and airlift slurry reactors", *Chem.Eng.J.Biochem.Eng.J.*, 62, No 3, 223-229
4. Obradovic, B., Dudukovic, A. and Vunjaknovakovic, G., 1994, "Local and overall mixing characteristics of the gas-liquid-solid airlift reactor", *Ind.Eng.Chem.Res.*, 33, No.3, 698-702
5. Bando, Y., Nishimura, M., Sota, H., Toyoda, K. and Suzuki, S., 1992, "Flow characteristics of bubble column with perforated draft tube-effects of equipment dimension and gas dispersion", *J.Chem.Eng.Japan.*, 25, No.1: 49-54
6. Kennard, M. and Janekeh, M., 1991, "2-phase and 3-phase mixing in a concentric draft tube gas-lift fermenter", *Biotech.Bioeng.*, 24, No.5: 680-682
7. Petrovic, D.L., Posarac, D. and Dudukovic, A., 1990, "Mixing time in gas-liquid-solid draft tube airlift reactors", *Chem.Eng.Sci.*, 45, No.9: 2967-2970
8. Allen, D.G. and Robinson, C.W., 1989, "Hydrodynamics and mass transfer in *Aspergillus niger* fermentations in bubble column and loop reactors", *Biotech.Bioeng.*, 34: 731-740
9. Koide, K., Kimura, M., Nitta, H. and Kawabat, H., 1988, "Liquid circulation in bubble column with draught tube", *J.Chem.Eng.Japan.*, 21, No.4: 393-399
10. Jones, A.G., 1985, "Liquid circulation in a draft tube bubble column", *Chem.Eng.Sci.*, 40, No.3: 449-462
11. Koide, K., Iwamoto, S., Takasaka, Y., Matsuura, S., Takahashi, E., Kimura, M. and Kubota, H., 1984, "Liquid circulation, gas holdup and pressure drop in bubble column with draught tube", *J.Chem.Eng.Japan.*, 17, No.6: 611-618

12. Pandit, A.B. and Joshi, J.B., 1983, "Mixing in mechanically agitated gas-liquid contactors, bubble columns and modified bubble columns" *Chem.Eng.Sci.*, 38, No,8: 1189-1215

13. Margaritis, A. and Sheppard, J.D., 1981, "Mixing time and oxygen transfer characteristics of a double draft tube air lift fermenter", *Biotech.Bioeng.*, 23: 2117-2135

14. Jirickova, E. and Rieger, F., 1995, "Mixing of suspensions in tall vessels with a draft tube", *Chem.Eng.J.Biochem.Eng.J.*, 59, No.3: 273-275

15. Carreau, P.J., Paris, J. and Guerin., P., 1994, "Heat-transfer to Newtonian and non-Newtonian liquids in a agitator and draft coil system", *Can.J.Chem.Eng.*, 72, No.6: 966-974

16. Kura, S., Nishiumi, H. and Kawase, M., 1993, "Oxygen transfer in a stirred loop fermenter with dilute polymer solutions", *Bioprocess.Eng.*, 8, No.5-6: 223-228

17. Kawase, Y. and Moo-Young, 1985, "Influence of non-Newtonian flow behaviour on mass transfer in bubble columns with and without draft tubes", *Chem.Eng.Comm.*, 40: 67-83

18. Rousseau, I and Bu'lock, J.D., 1980, "Mixing characteristics of a simple air-lift", *Biotech.Lett.*, 2, No.11: 475-480

19. Landau, J. and Procházka, J., 1964, "Studies on mixing. XVII. Relationship between energy consumption and rate of homogenisation", *Coll.Czech.Chem.Comm.*, 29: 1866-1877

20. Hoogendoorn, C.J. and Hartog, A.P., 1967, "Model studies on mixers in the viscous flow region", *Chem.Eng.Sci.*, 22: 1689-1699

21. Abradi, V., Rovera, G., Baldi, G., Sicardi, S., Conti, R., 1990, "Hydrodyanamics of a gas-liquid reactor stirred with a multi-impeller system", *Trans. I.Chem.E.*, 68, Part A: 516-522

22. Shuie, S.J. and Wong C.W., 1984, "Studies on homogenisation efficiency of various agitators in liquid blending", *Can.J.Chem.Eng.*, 62: 602-609

23. Shaw, J.A., 1994, "Understand the effects of impeller type, diameter, and power on mixing time", *Chem.Eng.Prog.*, February: 45-47

24. Ruszkowski, 1994, "A rational method for measuring blending performance , and comparison jof dirrent impeller types", *I.Chem.E. Symposium Series*, No. 136: 283-291

25. Sano, Y. and Usui, H., 1985, "Interrelations among mixing time, power number and discharge flow rate number in baffled mixing vessels", *J.Chem.Eng.Japan,* 18, No.1: 47-52

26. Joshi, J.B., Pandit., A.B. and Sharma, M.M., 1982, "Mechanically agitated gas-liquid reactors", *Chem.Eng.Sci.,* 37: 813-844

27. Khang, S.J. and Levenspiel, O., 1976, "New scale-up and design method for stirrer agitated batch mixing vessels", *Chem.Eng.Sci.,* 31: 569-577

28. Kramers, H., Baars G.M. and Knoll, W.H., 1953, "A comparative study on the rate of mixing in stirred tanks", *Chem.Eng.Sci.,* 2: 35-42

29. Cooke, M., Middleton, J.C. and Bush, J.R., 1988, "Mixing and mass transfer in filamentous fermentations", *Proc.2nd Int. Conf. Bioreactor Fluid Dynamics,* BHRA/Elsevier: 37-64

30. Biggs, R.D., 1963, "Mixing rates in stirred tanks", *A.I.Chem.E.,* September, 9, No 5: 636-640

31. Norwood, K.W. and Metzner, A.B., 1960, "Flow patterns and mixing rates in agitated vessels", *A.I.Chem.E.J.,* September, 6, No 3: 432-437

32. Rielly, C.D. and Britter, R.E., 1985, "Mixing times in stirred tanks", *Proc.5th.Euro.Conf.Mixing*, 365-375

33. Brennan, D.J. and Lehrer, I.H., 1976, "Impeller mixing in vessels influence of some parameters and formulation of a general mixing time equation", *Trans.I.Chem.E.,* 54: 139-152

34. Lundén, M., Stenberg, O. and Andersson, B., 1995, "Evaluation of a method for measuring mixing time using numerical simulation and experimental data", *Chem.Eng.Comm.,* 139: 115-136

35. Hass, V.C. and Nienow, A.W., 1989, *Chem.Ing.Tech.,* 61, No.2, 152-154

36. Langheinrich, C., Nienow, A.W., Stevenson, N., Emery, A.N., Clayton, T.H. and Slater, N.K.H., 1995, " Liquid homogenisation studies in stirred bioreactors under animal cell culture conditions", *IX Eng.Found.Conf.Biochem.Eng.*, Davos, Switzerland, May

37. Saito, F., Nienow, A.W., Chatwin, S. and Moore, I.P.T., 1992, "Power, gas dispersion and homogenisation characteristics of Scaba SRGT and Rushton turbine impellers", *J.Chem.Eng.Japan.,* 25: 281-287

38. Nienow, A.W., 1997, "On impeller circulation and mixing effectiveness in the turbulent flow regime", Chem.Eng.Sci., 52, No.15, 2557-2565

39. Reilly, C.D. and Burmester, S.S.H., 1993, "Homogenisation of liquids with different densities and viscosities, Industrial mixing technology", *A.I.Chem.E. Symposium Series*, 90, No.299: 175-180

40. Otomo, N., 1996, "A study of mixing with dual radial and dual axial flow impellers: Blending and power characteristics", *Ph.D. Thesis,* The University of Birmingham

41. Fasano, J.B., Bakker, A. and Penny, W.R., 1994, "Advanced impeller geometry boosts liquid agitation", *Chem.Eng.*, 101, No. 8: 110-116

42. Cronin, D.G., Nienow, A.W. and Moody, G.W., 1994, "An Experimental study of mixing in a proto-fermenter agitated by dual rushton turbines", *Trans.I.Chem.E.*, 72, Part C, March: 35-40

43. Nienow, A.W. and Elson, T.P., 1988, "Aspects of mixing in rheologically complex fluids", *Chem.Eng.Res.Des.,* 66, January: 5-15

44. Komori, S. and Murakami, Y., 1988, "Turbulent mixing in an unbaffled stirred tank with double impellers", *6th Euro.Conf.Mixing.*, Pavia, BHRA Cranfield: 63-68

45. Kumori, S. and Murakami, Y., 1988, "Turbulent mixing in baffled stirred tank with vertical-blade impellers", *A.I.Chem.E.J.*, June, 34, No 6: 932-937

46. Ando, K., Obata, E., Ikeda, K. and Fukuda, T., 1990, "Mixing time of liquid in horizontal stirred vessels with multiple impellers", *Can.J.Chem.Eng.,* 68, April: 278-283

47. Pörtner, R., Langer, G. and Werner, U., 1988, "Homogenization of non-Newtonian fluids in stirred tanks", *6th Euro.Conf.Mixing.*, Pavia, BHRA Cranfield: 521-526

48. Blakebrough, N. and Sambamurthy, K., 1966, "Mass transfer and mixing in fermentation vesssels", *Biotech.Bioeng.,* 8: 25-42

49. Einsele, A. and Finn, R.K., 1980, "Influence of gas flow rates and gas hold-up on blending efficiency in stirred tanks", *Ind. Eng. Chem. Process. Des. Dev.,* 19, 600-603

50. Manikowski, M., Bodemeier, S., Lübbert, A., Bujalski, W. and Nienow, A.W., 1994, "Measurement of gas and liquid flows in stirred tank reactors with multiple agitators", *Can.J.Chem.Eng.,* 72, October: 769-781

51. Zlokarnik, I.M., 1967, "Eignung von rührern zum homogenisieren von flüssigkeitsgemischen", *Chem.Ing.Tech.,* 39: 539-548

52. Cronin, D., S., 1988, "The design of a pilot-scale protofermenter and its application to mixing, power consumption, heat-transfer and mass transfer studies" *PhD Thesis,* University Of Birmingham

53. Landau, J. and Procháka, J., 1961, "Studies on mixing XI. Experimental methods for homogenisation of miscible liquids by rotary mixers", *Coll.Czech.Chem.Comm.,* 26: 1977-1989

54. Carreau, P.J., Patterson, I. and Yap, C., Y., 1978, "Mixing of viscoelastic fluids with helical ribbon agitators", *Can.J.Chem.Eng.*, 56: 135-142

CHAPTER 8

CIRCULATION TIME DISTRIBUTIONS

8.1 Introduction

The characterisation of mixing is of great importance when considering the optimal design of agitation systems. This is especially the case in viscous fermentation broths, where poor or incomplete mixing can severely reduce yield due to the creation of concentration gradients within the reactor, leading to possible nutrient/oxygen starvation. The previous chapter described mixing time measurements, incorporating the injection of a pulse tracer, to characterise the macromixing process. Although the effects of both impeller speeds on terminal mixing time were fully described through the tracer techniques, only a qualitative explanation for the mixing mechanism was obtained via the decolorisation method. It was therefore decided to employ a quantitative method for the determination of the mechanisms of the mixing process.

The flow follower technique generates mean circulation times and circulation time distributions which can be used to characterise the mixing process. The technique offers other advantages over the tracer methods for use in real fermentations since:

1. it does not affect the course of the fermentation or alter broth properties (pH, temp, rheology etc.);
2. there is no problem with background concentrations reducing the sensitivity of the measurement.

A single fluid element is labelled by a neutrally buoyant flow follower, and its path inside the reactor is followed. The time between two successive passes of the flow follower through a

fixed position within the vessel is termed the circulation time. In a stirred tank it is convenient to take the impeller region as the fixed point or volume[1]. The circulation time is widely distributed about its mean, since the path of the flow follower is highly variable. The passage of the fluid element may comprise of a single loop (Figure 8.1-1(a)) or it may follow a longer path consisting of multiple loops (Figure 8.1-1(b)) before it returns to the reference point.

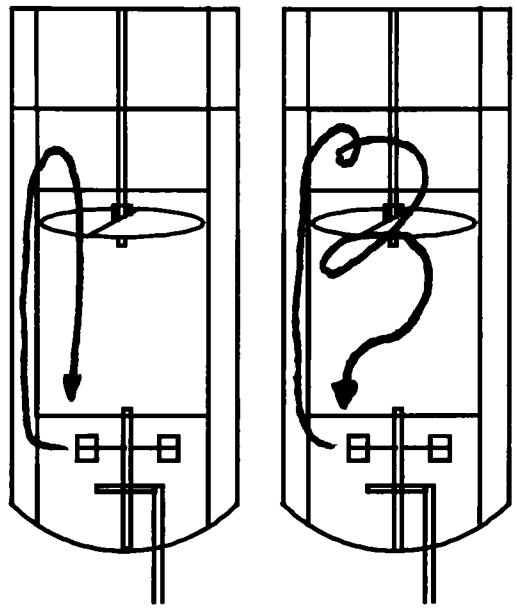

Figure 8.1-1 Possible flow paths experienced by magnetic pill

The most simplistic flow follower technique involves visual observation of plastic chips [2]. However, the procedure is monotonous, labour intensive and requires the use of glass/Perspex vessels with a clear test fluid. The method is therefore unsatisfactory for in-situ investigations into the mixing characteristics of opaque fermentation broths, which are usually carried out in stainless steel vessels. Bryant[3] introduced a flow follower technique that eliminated the need for visual observation. The "radio pill" consisted of two plastic hemispheres which were screwed together to house a small radio-transmitter and a mercury battery. A loop of wire surrounding the impeller region acted as the receiving aerial. The signal from the receiver was amplified and used to activate a data logger. The frequency of the receiver was adjusted so that when the radio-pill passed through the active region the signal strength was just enough to activate the data logger. Analysis of the frequency pattern for passage of the radio-pill through

the impeller region provided the mean, standard deviation and distribution of the circulation times.

Inverse proportionality between mean circulation time, standard deviation and impeller speed has been frequently reported [1,3,4,5,6]. In addition, researchers using the radio-pill have suggested that the distribution of circulation times, $f(t)$, could be represented by a log-normal distribution and used to predict the terminal mixing times in the following manner[1,3,4,5].

The proportion of circulation times between time t and $(t + dt)$ is given by $f(t)dt$. Therefore the proportion of particles returning to the impeller zone t seconds after the assumed injection of a pulse of tracer is given by

$$f_1(t) = f(t)dt \tag{8.1}$$

The proportion returning to the active region after two successive circulations in the same time, t, is formed by the fraction initially circulating in time t_2, then undergoing a second circulation in time $(t\text{-}t_2)$, where $0 < t_2 < t$. Therefore,

$$f_2(t) = \int_0^t f(t - t_2) f(t_2) dt_2 \tag{8.2}$$

Similarly, the fractions returning to the impeller after three, four or more circulations can be obtained via the same method. The effective concentration, obtained had a tracer pulse been injected, is described by

$$C(t) = \sum_{n=1}^{\infty} f_n(t)dt \tag{8.3}$$

where $f(t)$ approximates to a log-normal distribution, *i.e.*

$$f(t)dt = \frac{1}{t\sqrt{2\pi\sigma_l^2}} e^{-\frac{(\ln(t)-\mu)^2}{2\sigma_l^2}} dt \tag{8.4}$$

where t is the normalised circulation time, μ is the logarithmic mean and σ_l is the logarithmic standard deviation. They are related to the normalised values by

$$\bar{t} = e^{\left(\mu - \frac{\sigma^2}{2_l}\right)} \tag{8.5}$$

$$\sigma^2 = \bar{t}^2 (e^{\sigma_l^2} - 1) \tag{8.6}$$

The assumption that mixing is 99% complete after 5 mean circulation times[7,8,9] was deemed in need of modification according to the size of the vessel[1]. Following experiments at three different scales (0.18m^3, 0.6 m^3, 1.8 m^3) Middleton discovered a good correlation for mean circulation time and standard distribution using the empirical equations for vessels of H=T (0.18-1.8 m^3).

$$\bar{t} = 0.5V^{0.3}\left(\frac{1}{N}\right)\left(\frac{T}{D}\right)^3 \tag{8.7}$$

$$\sigma = 1.23V^{1.45}\left(\frac{1}{N}\right)\left(\frac{1}{D}\right)^{2.5} \tag{8.8}$$

Similarly, Bryant *et al.*[5] correlated mean circulation time and standard deviation using

$$\bar{t} = Hk_1\left(\frac{1}{N}\right)\left(\frac{1}{D}\right)^3 \tag{8.9}$$

$$\sigma = H^{7/3}k_2\left(\frac{1}{N}\right)\left(\frac{1}{D}\right)^3$$

(8.10)

where k_1 and k_2 are proportionality factors (not given). They also proposed that terminal mixing times could be calculated from

$$\theta_m = B\frac{k_1}{k_2^{\,2}}H^{11/3}\left(\frac{1}{N}\right)\left(\frac{1}{D}\right)^3 \tag{8.11}$$

where the dimensionless constant B represents the degree of uniformity required.

Using the radio-pill, Schmitz[6] recently confirmed the good approximation of a log-normal distribution to describe the circulation time data. The mean circulation time and standard deviation were inversely proportional to impeller speed and were expressed as

$$\bar{t} = 3.78\left(\frac{1}{N}\right) \tag{8.12}$$

$$\sigma = 7.56\left(\frac{1}{N}\right) \tag{8.13}$$

for a vessel of H=T=0.61 m (6RT with D=T/3).

However, the radio-pill exhibited limitations when characterising the mixing in viscous non-Newtonian solutions, so a smaller magnetic pill was employed[6]. Due to its size (0.8 cm compared to 2.5 cm for the radio-pill), the magnetic pill was thought to measure the true liquid circulation times more closely. In addition, since detection by the aerial was a function of both speed and proximity, a signal was only produced when the pill passed the aerial in the direct discharge stream or the entrainment flow of the impeller. This suggested that a more accurate detection zone, representing the impeller region, could be achieved with the magnetic aerial set-up. In water, the magnetic pill and radio-pill gave statistically similar mean circulation times and standard deviations, but the shapes of the distributions produced were very different.

The magnetic-pill technique was first introduced by Mukataka *et al.*[10]. The flow follower consisted of a magnet (1.15 x 1.15 x 3.0 mm) placed in a hollow plastic sphere 5 mm in diameter. When the pill passed the aerial (a coil of enamelled copper wire) a current/electromotive force was induced in the coil due to the changes in magnetic force. The strength of the signal was dependent on the velocity of the magnet and its distance from the aerial. Using a variety of test fluids, at differing scales (0.0017 m^3 to 0.03 m^3), Mukataka *et*

al.[11,12,13] reported a log-normal distribution of circulation times. They also discovered that, for constant power inputs, mean circulation time and standard deviation increased with an increase in scale and an increase in viscosity [11]. In water, impeller diameter and liquid height had no influence over mean circulation time or standard deviation[12]. However, in paper pulp suspensions, at low power inputs, there was a slight dependence on impeller diameter [12]. In dual impeller systems, distributions around each impeller were well approximated by a log-normal probability [13]. In fact, the distributions were identical to previous research using single impellers [13]. Circulation time data from tests using various fluid rheologies ($3.1<K<30$, $0.37<n<0.5$) in single and dual impeller systems could be correlated by:

$$\bar{t} = 7.8\left[n^3 \left(0.35 \frac{P}{VT^2} \right)^{\frac{(2-n)}{3}} \left(10^2 D\right)^{(1-n)} \right]^{-1} \qquad (8.14)$$

or more simply, for turbulent conditions

$$\bar{t} = \frac{7.8}{N} \qquad (8.15)$$

In a 6L tank stirred by a RT, using a magnetic pill, Funahashi *et al.*[14] discovered that the circulation times followed a bimodal distribution in water and low concentrations of xanthan gum ($K \leq 26.4$, $n \geq 0.12$). The first peak in the distribution, corresponding to the faster circulation times, was credited to circulations occurring in the "micromixer" (impeller region) and the second peak, at slower circulation rates, was due to circulations taking place in the "macromixer" (remainder of vessel). Roberts *et al.*[15] found a bimodal distribution of circulation times for a range of impeller types and sizes using a magnetic pill in water.

However, large diameter pitched blade turbines (D=T/2) gave a unimodal distribution. For the Rushton turbine, the mean circulation time could be correlated by:

$$\bar{t} = 0.641\left(\frac{1}{N}\right)\left(\frac{T}{D}\right)^2 \qquad (8.16)$$

In agreement with Funahashi *et al.*[14] and Roberts *et al.*[15], when using the magnetic-pill, a deviation from log-normal distribution was observed by Schmitz [6]. Compared to the radio pill technique, longer mean circulation times were encountered which could be represented by

$$\bar{t} = \frac{A}{N} \qquad (8.17)$$

where A = 15.15 and 20.08 for flat and dished bottomed vessels respectively. Employing a three aerial magnetic pill technique, Schmitz[6,16] investigated the flow structure which gave rise to the bimodal distribution observed when using only one aerial as the reference point. The method permitted the "break down" of the circulation time distributions into a:

1. tank distribution,
2. lower compartment distribution,
3. upper compartment distribution,
4. both compartment distribution (pill movement without travelling through the impeller region).

The majority of fast circulations, represented by the initial large peak, occurred in the lower region. This was probably due to the more defined flow pattern, in the lower compartment, aided by the presence of the solid tank base. Summation of the upper and lower distributions gave the overall tank distribution. The contribution to the overall shape of the tank distribution of circulations through both compartments was considered negligible.

It was proposed to examine the mechanisms of mixing within the $0.64m^3$ proto-fermenter fitted with the draft tube. The magnetic pill technique was applied since more realistic circulation time data have been obtained using this method[6].

8.2 Materials and methods

All experiments described in this chapter used a magnetic pill in water. The flow follower technique was based on the original design of Mukataka *et al.*[10] which was successfully employed by Schmitz [6].

8.2.1 Flow follower and aerial

The flow follower consisted of two hemispheres of polyethylene glued together to house a cubical neodymium-iron-boron magnet (Figure 8.2-1). The magnet was two cubic millimetres with a strength of 1.3 Tesla. The total diameter of the pill was 8 mm. Since polyethylene is less dense than water, neutral buoyancy was achieved by removing thin layers of material from the surface of the pill and subsequent testing in a beaker of water. For aerated experiments the buoyancy of the pill was tested in aerated tank. However, it was difficult to assess if the pill was truly neutrally buoyant since the liquid flow produced by the density difference meant the pill was constantly moving. This problem is universal to this technique but is reduced by using the smallest pill size possible.

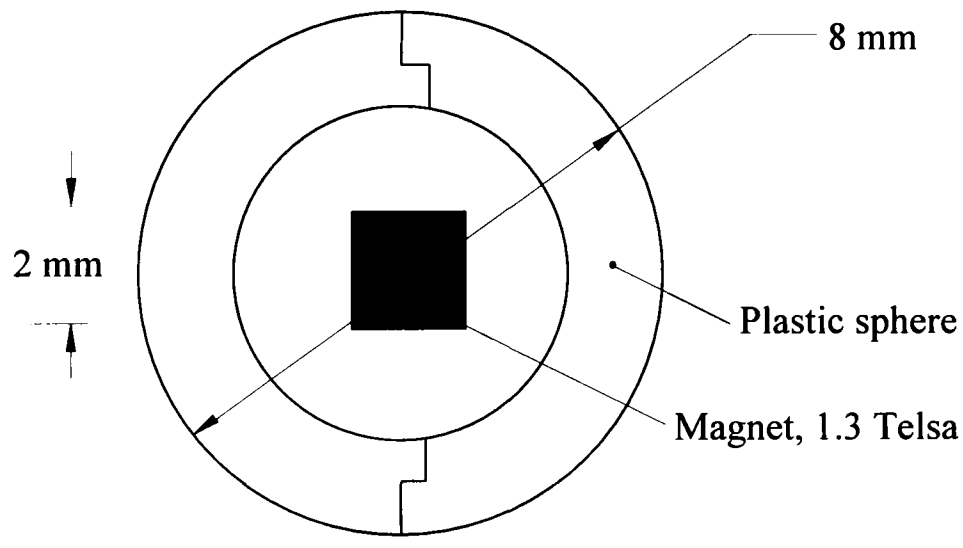

Figure 8.2-1 Schematic of magnetic pill

To form the aerial, a coil of 120 turns (enamelled 0.4mm copper wire (RS Components Ltd., Northants, U.K.)), was surrounded with insulation tape (RS electronics) and covered with a

second layer of copper, to avoid external pick-up. Finally two layers of self-amalgamating tape were applied to the aerial for water-proofing.

The sensitivity of the aerials was adjusted by visual observation. A two aerial (diameter 53cm) technique was employed. One aerial was positioned at the lower impeller (6RT) level and a second aerial was attached to the top of the draft tube, in the upper section of the vessel (Figure 8.2-2). This configuration permitted the circulation time distribution to be broken down into two parts. The distribution of circulation times for the overall tank was detected by the lower aerial (L-L), *i.e.* two consecutive pulses produced by the lower aerial. If the pill departed from the 6RT impeller region and travelled upwards in the annulus, flowing back down through the draft tube, a signal was generated in the lower aerial followed by the upper aerial, with a further signal produced, once more, in the lower aerial (L-U-L). This produced a distribution of circulation times which showed the frequency of liquid movement around the draft tube. In addition, the overall bulk (top to bottom) circulation was detected by using the upper aerial only (U-U). Here, two consecutive signals produced by the upper aerial gave a circulation time which represented the frequency of the passage of the pill through the upper part of the vessel. In this case, circulation times of less than 2 seconds were due to the motion of the pill around the aerial before entering the draft tube and were ignored.

8.2.2 Signal processing

The signal processing, identical to that performed by Schmitz for the magnetic pill, is outlined below (Figure 8.2-2).

When the pill (A) passed the copper aerial (B) a pulse of current was induced which was detected by the receiver (C). If the signal strength was above the previously determined threshold value then the output from the receiver changed from 0 V to 5 V. The pulses from

the receiver were collected by a data acquisition card (National Instruments, Austin, U.S.A.) which was controlled by LabVIEW (National Instruments, Austin, U.S.A.), a graphical software language (E). On-line and off-line data analysis was also undertaken using LabVIEW.

For aerated experiments, the receiver was pre-tuned to the sensitivity required under the same unaerated conditions since the opaque nature of the distribution made visual observation of the pill impractical.

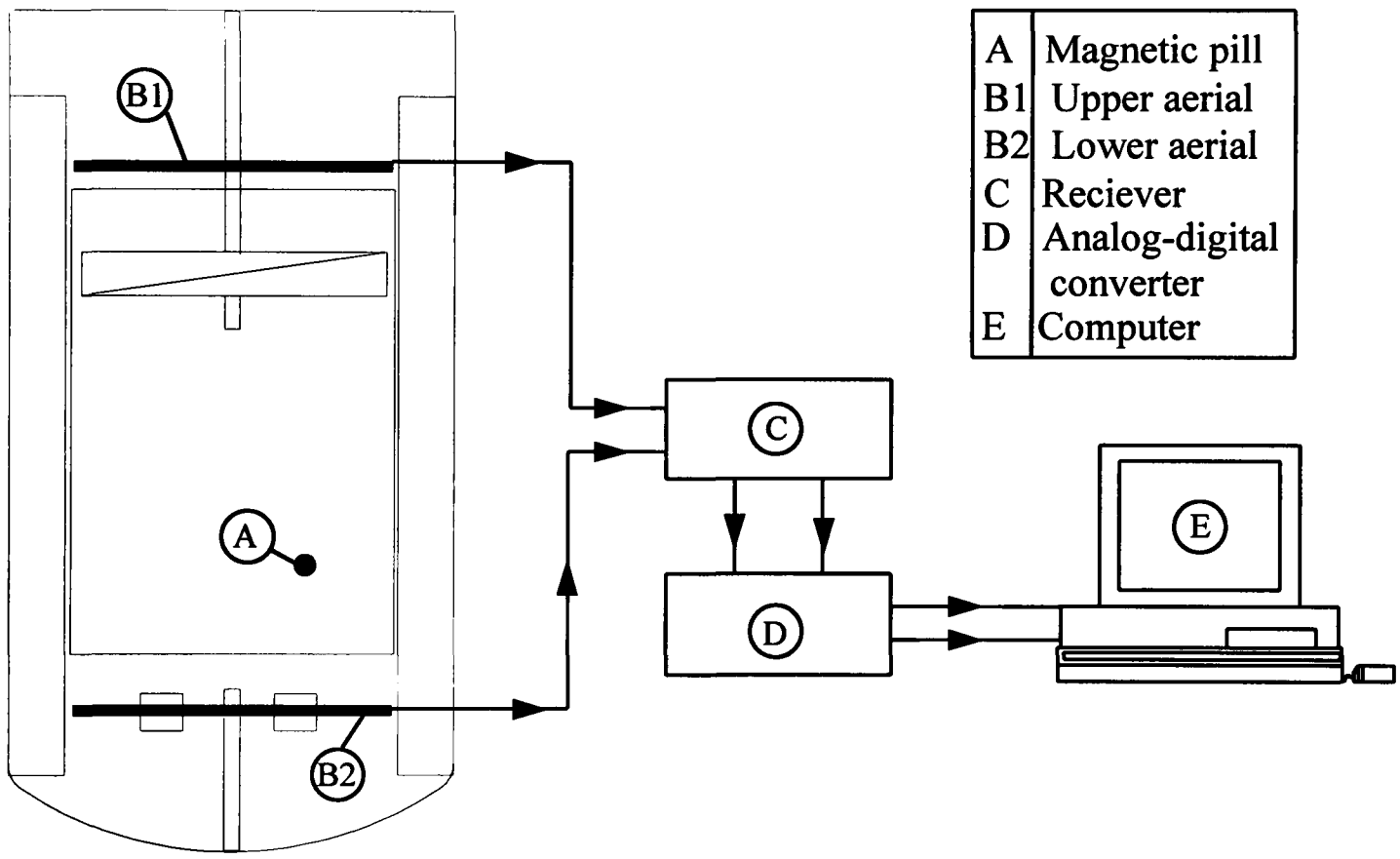

Figure 8.2-2 Signal processing for magnetic pill circulation time experiments

A program constructed by Schmitz was applied for the analysis (Appendix V). The time between two successive signals was measured by the internal clock to within one tenth of a second accuracy *i.e.* a 10Hz sampling frequency. This allowed the acquisition of 300 to 4000 circulation times within 4 hours without causing an overflow of data due to limited computer space. Off-line analysis of the data involved, for each set of conditions, the calculation of the mean circulation time, the standard deviation and the distribution in the form of a probability density function. The mean circulation was found from

$$\bar{t} = \frac{\sum_i t_i}{n_t} \tag{8.18}$$

where t_i is the circulation time and n_t is the total number of circulations. The standard deviation was calculated from

$$\sigma = \sqrt{\frac{\sum_i \left(t_i - \bar{t}\right)^2}{n_t - 1}} \tag{8.19}$$

and the probability density function was given by

$$f(t) = \frac{n_i}{n_t \Delta t_i} \tag{8.20}$$

where n_i represents the number of circulations occurring in the time Δt_i. The sampling frequency of the data acquisition card governed the value of Δt_i. Throughout the work a 10 Hz sampling frequency was used, *i.e.* Δt_i was 0.1 seconds.

8.3 Results and Discussion

8.3.1 Unaerated circulation time distributions (CTD) in water

In order to determine the mechanistics of the mixing process and to create a link between the circulation studies and the mixing time measurements, a sample of single and dual impeller configurations were examined.

8.3.1.1 Single 6RTDT

Figure 8.3-1 shows, using the lower aerial as a reference point (L-L), the change in CTD shape with increasing 6RT speed. It is evident that on increasing impeller speed, a narrower, higher initial peak is produced. In addition, the peak has shifted towards the left axis. This indicates that at higher impeller speeds, due to the increased pumping action of the 6RT, faster circulation times occur. They also appear more frequently. These changes can be characterised by the mean and the standard deviation of the distribution (Table 8.3-1). Although operating at an aspect ratio of 2:1, the mean circulation times were very similar to those predicted by Schmitz[6] when using the magnetic pill, a dished bottom and $H=T$, *i.e.*

$$\bar{t} = \frac{20}{N} \tag{8.21}$$

This was because the majority of the circulations took place in the lower 6RT circulation loop while only a small number passed around the draft tube (see below). The standard deviations, however, could not be described in a similar manner.

Closer examination of the curves revealed the presence of a bimodal distribution, similar to those reported by Funahshi *et al.*[14], Roberts *et al.*[15] and Schmitz[16]. Therefore, a second aerial was positioned above the draft tube to determine the source of the second peak. For this situation, an "upper loop" circulation time was indicated by the signal sequence: lower aerial-

upper aerial-lower aerial (L-U-L) and is shown for the single RTDT in Figure 8.3-2. Clearly, the main peaks in the "upper loop" distribution, at approximately 5 s and 8 s for the 6RT at 200 and 300 rpm respectively (Figure 8.3-2), correspond to the secondary peaks of the lower aerial distribution (Figure 8.3-1), thus confirming that the bimodal shape is due to pill motion in the upper and lower parts of the vessel. The initial peak in the 6RT 300 rpm L-U-L distribution could not be explained.

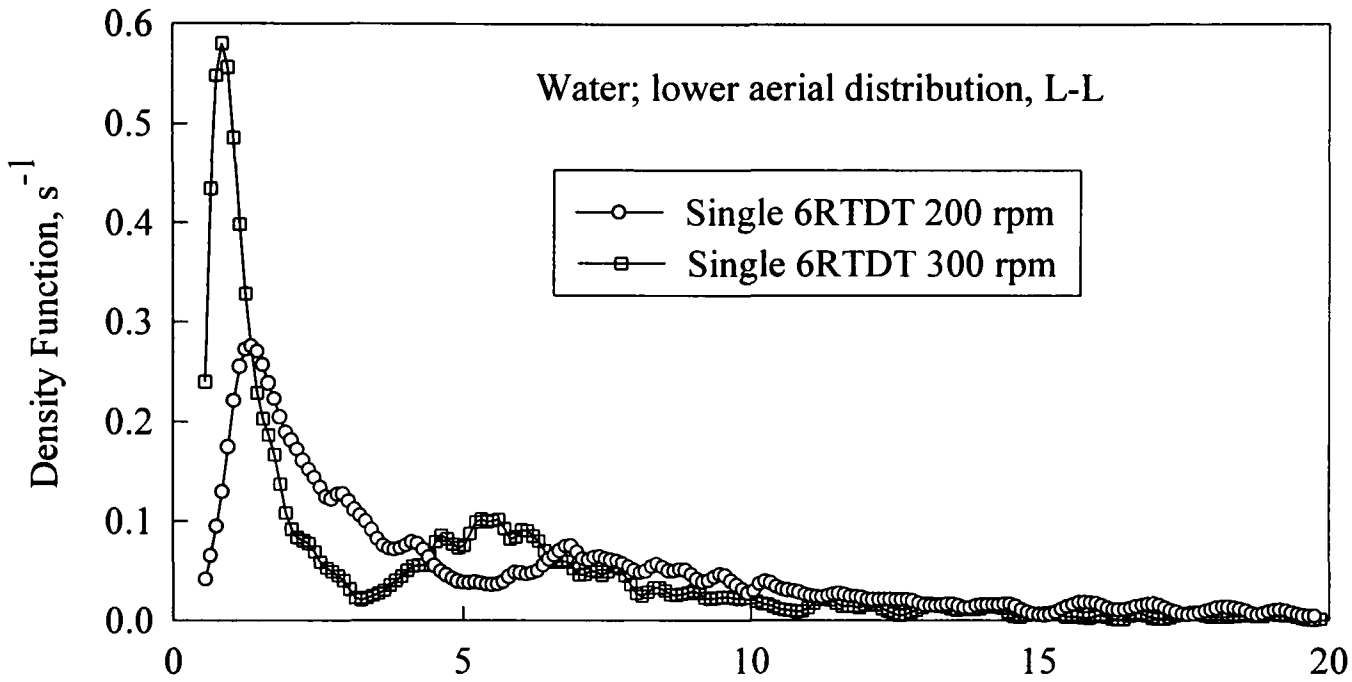

Figure 8.3-1 Circulation time distributions for single 6RTDT in water; lower aerial (L-L)

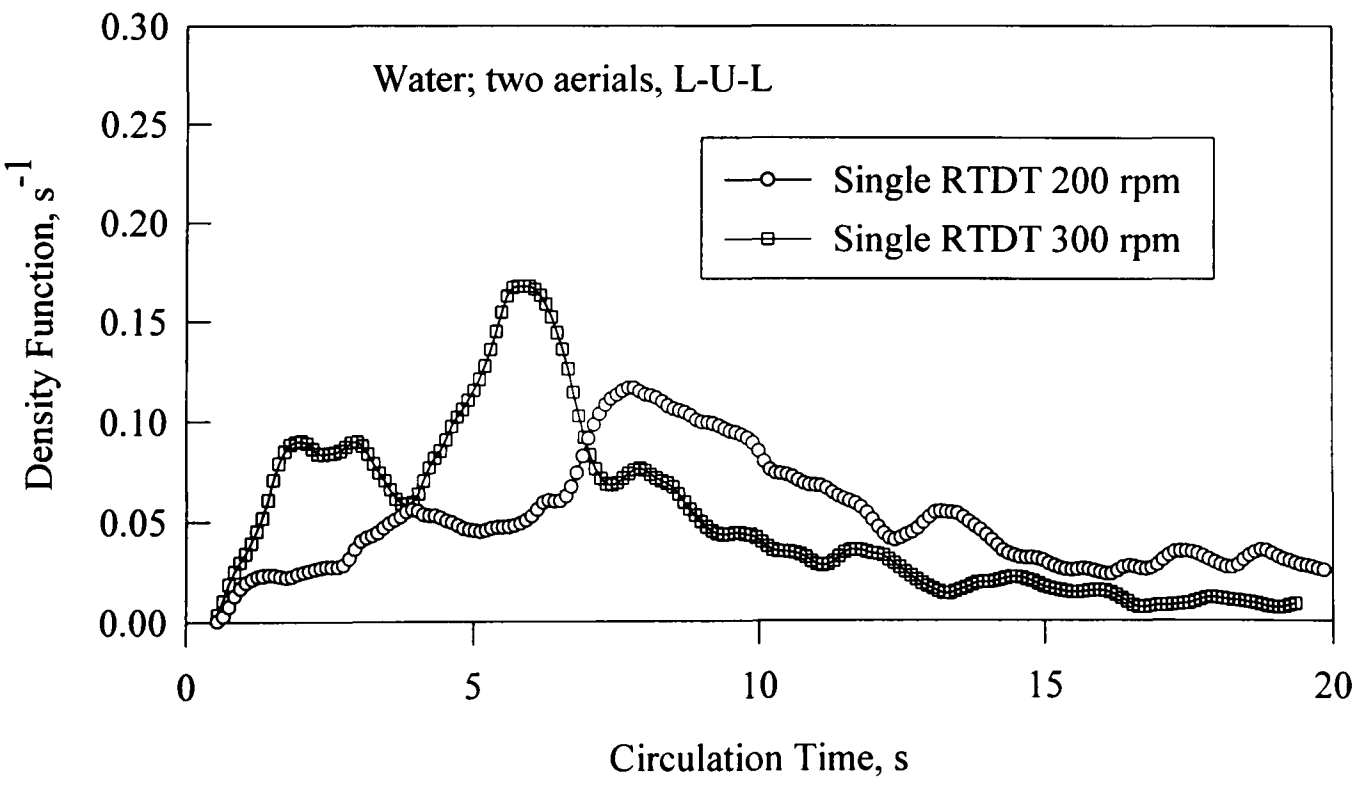

Figure 8.3-2 Circulation time distributions around the draft tube for single 6RTDT in water;two aerial method (L-U-L)

The mean circulation times for the upper circulation loop ($\bar{t}_u$) were approximately double that of the lower aerial means ($\bar{t}_l$). In addition, they occurred less frequently. The above analysis describes the circulation times using the lower aerial as a reference point and provides information on the frequency of the passage of the pill (or cells in a microbial environment) into a well mixed high shear zone (or a highly oxygenated zone if aerated). However, it provides little information on the efficiency of top to bottom mixing which is an essential consideration if the influence of concentration gradients on cell productivity is to be investigated. Using the upper aerial as a reference point allowed the overall top to bottom mixing to be assessed. The time for one circulation around the draft tube was represented by the time taken between two successive signals received by the upper aerial (irrespective of lower aerial signals) and was termed a "bulk circulation", $\bar{t}_{bc}$ (U-U).

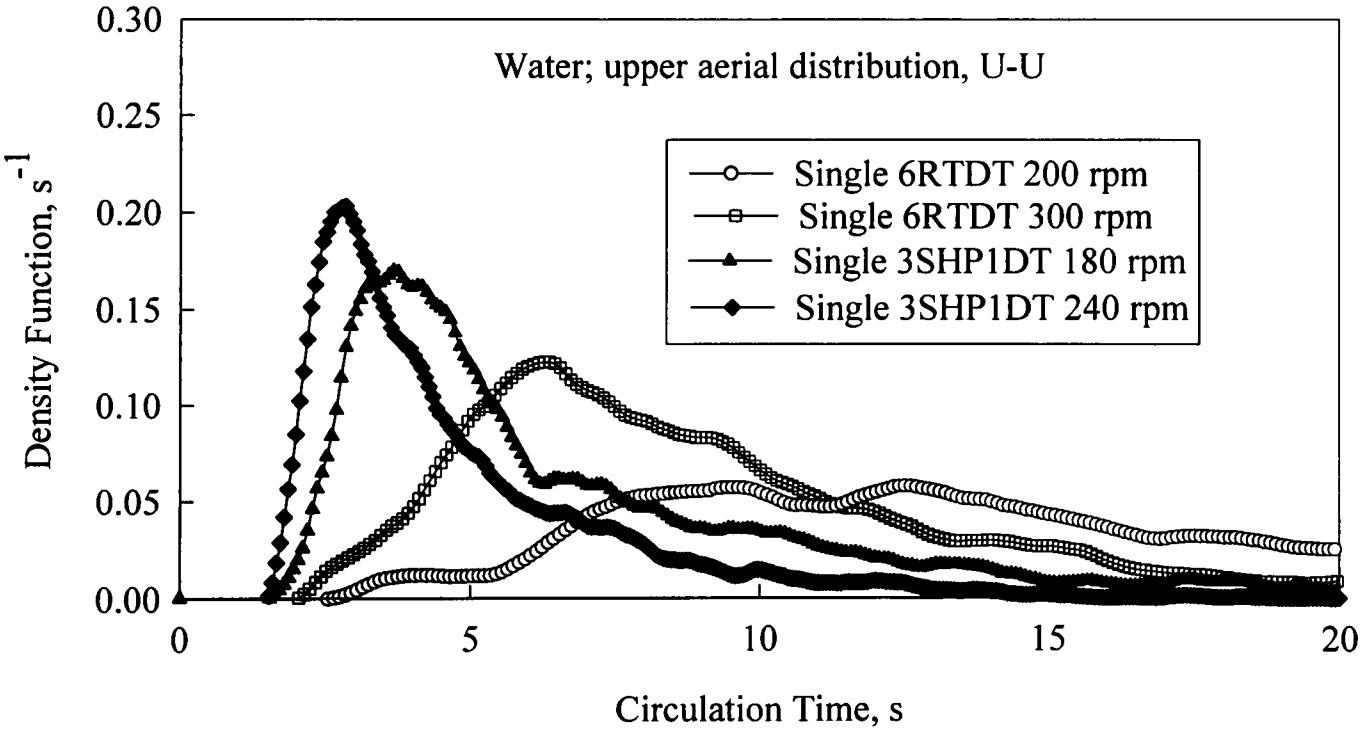

Figure 8.3-3 Bulk circulation time distributions for single impellers in water;upper aerial method (U-U)

The bulk CTD for the RTDT is shown in Figure 8.3-3. Very long bulk circulation times were exhibited by the single RTDT (Table 8.3-1) with a very wide distribution. This was especially evident at the lower impeller speed (200 rpm). This indicated that the pill tended to become trapped in the strong circulation flow loop formed below the RT and hence did not return

immediately to the upper aerial. For example, at 200 rpm, since the mean upper circulation time was ~ 9 s and the mean bulk circulation time was ~ 17 s, then the pill possibly spends ~ 8 s (circa 4 "lower loop" circulations) in the lower region of the vessel before returning to the upper aerial. No reason could be found for the "shoulder" on the CTD for the 3SHP1DT at 180 rpm.

8.3.1.2 Single 3SHP1DT

The single 3SHP1 was analysed in terms of bulk circulations only, since the lack of a lower impeller made the other distributions irrelevant. In contrast to the single RTDT, the CTD for the 3SHP1 exhibited a pronounced first peak followed by monotonic decline (Figure 8.3-3). Increasing the speed narrowed the peak and shifted the distribution to the left. The much lower mean bulk circulation times (compared to RTDT, Table 8.3-1) were due to the axial pumping capacity of the 3SHP1 improving top to bottom mixing.

8.3.1.3 IDDIDT

The effect on lower and upper CTD's of running both impellers simultaneously is shown in Figure 8.3-4 and Figure 8.3-5 respectively. Initiating the 3SHP1 changed the shape of the lower distribution in two ways. Firstly, the initial peak, which was in approximately the same position as with the RTDT, was larger for the IDDIDT and therefore indicated "lower loop" circulation times of similar magnitude but of increased frequency for the IDDIDT compared to the RTDT. This suggested that the lower loop circulation times were defined by the RT speed. Secondly, the secondary peak had shifted considerably to the left implying faster upper loop circulation times. Indeed, the faster upper circulation times were verified by a shift in the peak of the upper CTD which corresponded with the change in the secondary peak of the lower CTD.

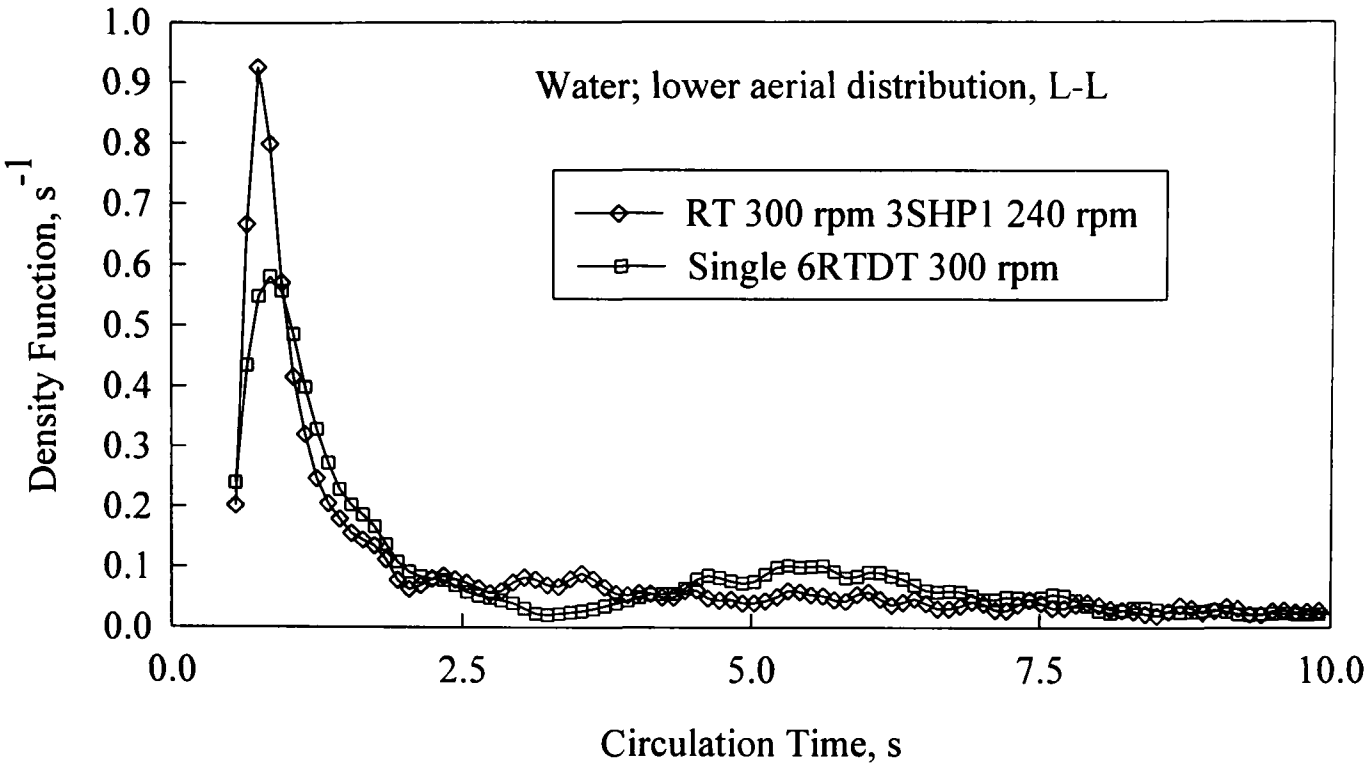

Figure 8.3-4 Comparison of circulation time distributions for IDDIDT and single 6RTDT in water; lower aerial

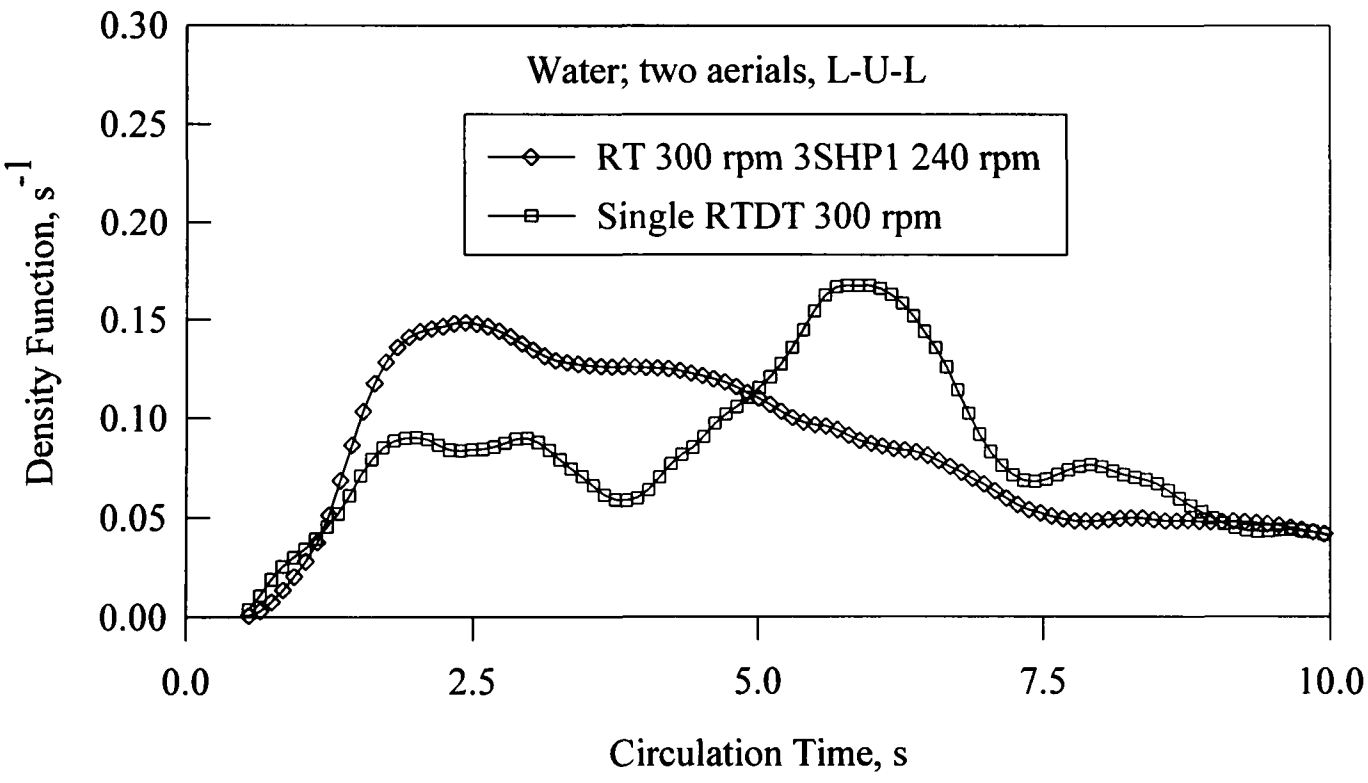

Figure 8.3-5 Comparison between circulation time distributions for the IDDIDT and the single 6RTDT in water; two aerial method (L-U-L)

As expected, the inclusion of the 3SHP1 greatly improved the bulk circulation in comparison to the single RTDT, exhibiting very similar distributions to those encountered with the single 3SHP1DT (comparing Figure 8.3-6 and Figure 8.3-3). Overall, the distributions were narrower and shifted towards faster circulation times at the higher 3SHP1 impeller speeds.

Although increasing the 6RT speed tended to move the distribution left, the height of the peak was reduced.

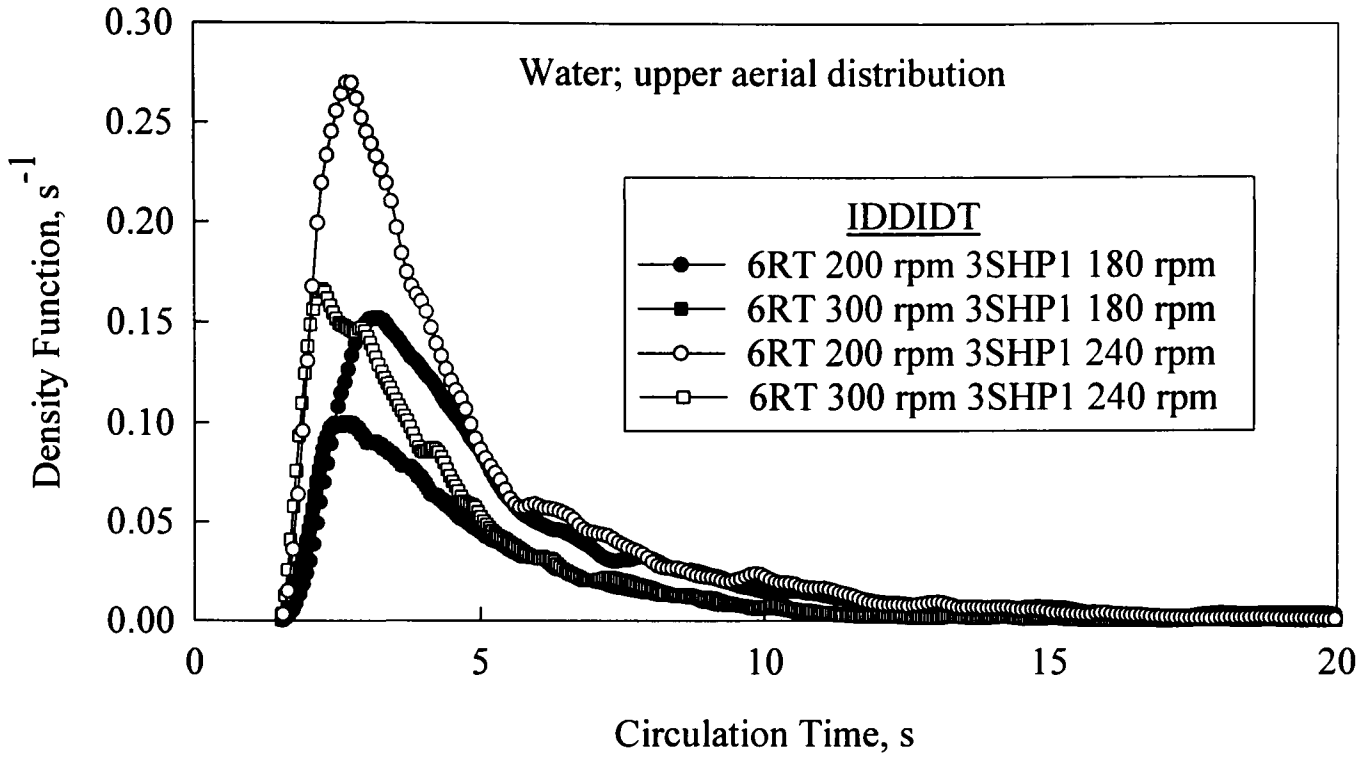

Figure 8.3-6 Comparison between bulk circulation time distributions for the IDDIDT and the single 6RTDT in water; upper aerial method (U-U)

Table 8.3-1 Mean circulation times and standard deviations for single and dual impellers; unaerated, water

RT	3SHP1	Lower aerial, $\bar{t}_l$ (L-L)		Lower and Upper aerial, $\bar{t}_u$ (L-U-L)		Upper aerial, $\bar{t}_{bc}$ (U-U)	
rpm	rpm	t	σ	t	σ	t	σ
200	0	5.42	2.75	9.22	8.36	13.86	6.68
300	0	3.94	2.98	6.76	5.37	8.86	4.89
0	180	-	-	-	-	6.23	4.53
200	180	4.24	2.12	7.00	4.77	5.29	4.00
300	180	3.67	2.14	6.33	4.04	4.39	2.62
0	240	-	-	-	-	4.41	2.89
200	240	-	-	-	-	4.50	3.58
300	240	3.84	2.01	6.1	3.45	3.96	2.59

8.3.2 Relationship between mixing times and circulation times

The tracer responses produced by the conductivity measurements can be linked to bulk flow characteristics through the decolorisation and the CTD results. The progress of mixing for the IDDIDT (subscript 1, Figure 8.3-7) and RTDT (subscript 2, Figure 8.3-7) can be explained through a parallel comparison between the concentration transients and the bulk flow patterns. The techniques have been considered separately in Chapter 7.

Immediately following the pulse injection (A), no change in concentration was detected by the conductivity probes and the vessel contents remained dark brown due to the presence of iodine. At point B, decolorisation occurred around the 6RT, in the lower region of the vessel, which corresponded to the initial response detected by the lowest probe (Probe 1). Due to upward flow through the annulus a response was then observed by the uppermost probe (Probe 2) which coincided with decolorisation in that part of the vessel (C). An approximation of the liquid velocity in the annulus could be made from the time delay between the two probe responses ((C)-(B)) and has been addressed previously (Section 7.3.2.3). At D, the Probe 2 response had reached a minimum and the remainder of the unreacted iodine solution had flown from the annulus into the draft tube. Total decolorisation took place approximately at the minimum of the Probe 2 response (E).

Using the bulk flow model, the circulation time was previously considered to be represented by the time between two peaks of an idealised tracer response[17] and was defined as

$$\theta_C = \frac{V}{Q}$$

for an aspect ratio of 1. Due to the well defined bulk flow pattern, an idealised tracer response enabled the time between peaks (or troughs) to be measured easily ((E)-(C)). However, the

distance between the peaks was always slightly higher with Probe 2 and therefore this value was taken as it represented the worst case scenario.

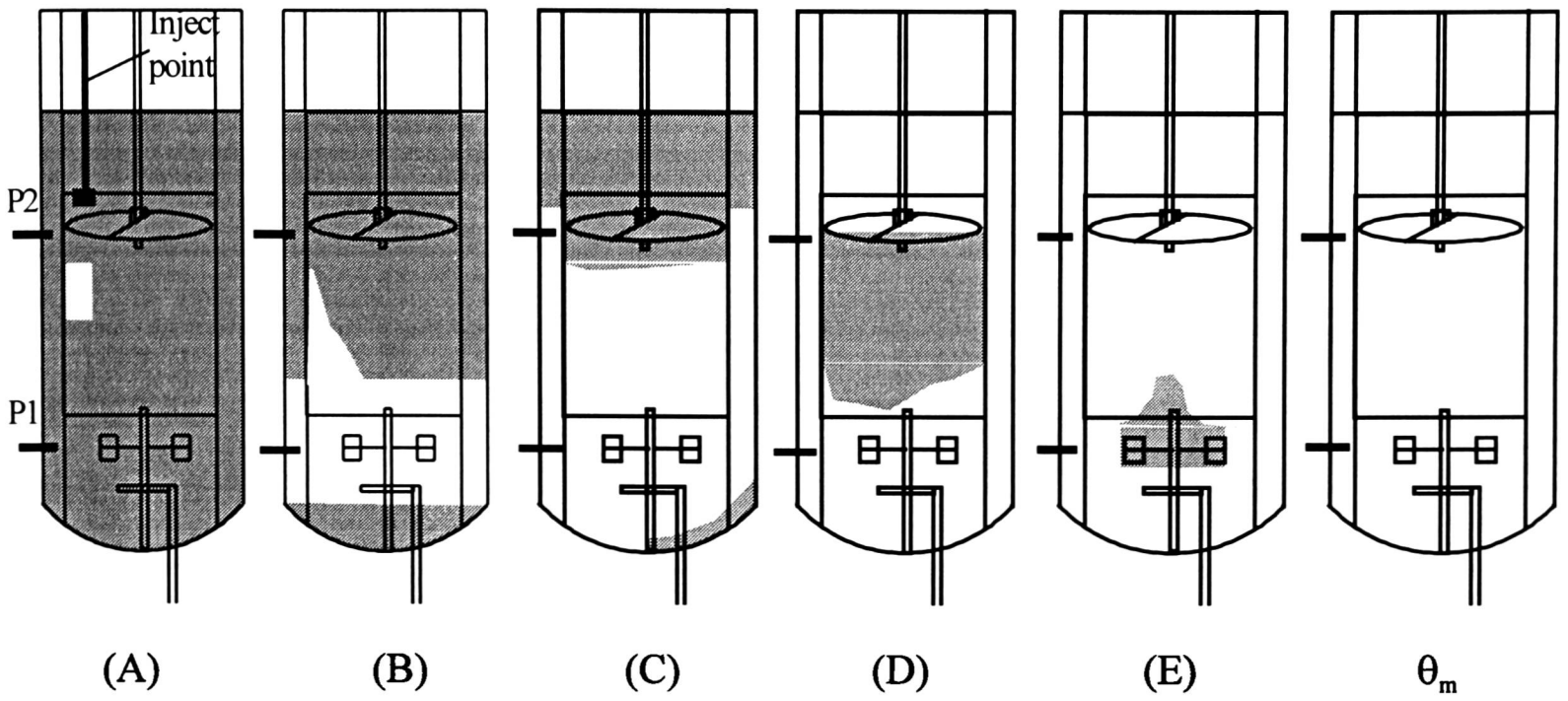

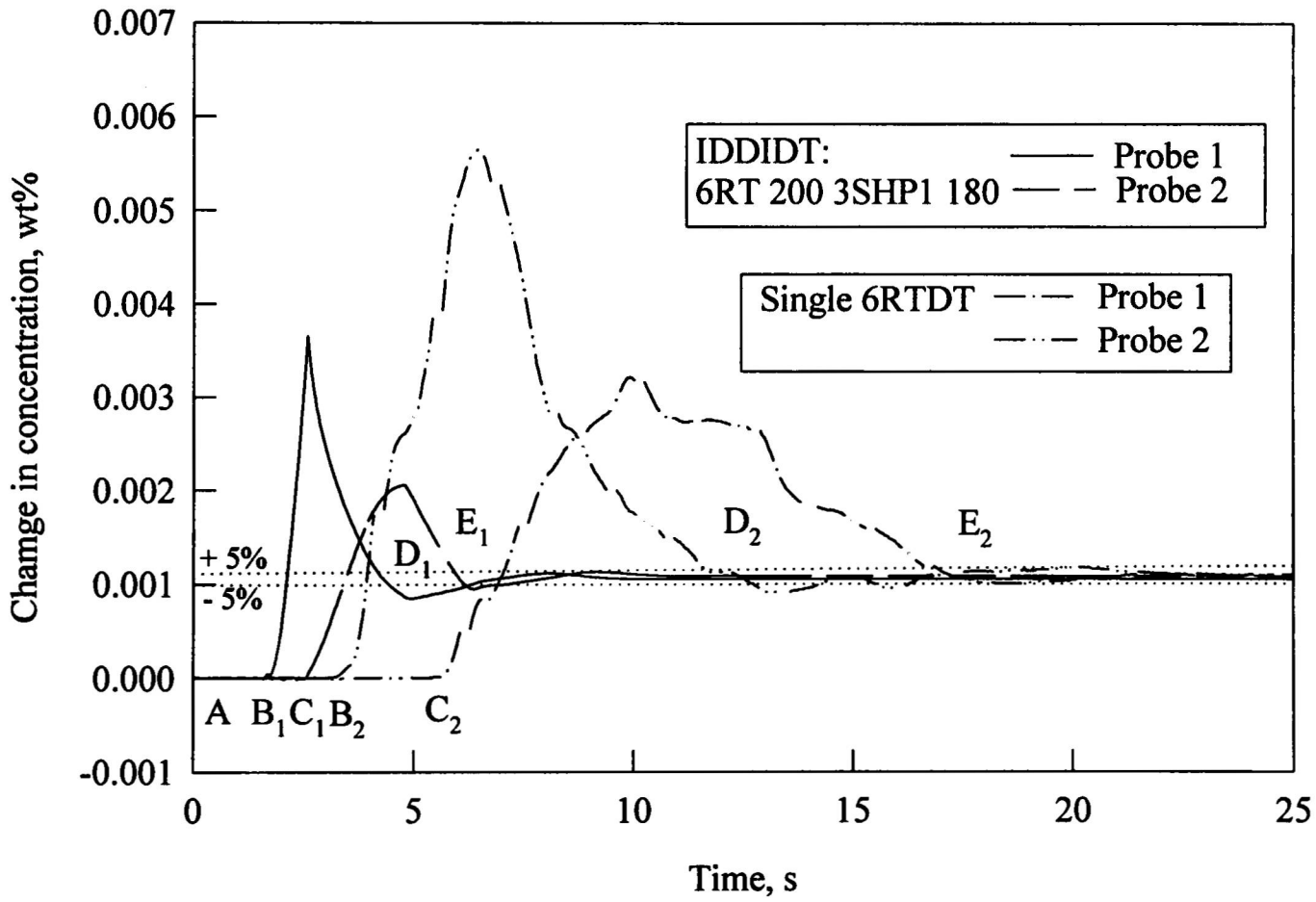

Figure 8.3-7 Comparison between decolorisation and conductivity mixing experiments in relation to the circulation time

The values of θ_C gave reasonably good agreement with the mean circulation times calculated from the bulk circulation time distribution, $\bar{t}_{bc}$ (Table 8.3-2). This indicated the importance of top to bottom mixing in the blending process *i.e.*, although $\bar{t}_u$ was not much greater for the

RTDT compared to the IDDIDT, the pills tendency to become trapped in the lower loop significantly increased θ_C (or $\bar{t}_{bc}$) and hence increased θ_m.

Table 8.3-2 Comparison of mean circulation times, peak to peak times (P-P) and mixing times

RT	3SHP1	t_{bc}	P-P	Mixing Time	
rpm	rpm	s	s	$\theta_{m\text{-}p1}$, s	$\theta_{m\text{-}p2}$, s
200	0	13.86	13	23.71	19.92
300	0	8.86	8	19.13	12.94
0	180	6.23	5	7.7	7.1
200	180	5.29	4.4	7.5	6.6
300	180	4.39	4.5	7.1	5.75
0	240	4.41	3.5	5.8	5.8
200	240	4.50	3.0	5.5	4.43
300	240	3.96	3.5	5.6	4.65

The mixing times correlated well with the mean "bulk" circulation times giving

$$\theta_m = A\,\bar{t}_{bc}$$

where A was constant and equal to 1.4 for Probe 1 (r^2=0.96) and 1.73 for Probe 2 (r^2=0.91). In contrast to others[7,9,17], a similar trend was also observed from the response curve, where the cross-section of the ±5% line and the concentration transient usually occurred shortly before the second peak, *i.e.* not long after one circulation. In fact, the traditional assumption of $\theta_m = 4 \times \bar{t}_{bc}$ gave mixing times very similar to those predicted by Cooke *et al.*[18] for the single RT and the single 3SHP1 at H=2T configuration (Section 7.1.3.1.1). *e.g.* 3SHP1 at 180 rpm; θ_m = 7.7 s, θ_m (Cooke *et al.*) = 25 s, $4 \times \bar{t}_{bc}$ = 24.92 s.

8.3.3 Aerated circulation time distributions

In addition to unaerated experiments, preliminary aerated CTD's were measured. The introduction of air had a profound effect on the mean, standard deviation and shape of the circulation time distributions (Figure 8.3-8 and Figure 8.3-9). It is clear that the primary peak of the distribution was much smaller and had shifted to the right indicating longer circulation times under aerated conditions (Figure 8.3-8). The lower aerial mean circulation time, $\bar{t}_l$, and standard deviation increased by about 100 % and 200 % respectively, at the conditions examined. Similarly, the bulk circulation time distribution shifted considerably to the left and exhibited a damped peak compared to the unaerated case. In addition, the CTD was much wider implying a more varied flow pattern. This was also reflected in the shift, and elongation of, the secondary peak, in the lower aerial CTD, from about 2.5 s to above 6 s. However, too few data were obtained for a complete analysis on the influence of aeration and therefore a full explanation of the changes was difficult. The trend of a longer bulk CTD agreed with the slower annular velocities reported in Section 7.3.2.3 and was considered to be due to the reduction of the pumping capacity of the 3SHP1. Figure 8.3-10 compares the tracer response of the unaerated and aerated conditions described above and confirms a longer circulation time, θ_C, for the latter. Since $\bar{t}_{bc}$ approximately doubled on aeration it was surprising that only slight increases in θ_m were observed (Section 7.3.2.3). In contrast to the unaerated case, it was apparent that 95 % homogeneity was accomplished shortly before the second trough, *i.e.* in less than one circulation, and was probably due to the effect of the gas mixing increasing the dispersion during circulation. Alternatively, the longer circulation times encountered in aerated systems could stem from an inadequacy in the measurement technique. Although a small pill was employed, problems still arose in attaining its neutral bouyancy. Therefore, whether the aerated CTD is representative of the liquid flow is questionable.

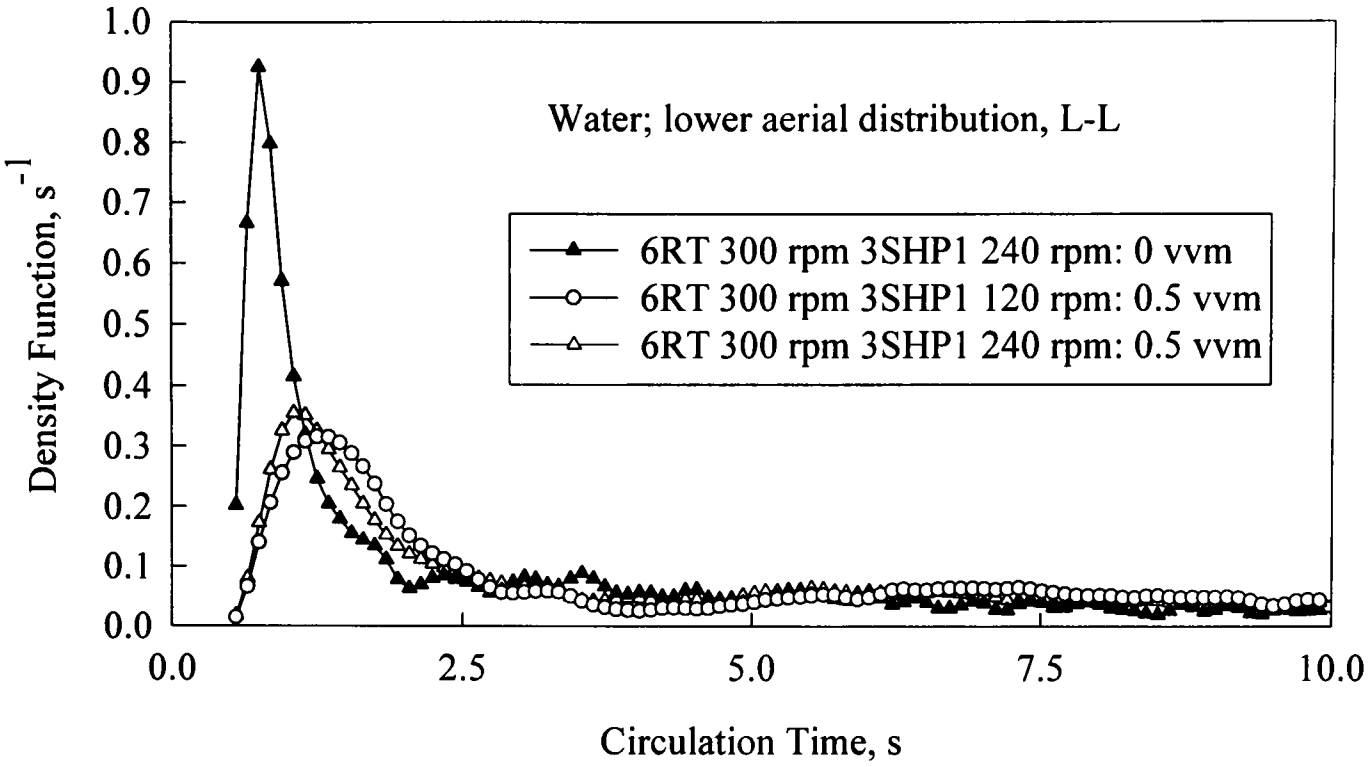

Figure 8.3-8 Effect of aeration on the lower aerial circulation time distribution (L-L)

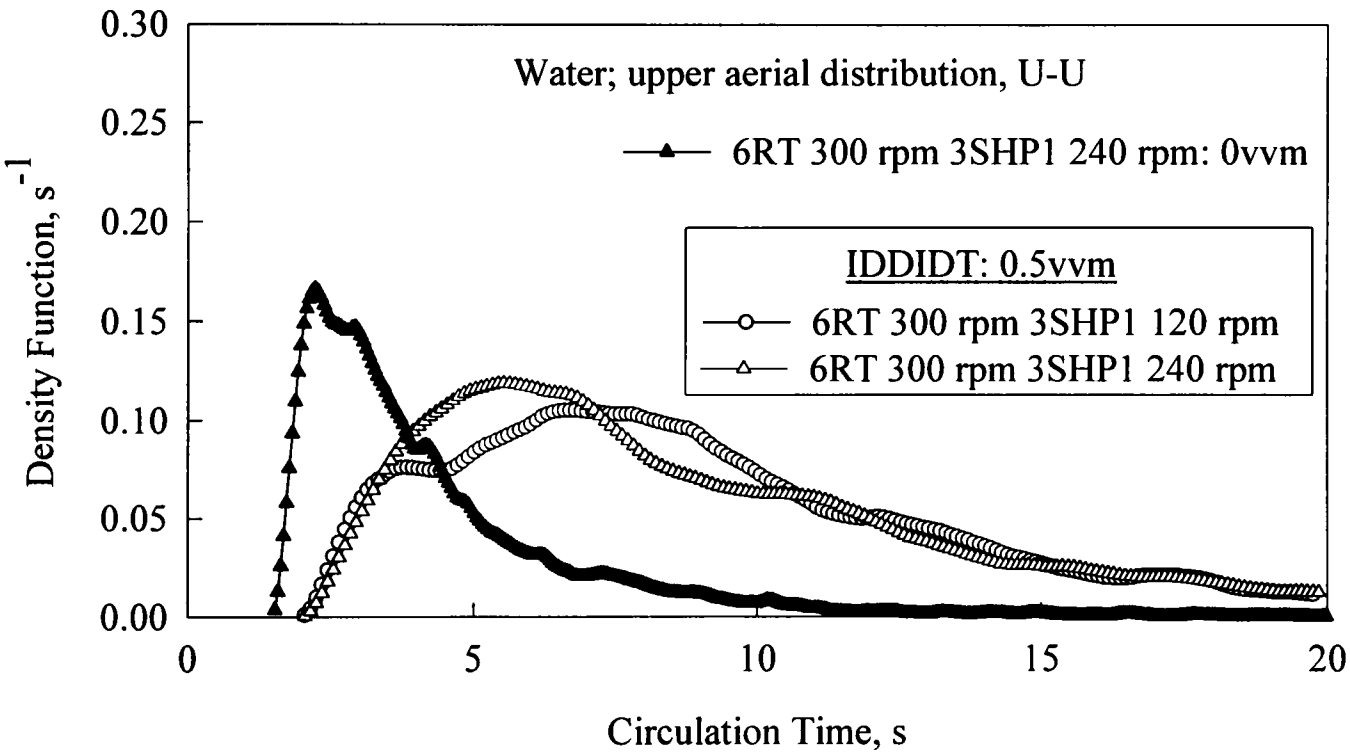

Figure 8.3-9 Effect of aeration on the bulk circulation time distribution (U-U)

8.3.4 Circulation time distributions in *Aspergillus niger* fermentation broths

Originally, two experiments were planned for the *A.niger* system. However, due to technical problems in the second fermentation, which incorporated two aerials, only preliminary data from the first fermentation, using one aerial, was used to assess CTD's acquired in real fermentation broths. The continually changing morphological and rheological environment experienced by the pill provided additional uncertainties in the measurement.

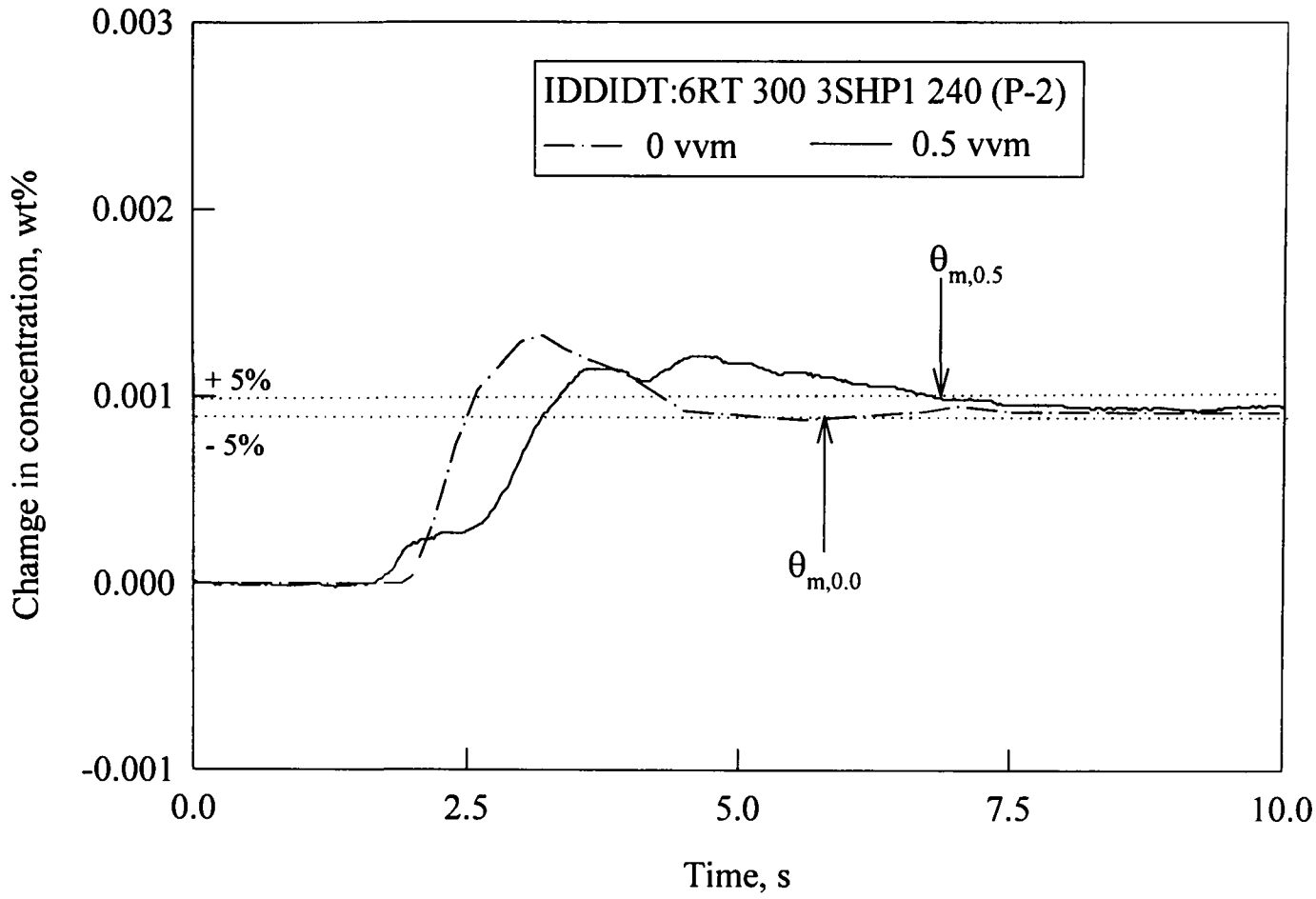

Figure 8.3-10 Comparison of unaerated and aerated tracer response

The CTD's (Figure 8.3-11) exhibited similar trends to those seen in water, *e.g.* a large initial peak followed by a tail which contained a secondary peak. In addition, increasing the gas flow rate from 0.5 to 0.62 vvm changed the shape of the CTD; lowering, widening and shifting the first peak to the left (even after an increase in 3SHP1 speed). Alternatively, the difference may have been caused by the highly increased viscosity encountered towards the end of the fermentation. Such a phenomena was reported by Schmitz[6] when examining CTD's in *Penicillium chrysogenum* fermentations.

In the earlier stages, increases in biomass concentration (over 4 hour periods) tended to have little effect on the CTD's. Mixing experiments executed between data collection times, resulted in gross changes in morphology and rheology (which may reduce circulation time). This, coupled with the increased biomass (which may increase circulation time) possibly caused the similarities in the CTD's. Alternatively, the well defined flow pattern provided by

the IDDIDT may not have been significantly altered by the relatively small changes in biomass concentration.

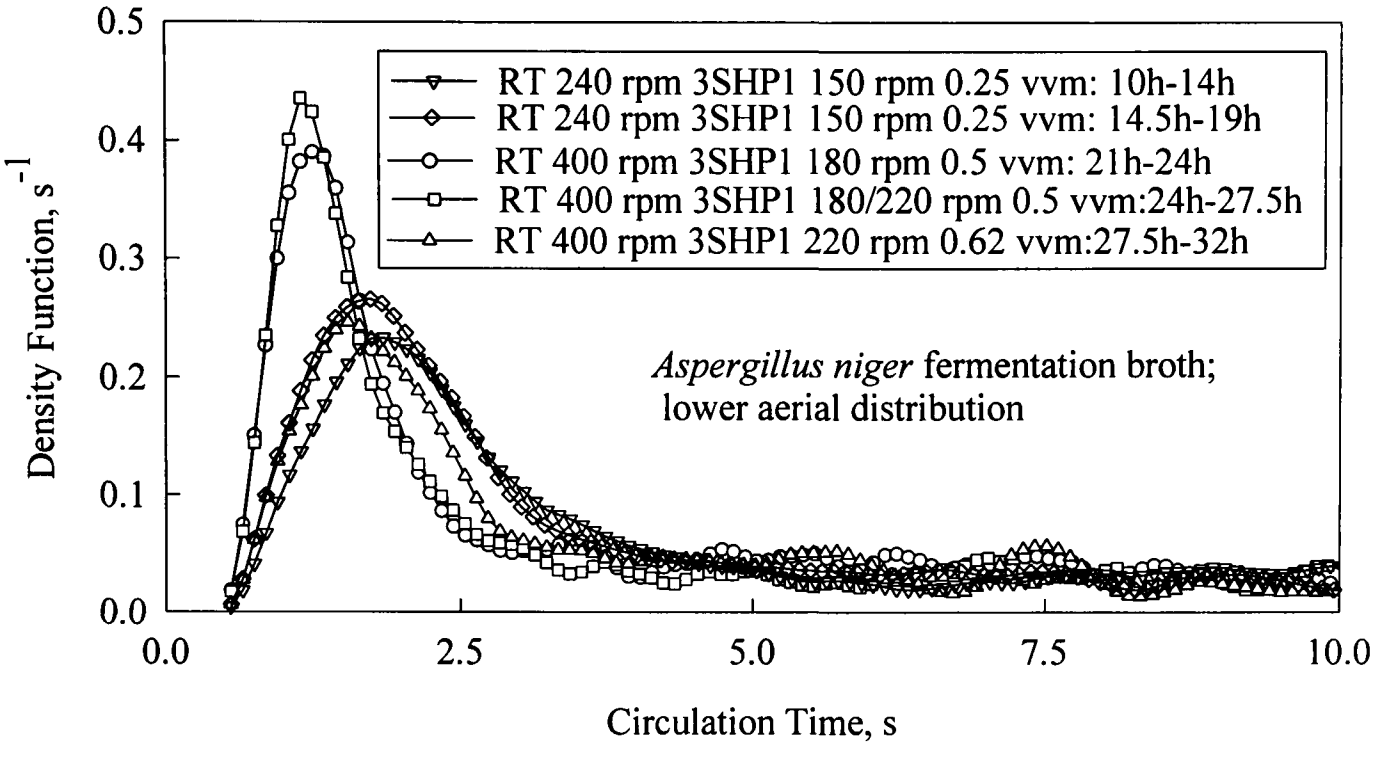

Figure 8.3-11 Circulation time distributions in *A.niger* fermentation broth

8.4 Conclusions

Aerated and unaerated circulation time distribution measurements, carried out in water and *Aspergillus niger* fermentation broths, aided the characterisation of the mixing process for the IDDIDT from which the following could be concluded:

1. With the lower aerial as a reference point the CTD could be described as bimodal. Using two aerials, it was discovered that the first peak was due to circulations in the region below the 6RT and the second peak to circulations which occurred around the draft tube,

2. The blending performance was dependant on the efficiency of top-to-bottom mixing and could be well described by CTD's using the upper aerial as a reference point, giving

$$\theta_m = A\,\bar{t}_{bc}$$

where A=1.4 or 1.7 for Probe 1 and 2 respectively. This suggested the well defined flow pattern produced by the IDDIDT was responsible for the low mixing times reported in Chapter 7,

3. Preliminary aerated studies in water and *A.niger* broths showed an influence of aeration and morphology/rheology on the CTD's, however not enough data were obtained to make any definite conclusions. Collecting sufficient CTD data from fermentations would require many fermentations operated at the same conditions, which is time consuming and expensive. Alternatively, CTD experiments using test fluids with rheological characteristics mimicking those of the fermentation broth would give representative results.

8.5 References

1. Middleton, J.C., 1979, "Measurement of circulation within large mixing vessels", *3rd Euro.Conf.Mixing*, BHRG, Cranfield, U.K., Paper A: 15-36
2. Sykes, P., 1965, "Particle circulation time in propeller stirred tanks", *Chem.Eng.Sci.*, 20:1145-1146
3. Bryant, J., 1977, "The characterisation of mixing in fermenters", *Advn.Biochem.Eng.*, 5: 101-123
4. Bryant, J. and Sadeghzadeh, S., 1979, " Circulation rates in stirred and aerated tanks", *3rd Euro.Conf.Mixing.*, U.K., Paper F3:325-336
5. Bryant, J. and Sadeghzadeh, S., 1982, "Terminal mixing times in stirred tanks", *4th Euro.Conf.Mixing.*, Netherlands, Paper B4, BHRG, Cranfield, UK: 49-56
6. Schmitz, R, 1996, "Circulation time studies in Newtonian and non-Newtonian fluids in stirred tanks", *PhD Thesis*, University of Birmingham, U.K.
7. Holmes, D.B., Voncken, R.M. and Dekker, J.A., 1964, "Fluid flow in turbine-stirred, baffled tanks-I Circulation time", *Chem.Eng.Sci.*, 19:201-208
8. Voncken, R.M., Holmes, D.B. and Dekker, J.A., 1964, "Fluid flow in turbine-stirred, baffled tanks-II Dispersion during circulation", *Chem.Eng.Sci.*, 19:209-213
9. Khang, S.J. and Levenspiel, O., 1976, "New scale-up and design criteria for stirrer agitated batch vessels", *Chem.Eng.Sci.*, 31:569-577
10. Mukataka, S., Kataoka, H. and Takahashi, J., 1976, "Measurements of mean circulation time of a mycelial suspension in a stirred tank", *Kagaku Kogaku Ronbunshu*, 2:628-630
11. Mukataka, S., Kataoka, H. and Takahashi, J., 1980, "Effects of vessel size and rheological properties of suspensions on the distribution of circulation times in stirred vessels", *J.Ferm.Tech.*, 58: 155-161
12. Mukataka, S., Kataoka, H. and Takahashi, J., 1980, "Circulation times of various fluids in stirred fermenters", *Adv.Biotech.*, 1: 523-528
13. Mukataka, S., Kataoka, H. and Takahashi, J., 1981, "Circulation time and degree of fluid exchange between upper and lower circulation regions in a stirred vessel with a dual impeller", *J.Ferm.Tech.*, 59: 303-307

14. Fuhanashi, H., Harada, H., Taguchi, H. and Yoshida, T., 1987, "Circulation time distribution and volume of mixing regions in highly viscous xanthan gum solution in a stirred vessel", *J.Chem.Eng.Japan*, 20, No.3:277-282

15. Roberts, R.M., Gray, M.R., Thompson, B. and Kresta, S.M., 1995, "The effect of impeller and tank geometry on circulation time distributions in stirred tanks", *Trans.I.Chem.E.*, 73, Part A:78-86

16. Schmitz, R., McFarlane, C.M. and Thomas, C.R., 1996, "Bioreactor mixing studies using two flow follower techniques", *Proc.I.Chem.E.Res.Event.*, 1:58-60

17. Nienow, A.W., 1990, "Agitators for mycelial fermentations", *Trends in Biotech.*, 8:224-233

18. Cooke, M., Middleton, J.C. and Bush, J.R., 1988, "Mixing and mass transfer in filamentous fermentations", *Proc.2nd Int.Conf. Bioreactor Fluid Dynamics*, BHRA/Elsevier, UK: 37-64

CHAPTER 9

ASPERGILLUS NIGER FERMENTATIONS

9.1 Introduction

As previously discussed, filamentous micro-organisms, grown in submerged culture, are used in a large number of industrial fermentation processes. Such processes include the fermentation of *Penicillium chrysogenum* for the production of penicillin and the use of *Aspergillus niger* to produce citric acid, which has an extensive use in the soft drinks industry. For such micro-organisms, two categories of mycelial growth have been reported. Firstly, a dispersed form in which the hyphae become dispersed throughout the culture potentially producing a highly viscous non-Newtonian fermentation broth and, secondly, a pelleted form where the mycelium grows into tightly packed hyphal masses, often as relatively uniform spheres producing broth which is less viscous but can still behave in a non-Newtonian manner. The dispersed form can be divided into "freely dispersed" and "clumps", the former often subdivided into "unbranched", "branched" and "loops" for measurement purposes (Table 9.2-3). The pelleted structure of the fungi can vary considerably and has been classified by various authors [1,2,3]:

- Fluffy loose pellets - compact centre with a much looser outer zone
- Compact smooth pellets - spherical compact pellet with a smooth surface
- Hollow smooth pellets- a smooth spherical pellet with a hollow centre formed by autolysis

In either case fluids are generally pseudoplastic and can be described by the power law model (Chapter 2).

These complex broth rheologies can lead to heat and mass transfer difficulties due to incomplete mixing, with the possible onset of dead zones (regions of stagnant fluid). They have been studied extensively in agitated tanks using Perspex vessels utilising model test fluids such as Carbopol and CMC. Chapters 4 to 8 have reported a possible improvement in performance for a vessel fitted with dual independently driven impellers and a draft tube (IDDIDT) compared to more conventional systems (RT-RT). However, little literature has been published concerning the use of real fermentation broths in this novel system. As the vessel is constructed of Perspex only a limited degree of sterility is achievable because the vessel is not steam sterilisable. However it was possible to undertake fermentations with hygienic conditions alone, and the vessel has therefore been described as a proto-fermenter.

9.1.1 Research considerations

Initially, two major problems had to be tackled. They were:

a) growing a fungus non-aseptically (avoiding contamination from bacteria) to produce a model, mixing sensitive fermentation broth in the dispersed form;

b) undertaking the fermentation in an environment not designated for microbial bioprocesses. Therefore, a minimal fermentation time was required to comply with strict safety regulations.

To solve (a), a food grade strain of *Aspergillus niger* (A1233/citrate) was chosen. This organism will grow at very low pH, minimising the risk of bacterial contamination even under non-aseptic conditions. However, *A.niger* tends to grow in the pelleted form and, therefore, small scale work was required to optimise the conditions needed to stimulate filamentous growth (Section 9.3.1).

To solve (b), in the final fermentation process a vegetative inoculum was grown from spores in a 75 l stainless steel fermenter injected into the proto-fermenter to give a batch fermentation time of circa 35 hours (Section 9.3.2).

The author would like to acknowledge the work of the research team without whose help the large scale fermentations (640 l) would not have been possible.

9.2 MATERIALS AND METHODS

9.2.1 Selected organism

The organism used for the mixing studies on filamentous fermentation broths was the food grade strain of *Aspergillus niger* (A1233/citrate) usually employed for the production of citric acid. It was deposited at IMI under the number 075353 and was isolated in Canada in 1952.

9.2.2 Sporulation media

Potato Dextrose Agar (PDA) was employed for the sporulation and growth of the *A. niger* (A1233/citrate). 39 g/l of PDA (OXOID, Unipath Ltd, Basingstoke) was dissolved in boiling distilled water. Upon dissolution of the PDA, rendering a clear solution, the media was transferred to 50 ml agar slopes (10 ml of media) and 250 ml medical flats (170 ml of media). The containers were bunged with cotton wool, covered with aluminium foil and sterilised at 121°C, 15 psig for 40 minutes. Once solidified, the agar slopes were aseptically inoculated from the spore stock using a heated loop and then incubated at 25°C. After 5 days the spores were transferred to medical flats using 15 ml of pre-sterilised 0.02% Tween 80 solution or sucrose solution containing glass beads. The Tween 80 is a surface active agent that encourages the release of the spores from the agar surface which are then distributed in the medical flats with the help of the glass beads. Following a further 5 days of incubation at 25°C, the fermentation inoculum was obtained from these flats in a similar method (using ~60ml of sucrose solution per medical flat).

9.2.3 Fermentation media

Three types of fermentation media were used for the growth of *A.niger* in submerged culture: a defined medium (medium I) designed by Professor G. Solomons (RHM); a molasses medium

(medium II) developed by Ms. H. Jennings at the University of Birmingham; and a medium (medium III) based upon the work of Roehr *et al.* [4] (Table 9.2-1).

Table 9.2-1 Media for *A.niger* fermentations

Media	Sugar g/l	Molasses %	$(NH_4)_2SO_4$ g/l	KH_2PO_4 g/l	$MgSO_4$ g/l	$ZnSO_4$ g/l	$MnSO_4$ g/l	$FeSO_4$ g/l	$CaCl_2$ g/l	Nacl g/l
I	65	-	15	2.5	0.5	0.25	0.05	0.02	-	-
II	-	5	1.25	1.5	0.1	-	-	-	-	-
III	50-65	-	-	0.15	1.1	0.0015	-	-	0.55	0.15

The defined medium was made up as follows:

The ammonium sulphate was dissolved in 100 ml of water and its pH adjusted to 5, 3 or 2 with sulphuric acid. The phosphate was dissolved in 50 ml of water, but its pH was not adjusted. The trace elements were dissolved altogether in 100 ml. These non-sugar components were then added to a conical flask which was then plugged and sterilised in the autoclave. The sucrose was dissolved in the remainder of the water (to make up the working volume) and its pH adjusted to 5, 3 or 2. This solution was then placed into the fermenter and autoclaved at 121°C, 15 psig for 15 minutes. The sugar was sterilised separately from the rest of the components to prevent the sugar browning due to the Maillard reaction. When cooled the inorganics were added to the fermenter aseptically and the pH adjusted to the required level with sulphuric acid.

9.2.4 Fermentation vessels

The geometric dimensions of the fermentation vessels employed for the production of *Aspergillus niger* are summarised in Table 9.2-2.

All bench scale fermentations were undertaken in 5 l glass vessels, with a working volume of 4l, agitated by a single or dual standard Rushton turbine (Table 9.2-2). The final fermentation process involved the growth of a vegetative inoculum, from spores, in a 75 l stainless steel fermenter. This was then injected into the 640 l IDDIDT proto-fermenter.

9.2.5 Analysis/monitoring

Variables (pH, dO_2, temperature, impeller speed) for the 75 l fermentations were logged using a commercially available computer control and monitoring system (SETCIM), whereas the changing variables in the proto-fermenter were followed using chart recorders. The bench scale variables were recorded manually. Exit gas from all the fermentations was analysed by a mass spectrometer (VG MM8-80 Gas Analysis Systems Ltd., Middlewich, UK)[5] and recorded by SETCIM via an interface program, enabling the oxygen uptake rate (OUR), carbon dioxide production rate (CPR) and respiratory quotient (RQ) to be calculated throughout the course of the fermentation.

Cell morphology and broth rheology were analysed throughout the larger scale fermentations and on the completion of a 5l fermentation. Morphology was assessed using a well developed image analysis procedure (Section 9.2.5.2) and rheology data was obtained from a Contraves disc turbine rheometer (Chapter 2).

Table 9.2-2 Pilot plant fermentation vessels

Vessel	Electrolab (5l)	In-house (5l)	75l
Diameter, T	0.15	0.15	0.79
Height, H	0.30	0.30	0.87
Working volume, l	4	4	60
Impeller type	2 -6 bladed turbines	Rushton turbine	2-Rushton turbines
Clearance	0.02	0.02	0.262
Speed range, rpm	0-1000	0-1000	0-800
Control mechanism	Electrolab	In-house	SETCIM

9.2.5.1 Dry cell weight

Dry cell weight was determined by filtering 10 ml of broth through a small Buchner funnel, containing 0.35μm cellulose filter paper (Whatman Int. Ltd., Maidstone, Kent), washing well with distilled water to dislodge any remaining sugar and drying at 100°C for 24 hours. The cellulose paper was dried and pre-weighed before filtration took place to ensure a true dry weight value.

9.2.5.2 Morphology

Mycelia morphology was assessed by a well developed image analysis technique established at the University of Birmingham[6,7,8,9,10] using the Quantimet 570 image analyser (Leica Cambridge Ltd., Cambridge, UK). Immediately after taking a sample, 1 ml of broth was fixed and stained with a few drops of lactophenol cotton blue (Fluka Chemika-BioChemika, Dorset,

UK). The fixed sample was diluted with 10/20% sucrose solution, to prevent quick evaporation[9], and 40 µl was placed on a slide and covered with a coverslip. The biomass concentration of the diluted sample was typically 0.2-0.5 g/l and a magnification of ×50 was used.

Analysis of freely dispersed mycelia (unbranched and branched) and clumps was necessary for an in-depth characterisation of morphological changes throughout the fermentation. The image classifications and processing stages were described by Paul and Thomas[11] and have been summarised by Jüsten[9]. Major parameters of interest are shown in Table 9.2-3.

Table 9.2-3 Morphological parameters of interest to this study [9,11]

UH - unbranched hyphae; BH - branched hyphae; LH - mycelia with 1- 3 loops; C - clumps

Parameter	Definition	Classification of
Projected area	Area of the projection of a three dimensional object (the mycelium) into a two-dimensional image.	UH, BH, LH, C
Perimeter	Length of the boundary of the projected area of mycelium.	UH, BH, LH
Fibre length	The length of a rectangular object having the same projected area and perimeter as the hypha.	UH, BH, LH
Total length	Sum of main hyphal length and all branches	UH, BH, LH
No. objects	Number of specific objects (freely dispersed or clumped) counted for a given sample.	UH, BH, LH, C
No. of tips	The mean number of tips per mycelium.	UH, BH, LH

9.3 Results and Discussion

9.3.1 Small scale studies (5l)

In order to produce the required viscous non-Newtonian dispersed form of *A.niger*, several 5 l bench scale fermentations, each with differing initial operating parameters or media constituents, were undertaken (Table 9.3-1). The traditional approach employed by the bioprocess industries is to inoculate a small inoculum fermenter with spores grown on a solid medium[12] and use this fermentation broth to inoculate a larger fermenter. Typically 10% of the larger vessel volume is used for the inoculum volume. In order to minimise the overall fermentation time (time to reach maximum biomass concentration, *i.e.* the stationary phase) hygienic fermentations were inoculated with 10% volume of final broth produced by a previous aseptic fermentation. A number of factors affected the growth and productivity of the micro-organisms as discussed below although the final rheological characteristics of the majority of the fermentation broths were similar. All small scale fermentations were at 25.0±0.1°C. A "trial and error" process was employed and is set out below.

9.3.1.1 Fermentation 1

Trager *et al.*[13] observed that provided the dissolved oxygen tension was greater than or equal to 100% of saturation throughout the lag phase then the final biomass concentration was not significantly influenced by the DOT. It has also been reported that *Aspergillus oryzae* fermentations will not be oxygen limited provided the critical oxygen concentration of 0.020 mmol/l[14] is surpassed (~10% DOT). To ensure an initial DOT close to 100%, fermentation 1 was conducted with an initial impeller speed of 800 rpm and a gas flow rate of 1 vvm. This proved unsatisfactory however because the *A.niger* spores tended to 'blow out' of the fermentation broth (possibly due to their high hydrophobicity) resulting in a distinct lack

of growth. Similarly, van Suijdam *et al.*[15] investigated the influence of inoculum type on *Aspergillus niger* and found that when using a spore inoculum in a bubble column *A. niger* failed to grow due to the high degree of hydrophobicity exhibited by the spores which consequently floated on the surface.

9.3.1.2 Fermentations 2 and 2(i)

To avoid spores being "blown out" of the broth, Fermentation 2 was operated at an initial gas flow rate of 0.2 vvm and an impeller speed of 200 rpm. Following the drop in dO_2, as biomass production occurred, impeller speed and gas flow rate were incrementally increased (manually) to obtain a DOT of at least 25%. Under these conditions 19.7 g/l of biomass was produced in 75 hours, giving an average growth rate of 0.27 g biomass/l/h. Ten percent (0.4 l) of this broth was used to vegetatively inoculate a second (hygienic) fermentation (fermentation 2(i)). Sixteen g/l of biomass was finally produced and the time required for its production was only 40 hours. In comparison to fermentation 2, this increased the average growth rate by approximately a third, to 0.40 g/l/h. The predominant factor in reducing the fermentation time was the decrease in the lag phase from well over 20 hours for spores to approximately 5 hours for a vegetative inoculum. However, in both cases the broth was pelleted so further work was required to optimise the conditions for dispersed growth.

9.3.1.3 Fermentation 3

It has been documented for moulds[15] that a low spore concentration in the inoculum ($<10^8$ spores/ml) will result in the formation of pellets, whereas with a concentration greater than 10^9 spores/ml, dispersed growth will occur. However, studies on *Aspergillus niger* have shown that pellet formation occurs at all spore concentrations when grown in shake flasks [16]. Here, increasing the spore concentration from 10^6 spores/ml to 10^7 spores/ml had little effect on the fermentation progress or morphology. It was observed that at the core of the pellets an

agglomeration of spores was present. To overcome this a high agitator speed (800 rpm) was utilised in fermentation 4.

9.3.1.4 Fermentation 4

It has been suggested that high agitator speeds will impede the agglomeration of spores and hence increase the possibility of dispersed phase growth[17]. However, operating at a high agitator speed (800 rpm) (with a low gas flow rate of 0.2 vvm to avoid spore "blow out") very little growth was observed, the fermentation taking 140 hours to produce 10.5 g/l of biomass. This phenomenon has recently been observed when growing *A. niger* at pH 2.0 using high impeller speeds and was attributed to a weaker cell wall at the low pH being more sensitive to high stresses[18]. Due to the poor inoculum stage the hygienic fermentation 4(i) failed to grow.

9.3.1.5 Fermentation 5 and 5(i)-(iv)

The fifth set of fermentations examined the possibility of growing an inoculum in a molasses medium, controlled at pH 5 (which gave a dispersed growth in previous shake flask research undertaken at the centre) and using this to hygienically inoculate four fermentations (Fermentations 5(i)-5(iv)) using media I and II with initial pH values of 3 and 5. Fermentation 5 produced a dispersed growth, although a lower biomass concentration, compared to Fermentation 2, of 7.6 g/l was obtained.

Fermentations 5(i) to (iv): The lack of growth using the molasses medium at low pH (fermentation 5 (ii)) has been reported previously[3] and was attributed to the prevention of germination due to the presence of acetic acid. The remaining three fermentations (5(i)(iii)(iv)) all grew in the pelleted form although Fermentation 5(iii) produced small fluffy pellets and hence gave a more viscous fermentation broth (higher K value). Once again it was evident that the average growth rate (maximum biomass/time to reach maximum) increased from 0.21 g/l/h with a spore inoculum to over 0.4 g/l/h when a vegetative inoculum was

utilised. However since the vegetative inoculum was pelleted then the subsequent fermentation broths also become pelleted, although the size and extent of pelleting was very dependent on the media constituents.

9.3.1.6 Fermentation 6(a-d) and 6(c,i)

It was suggested by Steel *et al.*[3] that acidic pH's favoured growth of *A.niger* in the dispersed form. Similarly, Galbraith and Smith[19] observed "filamentous" or dispersed growth at a pH of 2.1, probably due to the electrostatic repulsion of spores which prevented agglomeration and hence impeded the production of pellets. Therefore a series of fermentations (6(a) to (d)) were undertaken using medium III, the best of which (highest biomass) was used to inoculate a hygienic fermentation (6(c,i)). It is evident (Table 9.3-1) that at a pH of 2 a completely dispersed mycelium broth was produced (fermentations (a) and (c)) whereas when the fermentation was initiated at pH 5 and left to drift down to pH 2 pelleted growth occurred (fermentations (b) and (d)). In contrast to fermentation 4, the high impeller speeds had little effect on the end biomass or average growth rate of the fermentations.

The hygienic fermentation (6(c,i)), inoculated using the final broth of fermentation 6(c), inexplicably failed to produce biomass.

9.3.1.7 Fermentations 7(a) and (b)

Both fermentations 7(a) and 7(b), with pH controlled at 2, gave a dispersed growth of *A. niger*. Since the fermentation utilising medium I produced about three times as much biomass as that of fermentation 7(b) and was previously successfully employed as a hygienic inoculum stage (fermentation 2(i)) it was decided that this would be the most satisfactory 640 l inoculum stage, *i.e.* to grow *Aspergillus niger* at pH 2 utilising medium I, yielding a highly viscous rheologically complex broth (high K, low n).

Table 9.3-1. Small scale fermentation operating conditions and results
A-Aseptic, H-Hygienic; Q_G - gas flow rate; rpm-impeller speed; X-Biomass concentration; μ_{AV} -average growth rate; F-filamentous, P-pelleted; *controlled at this pH, otherwise left to drift

Ferm No.	A/H	Media	spores /ml (A) or g/l (H)	pH	Q_G vvm	rpm	Time h	X g/l	μ_{AV} g/l/h	P/F	K	n
1	A	I	10^6	3	1	800	-	-	-	-	-	-
2	A	I	10^6	3	0.2	200	75	19.7	0.27	P	1.8	0.24
2 (i)	H	I	1.97	3	0.2	200	40	16.0	0.40	P	1.5	0.25
3	A	I	10^7	3	0.2	200	58	20.2	0.34	P		
4	A	I	10^6	3	0.2	800	140	10.5	0.08	P		
4 (i)	H	I	0.5	3	0.2	200	-	-	-	-		
5	A	II	10^6	5*	0.2	200	46	7.6	0.21	F	2.8	0.36
5 (i)	H	II	0.96	5	0.2	200	21	9.2	0.43	P	2.2	0.20
(ii)	H	II	0.96	3	0.2	200	-	-	-	-	-	-
(iii)	H	I	0.96	5	0.2	200	45	21.3	0.47	P	3.3	0.23
(iv)	H	I	0.96	3	0.2	200	50	20.1	0.41	P	1.9	0.19
6 (a)	A	III	10^6	2*	0.2	800	40	8.3	0.21	F	0.7	0.22
(b)	A	III	10^6	5	0.2	800	40	7.1	0.18	P	0.1	0.44
(c)	A	III	10^6	2*	0.2	200	40	10.0	0.25	F	0.5	0.25
(d)	A	III	10^6	5	0.2	200	40	4.5	0.11	P	-	-
6 (c,i)	H	III	0.99	2*	0.2	200	40	-	-	-	-	-
7(a)	A	I	10^6	2*	0.2	200	54	22.2	0.41	F	3.2	0.17
(b)	A	III	10^6	2*	0.2	200	36	7.7	0.21	F	2.3	0.18

9.3.2 Mixing studies in the 640 l proto-fermenter

The protocol, formed from small scale work, enabled pilot scale (640l) mixing experiments using real fermentation broths. Three hygienic fermentations were executed in the proto-fermenter, one using a dual Rushton turbine common shaft simulation and the other two using IDDIDT. The fermentations were termed hygienic as the vessel and addition/sampling ports

could not be steam sterilised. Therefore, prior to inoculation, the vessel was cleaned using a solution of Decon 75 (Decon Laboratories Ltd, Hove, E.Sussex) and rinsed with distilled water. Medium I was made up and sterilised batch wise (as described in Section 9.2.3) and, in order to minimise the risk of contamination, was placed into the vessel immediately before the inoculation with *A.niger*.

For each fermentation, an inoculum was grown up from spores (10^6 spores/ml in the vessel), using medium I initially and controlled at pH 2 within the 75l stainless steel fermenter. The dispersed broth produced (after ≅ 70 hours) was used to inoculate the 640 l hygienic proto-fermenter, whose pH was also controlled at 2.0. Power, hold-up and k_La experiments were performed. HPLC analysis, CTD's and also full morphological data for different stages of the fermentation were collected. Fermentations II and III were controlled at 25.0±0.1°C but Fermentation I had no provision for temperature control.

The pilot scale (75 l to 640 l) fermentation work required the co-operation and hard work of fourteen people (from the biocentre, workshops and engineering department) to ensure the successful and safe completion of the project.

9.3.2.1 Regime analysis

An overall idea of the rate limiting steps for *Aspergillus niger* production was obtained by regime analysis (Chapter 2). Table 9.3-2 shows the time constants of the sub-processes that may affect the productivity. Evidently the time constants for growth and substrate utilisation are much greater than the time constants for the transport processes. Therefore they are not rate limiting sub-processes, but do govern the overall fermentation time.

Table 9.3-2 Time constants important for *A. niger* production, based on water values

(calculations in Appendix VI)

Sub-process	Time constant, seconds
IDDIDT (transport)	
Oxygen transfer ($1/k_La$); $t_{ot\text{-}ID}$	10-33
Circulation of liquid (θ_m); $t_{m\text{-}ID}$	5-30
RT-RT (transport)	
Oxygen transfer ($1/k_La$); $t_{ot\text{-}RT}$	10-67
Circulation of liquid (θ_m); $t_{m\text{-}RT}$	50-100
Microbial (conversion)	
Oxygen consumption, zero order; $t_{oc\text{-}0}$	47.3
first order; $t_{oc\text{-}1}$	3.55
Substrate consumption, zero order (C_s/r_{smax}); t_{sc}	$\sim 16\times10^4$
Growth ($1/\mu$); t_G	9×10^4

The times for oxygen consumption and oxygen transfer are of the same order of magnitude, suggesting oxygen limitation may occur. In addition, the liquid circulation time is of the same order of magnitude so oxygen gradients are likely to occur. Since the transport time constants are based on measurements made in water, their magnitudes will be much higher in fermentation broths due to the effect of viscosity (Chapters 6 and 7). Consequently the likelihood of oxygen gradients developing in the latter parts of the fermentation (when consumption is at a maximum and k_La and blending efficiency are at a minimum) is very high. The improvements in blending efficiency (Chapter 7) and mass transfer (Chapter 6) when using the IDDIDT configuration (compared to RT-RT) suggest a possible improvement in performance by lowering the time constants for the rate limiting mechanisms (t_m and t_{ot}).

Experimental design was necessary to provide a basis for the comparison between the efficiency of the IDDIDT and that of the RT-RT configuration. The possible approaches to the design of the fermentations were:

a) keep the agitation (P/V) and aeration (Q_G) conditions constant. This may result in loss of yield due to oxygen limitation,

b) attempt to match the DOT profile by changing the impeller speeds (P/V) and gas flow rate (Q_G) resulting in similar yields but with possible differences in the power demand between the fermentations.

The potential improvement in performance when using the IDDIDT comes from the separation of the agitator functions (gas dispersion and bulk blending) and the controllability of the local energy inputs, *i.e.* the 3SHP1 is operational only when the process requires an increase in bulk blending. Therefore to witness the possible merits of the configuration it was decided to use approach (b), which permitted impeller speed changes throughout the fermentation. Secondly, approach (b) would maximise the biomass production, giving a more viscous rheologically complex broth to be used for the mixing experiments (power, k_La, hold-up). However, due to the differing impeller speeds required to match the total energy inputs throughout the fermentation, the morphological (and hence rheological) profiles of the broths may differ. Consequently, differences in reactor performance may not be unequivocally due to system geometry.

9.3.2.2 Growth/biomass curves

Matching the final biomass concentrations and therefore omitting an initial unexplainable lag phase (10 hours) for the second IDDIDT fermentation, showed that the fermentation times (from the beginning of exponential phase to the stationary phase) were approximately equal (about 30 hours) for all three fermentations giving an average exponential growth rate of

0.039 h^{-1} (Figure 9.3-1), despite no temperature control in Fermentation I. The rheological characteristics of the broths were similar with the consistency index, *K*, reaching 0.25-1.0 and the flow behaviour index, *n*, reducing to approximately 0.22 (Figure 9.3-2).

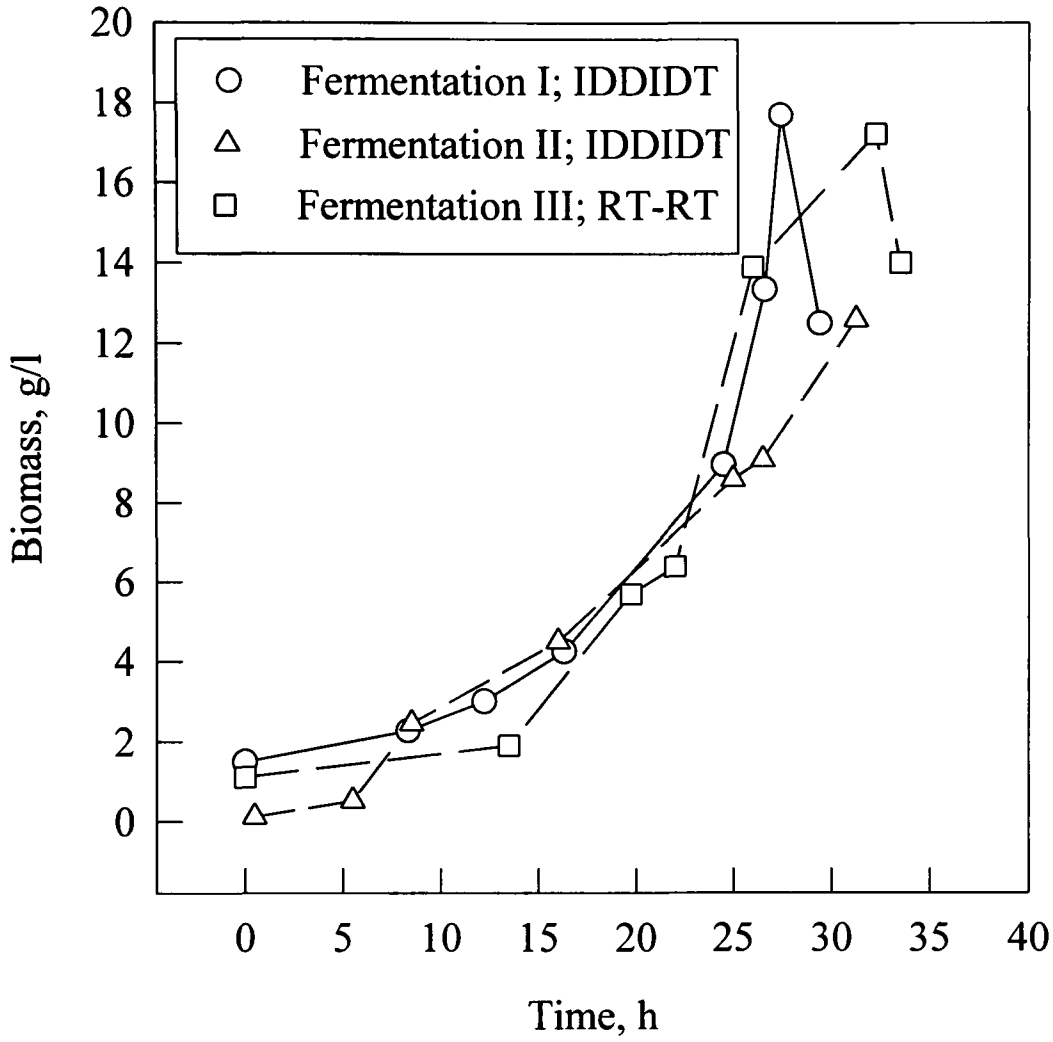

Figure 9.3-1 Biomass as a function of time for Fermentations I (IDDIDT), II (IDDIDT) and III (RT-RT)

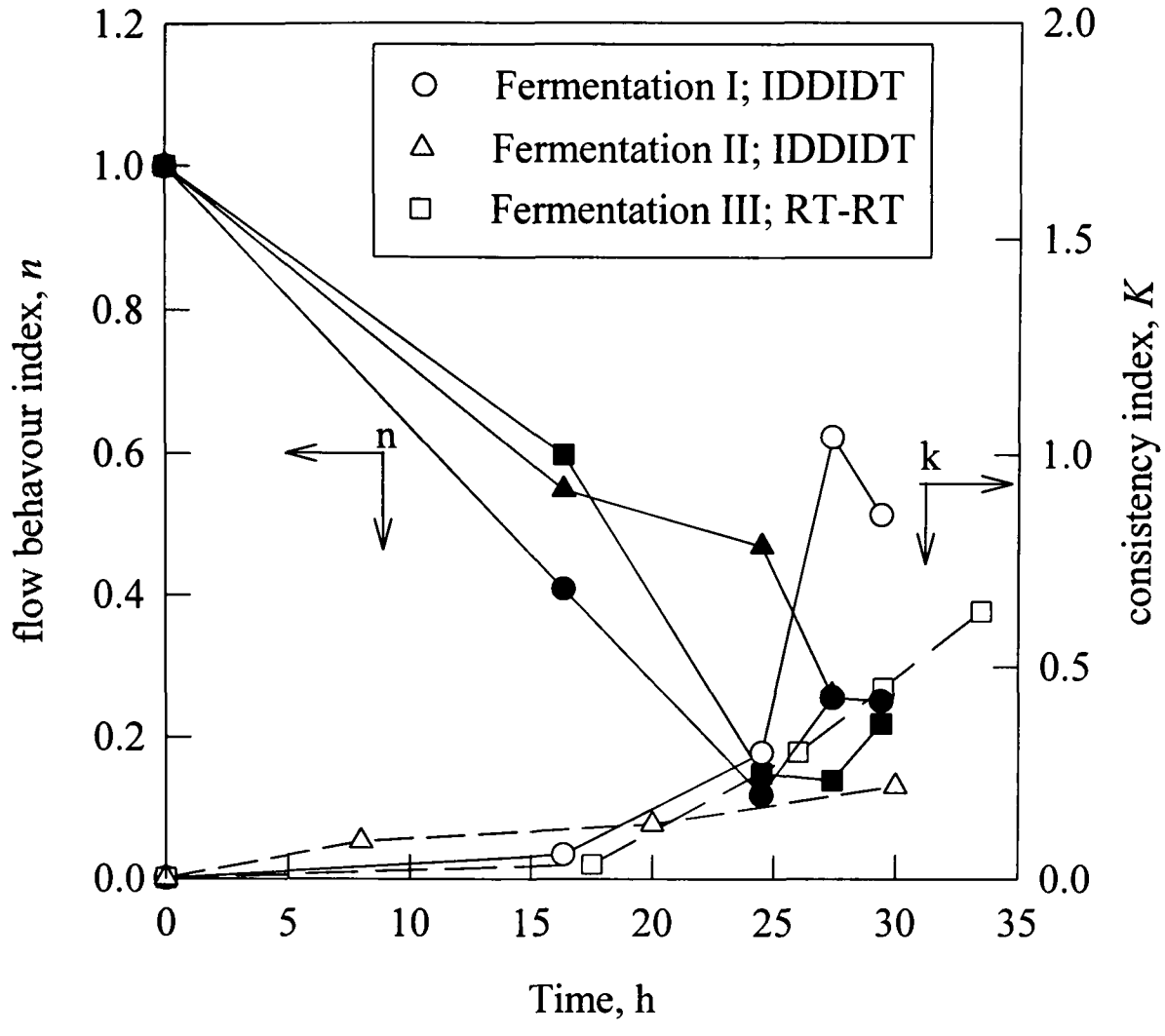

Figure 9.3-2 Rheological properties of *A. niger* fermentations

Overall approximately 16 % more power was required to provide similar dissolved oxygen concentrations (Figure 9.3-3) and mass transfer coefficients (Figure 9.3-4) for the RT-RT (22.2 kWh) compared to the IDDIDT (19.5 kWh). It was only in the latter stages of fermentation III (last 5 hours) that provision of adequate dissolved oxygen became problematic. Fermentation II did not reach such a high level of viscosity, thus making a direct comparison in terms of energy consumption difficult. Consequently, the advantages of the improved blending and mass transfer, previously noted for the IDDIDT, were not apparent. Similarly, Clark and Lentz[20] observed that the possibility of increased mass transfer due to increases in aeration rate and impeller speed did not improve citric acid production in *A.niger* fermentations. A longer fermentation time, a more viscous fermentation broth or an organism more sensitive to oxygen fluctuations could further highlight the advantages of the IDDIDT. Mass transfer experiments in these fermentation broths gave similar $k_L a$ values, at similar gas flow rates and power inputs, for the IDDIDT and RT-RT configurations (Figure 6.4-11 and

Figure 9.3-4). Therefore, if the liquid circulation around each impeller in the RT-RT system was high enough to ensure that oxygen starvation was avoided, a similar performance to the IDDIDT configuration was not unexpected. It may be noted that the reduced blending efficiency for the RT-RT system was due to the reduced fluid exchange between the upper and lower compartments (top to bottom mixing), and since oxygen transfer is dependent upon the circulation of a micro-organism into any well mixed region (either top or bottom RT) then the consequences of the reduced blending efficiency may not be a problem. However, in many industrial fermentations good top-to-bottom mixing is important for pH control or for the supply of nutrients in fed-batch/continuous fermentations. In these cases the IDDIDT would offer a distinct advantage.

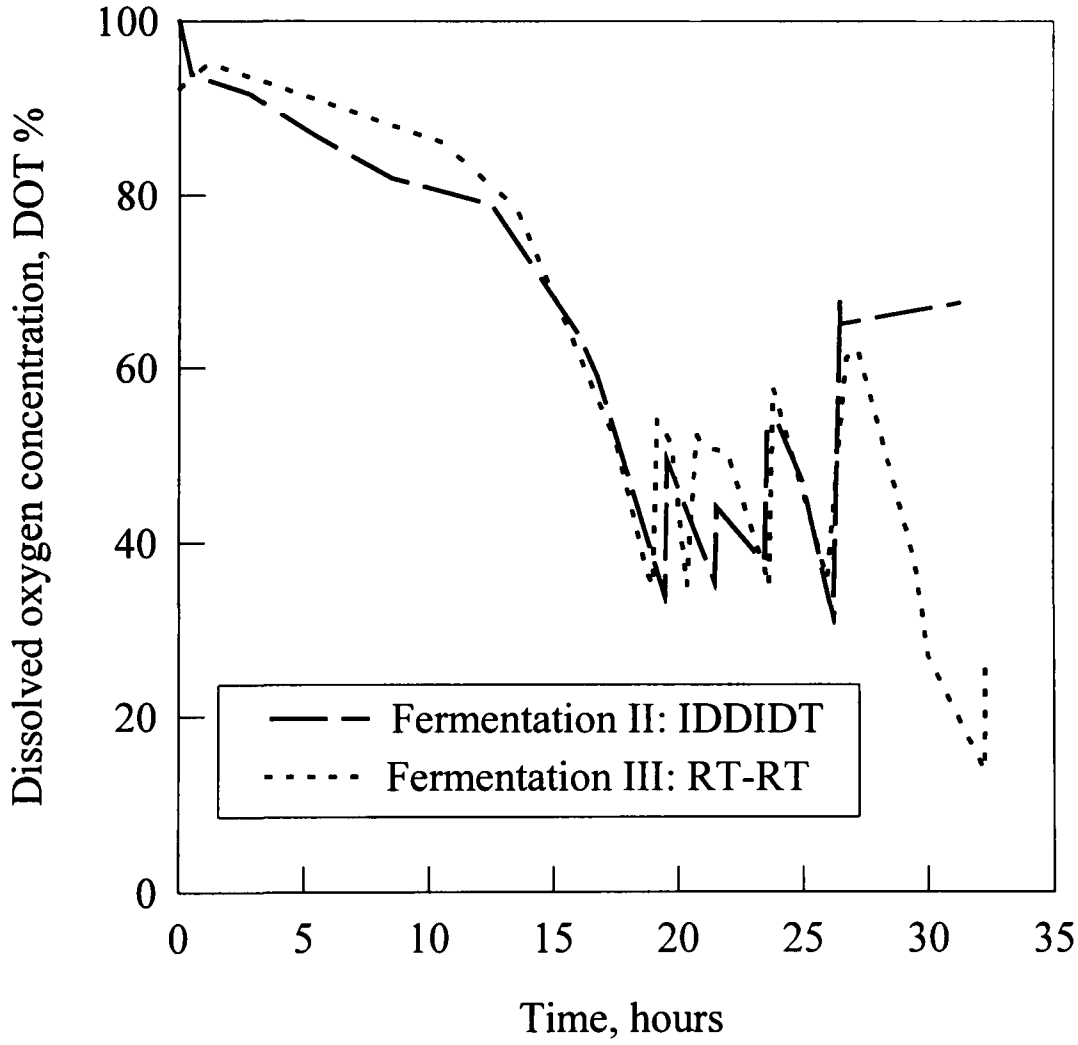

Figure 9.3-3 DOT profile for fermentations II and III

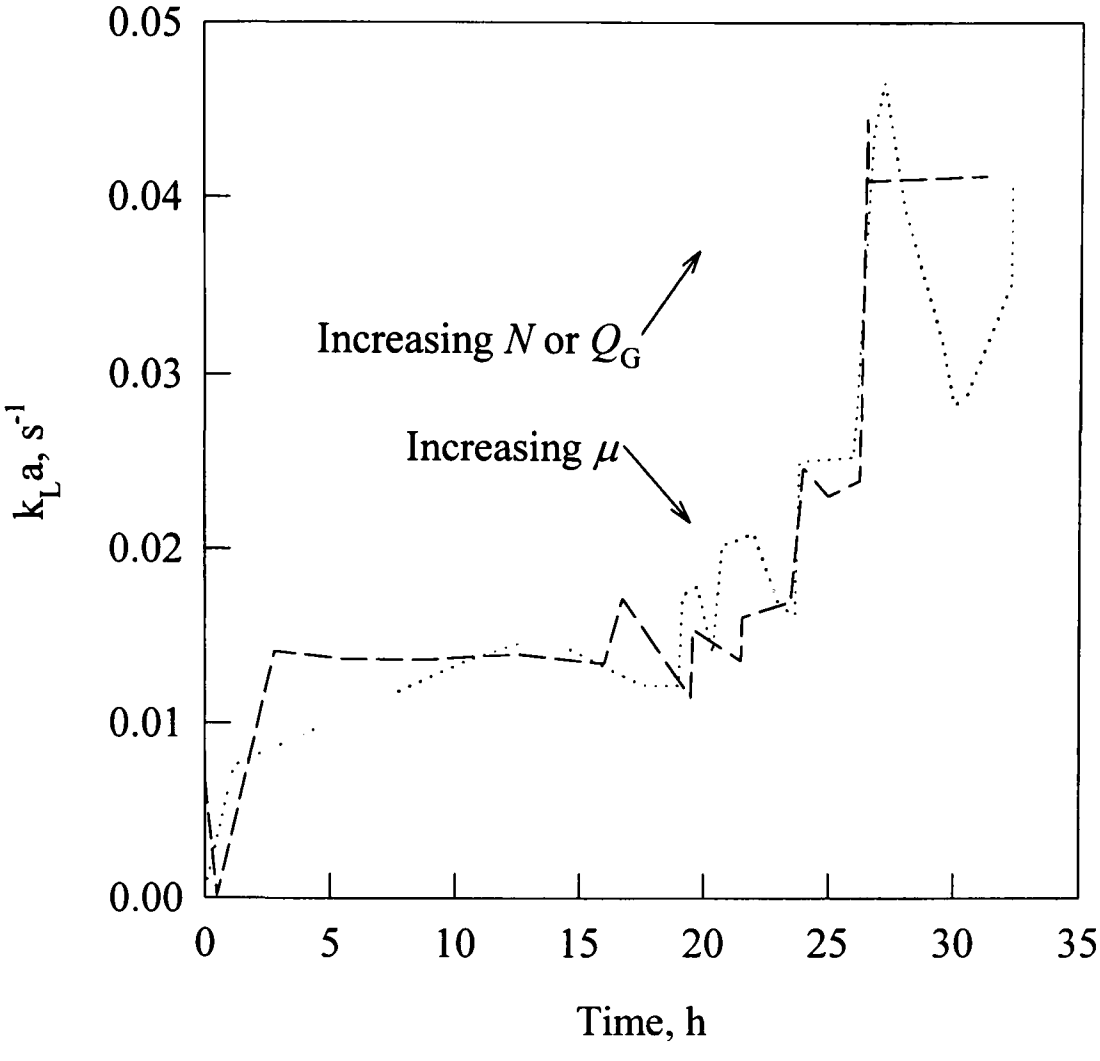

Figure 9.3-4 Mass transfer profile for fermentations II and III

9.3.2.3 Morphology

The morphological parameters mean projected area (85-98 % of broth) and hyphal length (2-15% of broth) were followed with fermentation time. Changes in impeller speed, for mixing experiments or to increase the DOT, had a dramatic effect on both parameters. Recently, Jüsten[9,21] has related the fragmentation of *Penicillium chrysogenum* to the "energy dissipation/circulation function":

$$\frac{P}{kD^3 t_c} \tag{9.1}$$

where k is an impeller geometric factor equal to

$$\left(\frac{\pi}{4}\right)\left(\frac{W}{D}\right) \tag{9.2}$$

with *W/D* being the blade height/diameter ratio for radial impellers and projected blade height/impeller ratio for axial impellers. The author reported, for off-line experiments, both mean projected area and mean hyphae length correlated well with this function at scales from 1.4 to 180 l. Although mean projected area could be correlated with the "energy dissipation/circulation function" (DCF) for constant impeller speed fed-batch processes, no data was presented for morphological changes due to step changes in impeller speed during a fermentation.

The *A.niger* broths consisted largely of clumps (~98%) with only a small fraction of the biomass being freely dispersed (~2%). It was evident that an increase in either 3SHP1 speed or 6RT speed, and hence the DCF, dramatically reduced the clump mean projected area (Figure 9.3-5 and Figure 9.3-6), *e.g.* a ~150% increase in DCF (from 48-140 $kW/m^3/s$) gave a 60% reduction in mean projected area (Fermentation I) and a ~160 % increase in DCF reduced clump size by 85% (Fermentation II). Similarly, 35 minutes of mixing experimentation (DCF up to 140 $kW/m^3/s$) reduced the area by 50% (Fermentation I (M(i))) and 75 minutes of experimentation lowered the size by 66% in Fermentation II (M(i)). As previously reported [9,22] erosion of the outer surface was the probable cause of the reduction. The fraction (by mean projected area) of clumps fell, to circa 86%, following any increases in impeller speeds due to the release of the free mycelia into the medium. However, on returning to the initial agitation conditions clump size and percentage clumps increased rapidly presumably due to a combination of growth and agglomeration effects (see below).

Growth effects:

Assuming area to be directly proportional to the biomass

$$\frac{A_i}{A_o} = \left(\frac{X_i}{X_o}\right) \qquad (9.4)$$

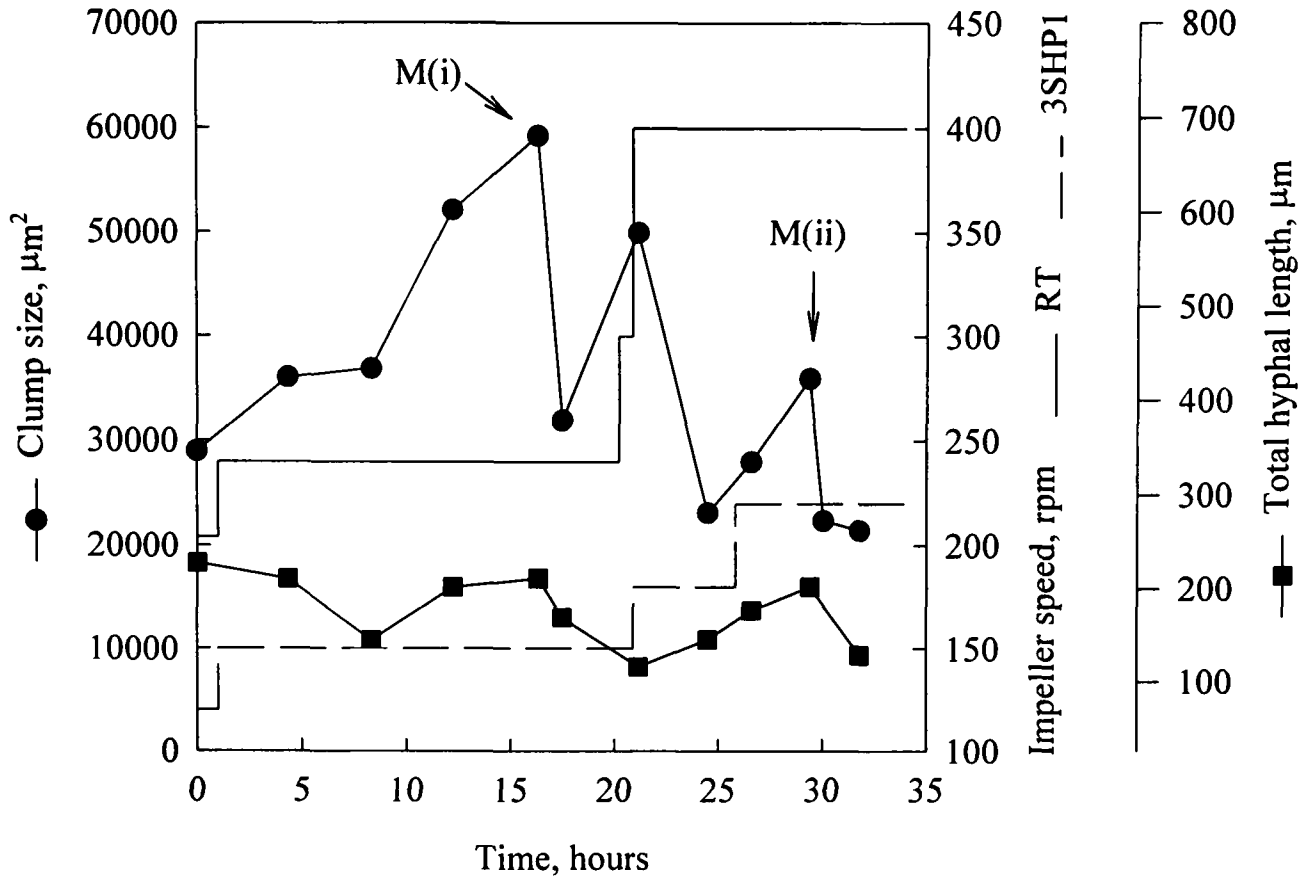

Figure 9.3-5 Morphology profile for fermentation I

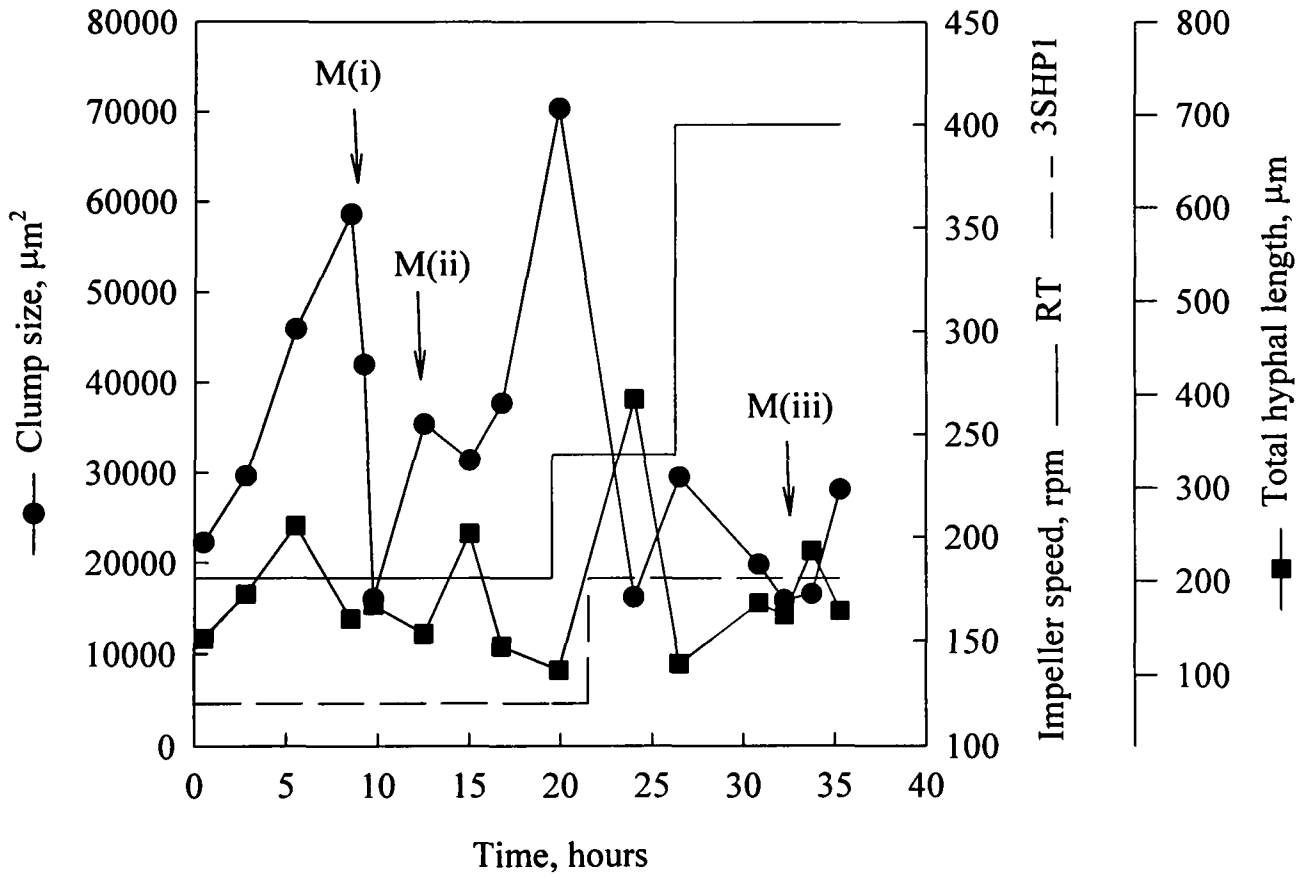

Figure 9.3-6 Morphology profile for fermentation II

M(i), M(ii) and M(iii) represent a series of mixing experiments (hold-up, power draw, $k_L a$)

where A_i is the mean projected area at $t=i$ and X_i is the biomass concentration at $t=i$. Taking examples:

- Fermentation I: Conditions immediately following M(i):

t_o = 17.5 h, X_O = 3.2 g/l, A_O = 20000 μm^2.

After four hours: t=21.6 h, X_t = 6.4 g/l. Using equation (9.4) the new clump area due to growth, A_t, was calculated to be 40000 μm^2. However, the experimentally determined value was 50000 μm^2 (~20% greater), *i.e.* growth could only account for a 20000 μm^2 increase in area compared to the 30000 μm^2 change encountered.

- Fermentation II, immediately following M(ii):

t_O = 15 h, X_O = 4 g/l, A_O = 30000 μm^2.

After five hours: t=20 h, X_t = 6.1 g/l. Using equation (9.4) the new area due to growth, A_t, was calculated to be 45700 μm^2, whereas the measured value was 70000 μm^2 (65 % larger). This suggests the existence of a secondary mechanism, agglomeration, which is further highlighted when examining the freely dispersed mycelia.

Freely dispersed mycelia

The effect of agitation rate on total length of unbranched (UH), branched (BH) and loops (LH) was difficult to determine due to a complex interaction between the clumps and the dispersed hyphae. In addition, the continual switching of hyphae between the groups, and the low fraction of freely dispersed hyphae, led to difficulties in the measurement. In contrast to previous studies[9], the total hyphal length (UH+BH+LH) did not unequivocally decrease when exposed to an increase in the DCF. In fact, throughout the majority of fermentation II the mean total length exhibited an inverse functionality to the clump area, *i.e.* increases in total length coincided with reductions in clump area and vice versa. This was most likely due to the

increased impeller speed promoting clump fragmentation producing freely dispersed hyphae with an average total length greater than that measured in the previous sample. The reduction in mean total length, which coincided with the increased projected area, reinforces the theory that agglomeration effects, as well as growth, was influencing the clump size. In addition, the fraction of clumps in the broth increased, when returning to lower impeller speeds, suggesting that aggregation of freely dispersed hyphae had resulted in the formation of larger clumps (Figure 9.3-7). A more in-depth investigation is necessary (and is on-going within the research program of the centre) to completely understand the mechanisms behind the morphological changes outlined here.

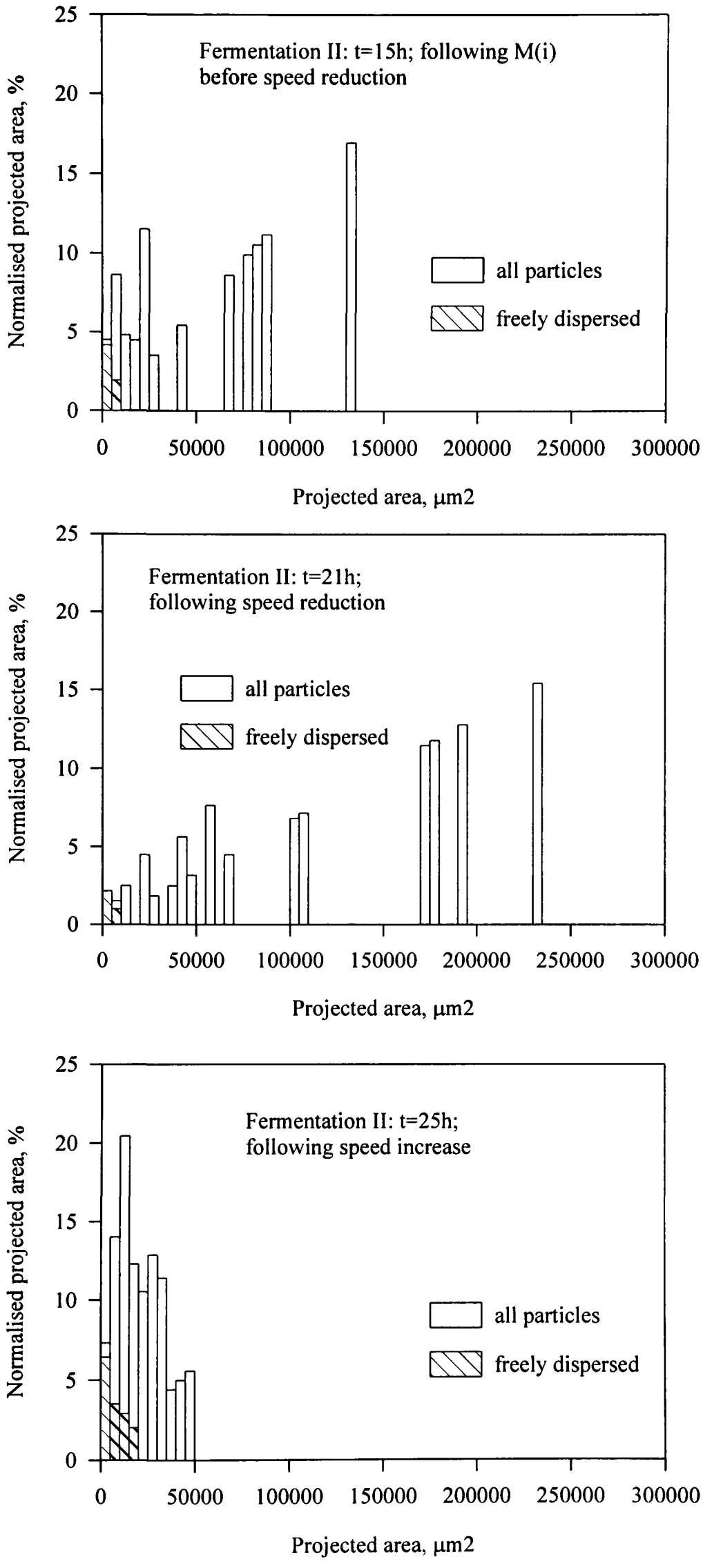

Figure 9.3-7 Projected area distributions of freely dispersed hyphae and all particles in fermentation II

9.4 Conclusions

The optimum process parameters for the production of a filamentous fermentation broth, under hygienic conditions, were obtained on the small scale; pH 2, Media I, Temperature 25°C, Initial low aeration (0.2vvm) and agitation (200rpm) conditions.

- *Aspergillus niger* was successfully grown under hygienic conditions in the 640l Perspex proto-fermenter which was operated using the IDDIDT and RT-RT configurations. 'Pulp like' non-Newtonian filamentous broths with final biomass concentrations of ~15g/l were achieved for each set-up. These broths were used for standard mixing experiments, *e.g.* Power draw, Hold-up, k_La, and used to draw a comparison between real broths and model solutions (Chapter 4 - Chapter 8).

- The mass transfer coefficients, k_La, throughout the fermentations were found to be a function of air flow rate and overall power input into the system irrespective of geometry. In addition, the productivity (g/l/kWh) was similar for both configurations.

- Increasing impeller speeds throughout the fermentation, as well as during short term mixing experiments, resulted in a profound change in the morphological characteristics of the broth due to the fragmentation at the high speeds of the mixing studies followed by rapid agglomeration on return to the lower speeds required for further biomass production.

- Although it was feasable to undertake hygienic fermentations within the proto-fermenter it is questionable whether the extra expense and manpower was justified. Matching the rheological characteristics of fermentation broths by using model solutions, such as CMC, provided similar power and hydrodynamic characterisitics without the neccesity for costly fermentations. In addition, obtaining fermentation broths with reproducable rheological and morphological characteristics is very difficult as many of the operating parameters are

inter-dependent, *e.g.* impeller speed/type, dO_2, growth rate, morphology, rheology. When comparing different systems, this makes drawing definate conclusions extremly difficult.

9.5 References

1. Whitaker, L. and Long, P.A., 1973, "Fungal Pelleting", *Process.Biochem.*, Nov:27-31

2. Clark, D.S., 1962, " Submerged citric acid fermentation of ferrocyanide treated beet molasses: morphology of pellets of *Aspergillus niger*", *Can.J.Microbiol.*, 8: 133-136

3. Steel R., Martin, S.M. and Lentz, C.P., 1954, "A standard inoculum for citric acid production in submerged culture", *Can.J.Microbiol.*, 1: 150-157

4. Roehr, M, Zehentgruber, O. and Christian, P., 1981, "Kinetics of biomass formation and citric acid production by *Aspergillus niger* on pilot plant scale", *Biotech.BioEng.*, 23: 2433-2445

5. Ammanullah, A, 1994, "Scale down models of mixing performance in large scale bioreactors", *Ph.D Thesis*, University of Birmingham, UK

6. Adams, H.L. and Thomas, C.R., 1988, "The use of image analysis for morphological measurements on filamentous micro-organisms", *Biotech.Bioeng.*, 32:707-712

7. Tucker, K.G., Kelly, T., Delgrazia, P. and Thomas, C.R., 1992, "Fully-automatic measurement of mycelial morphology by image analysis", *Biotech.Prog.*, 8: 353-359

8. Cox, P.W. and Thomas, C.R., 1992, "Classification and measurement of fungal pellets by automated image analysis", *Biotech.Bioeng.*, 39: 945-952

9. Jüsten, P., 1997, "Dependence of *Penicillium Chrysogenum* growth, morphology, vacuolation and productivity on impeller type and agitation intensity", *Ph.D. Thesis*, University of Birmingham, UK.

10. Olsvik, E., Tucker, K.G., Thomas, C.R. and Kristiansen, B., 1993, "Correlation of *Aspergillus niger* broth rheological properties with biomass concentration and the shape of mycelial aggregates", *Biotech.BioEng.*, 42: 1046-1052

11. Paul, G.C. and Thomas, C.R., "Characterisation of mycelial morphology using image analysis", In: K. Schügerl (Ed.), *Relation between Morphology and Process Performance., Adv. in Biochemical Engineering/Biotechnology* : (in press)

12. Foster, J,W., 1979, "Chemical activities of fungi", (Ed. F.W. Foster), Academic Press, New York

13. Trager M., Qazi, G.N., Buse, R. and Onken, U., 1992, "Influence of constant and oscillating dissolved oxygen concentration on *Aspergillus niger*", *J.Ferm.Bioeng.*, 74, No. 5: 282-287

14. Bailey, J.E. and Ollis, D.F., 1986, "Biochemical Engineering Fundamentals", 2nd Ed. (Eds. McGraw Hill)

15. van Suijdam, J.C., Kossen, N.W.F. and Paul, P.G., 1980, "An inoculum technique for the production of fungal pellets", *Euro.J.Appl.Microbiol.*, 10: 211-221

16. Seviour, R.J. and Read, M.A., 1985, "Electrophoretic mobility of Conidia of *Aspergillus niger*, and the role of their surface properties in pelleting", *Trans.Br.Mycol.Soc.*, 84: 745-747

17. Mitard, A. and Riba, J.P., 1988, "Morphology and growth of Aspergillus niger ATC 26036 cultivated at several shear rates", *Biotech.Bioeng.*, 32: 835-840

18. Priede, M., Personal communication

19. Galbraith, J. C. and Smith, J.E., 1969, "Filamentous growth of *Aspergillus* niger in submerged shake culture", *Trans.Brit.Mycol.Soc.*, 52 (2): 237-246

20. Clark, D.S. and Lentz, C.P., 1963, "Submerged citric acid fermentation of beet molasses in tank-type fermenters", *Biotech.Bioeng.*, 5: 193-199

21. Jüsten, P., Paul, G.C., Nienow, A.W. and Thomas, C.R., 1996, "Dependence of mycelial morphology on impeller type and agitation intensity", *Biotech.Bioeng.*, 52: 672-684

22. Taguchi, H., Yoshida, T., Tomita, Y. and Teramoto, J., 1968, "The effects of agitation on disruption of the mycelial pellets in stirred fermentors", *J.Ferm.Technol.*, 46: 814

CHAPTER 10

CONCLUSIONS AND RECOMMENDATIONS

10.1 Conclusions

A novel reactor used to improve gas-liquid processing has been examined. Hold-up, mixing times, circulation times and $k_L a$ have been investigated and correlated with total power input to the system. In addition to using test fluids such as water and CMC, it was possible to undertake hygienic *Aspergillus niger* fermentations within the vessel. The resultant broth was used for hold-up, power draw and $k_L a$ measurements in live cultures. The following conclusions can be drawn:

- The incorporation of the draft tube and a lower Rushton turbine eliminated the potential problems associated with instabilities in the bulk flow patterns previously reported for single hydrofoils and mixed flow systems.

- The minimum 6RT impeller speed required to prevent flooding could be calculated from

$$(Fl_G)_F = 30\left(\frac{D}{T}\right)^{3.5}(Fr)_F$$

provided the 3SHP1 was operational. At high 3SHP1 speeds the loading regime was narrowed. The single 6RT tended to flood more easily due to a disruption in the radial flow pattern by the draft tube and the above equation no longer holds.

- At low gas flow rates, hold-up results suggested an increased specific area, a, and hence improved mass transfer performance for IDDIDT compared to the configurations without a draft tube. The improvement was most marked with the 3SHP1 operational. However, at

0.5 vvm the performance was similar irrespective of geometry or impeller type. Hold-up was correlated by the empirical equation

$$\varepsilon_G = 17.9\left(\frac{P}{V}\right)^{0.30}(u_s)^{0.70}$$

for water.

Increasing the viscosity tended to reduce hold-up due to the greater amount of large bubbles present. However, hold-up values in fermentation broths were greater than those in CMC solutions due to the presence of salts which inhibited coalescence. For CMC solutions the hold-up could be predicted by

$$\varepsilon_G = 20.7\left(\frac{P}{V}\right)^{0.20}(u_s)^{0.35}(\mu_a)^{-0.39}$$

however only a medium ($0.26<r^2<0.64$, Appendix III) correlation could be found for the fermentation broths.

- Using the IDDIDT, for both water and fermentation broths, the mass transfer coefficient was found to be a function of total agitation power input and air flow rate, although independent of which impeller inputs the power. At the low gas flow rates, k_La's were higher using the IDDIDT compared to the dual Rushton system as was suggested by the increased hold-up values for the same operating conditions. Similarly, mass transer rates at 0.5 vvm were approximately equal for all configurations. Although hold-up values for *A. niger* broths were similar to those encountered using water, the equivilant k_La's were markedly lower. This discrepancy emphasises the care which must be taken when using hold-up values as an approximation of the gas-liquid mass transfer performance in fermentation broths.

The mass transfer coefficients for the IDDIDT could be calculated by

$$k_L a = 0.00029\left(\frac{P}{V}\right)^{0.70}(u_s)^{0.40}(\mu_a)^{-0.36}$$

for water and *Aspergillus niger* fermentation broths.

- Mixing times were studied by decolorisation and conductivity techniques. For each set of operating conditions similar results were obtained using both methods. Overall, rapid mixing times, up to a magnitude faster than were predicted using the correlations of previous workers, were observed. In addition, mixing times for the IDDIDT were circa 50 to 85 % lower, on an equal power basis, than experimentally determined values when using a dual Rushton turbine configuration. The increase in blending performance was directly controllable by the speed of the 3SHP1 impeller. In fact, in viscous solutions very little blending occured unless the 3SHP1 was operational. The unaerated mixing times could be accurately predicted from

$$\theta_m = 5.6\left(\frac{P_{SC}}{V}\right)^{-0.25}\left(\frac{P_{RT}}{V}\right)^{-0.08}$$

Under aerated conditions, the importance of the 6RT became evident as mixing times tended to increase dramatically if the impeller was flooded. However, at the highest speeds aerated and unaerated times were similar and less than standard dual impeller configurations.

- The mechanisms of the mixing process were quantitatively assessed by circulation time distribution data obtained using a magnetic pill technique. The provision of a well defined flow pattern was responsible for the low mixing times found with the IDDIDT. The bulk circulation time was related to the mixing time by:

$$\theta_m = A\,\bar{t}_{bc}$$

where A = 1.4 or 1.7 for Probe 1 and 2 respectively.

The configuration gives controllability of local energy inputs, increasing the flexibility of the system. Thus the 6RT can be used for gas dispersion and the 3SHP1 impeller speed can be altered to meet the process mixing requirements. Mass transfer rates can be controlled by either impeller since k_La's are independent of which impeller type inputs the majority of the power.

10.2 Recommendations for future work

10.2.1 Improving correlations

Empirical correlations for estimating bulk blending, gassed hold-up and mass transfer were formed from experiments conducted at one scale of operation using a limited range of gas flow rates. Experiments at different scales would highlight any scale effects and enable more reliable correlations to be constructed. In addition, investigation of the gas-liquid hydrodynamics at higher gas flow rates (>1 vvm) is necessary to establish the stability of hydrofoil in conditions that are likely to be encountered in industry.

Gassed power (P_g/V) is a satisfactory parameter for comparative purposes, however, as a design tool it is limited because of the interaction between the gas rate and the two-phase hydrodynamics around the impeller. Additionally, the work presented in this thesis assumes that the fermenter is uniformly mixed, and that oxygen concentrations and hold-up values are constant throughout the tank. A more clear understanding of energy dissipation rates, bubble size distributions, local hold-up values and local mass transfer values would enable multi-compartment modelling of the process which could be used for optimising operating conditions. Developments in computer hardware and software have led to the improvement

of computational fluid dynamic (CFD) simulations that can aid the design of these fluid flow systems. However, experimental methods are still required to specify the boundary conditions and to verify the models produced.

10.2.2 Geometry

The separation of the agitator functions (gas dispersion and bulk blending) was considered to be the major advantage of the IDDIDT configuration. Inclusion of the draft tube coupled with a large diameter hydrofoil significantly improved the blending performance, provided the lower impeller (6RT) was not flooded. Since blending efficiency was not affected by the 6RT and mass transfer was independent of impeller type then a significant improvement in the design could be achieved by improving the method of gas dispersion. Incorporation of a curved blade disc turbine (such as the SCABA 6SRGT), which can handle up to three times as much gas as an RT, would significantly reduce the energy requirements of gas dispersion and improve the efficiency of the reactor. Alternatively, removal of the lower agitator with gas dispersion into the annulus would eliminate costs associated with a bottom driven impeller and still ensure the stable operation of the hydrofoil. However, changes in the bubble size distribution would probably lead to losses in mass transfer, for given gas flow rates, and an economic evaluation would be necessary.

10.2.3 Fermentations

Pilot scale fermentation work (640 l) showed that care must be taken when using model solutions to describe hold-up or mass transfer characteristics. Here, it is important to match coalescence characteristics, in addition to the rheological parameters, if reliable representations are to be made. Power draw and flow patterns were well mimicked by the model solutions. Therefore, the extra work and cost required to produce a reproducible fermentation broth to be used for mixing studies could be considered excessive.

Assessing the overall fermenter performance requires a re-assesment of the experimental design. Interactions between impeller speed/type, dO_2, growth rate, nutrient/O_2/pH gradients, biomass concentration, morphology and rheology make drawing conclusions difficult. Investigating the influence of each parameter independently would greatly increase the value of the results. However, on such a large scale such an approach would be time consuming and expensive. Alternativley, the large scale fermentations could be simulated by scale-down equipment (Section 10.2.3.1).

10.2.3.1 Scale down

Expanding the quantity of circulation time data, to include a wider variety of conditions, and using the results to create a mathematical model to describe the flow behaviour in the vessel would provide a valuable basis for scale-down work. The scale down experiments could be used to compare the fermentation performance of the IDDIDT with more common configurations without the necessity for expensive large-scale fermentations. In addition, separation of the parameters is possible, enabling the effects of each, on biological performance, to be found.

10.2.3.2 Morphology

Agitation intensity was shown to have a profound influence on the morphology of *Aspergillus niger* due to the fragmentation, at high speeds, followed by rapid agglomeration, on return to the lower speeds. Fragmentation of the clumps by continual erosion has been previously reported, however the mechanisms behind the rapid agglomeration are still unknown. Agglomeration was not found in off-line experiments (previous unpublished work undertaken at the biocentre), suggesting that extracellular compounds (polysaccharides, proteins), which are excreted in the growth phase, may be influencing the mechanism. Further work is

required to determine the nature of the agglomeration and also investigate its influence on productivity (enzyme, carboxylic acid).

APPENDIX I

NOMENCLATURE

A	Contact area between gas and liquid phase	m^2
A	Constant in equation (8.17)	
a	Specific interfacial area	m^{-1}
C	Impeller clearance from vessel bottom	m
C'	Constant in equation (6.10)	-
CF	Calibration factor	-
CPR	Carbon dioxide production rate	mmol L^{-1} h^{-1}
C_L	Concentration of oxygen in the bulk liquid	mg L^{-1}
C_s	Substrate concentration	mg L^{-1}
C_i	Concentration of oxygen at the gas-liquid interface	mg L^{-1}
C_L^*	Liquid phase concentration of oxygen in equilibrium with the gas phase	mg L^{-1}
D	Impeller diameter	m
DOT	Dissolved oxygen tension	%
D_{DT}	Draft tube diameter	m
D_{SP}	Sparger diameter	m
d_B	Sauter mean bubble diameter	m
d_p	Distance between conductivity probes	m
H	Liquid height	m
H'	Henrys law constant	-
$[H_2O_2]$	Hydrogen peroxide concentration	mol m^{-3}
K	Consistency index	Pa s^n
k	Proportionality constant in equation (5.3)	-
k	Geometrical factor per impeller	-
k_C	Casson viscosity	-
k_G	Gas phase oxygen transfer coefficient	m s^{-1}

k_L	Liquid film oxygen transfer coefficient	$m\ s^{-1}$
k_La	Volumetric oxygen transfer coefficient	s^{-1}
k_s	Metzner-Otto shear rate constant	-
F	F statistic	-
Fl_g	Gas flow number	-
Fr	Froude number	-
g	Gravitational acceleration	$m\ s^{-2}$
M	Torque	N m
N	Impeller speed	s^{-1}
N_A	Mass flux	$mol\ s^{-1}\ m^{-3}$
N_C	Critical speed to avoid instabilities	s^{-1}
n	Flow behaviour index	-
n_t	Number of circulations	-
OTR	Oxygen transfer rate	$mg\ L^{-1}\ h^{-1}$
OUR	Oxygen uptake rate	$mmol\ L^{-1}\ h^{-1}$
P	Power input	W
Po	Power number	-
p_g	Gas phase oxygen partial pressure	atm
p_i	Interfacial oxygen partial pressure	atm
Re	Reynolds number	-
RQ	Respiratory Quotient (moles CO_2 formed/moles O_2 consumed)	-
r	Mass transfer rate	$mol\ s^{-1}$
r^2	Correlation coefficient	-
r_{smax}	Maximum substrate consumption rate	$mg\ L^{-1}\ s^{-1}$
rpm	Revs/minute	min^{-1}
T	Vessel diameter	m
T	Temperature	°K
t	Time	s
$\bar{t}$	Mean circulation time	s
$\bar{t}_{bc}$	Mean circulation time - bulk recirculation	s
$\bar{t}_l$	Mean circulation time - lower aerial	s
$\bar{t}_u$	Mean circulation time - upper aerial	s

Q_G	Gas flow rate	$m^3 s^{-1}$
u_s	Superficial gas velocity	$m s^{-1}$
vvm	Volume of gas/minute/volume of vessel contents	m^{-1}
V	Liquid volume	m^3
V	Voltage	V
W	Impeller blade width	m
w	Water vapour pressure	atm
X	Biomass concentration	$g L^{-1}$
x_l	Disc thickness	m

Greek

α	Constant in equations (5.3),(6.10)	-
β	Constant in equations (5.3),(6.10)	-
δ	Constant in equations (5.3),(6.10)	-
ΔC_{LMCD}	Log mean concentration difference	$mg L^{-1}$
ε_G	Gassed hold-up	%
ε_T	Specific energy input	$W kg^{-1}$
$\dot{\gamma}$	Shear rate	s^{-1}
$\dot{\gamma}_{AV}$	Average shear rate	s^{-1}
η	Coefficient of rigidity	-
θ_m	Mixing time	s
θ_R	Initial response time	s
σ	Standard deviation	-
ρ	Density	$kg m^{-3}$
τ	Shear stress	$N m^{-2}$
τ_o	Yield stress	$N m^{-2}$
μ	Specific growth rate	h^{-1}
μ	Dynamic viscosity	$N s m^{-2}$
μ_a	Apparent viscosity	$N s m^{-2}$

Subscripts

AV	Average
CD	Complely dispersion
F	flooding
DT	draft tube
g	under gassed conditions
gas	gas (air)
RT	Rushton turbine
SP	Sparger
SC	Scaba 3SHP1
T	Total

Abbreviations

A315	Lightin' A315 hydrofoil
CBRT	Curved blade disc turbine
CMC	Carboxy-methyl-cellulose
CTD	Circulation time distribution
DPM	Down pumping mixed flow impeller
DT	Draft tube
IDDIDT	Independently-driven dual impellers with draft tube
IDDINT	Independently-driven dual impellers with no draft tube
PBT	Pitched blade turbine
PMT	Prochem Maxflo T
RT	Rushton turbine
UPM	Upward pumping mixed flow impeller
3SHP1	Scaba 3SHP1 impeller

APPENDIX II

CALIBRATION OF RHEOMETER

The calibration of the Rushton turbine rheometer has been previously described[1,2] and was recently employed by Schmitz[3] for the calibration of the rheometer used in this work. In the laminar region, the average shear stress is related to torque, M, and impeller diameter, D, by [1,2,3]

$$\tau_{AV} = \frac{2\pi M k_s}{CD^3} \qquad \text{(AII.1)}$$

where C is the shape factor and k_s is the proportionality factor. k_s is geometry dependent and is related to the average shear rate and impeller speed by[4]

$$\dot{\gamma} = k_s N \qquad \text{(AII.2)}$$

For the Rushton turbine rheometer, the constants C and k_s were determined from the calibration outlined below.

AII.1 Determination of C

The torque readings, over the upper speed range, were measured in Brookfield silicon oil 1000 and 12500 at 23 ±0.3°C.

Since

$$Po = \frac{C}{\mathrm{Re}} \qquad \text{(AII.3)}$$

in the laminar regime, a log-log plot of *Po* versus *Re* will give a gradient of -1 and an intercept equal to *C*. Using the reported viscosities of 0.943 Pas and 12.25 Pas, for the Brookfield silicon oil 1000 and 12500 respectively, *C* was found to be 79.4.

AII.2 Determination of k_s

As previously explained (Chapter 3) the apparent viscosity for non-Newtonian fluids is defined as

$$\mu_a = \frac{\tau}{\dot{\gamma}} \tag{3.2}$$

Substituting for *Re* and *Po* in equation (AII.3) and re-arranging gives

$$\mu_a = \frac{P}{CN^2D^5} \tag{AII.4}$$

Since

$$\mu_a = K(k_s N)^{n-1} \tag{3.10}$$

then

$$P = CD^3 K k_s N^{n+1} \tag{AII.5}$$

For non-Newtonian fluids Carbopol 934 and Carbopol 940, at various concentrations and pHs, the values of *K* and *n* were calculated from measurements made with the concentric cylinder apparatus, *i.e.* a *log-log* plot of shear stress versus shear rate gave an intercept *log K* and gradient *n*. The power, *P*, was calculated directly from the torque readings and the constant *C* was already known. Therefore, plotting *log P* versus *log N* gave a slope of *n+1* and an intercept CD^3Kk_s from which k_s was calculated (TableAII-1).

Average values of 79.4 and 12.48 for C and k_s respectively are in good agreement with previous values obtained by Tucker (80.9±5.5 and 12.5±1.0).

Table AII-1 Consistency index, K, flow behaviour index, n, and k_s for non-Newtonian fluids

Carbopol Grade	Concentration w/w%	pH	K	n	Intercept	k_s
940	0.17	4.4	11.22	0.23	0.015	12.90
940	0.30	4.4	50.12	0.31	0.073	12.43
934	0.30	5.2	9.55	0.27	0.019	13.20
934	0.30	6.0	16.58	0.17	0.034	11.36

AII.3 References

1. Roels, J.A., van der Berg, J. and Voncken, 1974, "The rheology of mycelial broths", *Biotech. Bioeng.*, 16: 181-208
2. Bongenaar, J.J.T.M., Kossen, N.W.F., Metz, B., and Meijboom, F.W., 1973, "A method for characterising the rheological properties of viscous fermentation broths", *Biotech. Bioeng.*, 15: 201-206
3. Schmit, R., 1996, "Circulation time studies in Newtonian and non-Newtonian fluids in stirred tanks", *Ph.D. thesis*, University of Birmingham, UK
4. Metzner, A.B. and Otto, R.E., "Agitation of non-Newtonain fluids", 1957, *A.I.Chem.E.J.*, 3, No.3: 3-10

APPENDIX III

STATISTICAL ANALYSIS

AIII-1 Statistical Analysis

Throughout this work empirical correlations, such as the dependency of $k_L a$ on power input and gas flow rate, have been created using a Sigmaplot curve fitting package (Jandel Scientific Software, Erkrath, Germany) by the method of least mean squares. Here, the sum of the squares of the residuals is minimised by an iterative technique, *i.e.* the function

$$SSE = \sum (y - f)^2 \qquad \text{(AIII.1)}$$

is minimised. *SSE* is the sum of the squares of the residuals, y represents the experimental results and f is the predicted values calculated from the correlation. The goodness of the fit can be described by the regression coefficient (r) or by an F-statistic.

$$r^2 = 1 - \left[\frac{SSE}{SSM}\right] \qquad \text{(AIII.2)}$$

where *SSM* is the sum of the squares of the error about the mean and is calculated from

$$SSM = \sum \left(y - \bar{y}\right)^2 \qquad \text{(AIII.3)}$$

where $\bar{y}$ is the mean y value. The closer the value of r is to unity then the better the fit. Guidelines for the interpretation of the correlation coefficient are outlined in Table AIII-1[1].

The F-ratio, a ratio of two mean squares, provides information on the statistical significance of the correlation with respect to the experimental data and is found from

$$F = \frac{\left((SSM - SSE)/edof\right)}{\left(SSE/rdof\right)} \qquad \text{(AIII.4)}$$

where *edof* is the error degrees of freedom (number of non-zero parameters in correlation -1) and *rdof* is the regression degrees of freedom (total number of degrees of freedom-edof). The total number of degrees of freedom (*tdof*) is the total number of experimental points -1. To test the correlation at the n% level the F-ratio (F_{calc}) is compared to the tabulated $F_{n,edof,rdof}$ value. If $F_{calc} > F_{n,edof,rdof}$ then the correlation is significant. In comparing two correlations the one with the larger F-ratio will be most significant. In addition, to compare whether a statistical difference exists between the correlations an F-ratio of their respective error square means is calculated, *i.e.*

$$F_{ccorr1,corr2} = \frac{\left(SSE/rdof\right)_{corr1}}{\left(SSE/rdof\right)_{corr2}} \qquad \text{(AIII.5)}$$

and compared to the tabulated $F_{n,rdof1,rdof2}$. If $F_{corr1,corr2} > F_{n,rdof1,rdof2}$ then the correlations are significantly different at the *n*% level.

Table AIII-1 Interpretation of regression coefficients

r^2	r	**Interpretation**
0	0	no correlation
0-0.25	0-0.5	weak correlation
0.25-0.64	0.5-0.8	medium correlation
0.64-1	0.8-1	strong correlation
1	1	perfect correlation

Table AIII-2 shows the statistical analysis of the correlations formed for the prediction of hold-up and mass transfer, as discussed in Chapters 5 and 6.

Table AIII-2. Regression coefficients and F-ratios for the empirical correlations of Chapters 5 and 6

NS - no statistical difference between the correlations.

Correlation 1				Correlation 2					
Eqn.	**r^2**	**F_1**	**SSE/rdof**	**Eqn.**	**r^2**	**F_2**	**SSE/rdof**	**$F_{n,1,2}$**	**n% level**
5.4	0.98	2047	0.0588	5.9	0.96	798	0.1471	2.50	99.5
5.5	0.98	1692	0.0406	5.9	0.77	54.2	0.5273	13.00	99.5
5.7	0.99	478	0.0809	5.9	0.94	51.9	0.670	8.29	99.5
5.8	0.97	2380	0.1091	5.9	0.94	251.9	0.214	1.99	99.0
5.10	0.93	159	0.2916	5.13	0.92	96	0.3198	1.10	NS
5.11	0.95	416	0.1787	5.13	0.94	238	0.2065	1.16	NS
5.12 (1%)	0.85	60	0.9770	5.13	0.94	238	0.2111	4.63	99.5
5.12 (0.28,1%)	0.72	56	1.003	5.13	0.97	226	0.2163	4.64	99.5
5.14	0.98	305	0.0476	5.17	0.97	188.5	0.0515	1.08	NS
5.15	0.95	187.7	0.0307	5.17	0.95	110	0.0346	1.12	NS
5.16	0.67	40.4	0.502	5.17	0.98	503	0.0382	13.14	99.5
5.18	0.93	1000	0.110	5.19	0.93	1558	0.1263	1.15	NS
6.17	0.97	220.7	2.2×10^{-5}	6.20	0.61	11.9	2.7×10^{-4}	8.15	99.5
6.19	0.81	103.5	1.5×10^{-4}	6.20	0.76	75.5	1.97×10^{-4}	1.31	NS
6.17	0.97	220.7	2.2×10^{-5}	6.22	0.97	136.3	2.46×10^{-5}	1.18	NS
6.22	0.97	136.3	2.46×10^{-5}	6.24	0.74	24.1	1.86×10^{-4}	7.56	99.5
6.19	0.81	103.5	1.5×10^{-4}	6.23	0.87	107.2	1.54×10^{-4}	1.02	NS
6.23	0.87	107.2	1.54×10^{-4}	6.24	0.79	46.68	3.14×10^{-4}	2.03	97.5

The program used to create the one-way analysis of variance is set out below.

;**** Analysis of Variance (ANOVA) Table ******

;This transform takes regression or curve fit results and constructs an ANOVA table

;Required INPUT: y data, fitted y data, function parameters/coefficients

;RESULTS: sum of squares, degrees of freedom, mean squared, F-value, R-squared & R values, standard error of fit

;INPUT to be placed in (specify source columns):

```
y_col=27                          ;y data column number
fit_col=40                        ;fitted y data column number
param_col=39                      ;parameter column number
```

;ANOVA to be placed in column:

```
anova=55 ;                        ANOVA table starting column (5 columns x 10
rows)
y=col(y_col)                      ;define y values
f=col(fit_col)                    ;define fitted y values
p=col(param_col)                  ;define function parameters
n=count(y)                        ;number of y datapoints
tdof=n-1                          ;total degrees of freedom
r=count(if(p<>0,p,"--"))          ;the number of nonzero parameters
```

;***** ANOVA TABLE CALCULATION *******

```
rdof=tdof-if(r<count(p),r-2,count(p)-1) ;Regression Degrees of Freedom
edof=tdof-rdof                    ;Error Degrees of Freedom
SSE=total((y-f)^2)                Sum of Squares of Residuals
SSM=total((y-mean(y))^2)          ;Sum of Squares of Error about the Mean
SSR=SSM-SSE                       ;Sum of Squares of Error due to Regression
se=sqrt(SSE/rdof)                 ;Standard Error of Fit
f1=((SSM-SSE)/(edof))/(SSE/rdof)  ;F value
```

```
F=if(n<2,"n < 2 !",f1)
R2=(1-SSE/SSM)                    ;R squared

;****** PLACE ANOVA TABLE IN WORKSHEET *******
col(anova)={0/0,"REGRESSION","ERROR","TOTAL"}
col(anova+1)={"SUM OF SQUARES",SSR,SSE,SSM}
col(anova+2)={"DEG FREEDOM",edof,rdof,tdof}
col(anova+3)={"MEAN SQUARE",(SSR/edof),(SSE/rdof)}
col(anova+4)={"F",F}
col(anova,7)={"#POINTS","R SQUARED","R","STD ERR"}
col(anova+1,7)={n,R2,sqrt(R2),se}
```

AIII-2 References

1. Anderson, T.W. and Sclove, S.L., 1986, "The statistical analysis of data", 2nd Edition, Scientific Press, CA, USA

APPENDIX IV

MASS TRANSFER CALCULATIONS

AIV-1 Mass Transfer Calculations

The theory behind the technique and the derivation of the rate equation (Equation (6.6)) has been explained in Section 6.1.1. The following calculations are based on that theory.

The flux of oxygen from the gas phase to the bulk liquid is of particular interest in fermentation systems and is termed the oxygen transfer rate (OTR):

$$OTR = k_L a\left(C_L^* - C_L\right) \qquad \text{(AIV.1)}$$

The hydrogen peroxide decomposition technique for measuring mass transfer involved the stripping of an oxygen rich broth by the air flowing through the vessel. In this situation the oxygen was transferred from the bulk liquid into the gas phase and hence the driving force for mass transfer was reversed, therefore

$$OTR = k_L a\left(C_L - C_L^*\right) \qquad \text{(AIV.2)}$$

Assumptions:

- Ideal gas behaviour
- Well mixed liquid phase
- Volume fraction of oxygen in air is 0.2095

AIV-1.1 Calculation of oxygen transfer rate (OTR)

Mass balance

Consider a vessel ,volume V, with inlet gas flow $Q_{(i)}$ and exit gas flow rate $Q_{(o)}$

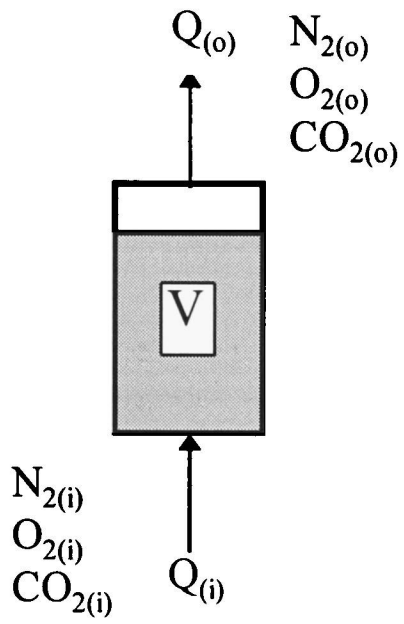

The oxygen concentration difference (OCD) is given by a mass balance over the reactor

$$OCD = \left(Q_{(i)}O_{2(i)} - Q_{(o)}O_{2(o)}\right) \qquad \text{(AIV.3)}$$

Since nitrogen is inert the exit gas flow rate can be calculated from a N_2 balance. Under steady state conditions and assuming no net accumulation

$$Q_{(o)}N_{2(o)} = Q_{(i)}N_{2(i)} \qquad \text{(AIV.4)}$$

$$Q_{(o)} = \frac{Q_{(i)}N_{2(i)}}{N_{2(o)}} \qquad \text{(AIV.5)}$$

Therefore,

$$OCD = Q_{(i)}\left(O_{2(i)} - O_{2(o)}\frac{N_{2(i)}}{N_{2(o)}}\right) \qquad \text{(AIV.6)}$$

and the Oxygen Transfer Rate in moles $O_2 m^{-3} s^{-1}$ is

$$OTR = Q_{(i)}\left(1-\left(\frac{w_{(i)}}{100}\right)\right)\left(O_{2(i)} - O_{2(o)}\frac{N_{2(i)}}{N_{2(o)}}\right)\left(\frac{p_i}{RT_{(i)}}\right)\left(\frac{1}{V}\right) \qquad \text{(AIV.7)}$$

$w_{(i)}$ is the water content of the inlet air (%)

R is the universal gas constant ($Jmol^{-1}k^{-1}$)

p_i/RT_i represents the molar volume of air at the inlet conditions

The hydrogen peroxide technique

At steady state conditions the rate of addition of hydrogen peroxide is equilibrated to the rate of decomposition of hydrogen peroxide (or the rate of stripping by the air) (Chapter 6)

$$r_d = \frac{Q_{H_2O_2}\left[H_2O_2\right]}{V} \qquad \text{(AIV.8)}$$

r_d is the rate of hydrogen peroxide decomposition (mol m^{-3} s^{-1})

$Q_{H_2O_2}$ is the feed rate of hydrogen peroxide (m^3s^{-1})

$[H_2O_2]$ is the concentration of hydrogen peroxide (mol m^{-3})

Since one mole of O_2 is produced from the decomposition of 2 moles of H_2O_2 then

$$\frac{r_d}{2} = OTR = k_L a\left(C_L - C_L^*\right) \qquad \text{(AIV.9)}$$

AIV-1.2 Calculation of driving force

At operating/ probe calibration conditions,

$$P_v = P_a + P_h + P_s \qquad \text{(AIV.10)}$$

P_v is the vessel pressure at calibration conditions (Nm^{-2})

P_a is atmospheric pressure (Nm^{-2})

P_h is the head pressure (Nm^{-2})

P_s is the static pressure (Nm^{-2})

The concentration of oxygen in the gas phase at operating conditions, C_G^{cal} (mol m^{-3})

$$C_G^{cal} = \frac{n}{V} = \left(\frac{P_v}{RT_i}\right)\left(\frac{100 - w_i}{100}\right)(0.2095) \qquad \text{(AIV.11)}$$

The liquid phase concentration of oxygen which is in equilibrium with the gas phase (interface concentration), C_L^*, can be calculated from

$$C_L^* = \frac{C_G^{cal}}{H'} \qquad \text{(AIV.12)}$$

H' is the dimensionless Henry's constant (mol m^{-3} gas/mol m^{-3} bulk liquid)

The concentration of oxygen in the bulk liquid (C_L) is obtainable from the dissolved oxygen probe reading ($dO_2\%$), such that

$$C_L = C_L^* \frac{dO_2\%}{100} \qquad \text{(AIV.13)}$$

To calculate ΔC the liquid phase oxygen concentrations in equilibrium with the inlet ($C_{L_{(i)}}^*$) and exit gas ($C_{L_{(o)}}^*$) is required, therefore

$$C_{L(i)}^* = \frac{C_G^{cal}}{H'} \qquad \text{(AIV.14)}$$

and

$$C_{L(o)}^* = \frac{C_G^{out}}{H'} \qquad \text{(AIV.15)}$$

where C_G^{out} is either established from the mass spectrometer data or obtained from the following equations (when using H_2O_2 decomposition):

$$C_G^{out} = \left(\frac{C_G^{cal} Q_{(i)} + OTR.V}{Q_{(o)}}\right) \qquad \text{(AIV.16)}$$

where

$$Q_{(o)} = Q_{(i)} + \left(\frac{OTR.V.R.T_v}{P_v} \right) \qquad \text{(AIV.17)}$$

Consequently the driving force for mass transfer is dependant upon the specified model:

(i) Fully back mixed gas phase

$$\Delta C = C_L - C^*_{L_{(o)}} \qquad \text{(AIV.18)}$$

(ii) Plug flow model

$$\Delta C = \frac{\left(C_L - C^*_{L_{(i)}}\right) - \left(C_L - C^*_{L_{(o)}}\right)}{\ln\left[\frac{\left(C_L - C^*_{L_{(i)}}\right)}{\left(C_L - C^*_{L_{(o)}}\right)}\right]} \qquad \text{(AIV.19)}$$

The mass transfer coefficient can now be calculated:

$$k_L a = \frac{OTR}{\Delta C} \qquad \text{(AIV.20)}$$

AIV-2 Worked example

Using the H_2O_2 technique and obtaining the oxygen transfer rate from both the hydrogen peroxide feed rate and the mass balance the method was checked.

Operating conditions:

P/V = 1 W/kg; 3SHP1, 252 rpm; 6RT, 200 rpm; 0.1 vvm

Temperature = 25 °C = 298.15°K

Head pressure, atmospheric, $P_h + P_a = 0 + 1.013\times10^5 = 1.013\times10^5\,Nm^{-2}$

Static pressure, $P_s = 0.36\times998\times9.81 = 0.0353\times10^5\,Nm^{-2}$

Operating pressure, $P_v = P_h + P_a + P_S = 1.048\times10^5\,Nm^{-2}$

Gas flow rate, $Q_{(i)} = 1.06\times10^{-3}\ m^3s^{-1}$

$V_L = 0.64\ m^3$

$w_{(i)} = 3.166\%$ at operating temperature and pressure[1]

$R = 8.314\ Jmol^{-1}K^{-1}$

Calculation of OTR

- Mass balance:

Substituting

$O_{2(i)} = 0.2095$

$O_{2(o)} = 0.2994$

$N_{2(i)} = 0.7903$

$N_{2(o)} = 0.6923$

into Equation (AIV.7) gives

$$OTR = 1.06 \times 10^{-3}\left(1 - \frac{3.166}{100}\right)\left(0.2095 - \frac{29.94 \times 0.7903}{0.6914}\right)\left(\frac{1.048 \times 10^{5}}{8.314 \times 298.15}\right)\left(\frac{1}{0.64}\right)$$

$$\boldsymbol{OTR = -0.00905\ molO_2\ m^{-3}s^{-1}}$$

The value is negative because oxygen is produced by the decomposition of H_2O_2. A positive value is found when fermentation broth is used as an oxygen sink.

- H_2O_2 feed rate

Substituting

$Q_{H_2O_2} = 1.23\times10^{-6}\ m^3\ s^{-1}$

$[H_2O_2] = 9251\ mol\ m^{-3}$

into Equation (AIV.8) gives

$$OTR = \frac{1.23 \times 10^{-6} \times 9251}{0.64}$$

$$\boldsymbol{OTR = 0.00938\ molO_2\ m^{-3}s^{-1}}$$

Calculation of the driving force

$$C_G^{cal} = \left(\frac{1.048 \times 10^5}{8.314 \times 298.15}\right)\left(1 - \frac{3.166}{100}\right)(0.2095) = 8.58 \text{ mol m}^{-3}$$

For water at 25°C,

Henrys constant[2] = 0.2663 mol O_2 m^{-3} atm.air^{-1} = 1.271 mol O_2 m^{-3} atm.O_2^{-1}

Which gives a dimensionless Henrys constant, H' = 32.161

$$C_L^* = \frac{8.58}{32.161} = 0.2669 \text{ mol m}^{-3}$$

dO_2 = 201.9 %

$$C_L = 0.2669 \frac{201.9}{100} = 0.5389 \text{ mol m}^{-3}$$

$C^*_{L(i)}$ = 0.2669 mol m^{-3}

The liquid phase oxygen concentration in equilibrium with the exit gas can be calculated from the mass balance or using the OTR found from the H_2O_2 feed rate:

- The mass balance:

$$C_G^{out} = \left(O_{2(o)}\right)\left(\frac{P_v}{RT_i}\right) = 0.2994 \times \frac{1.048 \times 10^5}{8.314 \times 298.15} = 12.65 \text{ mol m}^{-3}$$

$$C_{L(o)}^* = \frac{12.65}{32.161} = 0.3933 \text{ mol m}^{-3}$$

Substituting $C^*_{L(i)}$ and $C^*_{L(o)}$ into Equations (AIV.18) and (AIV.19) gives

Fully backmixed ΔC = 0.1453 mol m^{-3}

Plug Flow ΔC = 0.2021 mol m^{-3}

- H_2O_2 feed rate:

$$Q_{(o)} = 1.06 \times 10^{-3} + \left(\frac{0.00938 \times 0.64 \times 8.314 \times 298.15}{1.048 \times 10^5}\right) = 1.209 \times 10^{-3} \text{ m}^3 \text{ s}^{-1}$$

$$C_G^{out} = \frac{8.582 \times 1.06 \times 10^{-3} + 0.00938 \times 0.64}{1.209 \times 10^{-3}} = 12.54 \text{ mol m}^{-3}$$

$$C^*_{L(o)} = \frac{12.54}{32.161} = 0.3899 \text{ mol m}^{-3}$$

Substituting $C^*_{L(i)}$ and $C^*_{L(o)}$ into Equations (AIV.18) and (AIV.19) gives

Fully backmixed ΔC = 0.1488 mol m^{-3}

Plug Flow ΔC = 0.2042 mol m^{-3}

Calculation of $k_L a$

Substituting the driving force and OTR into Equation (AIV.20) gives

	***OTR*, molO$_2$ m^{-3}s^{-1}**	**ΔC, mol m^{-3} Fully backmixed**	**ΔC, mol m^{-3} Plug flow**	**$k_L a$, s^{-1} Fully backmixed**	**$k_L a$, s^{-1} Plug flow**
Mass balance	-0.00905	0.1453	0.2021	0.062	0.045
Feed rate	0.00938	0.1488	0.2042	0.063	0.046

APPENDIX V

LABVIEW PROGRAMS

AV-1 LabVIEW Data Acquisition Program

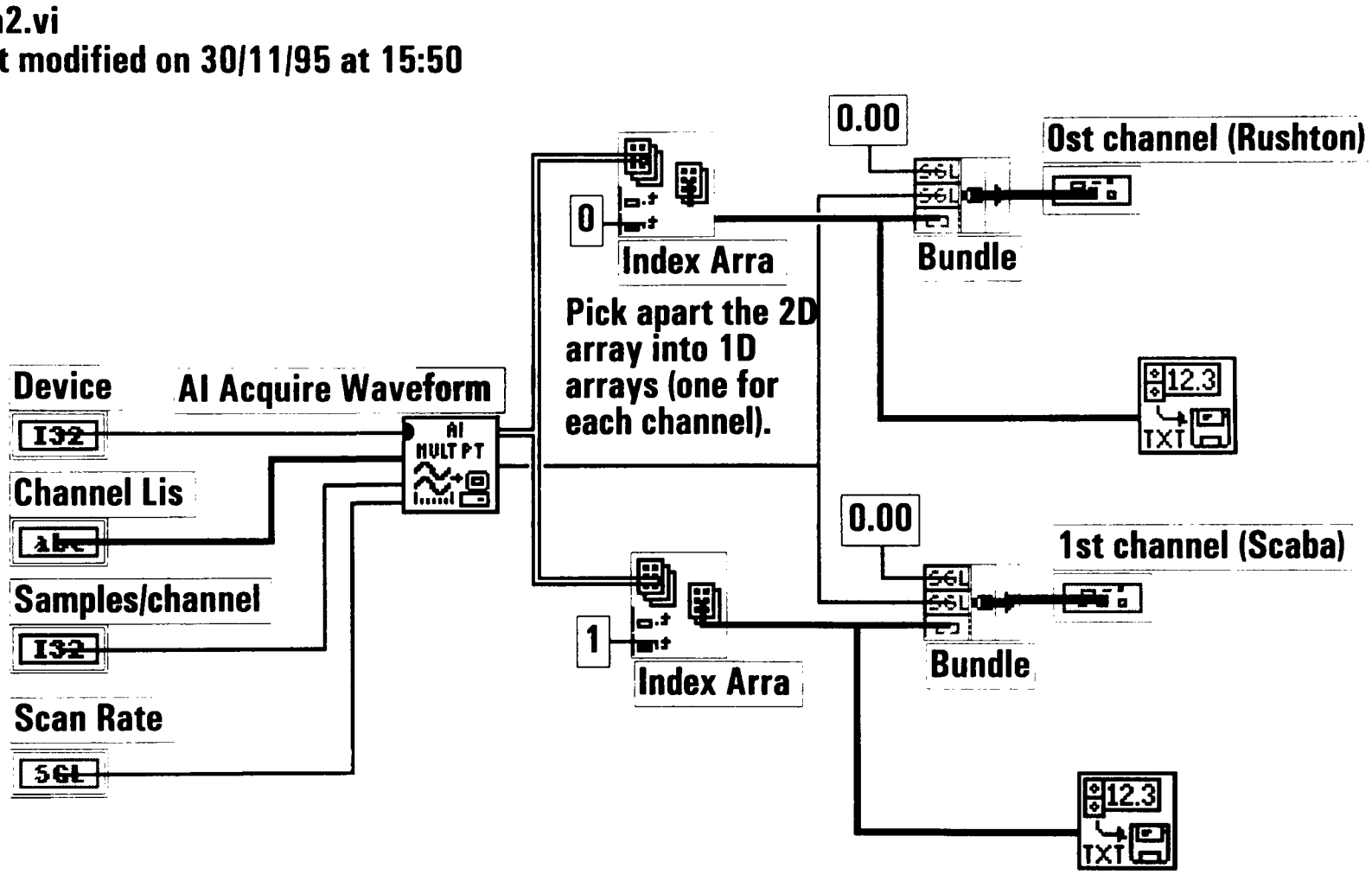

AV-2 LabVIEW Data Manipulation Programs

Single Impeller:

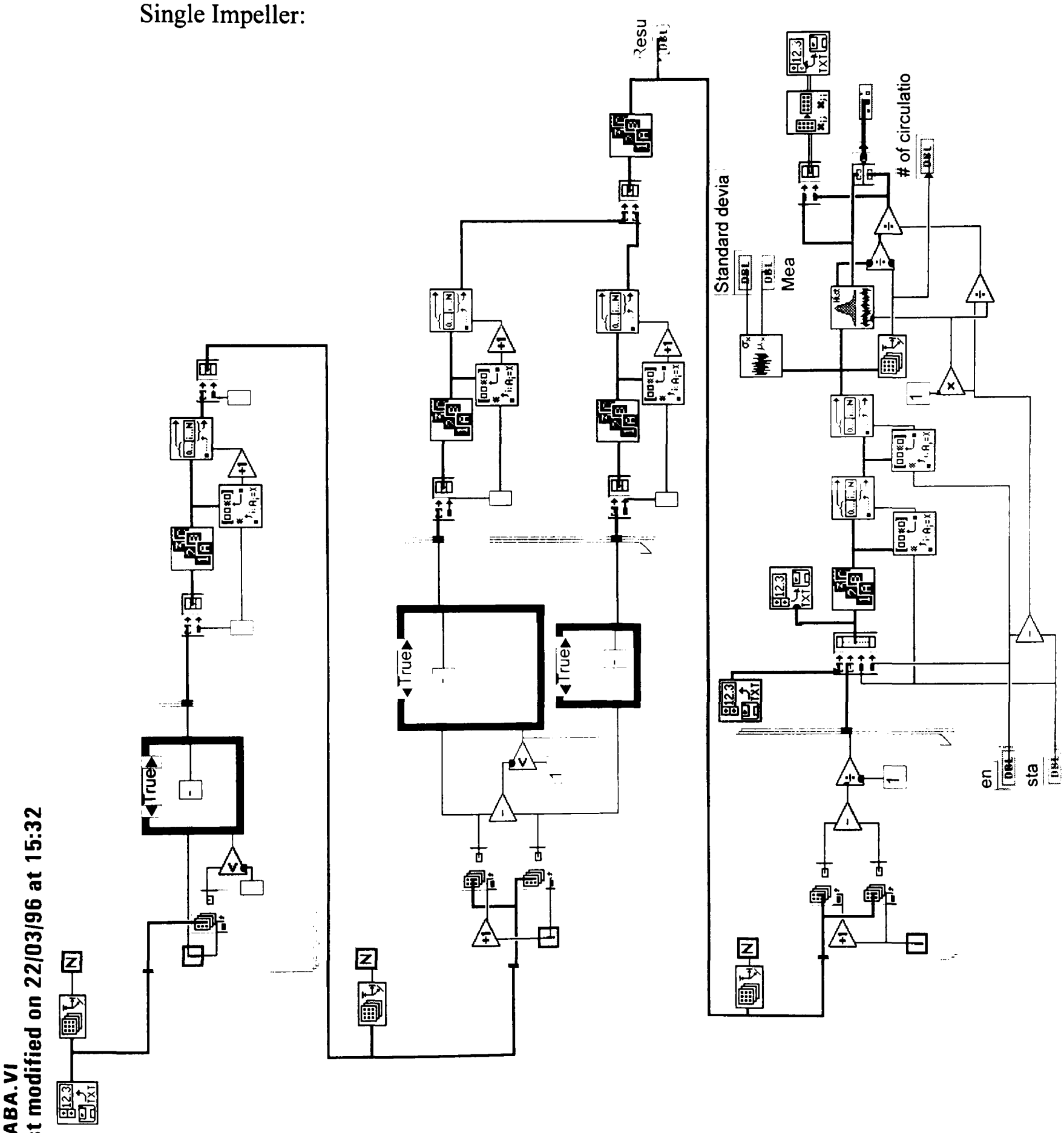

Dual impellers:

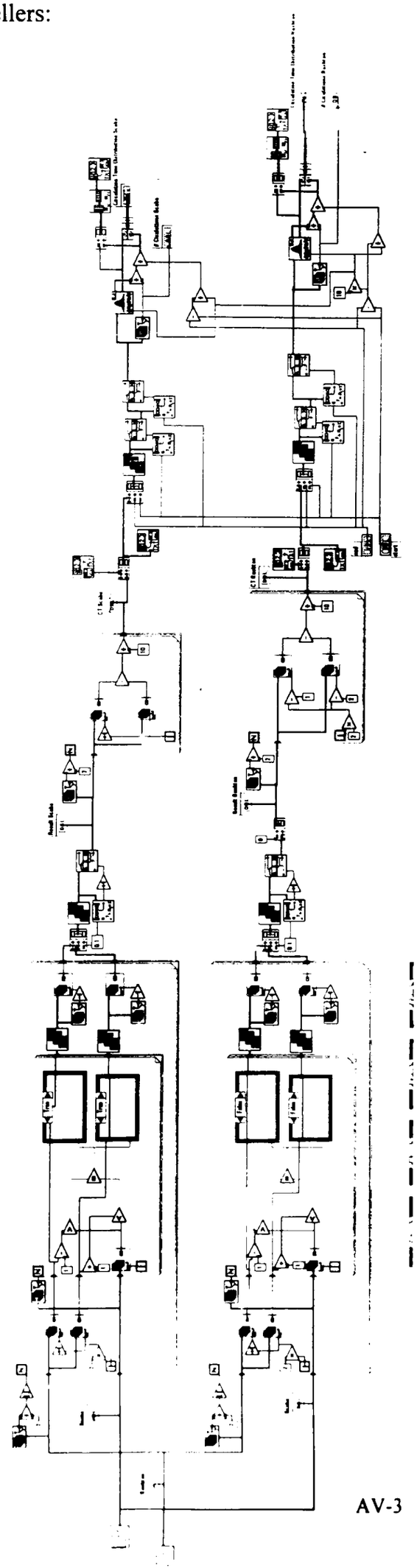

Block Diagram

APPENDIX VI

ASPERGILLUS NIGER FERMENTATIONS

AVI-1 MORPHOLOGY

AVI-1.1 Freely dispersed morphology for fermentations I and II

A breakdown of the freely dispersed hyphae for fermentations I and II is shown in the following figures. Evidently, there is a degree of switching between the groups, highlighting the problems associated with measuring the freely dispersed phase.

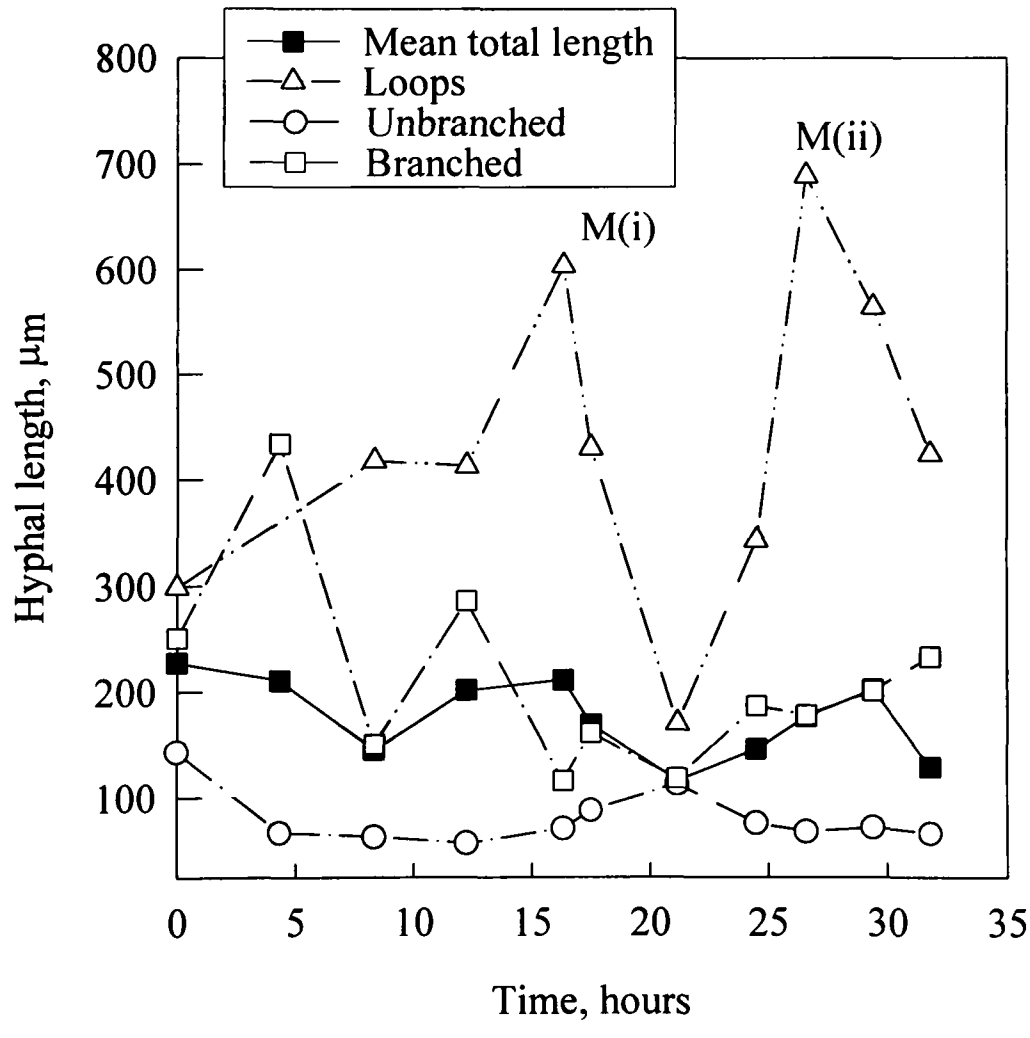

Figure AVI-1 Profile of freely dispersed hyphae for Fermentation I

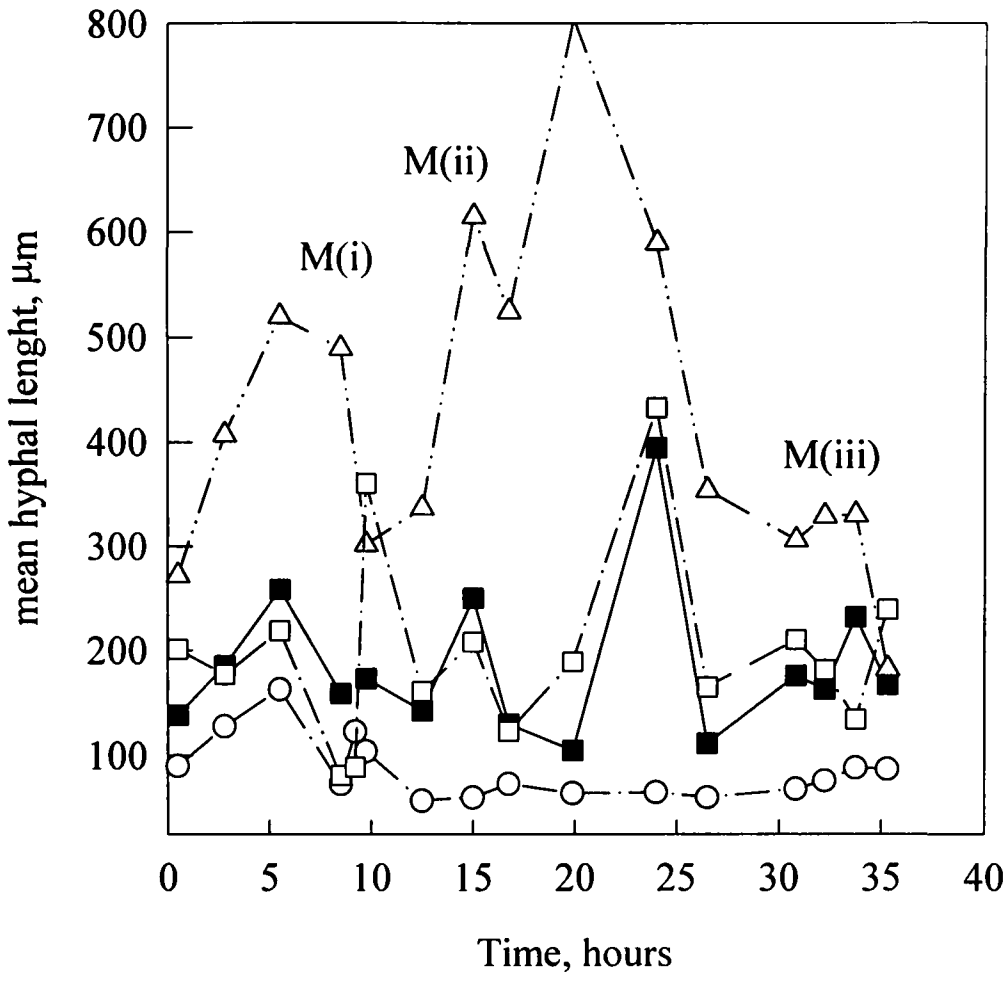

Figure AVI-2 Profile of freely dispersed hyphae for Fermentation II; symbols as Figure AV-1

AVI-1.2 Morphological profile for fermentation III

Comparison of the morphological profiles from each of the fermentations was difficult due to interuptions caused by higher impeller speeds used for the mixing experiments in fermentations I and II. The initial clump projected area and that after ~10 hours was similar (circa 30000 μm^2 and 60000 μm^2 respectively) for each fermentation irrespective of geometry. However, clump size dropped to 40000 $m\mu^2$ after approximately 12 hours in Fermentation III. This observation was possibly concealed in fermentations I and II by the increases in impeller speed used in the mixing experiments. As with fermentations I and II changes in impeller speed were seen to have a profound affect on the morphology of the system, *i.e.* clump reduction by fragmentation followed by a rapid recovery due to growth and agglomeration effects.

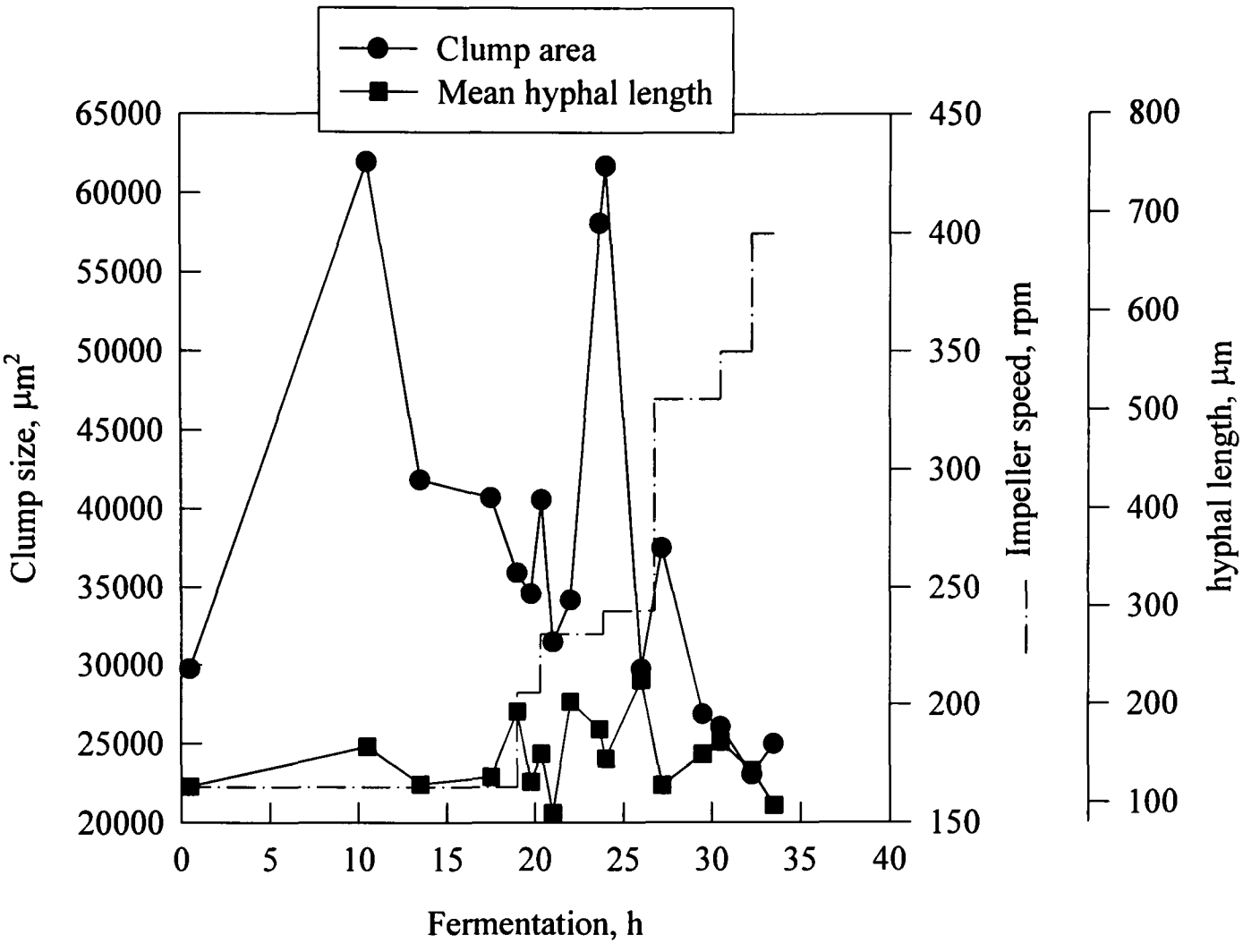

Figure AVI-3 Morphological profile for fermentation III

AVI-2 HPLC ANALYSIS

Figure AV-4 shows the detailed HPLC analysis for fermentation I. Unfortunately analysis for fermentations II and III produced very poor results, either due to experimental error or problems with the HPLC column. For fermentation I, the sucrose was very rapidly broken down into fructose and glucose which was subsequently metabolised by the *A. niger* producing biomass. Approximately 40 g/l of sugar was used to produce 14 g/l of biomass. This gave a yield of 0.35 g biomass/g sugar, 30% less than the theoretical yield (0.5 g/g) and suggested the 6 g/l sugar was utilised by the micro-organism to produce a by-product. In addition, 30 l of 4M NaOH, neutralising 120 moles of H^+, was required to control the pH at 2.0. Similarly, in the 5 l bench scale work pH dropped very rapidly (from 5 or 3) to a relatively constant value of about 1.1. This rapid acidification of the broth is characteristic of *A.niger* fermentations[1,2] even before the onset of extracellular citric acid production. Legisa

and Kidric[2] suggested that at sucrose levels greater than 5% enough intracellular glycerol is formed (by the pentose phosphate pathway) to inhibit $NADP^+$-specific ICDH (enzyme) causing a reduction in the metabolic flux through the TCA cycle. This flux reduction would increase the intracellular citrate level.

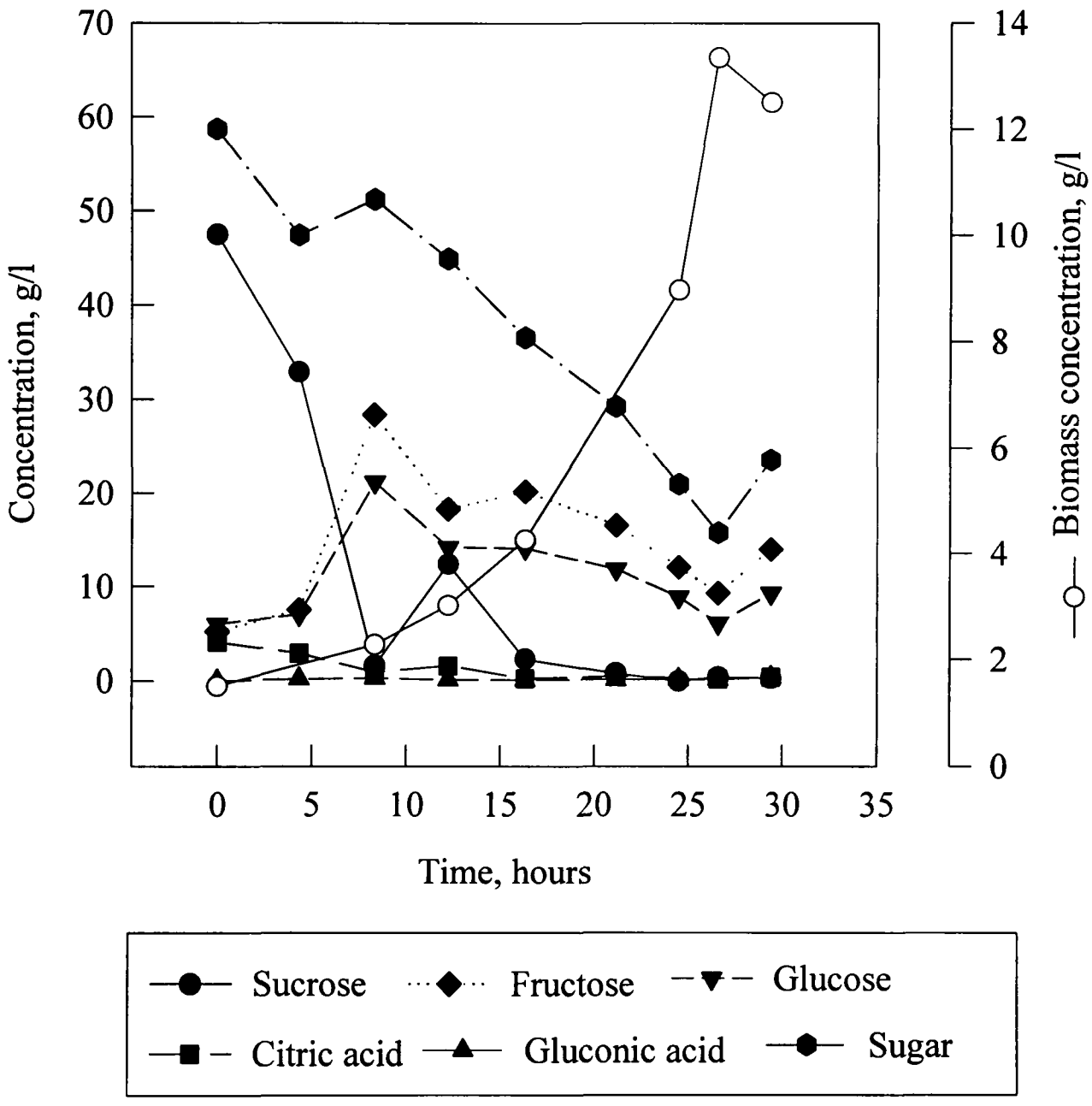

Figure AVI-4 HPLC analysis of fermentation I

At low pH values, protons are released by the cell, as the citrate is present in the ionic form. It was proposed that provided sufficient magnesium was present in the medium, citrate excretion would not occur. This would account for the scarcity of citric acid detected by the HPLC analysis on the fermentations performed in this project. Assuming the intracellular citric acid

was totally dissociated, 3 protons would be excreted per mole of citrate formed. Therefore, approximately 40 moles of intracellular citric acid were produced (~12 g/l if excreted) which would account for the 6g/l sugar not utilised for biomass production (Table AVI-1).

Table AVI-1 Carbon mass balance over reactor

(assuming total dissociation of citric acid and no citrate in biomass measurement)

	IN		OUT	
	Constituent g/l	Carbon g/l	Constituent g/l	Carbon g/l
Sucrose	50	19.67	0	0
Fructose	5	1.99	11	4.40
Glucose	5	1.99	9	3.60
Citric acid (intracellular)	-	-	12	4.50
Biomass	-	-	15	10.81
TOTAL	**60**	**23.65**	**47**	**23.31**

AVI-3 Calculation of the Time Constants

AVI-3.1 Transport phenomena

- **Oxygen transfer, t_{ot}**

This was defined as the reciprocal of the k_La (Chapter 6). For IDDIDT the range of k_La values in water at the fermenter operating conditions was 0.03 s^{-1} to 0.1 s^{-1}. Therefore $10s<t_{ot\text{-}ID}<33s$.

Simlarly, for the RT-RT: $0.015s^{-1}<k_La<0.1s^{-1}$ and $10s<t_{ot\text{-}RT}<67s$.

- **Circulation of liquid, t_m**

This was taken as the experimental blend times at the fermenter operating conditions.

For IDDIDT mixing times were between 5 and 30 seconds (Chapter 7).

For the RT-RT: $50s<t_{m\text{-}RT}<100s$ (Chapter 7)

AVI-3.2 Microbial conversion

- **Oxygen consumtion, t_{oc}**

The time constants for oxygen consumption are found from the Michaels-Menton equation:

$$OUR = \frac{(OUR_{\max})(C_L)}{(C_L + K_{O2})}$$

Where OUR_{max} is the maximum oxygen uptake rate and K_{O2} is the saturation constant for O_2.

For a *zero order* reaction ($C_L >> K_{O2}$):

$$t_{oc-o} = \frac{C_L^*}{OUR_{\max}}$$

From experimental data the maximum OUR was 5.643×10^{-3} mol.m^{-3} s^{-1}

and C^*_L at 25°C was 0.2669 mol.m^{-3}. Therefore t_{oc-o} was 47.3 s.

For a *first order* reaction ($K_{O2} > C_L$):

$$t_{oc-1} = \frac{K_{O2}}{OUR_{\max}}$$

K_{O2} can be estimated from[3]:

$$dO_{2,crit} \approx 3K_{O2}$$

where $dO_{2,crit}$ for *Aspergillus* is 0.02 mol.m^{-3} [3]. Therefore t_{oc-1} was 3.55 s.

- **Substrate consumption**

Assuming a first order reaction ($C_s > K_s$) then

$$t_{sc} = \frac{C_s}{r_{s\max}} = \frac{60}{3.7 \times 10^{-4}} = 16.2 \times 10^4 \text{ s}$$

where C_s is the initial sugar content (60 g/l), K_s is the saturation constant for sucrose and r_{smax} is the maximum rate of consumtion of sugar

(calculated to be 1.333 g/l/h (3.7×10^{-4} g/l/s))

- **Growth**

This is given by the reciprocal of the maximum specific gowth rate. The specific growth rate calculated for the exponential phase was $0.039h^{-1}$. Therefore:

$$t_G = \frac{1}{\mu_{max}} = \frac{1}{1.08 \times 10^{-5}} = 9.2 \times 10^4 \text{ s}$$

AVI-4 REFERENCES

1. Kristiansen, B. and Sinclair, C.G., 1978, "Production of citric acid in batch culture", *Biotech.BioEng.*, 20:1711-1722
2. Legisa, M. and Kidric, J., 1989, "Initiation of citric acid accumulation in the early stages of Aspergillus niger growth", *Appl.Microbiol.Biotechnol.*, 31: 453-457
3. Bailey, J.E. and Ollis, D.F., 1986, "Biochemical Engineering Fundamentals", 2nd Ed. (Eds. McGraw Hill)

APPENDIX VII

PUBLISHED WORK

Oral

- W. Bujalski, A.H.John, R. Sharpe, R.S. Badham, D. Bowden, P. W. Cox, T. Eddleston, R. Haddock, H.R. Jennings, D. Webb, D. Patel, G. Riley, R. Schmitz, G. L. Solomons, C. R. Thomas and A. W. Nienow, 1996, "A non-aseptic *Aspergillus niger* fermentation for characterising a dual impeller proto-fermenter: A Feasibility study", *Proc. 1996 IChemE Research Event/Second European Conference*, Leeds, UK: 13-15

- A.H. John, W. Bujalski, R. Schmitz, C.R. Thomas, A. W. Nienow, 1996, "Biological and physical aspects of mixing in a novel dual impeller proto-fermenter", *A.IChem.E. Annual Meeting*, Chicago, USA

Journal

- A.H. John, W. Bujalski, A. W. Nienow, A. Sanchez, L. Torres and E. Galindo, 1995, "Investigations into the performance of an independently driven, dual impeller proto-fermenter: Power and Hold-up", *Trans. I.Chem.E.*, 73, Part A: 535-541

- A.H.John, W. Bujalski and A.W. Nienow, 1997, "The performance of a proto-fermenter containing independently-driven dual impellers in a draft tube (IDDIDT): Mixing Times", *Trans. I.Chem.E.*, currently in construction

Poster/Conference proceedings

- A.H. John, W. Bujalski and A. W. Nienow, 1995, "Investigations into the performance of an independently driven, dual impeller proto-fermenter: Mixing times", *Proc. 1995 I.Chem.E. Research Event/First European Conference,* Edinburgh, UK: 710-713

- A.H. John, R. Schmitz, H. R. Jennings, W. Bujalski, G. L. Solomons, C.R. Thomas and A.W Nienow, 1996, "Large scale mixing experiments in non-aseptic *Aspergillus niger* fermentations", *Proc. 5th World Congress Chem. Eng.*, San Diego, USA, 2: 538-546

- A.H. John, W. Bujalski and A. W. Nienow, 1997, "A novel reactor with two independently-driven impellers for gas-liquid processing", *Proc. 9th European Conference on Mixing,* Williamsburg, Virginia, USA